UNIVERSITAT DE BARCELONA

Impact of cancer cell plasticity on tumor immune microenvironment and immunotherapy response

Laura Lorenzo Sanz

UNIVERSITAT DE BARCELONA

FACULTAT DE MEDICINA I CIÈNCIES DE LA SALUT

Programa de Doctorat en Biomedicina

IMPACT OF CANCER CELL PLASTICITY ON TUMOR IMMUNE MICROENVIRONMENT AND IMMUNOTHERAPY RESPONSE

Memòria de tesi doctoral presentada per **Laura Lorenzo Sanz** per optar

al grau de Doctor per la Universitat de Barcelona

Director: Dra. Purificación Muñoz Moruno

Tutor: Dr. Francesc Viñals Canals

Doctorand: Laura Lorenzo Sanz

Laura Lorenzo Sanz
Maig 2021

UNIVERSITAT DE BARCELONA

FACULTAT DE MEDICINA I CIÈNCIES DE LA SALUT

Programa de Doctorat en Biomedicina

IMPACT OF CANCER CELL PLASTICITY ON TUMOR IMMUNE MICROENVIRONMENT AND IMMUNOTHERAPY RESPONSE

Memòria de tesi doctoral presentada per

Laura Lorenzo Sanz

per optar al grau de Doctor per la Universitat de Barcelona

Aquesta tesi doctoral s'ha realitzat al Grup d'Envelliment i Càncer de l'Institut d'Investigació Biomèdica de Bellvitge (IDIBELL), sota la direcció de la Dra. Purificación Muñoz Moruno

Dra. Purificación Muñoz Moruno
Director

Dr. Francesc Viñals Canals
Tutor

Laura Lorenzo Sanz
Doctorand

Barcelona, Maig 2021

TABLE OF CONTENTS

TABLE OF CONTENTS

ABBREVIATIONS

ACN	Acetonitrile
ACT	Adoptive cell transfer
ADM	Adrenomedullin
AEs	Adverse events
AK	Actinic keratosis
AMP	Adenosine monophosphate
APCs	Antigen presenting cells
ARG1	Arginase 1
ATRA	All-trans-retinoic acid
B2M	Beta-2-microglobulin
BCC	Basal cell carcinoma
bFGF	Basic fibroblast growth factor
Bv8	Bombina variegate peptide 8
CAFs	Cancer-associated fibroblasts
CAR-T	Chimeric antigen receptor-T cell therapy
CCL	C-C motif chemokine ligand
CCR	C-C motif chemokine receptor
CD11b	Cluster of differentiation 11b or integrin alpha M (ITGAM)
CD11c	Cluster of differentiation 11c or integrin alpha X (ITGAX)
CD204	Macrophage scavenger receptor and cluster of differentiation 204
CD206	Macrophage scavenger receptor and cluster of differentiation 206
CD3	Cluster of differentiation 3
CD34	Hematopoietic Progenitor Cell Antigen CD34
CD4	Cluster of differentiation 4
CD45	Cluster of differentiation 45 or protein tyrosine phosphatase receptor type C
CD8	Cluster of differentiation 8
CD80	Cluster of differentiation 80 or B7-1
CD86	Cluster of differentiation 86 or B7-2
CDK	Cyclin-dependent kinase
CEACAM-1	Carcinoembryonic antigen cell adhesion molecule 1
cGAS	Cyclin GMP-AMP synthase
COX2	Cyclooxygenase-2
CR	Complete response
CSC	Cancer stem cell
cSCC	Cutaneous squamous cell carcinoma
CSF1R	Colony-stimulating factor-1 receptor
CTL	Cytotoxic T lymphocyte
CTLA-4	Cytotoxic T lymphocyte-associated molecule 4
CXCL	C-X-C motif chemokine ligand
CXCR	C-X-C motif chemokine receptor
DAPI	4’-6-Diamidino-2-phenylindole
DC	Dendritic cells
DCR	Disease control rate
DMBA	7,12-dimethylbenz(a)anthracene
DNA	Deoxyribonucleic acid
DNAM-1	DNAX accessory molecule-1 or CD226
DNMT	DNA methyltransferase
DTT	Dithiothreitol

ECM	Extracellular matrix
EGF	Epidermal growth factor
EGFR	Epidermal growth factor receptor
EMA	European Medicines Agency
EMT	Epithelial-to-mesenchymal transition
EMT-TF	Epithelial-to-mesenchymal transition transcription factor
Epit	Epithelial
EV	Extracellular vesicles
F4/80	EGF-like module-containing mucin-like hormone receptor-like 1
FACS	Fluorescence-activated cell sorting
FADD	Fas-associated death domain
FDA	U.S. Food and Drug Administration
FGFR	Fibroblast growth factor receptor
FGL-1	Fibrinogen-like protein 1
FoxP3	Forkhead box P3
GFP	Green Fluorescent Protein
GM-CSF	Granulocyte-macrophage colony-stimulating factor
GO	Gene ontology
GR1	Protein gamma response 1
GRHL2	Grainyhead-like transcription factor 2
GZMB	Granzyme B
HGF	Hepatocyte growth factor
HIF-1α	Hypoxia-inducible factor-1α
HLA	Human leukocyte antigen
HMGB1	High-mobility group protein 1
HNSCC	Head and neck squamous cell carcinoma
HPV	Human Papillomavirus
IC	Immune checkpoint
ICB	Immune checkpoint blockade
ICOS	Inducible costimulator
IDO	Indoleamine 2,3-dioxygenase
IF	Immunofluorescence
IFN	Interferon
IGF-1	Insulin-like growth factor 1
IGF-1R	Insulin-like growth factor 1 receptor
IHC	Immunohistochemistry
IL	Interleukin
iNOS	Inducible nitric oxide synthase
irAEs	Immune-related adverse events
IRF1	Interferon regulatory factor 1
JAK	Janus kinase
K14	Keratin 14
KIR	Killer immunoglobulin-like receptor
LAG-3	Lymphocyte activation gene-3 or CD223
LOF	Loss of function
LOX-1	Lectin-type oxidized receptor 1
LPS	Lipopolysaccharide
MAPK	Mitogen-activated protein kinase

MD	Moderately differentiated
MDSC	Myeloid-derived suppressor cell
Mes	Mesenchymal
MET	Mesenchymal-to-epithelial transition
MHC-I	Major histocompatibility complex class I
MHC-II	Major histocompatibility complex class II
miRNAs	microRNAs
Mix	Mixed
M-MDSC	Monocytic MDSC
MMPs	Matrix Metalloproteinases
NCR	Natural cytotoxicity receptor
NK	Natural killer
NMSC	Non-melanoma skin cancer
NO	Nitric oxide
NSCLC	Non-small cell lung cancer
ORR	Objective response rate
OVOL2	Ovo like zinc finger 2
P53	Tumor Protein P53
PBS	Phosphate-buffered saline
PD	Poorly differentiated or Progressive disease
PD/S	Poorly differentiated/spindle
PD-1	Programmed cell death protein 1
PDE-5	Phosphodiesterase-5
PDGF	Platelet-derived growth factor
PDGFR	Platelet-derived growth factor receptor
PD-L1	Programmed cell death ligand 1
PD-L2	Programmed cell death ligand 2
PDX	Patient-derived xenograft
PFS	Progression-free survival
PGE2	Prostaglandin E2
PKA	Protein kinase A
PMN-MDSC	Polymorphonuclear MDSC
PR	Partial response
PRRX1	Paired-related homeobox 1
PtdSer	Phosphatidyl serine
PyMT	Polyoma middle tumor-antigen
Rb	Retinoblastoma
RECIST	Response Evaluation Criteria in Solid Tumors
ROS	Reactive oxygen species
SC	Stem Cell
SCC	Squamous cell carcinoma
SD	Stable disease
SNAI1	Snail family transcriptional repressor 1 or Snail
SNAI2	Snail family transcriptional repressor 2 or Slug
SOX2	SRY-Box transcription factor 2
STAT	Signal transducer and activator of transcription
TAM	Tumor-associated macrophage
TAN	Tumor-associated neutrophil

TCR	T-cell receptor
TF	Transcription factor
TFA	Trifluoroacetic acid
TGF-β	Transforming growth factor β
Th1	T helper type I
Th2	T helper type II
TIGIT	T cell immunoglobulin and ITIM domain
TILs	Tumor-infiltrating lymphocytes
TIM-3	T cell immunoglobulin and mucin domain-containing molecule-3 or CD366
TMB	Tumor mutation burden
TME	Tumor microenvironment
TNF-α	Tumor necrosis factor α
TPA	12-O-tetradecanoylphorbol-13-acetate
TRAIL	TNF-related apoptosis-inducing ligand
Treg	Regulatory T cells
TREM2	Triggering receptor expressed on myeloid cells 2
TWIST1	Twist family bHLH transcription factor 1
UVR	Ultraviolet radiation
VEGF	Vascular endothelial growth factor
WD	Well differentiated
YAP1	Yes associated protein 1
ZEB1	Zinc Finger E-Box-Binding Homeobox 1
ZEB2	Zinc Finger E-Box-Binding Homeobox 2
α6	Integrin alpha-6

RESUMEN TESIS

IMPACTO DE LA PLASTICIDAD DE LAS CÉLULAS TUMORALES EN EL MICROAMBIENTE INMUNITARIO DEL TUMOR Y EN LA RESPUESTA A LA INMUNOTERAPIA

La mayoría de los carcinomas escamosos de piel (cSCCs) se tratan con éxito mediante escisión quirúrgica. Sin embargo, el 5-8% de los casos desarrollan recurrencias, las cuales están asociadas a un crecimiento agresivo, progresión de la enfermedad y una limitada supervivencia de los pacientes. Hasta hace unos años, los cSCCs avanzados y/o metastásicos eran tratados con quimioterapia y radioterapia con escasos beneficios clínicos. Sin embargo, recientemente se aprobó el uso de cemiplimab y pembrolizumab (anticuerpos anti-PD-1) para el tratamiento de este tipo de tumores. Estudios previos en otros tipos tumorales indicaron que las características de las células tumorales pueden influenciar el microambiente inmunitario y, a su vez, estas células inmunitarias pueden desempeñar un papel importante en la progresión de la enfermedad, en el desarrollo de la metástasis y en la respuesta a la terapia. El objetivo principal de esta Tesis es identificar el impacto de la plasticidad de las células tumorales en el microambiente inmunitario y en la respuesta a la inmunoterapia, con el fin de establecer las bases para el diseño de nuevas estrategias terapéuticas para los cSCCs avanzados y/o metastásicos.

Nuestros estudios realizados en modelos de ratón demuestran que las características de las células tumorales cambian durante la progresión del cSCC, pasando desde estadios en los que conservan rasgos de diferenciación epitelial (en WD-SCC) a estadios completamente mesenquimales (en PD/S-SCC), a través de la aparición de estadios híbridos epiteliales-mesenquimales (en MD/PD-SCC). Mediante ensayos de citometria de flujo y de immunohistoquímica, hemos observado que la aparición de las células tumorales híbridas y mesenquimales se correlaciona con un enriquecimiento de células T reguladoras, células mieloides supresoras (MDSCs) y macrófagos con polaridad M2 en muestras de cSCCs de ratón y de pacientes. Este ambiente inmunosupresor se asocia a su vez con un aumento de la infiltración de linfocitos T $CD8^+$ y de células natural killer (NK) inactivos en el tumor, que se caracterizó por un aumento de la expresión de receptores de puntos de control inmunitario (IC) tales como PD-1, TIM-3, LAG-3 y TIGIT. Además, se observó que las células tumorales epiteliales y mesenquimales desarrollan diferentes mecanismos de evasión inmunitaria mediante cambios de la expresión de ligandos de IC, así como a través de la pérdida de la expresión del complejo mayor de histocompatibilidad (MHC-I), el cual es necesario para su reconocimiento por parte de los linfocitos T $CD8^+$. En concreto, mientras que las células tumorales epiteliales expresan mayoritariamente los ligandos PD-L1, MHC-II, Galectina-9 y CD86, las células tumorales mesenquimales reducen la expresión de estos ligandos e inducen la expresión de CD80 y CD155. Estos resultados indican que el patrón de expresión de ligandos de IC podría tener un importante impacto en la respuesta a la inmunoterapia basada en inhibidores de IC por parte de los pacientes con cSCCs avanzados y/o metastásicos.

Posteriormente, evaluamos como el ambiente inmunosupresor y el patrón de expresión de ligandos de IC podría afectar a la respuesta a la terapia mediante el uso de inhibidores de IC o la depleción de poblaciones inmunosupresoras tales como las MDSCs o los macrófagos. Nuestros estudios demuestran que los WD-SCCs de ratón compuestos mayoritariamente por células tumorales epiteliales responden a la terapia anti-PD-L1. Esta respuesta es dependiente de la reactivación de los linfocitos T citotóxicos y de la reducción del reclutamiento de macrófagos de tipo M2 y M-MDSCs al tumor. No obstante, los tumores PD/S-SCCs de ratón compuestos por células tumorales de tipo mesenquimal son refractarios a la terapia anti-PD-L1, pero muestran una buena respuesta a la terapia anti-TIGIT, de acuerdo con la mayor expresión de su ligando CD155 por las células tumorales, los macrófagos de tipo M2 y las células dendríticas. Finalmente, la depleción parcial de MDSCs tras el tratamiento con anti-Gr1 bloquea la progresión de las células tumorales hacia el estado mesenquimal y reduce la infiltración de macrófagos de tipo M2, lo que podría contribuir a potenciar la respuesta antitumoral de los linfocitos T citotóxicos y las células NK. Además, el tratamiento con anti-CSF1R promueve una reducción de la infiltración de los macrófagos de tipo M1 y M2, así como de las M-MDSC al tumor, lo que podría contribuir a reducir el microambiente tumoral inmunosupresor.

En conjunto, nuestros datos indican que no solo la presencia de células tumorales híbridas y mesenquimales, sino también la inducción de la expresión de ligandos de IC alternativos y el reclutamiento de diferentes poblaciones de células inmunosupresoras en los cSCCs podría tener un papel muy importante en la respuesta a la inmunoterapia. Estos resultados abren las puertas a poder desarrollar terapias basadas en la combinación de varios inhibidores de IC o en la combinación de inhibidores de IC junto con la depleción de poblaciones inmunosupresoras con el fin de potenciar la respuesta inmunitaria adaptativa e innata en función de las características de las células tumorales. Por lo tanto, estas estrategias nos pueden permitir encontrar nuevas terapias para superar la resistencia primaria o adquirida a los tratamientos de inmunoterapia por parte de los pacientes con cSCCs avanzados y/o metastásicos.

INTRODUCTION

1. NON-MELANOMA SKIN CANCER

Non-melanoma skin cancer (NMSC) is the most frequently diagnosed cancer in humans (Leiter et al., 2014; Madan et al., 2010), and their pathogenesis is mainly associated with the mutagenic effects produced by ultraviolet radiation (UVR), genetic, epigenetic and microenvironment alterations, as well as immunosuppression (Didona et al., 2018).

The term NMSC includes cutaneous lymphomas, Merkel-cell carcinomas, adrenal tumors, and other rare primary cutaneous neoplasms, but it is mainly used to define basal cell carcinoma (BCC) and cutaneous squamous cell carcinoma (cSCC), as they represent for over 95% of total NMSC cases (Madan et al., 2010). Although they share many similarities, BCC and cSCC have different incidence rates, as an approximately 80% of diagnosed cases are BCCs, while cSCCs represent a 20% (Lomas et al., 2012). However, cSCCs show a more aggressive growth, a higher metastatic capacity and account for the majority of NMSC-related deaths (Burton et al., 2016). Due to their rising incidence and morbidity in the last years, NMSCs have carried a substantial global healthcare problem. Therefore, a better understanding of the pathogenesis mechanisms is essential to strengthen preventive measures and to boost the search of new therapeutic strategies.

1.1- Cutaneous squamous cell carcinoma (cSCC): risk factors and development

cSCC arises from the uncontrolled proliferation of epidermal keratinocytes, which are the main cells building the skin barrier that protects underlying tissues against mechanical stress, water loss, chemicals, and infections. The most important risk factor for cSCC is the exposure to UVR, which lead to cellular damage because of the reduction of cell-mediated immune responses, production of reactive oxygen species (ROS) and DNA alterations (Alam and Ratner, 2001; Didona et al., 2018). The incidence of cSCC has increased in the last 30 years, and can be mainly attributed to increased chronic sun and UVR exposure and a prolonged half-life of the population. Their incidence is also increased at lower latitudes, correlating with an increased intensity of ambient light. In 90% of cases, cSCCs arise on UVR-exposed areas such as the head and neck, the trunk, and the dorsal aspects of the hands and forearms (Stratigos et al., 2015).

Other environmental factors involved in cSCC development are the exposure to ionizing radiations and chemical agents, such as arsenic and polycyclic aromatic hydrocarbons, and the presence of long-lasting inflammatory processes such as those observed in chronic wounds, burns and ulcers (Stratigos et al., 2015). In addition, the immunosuppression derived from organ transplantation, classical immunosuppressives to treat immune diseases and chemotherapy are associated with an increased risk of cSCC development (Stratigos et al., 2015). cSCC development has also been associated with the human papillomavirus (HPV) infection, specifically the high-risk HPV16 variant (Kauvar et al., 2015). A high HPV16 viral load has been recorded in 80% of cSCCs of immune-

suppressed patients (Dubina and Goldenberg, 2009), whereas in immune-competent patients their frequency varies from 27% to 70% (Harwood et al., 2000). HPV16 produces the E6 and E7 viral oncoproteins upon integration into the genome of the host keratinocytes (Moody and Laimins, 2010), which leads to the inactivation of the key tumor-suppressor proteins p53 and retinoblastoma (Rb) by E6 and E7, respectively (Ghittoni et al., 2010). All these observations indicate than an impaired immune system can promote cSCC development (Kadakia et al., 2016).

cSCC development starts after an external stimulus such as UVR or the appearance of mutations in the keratinocytes, and more probably in the stem cells (SCs) of the epidermis (Dotto and Rustgi, 2016; Sánchez-Danés and Blanpain, 2018) (Figure 1). These alterations lead to the loss of normal skin architecture (cellular atypia) and the generation of a region of hyper keratinization called actinic keratosis (AK) (Stratigos et al., 2015) (Figure 1). Increased proliferation of atypical keratinocytes results in cSCCs in situ, which usually presents as Bowen's disease. The accumulation of further mutations in genes such as H-Ras and p53, among others, favors the emergence of more neoplastic properties and can lead to invasive growth, resulting in invasive cSCCs (Alam and Ratner, 2001; Ratushny et al., 2012) (Figure 1). Cancer cells can then migrate and reach the blood vessels, disseminate and metastasize to distant organs such as regional lymph nodes or lungs (Massagué and Ganesh, 2021) (Figure 1). About 97% of cSCCs are the result of the malignant progression of an AK and can be subdivided into four groups based on their histopathological grade (associated with the degree of nuclear atypia and keratinization) (Brantsch et al., 2008).

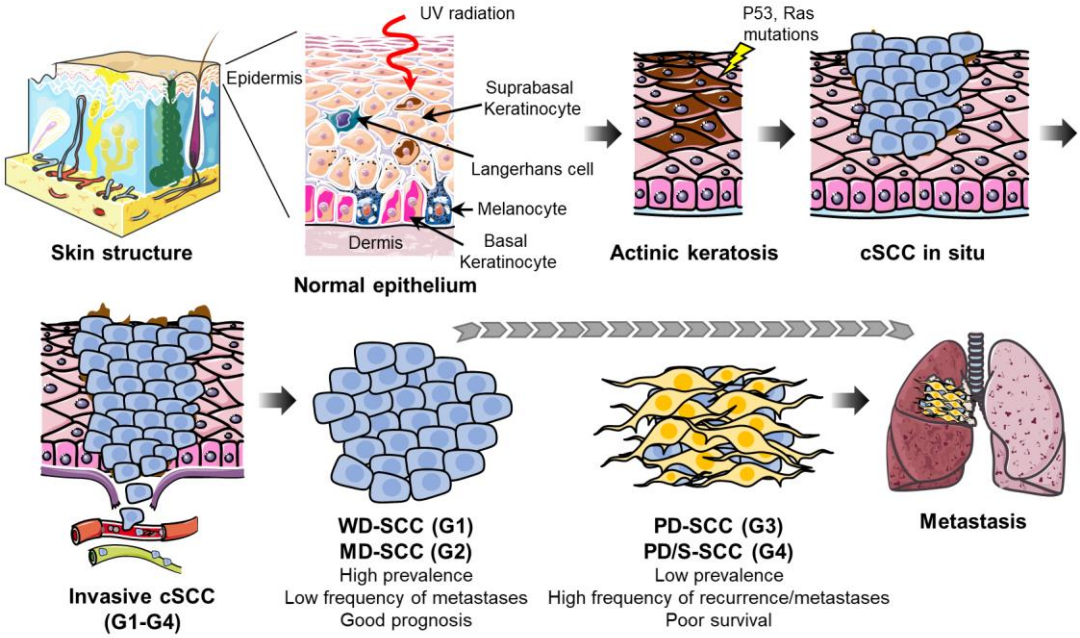

Figure 1. Stages of cSCC progression (original figure from Lorenzo-Sanz L)**.** After an external stimulus, such as UVR and/or the appearance of genetic alterations, keratinocytes begin to proliferate uncontrollably, giving rise to actinic keratosis. These keratinocytes can accumulate further mutations in genes such as H-Ras or p53, among others, promoting the generation of cSCCs in situ, which can eventually progress to invasive

carcinomas. These invasive carcinomas can be classified as well differentiated (G1), moderately differentiated (G2), poorly differentiated (G3) and/or sarcomatoid spindle cell carcinomas (G4), the latter two stages being those associated with high recurrence and metastatic capacity, which reduces patient survival.

Most cSCCs are well differentiated (WD-SCCs) or G1 tumors and retain features of epidermal differentiation. They are formed by cancer cells with atypical elongated nucleus and large cytoplasm, which promotes the formation of extracellular keratin pearls. These tumors are generally associated with low malignancy and low metastatic rate (0.5%-2%) (Brantsch et al., 2008; Brinkman et al., 2015) (Figure 1). A second subtype is the so-called moderately differentiated (MD-SCCs) or G2 tumors. These tumors show greater structural disorganization, nuclear and cytoplasmatic pleomorphisms, more numerous mitoses and limited keratin pearl formation (Figure 1). Poorly differentiated (PD-SCCs) or G3 tumors lose epithelial differentiation features and show a markedly reduction of keratin formation. These PD-SCCs present greatly enlarged and pleomorphic nuclei, and very frequent mitoses. Finally, undifferentiated/spindle (PD/S-SCCs) or G4 tumors are characterized by being completely anaplastic, lose any epithelial differentiation feature and may even reach a spindle-cell stage. Poorly differentiated G3 and G4 cSCCs have a high risk of developing metastasis (26%) and recurrence (28%) (Brantsch et al., 2008; Brinkman et al., 2015).

1.2- Treatment of cutaneous squamous cell carcinoma (cSCC)

In 90% of cases, the prognosis of cSCC patients is favorable and they are successfully treated with surgical excision (Yanofsky et al., 2011). However, some of these cSCCs can evolve into highly aggressive lesions. In contrast to BCCs, which rarely metastasize, 2%-5% of cSCCs develop metastasis, which is associated with a poor prognosis and a median patient survival of less than 2 years (Stratigos et al., 2015). Approximately 85% of metastases occur in regional lymph nodes, and in a smaller percentage of cases in the lungs, liver, brain, and bone. In addition, 4.6% of patients develop recurrences, of which 75% appear during the first 2 years and 95% during the first 5 years after resection (Brantsch et al., 2008). Unfortunately, most of these recurrent tumors present increased aggressiveness and metastatic capacity, which significantly reduces patient survival (Ashford et al., 2017).

The diagnosis of cSCCs is primarily based on clinical features. Patients presenting lesions of multiple AKs or cSCCs in situ are treated with surgical excision, which allows the removal of the total cancerous area (Kauvar et al., 2015). However, there are situations where surgical excision is contraindicated, such as in elderly patients, tumors in difficult resection areas, or advanced and metastatic cSCCs. In these cases, patients are treated with radiotherapy, conventional systemic chemotherapy (cisplatin, fluoropyrimidines, bleomycin, doxorubicin), 13-cis-retinoic acid (13cRA) and interferon α2a (IFN-α) (Cranmer et al., 2010; Guthrie et al., 1990; Sadek et al., 1990; Shin et al., 2016; Wollina et al., 2005). Unfortunately, these treatments have shown limited clinical

responses (Franco et al., 2013a), and patients with advanced and metastatic cSCCs are still challenging to treat and have a very poor prognosis. Therefore, it is necessary to identify the molecular, cellular and microenvironmental mechanisms underlying the regulation of cancer-cell proliferation and invasion at different stages of cSCC progression. This information will allow the design of new effective therapies for the treatment of patients with high-risk cSCCs.

Recently, several phase II trials based on inhibitors against the epidermal growth factor receptor (EGFR) such as cetuximab, gefitinib and erlotinib have been tested in patients with recurrent and/or metastatic cSCCs. The expression of EGFR is frequently detected in cSCCs and appears to be prognostically adverse, but the relevance of this signaling pathway is unclear (Cañueto et al., 2017; Maubec et al., 2005). In one of these trials, cetuximab was evaluated in 31 patients with unresectable or metastatic cSCCs that expressed EGFR and had not previously received chemotherapy, and yielded an objective response rate (ORR) of 28% and a disease control rate (DCR) of 69%. However, the disease progressed in 17%-19% of patients and the median progression-free survival (PFS) was shorter than 6 months (Maubec et al., 2011). In a phase II study with 40 patients with metastatic and recurrent cSCCs, gefitinib showed an ORR of 16% and a DCR of 51%. The median PFS was 3.8 months (William et al., 2017). Finally, in a phase II trial, erlotinib exhibited an ORR of 10%, a DCR of 72% and a median PFS of 4.7 months in patients with recurrent or metastatic cSCCs (Gold et al., 2018). All these clinical trials have revealed that the disease still progressed in a significant percentage of patients, making it necessary to investigate the mechanisms involved in resistance acquisition. In this line, a recent work from our laboratory has demonstrated that patient-derived xenografts (cSCC-PDXs) resistant to gefitinib and patients with cSCCs or head and neck SCCs (HNSCC) with short-term responses to cetuximab showed an activation of the fibroblast growth factor receptor (FGFR) signaling. The pharmacologic inhibition of this signaling overcame resistance to EGFR inhibitors (Bernat-Peguera et al., 2021). This study reveals that combinatorial EGFR- and FGFR-targeted therapies may be used to treat cSCCs and HNSCCs that are refractory to EGFR inhibitors, strengthening the response of this therapeutic strategy.

cSCCs present clinical and molecular features of tumors responsive to immunotherapy, as they contain a high tumor mutation burden (TMB) and the disease risk is strongly associated with immunosuppression (Chalmers et al., 2017; Pickering et al., 2014). In this sense, several immune checkpoint-blocking PD-1 antibodies have been tested in trials (Wessely et al., 2020). In these trials, response assessment is measured according to the Response Evaluation Criteria in Solid Tumors (RECIST) (Eisenhauer et al., 2009). Favorable responses include complete response (CR), which is the complete disappearance of all target lesions, and partial response (PR), where there is at least a 30% decrease in the diameter of the target lesion. Progressive disease (PD) is when there is a 20% increase in the diameter of the target lesion or the appearance of new lesions, and stable disease (SD) is when there is insufficient shrinkage or growth in target lesions to qualify for a PR or PD

(Eisenhauer et al., 2009). Midgen et al. presented the results of a phase I (NCT02383212) and phase II trials (NCT02760498) evaluating cemiplimab, an anti-PD-1 blockade antibody, for the treatment of advanced and metastatic cSCCs. In the phase I study, among the 26 patients, 50% experienced a PR, 23% had SD, and 12% had PD, resulting in an ORR of 50%. Among the 13 patients that had a response, 54% of them had a response exceeding 6 months (Ahmed et al., 2019; Migden et al., 2018). The phase II study includes 59 patients, and the ORR was 47.5%. In particular, 6.8% patients had CR, 40.7% had PR, 15% had SD, and 19% had PD. The duration of response exceeded 6 months in 57% of cases (Migden et al., 2018). The most common adverse events (AEs) for these patients included diarrhea (27.1%), fatigue (23.7%), and nausea (16.9%) (Migden et al., 2018). These studies lead to cemiplimab's approval by the U.S. Food and Drug Administration (FDA) and the European Medicines Agency (EMA) for the treatment of advanced and metastatic cSCCs in 2018.

The FDA has also approved pembrolizumab, an anti-PD-1 blockade antibody, for the treatment of advanced and metastatic cSCCs in 2020. Its final approval was supported by the KEYNOTE-629 trial (NCT03284424) (Grob et al., 2020). In this trial, Grob et al. presented that, of 105 patients with recurrent or metastatic cSCCs, 3.8% of them had CR, 30.5% had PR, 29.5% had SD with 18.1% lasting for at least 12 weeks, and 26.7% had PD (Grob et al., 2020). Thus, ORR was 34.3% and DCR was 52.4%. AEs such as pruritus, asthenia and fatigue, among others, occurred in 66.7% of patients. In total, 12.4% of patients discontinued the therapy due to AEs (Grob et al., 2020). Taken together, among patients with advanced or metastatic cSCCs, cemiplimab and pembrolizumab induced a favorable response in approximately 35-50% of patients, but still a significant percentage of patients showed disease stabilization (15-30%) or progression (12-27%). This situation makes it necessary to search for alternative therapies for advanced and metastatic cSCCs, investigating the mechanisms involved in immunotherapy resistance.

2. CELLULAR PLASTICITY IN CANCER

Over recent decades, several studies have described the existence of a great intertumoral and intratumoral heterogeneity, which has a strong impact on the response of cancer therapies (McGranahan and Swanton, 2017; Vitale et al., 2021). Intertumoral heterogeneity encompasses the genetic and phenotypic variability observed among patients with particular tumor types, whereas intratumoral heterogeneity involves the phenotypic and functional heterogeneity that arises among cancer cells within the same tumor (Bedard et al., 2013; da Silva-Diz et al., 2018). Intratumoral heterogeneity can be originated by genetic variability, differences in gene regulation, transitions between cellular states or environmental alterations (Junttila and de Sauvage, 2013; Meacham and Morrison, 2013). The origins of intratumoral heterogeneity have been extensively debated and several models have been postulated to describe the mechanisms that give rise to cellular diversity: the clonal evolution model, the cancer stem cell (CSC) model, and the cell plasticity model.

2.1- Models of intratumoral heterogeneity

The clonal evolution model, initially introduced by Dr. Nowell in 1976, proposes that intrinsic differences among cancer cells are caused by stochastic genetic and/or epigenetic alterations in individual cells (Baylin and Jones, 2011; Nowell, 1976). Subsequently, this genomic instability would allow the selection of better-adapted clones and the eradication of disadvantaged clones by the immune system or antitumoral treatments (Figure 2a). In addition, it proposes that cells of different dominant populations would possess similar tumorigenic potential and would be responsible for driving tumor progression (Figure 2a). Finally, it was pointed out that each patient requires a specific individual therapy, but this could be frustrated by the emergence of a genetically different subclone that could be resistant to the treatment (Nowell, 1976).

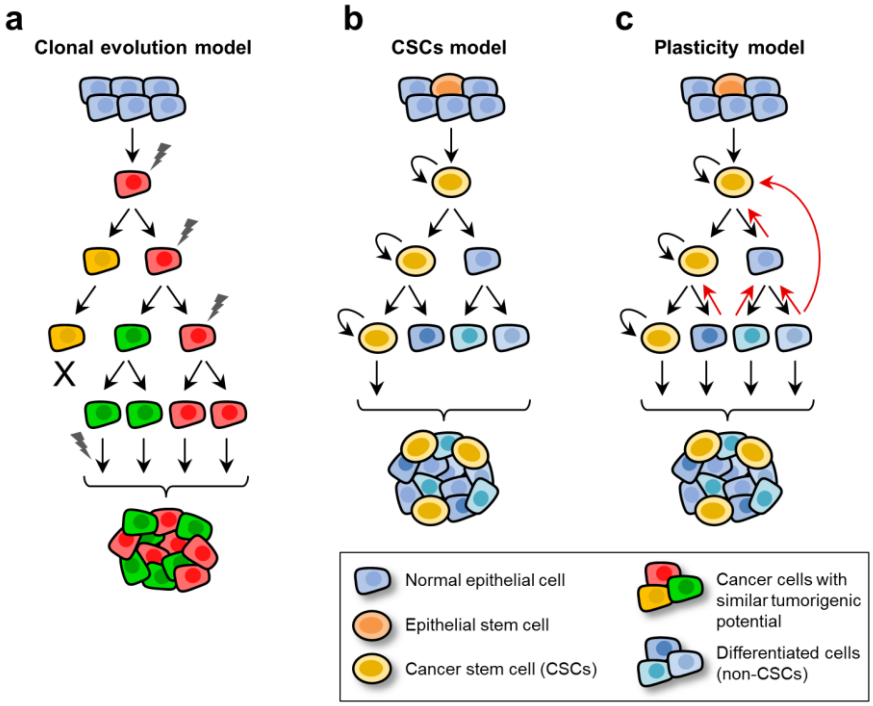

Figure 2. Proposed models to describe the mechanisms that give rise to intratumoral heterogeneity (adapted from Marjanovic et al., 2013)**. a.** The clonal evolution model considers that each cancer cell has a similar tumorigenic potential. **b.** The CSC model assumes that CSCs are the source of intratumoral heterogeneity because of their capacity to self-renew or differentiate into non-CSCs. **c.** The cell plasticity model proposes an equilibrium of bidirectional conversions between CSCs and non-CSCs.

The CSC model postulates that only a subset of undifferentiated cancer cells, the CSCs, have the ability to self-renew and the potential to initiate and maintain long-term tumor growth (Clevers, 2011; Lapouge et al., 2012; Malanchi et al., 2008; Visvader, 2011) (Figure 2b). The rest of the tumor would consist of cancer cells with a high degree of differentiation and limited proliferative and tumorigenic potential (non-CSCs) (Pattabiraman and Weinberg, 2014). In this sense, tumors follow a hierarchical organization where CSCs are responsible for giving rise to the bulk of non-CSCs, thus

contributing to intratumoral heterogeneity (Figure 2b). Skin SCC CSCs have been identified and characterized by the expression of α6-integrin and CD34, which are markers of hair follicle SCs (Arwert et al., 2012; Blanpain et al., 2004; Trempus et al., 2007). $CD34^+$ CSCs are able to regenerate all cell types of parental SCCs after serial transplantation into immunodeficient mice, driving long-term tumor growth and disease progression (Lapouge et al., 2012; Malanchi et al., 2008). In addition, Sox2, a transcription factor expressed in various types of embryonic and adult SCs, is induced in mouse and human SCC CSCs, promoting CSC self-renewal and tumor growth (Boumahdi et al., 2014; Siegle et al., 2014). In addition, it has been described that CSCs have several clinical consequences, being responsible for tumor growth, therapy resistance, tumor recurrence and metastasis development (Chen et al., 2012; Clevers, 2011; Mani et al., 2008; Zhang et al., 2014).

Recently, cellular plasticity has been proposed as an important mechanism that contributes to intratumoral heterogeneity (da Silva-Diz et al., 2018) (Figure 2c). Several studies have provided evidences that some cancer cells are plastic and capable of undergoing dynamic transitions between non-CSC and CSC states in response to appropriate stimuli (Batlle and Clevers, 2017; Gupta et al., 2011; Meacham and Morrison, 2013). This cellular plasticity results from different mechanisms, such as genetic and epigenetic alterations, microenvironmental-derived signals and/or treatment-imposed selective pressures, thereby contributing to tumor heterogeneity, immune evasion and therapy resistance (Dagogo-Jack and Shaw, 2018; McGranahan and Swanton, 2017; da Silva-Diz et al., 2018; Vitale et al., 2021; Yuan et al., 2019). In addition, this plastic behavior has been associated with the induction of the epithelial-to-mesenchymal transition (EMT) program, which results into the transition from epithelial to mesenchymal phenotypes through plastic intermediate states (Nieto et al., 2016) (see section 2.2 and 2.3). A better understanding of the mechanisms that contribute to cellular plasticity may open new avenues for the development of novel therapeutic strategies.

2.2- The EMT program and CSC state in tumor progression and metastasis

The EMT program is a dynamic process that is essential for embryonic development and wound healing (Nieto et al., 2016; Polyak and Weinberg, 2009). Moreover, the EMT program is activated during cancer pathogenesis and tissue fibrosis (Thiery, 2002; Thiery et al., 2009). This process involves a complex transcriptional program mediated by several transcription factors (TFs), such as Snail, Snai2, Twist1, Zeb1 and Zeb2, which leads to the repression of genes that are necessary for the maintenance of the epithelial state, the loss of intercellular connections and apical-basal polarity, the reorganization and expression of cytoskeletal proteins, and the production of extracellular matrix (ECM)-degrading enzymes (Comijn et al., 2001; Savagner et al., 1997; Yang et al., 2004, 2020) (Figure 3). The activation of the EMT program in epithelial cancer cells endows them with a mesenchymal-like phenotype that facilitates migration, invasion, and metastasis (Brabletz, 2012; Chaffer et al., 2016; Lamouille et al., 2014; Nieto et al., 2016; Ye and Weinberg, 2015).

The EMT program can be regulated by epigenetic modifications, transcriptional control and specific signaling pathways. EMT-TFs act as transcriptional repressors of epithelial genes, including E-cadherin and claudins (Batlle et al., 2000; Cano et al., 2000), and induce the expression of genes associated with the mesenchymal state as fibronectin, Vimentin, and N-cadherin (Lamouille et al., 2014; Peinado et al., 2007) (Figure 3). In addition, p53, Grhl2, Ovol2 and miRNAs play a significant role by inhibiting the EMT program (Craene and Berx, 2013) (Figure 3). These EMT regulators are integrated into a network of complex loops that lead to a dynamic activation of EMT, such as the mutually inhibitory loops miR-34/SNAI1 and miR-200/ZEB1. Epithelial cancer cells express high levels of miR-200 and miR-34 and, when they are activated by p53, this leads to the inhibition of SNAI1 and ZEB1 expression (Burk et al., 2008; Park et al., 2008). EMT-inducing signals such as transforming growth factor β (TGF-β), epidermal growth factor (EGF), and hepatocyte growth factor (HGF) induce SNAI1 and ZEB1 expression, which in turn reduce the expression of miR-34 and miR-200 in mesenchymal cancer cells (Craene and Berx, 2013). OVOL2 and GRHL2 participate in this regulatory network by protecting the epithelial phenotype (Qi et al., 2018), and PRRX1 cooperates with TWIST1 to induce the mesenchymal state (Ocaña et al., 2012) (Figure 3). Each of these EMT-TFs have a differential potential to suppress the epithelial phenotype or to induce the mesenchymal state. Indeed, PRRX1 and TWIST1 are more potent as mesenchymal inducers than epithelial repressors, while SNAI1 and ZEB1 strongly repress the epithelial phenotype and weakly induce the mesenchymal phenotype (Nieto et al., 2016). In addition to transcriptional and miRNA regulation, post-translational modifications and epigenetic changes also contribute to the EMT phenotype (Craene and Berx, 2013). For instance, DNA methylation and histone repressive marks are associated with the mesenchymal phenotype, whereas poised chromatin allows a more plastic intermediate EMT phenotype (Tam and Weinberg, 2013). EMT induces the hypermethylation of CpG islands in the E-cadherin promoter of various cancer cell lines, which is associated with the recruitment of DNMT1 to these sites by interacting with SNAIL and ZEB1/2 (Fukagawa et al., 2015; Lim et al., 2008). The expression of TWIST1/2 in colon cancer cells (Galván et al., 2014) and of ZEB2 in pancreatic and liver cancer cells is also regulated by the DNA methylation of their promoters (Acun et al., 2011; Li et al., 2010). In addition, the chromatin landscape is altered during the EMT program. Indeed, the chromatin of epithelial genes shifts from an active state that is associated with histone H3 acetylation (H3Kac) and active methylation marks (H3K4me3), to an intermediate bivalent state identified by the coexistence of the repressive H3K27me3 and the active H3K4me3 marks, finally being repressed by H3K27me3 and H3K9me3 marks. Cancer cells use this bivalent chromatin state to modulate the expression of differentiation, stemness or EMT genes. This poised state may underpin the phenotypic plasticity of cancer cells, which enables them to respond rapidly to EMT-inducing signals (Ke et al., 2010). Likewise, Blanpain's group demonstrated that the chromatin and transcriptional state of the cancer cell-of-origin prime skin SCs to generate mesenchymal tumors with an increased metastatic potential (Latil et al., 2017). In this sense, SCCs

derived from the interfollicular epidermis were mostly WD-SCCs, containing epithelial cancer cells, whereas those derived from hair follicle SCs were mixed tumors (MD-SCCs), containing epithelial $EpCAM^+$ and mesenchymal $EpCAM^-$ cancer cells. This implies that hair follicle SCs have a greater plasticity for switching from an epithelial to a mesenchymal phenotype (Latil et al., 2017).

Several studies have described that the expression of EMT-TFs leads to the acquisition of SCs features in cancer cells, and that CSCs exhibit an induced EMT program (Gupta et al., 2009; Morel et al., 2008; Puisieux et al., 2014). The expression of Snail or Twist in breast epithelial cells induces the EMT program and the acquisition of SCs features (Mani et al., 2008). Zeb1 expression maintains the stemness state of pancreatic cancer cells, repressing the expression of the miRNAs that negatively regulate this process (Wellner et al., 2009). Moreover, Snail expression induces an expansion of colorectal CSCs through symmetrical cell divisions, which allowed to associate EMT program with an increase in CSCs (Hwang et al., 2014). In agreement with this work, our laboratory demonstrated that there is an expansion of the CSC population (α6-$integrin^+/CD34^+$ cells) concomitant with a robust induction of the EMT program during SCC progression (Silva-Diz et al., 2016). In addition, the regulatory mechanisms controlling CSC proliferation, survival and dissemination changed. Indeed, whereas β-catenin and EGFR signaling controlled CSC proliferation and survival in WD-SCCs, these pathways were strongly downregulated in CSCs of advanced PD/S-SCCs. Autocrine FGFR1c and PDGFRα signaling were specifically induced in CSCs of advanced PD/S-SCCs, being responsible for promoting an aggressive growth and metastasis development, respectively (Silva-Diz et al., 2016). These findings suggest that therapeutic strategies should be adapted to the cancer cell features that can switch at various stages of progression.

Despite multiple evidences have reported the relationship between stemness and the EMT program, other studies indicate that they could not be directly coupled. Indeed, the mesenchymal-to-epithelial transition (MET) program is necessary for cancer cells to seed metastases, which involves the repression of EMT-TFs and the maintenance of tumor-initiating ability (Ocaña et al., 2012; Tsai et al., 2012). In addition, CSC features and EMT induction can depend on different doses of EMT-TFs, as low levels of Twist are necessary to induce stemness in mouse skin SCC cells and tumor development, whereas high levels of Twist are related to EMT induction (Beck et al., 2015). In contrast, the constitutive expression of Snail in prostate and bladder cancer induced EMT and repressed stemness (Celià-Terrassa et al., 2012), indicating that both processes were decoupled.

2.3- Partial EMT, CSC state and metastasis development

Recent works have shown that EMT does not represent a linear process, understood as the transformation of cancer cells from an epithelial to a mesenchymal-like state (Yuan et al., 2019). Rather, cancer cells oscillate between these two states through a spectrum of intermediate/hybrid phenotypes that present different competence to invade, disseminate and seed metastatic deposits

(Dongre and Weinberg, 2019; Jolly et al., 2016) (Figure 3). This plasticity has led to the recognition of cells having a partial EMT state, where cells can retain epithelial features together with newly acquired mesenchymal ones (Figure 3). These characteristics provide cancer cells with an increased adaptability to respond to a variety of external cues and physiological stresses (Chaffer et al., 2016; Santamaria et al., 2017). These hybrid epithelial-mesenchymal cancer cells have been identified in breast (Yu et al., 2013), ovarian (Strauss et al., 2009), HNSCC (Puram et al., 2017), pancreatic and prostate cancers (Rhim et al., 2012; Ruscetti et al., 2015), and its presence has been correlated with poor patient survival and resistance to chemotherapy (Grosse-Wilde et al., 2015; Smith and Bhowmick, 2016; Yamashita et al., 2018). However, still unresolved is whether these intermediate states are metastable, suggesting an intermediate step in the transition of cancer cells, or whether partial EMT represents a stable state of its own (Jolly et al., 2016).

The co-expression of epithelial and mesenchymal genes in cancer cells has been associated with an increased stemness capacity and tumorigenic potential (Grosse-Wilde et al., 2015; Ruscetti et al., 2015; Strauss et al., 2009). Partial EMT states also facilitate the migration of cancer cells (Aiello et al., 2018; Armstrong et al., 2011), leading to the formation of metastatic circulating cell clusters (Aceto et al., 2014; Maddipati and Stanger, 2015; Massagué and Ganesh, 2021). In addition, partial EMT states confer cancer cells with a higher degree of metastatic competence as compared with cancer cells that have advanced through an entire EMT program (Schmidt et al., 2015; Tran et al., 2014; Tsai et al., 2012). In this sense, the initial acquisition of mesenchymal traits can enable cancer cells with disseminating features and homing to distant tissues, while the conservation of epithelial features might facilitate the reprogramming to the epithelial state and the outgrowth of metastatic colonies (Gunasinghe et al., 2012; Ocaña et al., 2012). Considering the enhanced tumorigenic potential and the resistance to conventional therapeutic agents of hybrid and mesenchymal cancer cells, several studies have proposed to force these populations toward a more differentiated epithelial state. Preliminary findings suggested that the activation of the protein kinase A (PKA) induces a MET process in mesenchymal mammary cells, which was accompanied by the sensitization of these cancer cells to conventional chemotherapies (Pattabiraman et al., 2016). Although attractive, this strategy is not exempt from controversy. Given the requirement for reversion of the EMT program at the last step of the metastatic cascade (Ocaña et al., 2012; Tsai et al., 2012), therapies that promote the switch from the mesenchymal to the epithelial phenotype may favor the formation of secondary tumors from already disseminated cancer cells.

The progression of cancer cells along the EMT spectrum can generate a strong phenotypic heterogeneity within tumors (Figure 3). Multiple epithelial-mesenchymal cell populations have been reported in skin SCCs and mammary primary tumors. In particular, the screening of the cell surface markers CD61, CD106, and CD51 identified several cancer cell populations that were associated with different EMT phenotypes (Pastushenko et al., 2018). Cancer cells with a hybrid phenotype

were more efficient in reaching the circulation, colonizing and forming lung metastases. In addition, cells exhibiting this intermediate EMT state had a greater plasticity, since they gave rise to the other mesenchymal cancer cell phenotypes when engrafted in mice (Pastushenko et al., 2018). A recent work have revealed that the loss of function of FAT1, which encodes a protocadherin commonly expressed in epithelial tissues (Morris et al., 2013), promotes tumor stemness and metastasis through the induction of a hybrid EMT state in mouse and human SCCs (Pastushenko et al., 2021). This study demonstrated that the loss of function of FAT1 promotes ZEB1 expression, which stimulates the acquisition of a mesenchymal state. At the same time, FAT1 loss of function inactivates EZH2 and promotes SOX2 expression, which sustains the epithelial state. All these studies have indicated that cancer cells can transit from a stable epithelial phenotype to a partial EMT, and finally to a stable mesenchymal phenotype. This transition can depend on the tumor type and the stage of progression of the particular tumor. In fact, while partial EMT induction might be regulated by tumor microenvironment (TME) signals at earlier stages of progression, cancer cells may become more independent of external signals to maintain the mesenchymal phenotype, relying on a stable configuration of the chromatin or the acquisition of autocrine signaling loops (da Silva-Diz et al., 2018) (Figure 3).

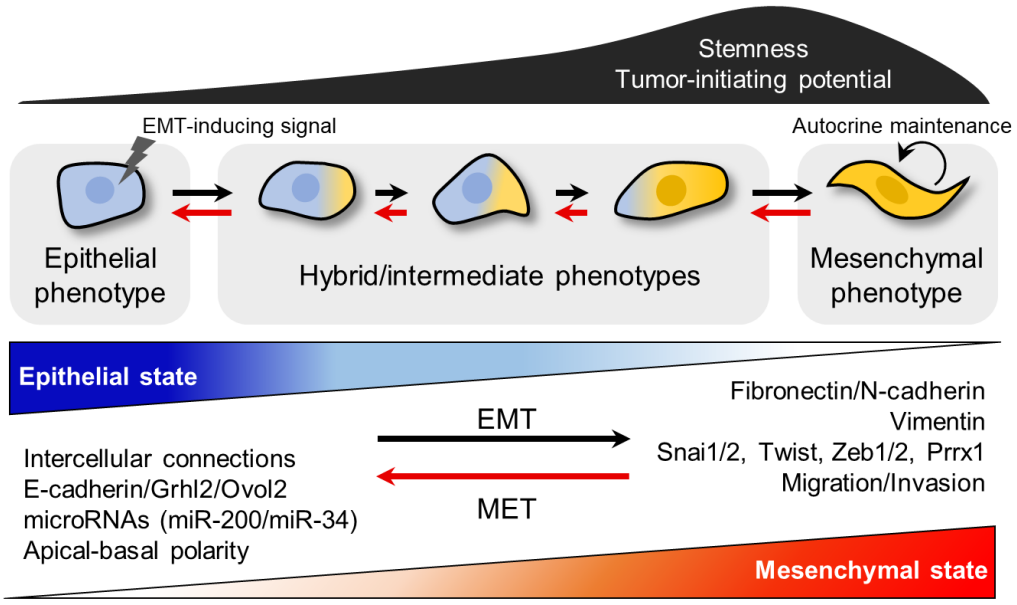

Figure 3. Spectrum of EMT phenotypes in cancer (adapted from Chaffer et al., 2016)**.** Some epithelial cancer cells can respond to EMT-inducing signals (hypoxia, inflammatory signals, EMT-TFs, growth factors and cytokines), leading to the disruption of the pathways that maintained the epithelial state and initiating a transition toward the mesenchymal state. Once cancer cells have undergone a complete EMT state, autocrine signaling can maintain the mesenchymal phenotype in the absence of EMT-inducing signals. During this transition, cancer cells undergo hybrid/intermediate partial EMT states, which are reversible, transient and have different competence to invade, disseminate and seed metastases. These hybrid states are also associated with the acquisition of stemness and tumor-initiating potential features.

3. TUMOR MICROENVIRONMENT AND THERAPEUTIC STRATEGIES

The TME is composed of several immune cells, as T and B lymphocytes, natural killer (NK) cells, tumor-associated macrophages (TAMs) and neutrophils (TANs), myeloid-derived suppressor cells (MDSCs), and dendritic cells (DCs); stromal cells such as cancer-associated fibroblasts (CAFs), pericytes, and mesenchymal stromal cells; the ECM and other secreted molecules, such as growth factors, cytokines, chemokines, and extracellular vesicles (EV); and the blood and lymphatic vascular networks (Tlsty and Coussens, 2006). All these components are in communication with each other and with the cancer cells, forming the complex environment in which a tumor develops (Bejarano et al., 2021). It is well known that the immune system identifies and eliminates transformed malignant cells through the activation of innate and adaptive immune responses. Cytotoxic T lymphocytes (CTLs) and NK cells are the immune cell populations responsible for immunosurveillance and for eliminating target cells. Cancer cells can be identified by CTLs by the expression of mutated or altered antigens displayed by the major histocompatibility complex (MHC) proteins (Schumacher and Schreiber, 2015). However, cancer cells with defects in antigen presentation can escape T-cell immune control. In these cases, NK cells can identify and target cancer cells lacking MHC expression. Despite this, cancer cells are able to evade the host's immune response through a process called immune evasion (Hanahan and Weinberg, 2011). Tumors achieve this by creating an immunosuppressive network enriched in specific immune cell populations or by hijacking the so-called immune checkpoint (IC) pathways (Lorenzo-Sanz and Muñoz, 2019). TAMs, MDSCs and regulatory T (Treg) cells release soluble factors that reduce the effector functions of cytotoxic cells. In addition, cancer cells and several immune populations can induce the expression of IC ligands that, when interacting with CTL and NK coinhibitory receptors, contribute to their dysfunctional state (Kim et al., 2016; Pardoll, 2012). Tumors with a strong immunosuppressive TME are associated with impaired immune cytotoxicity, are more aggressive, and have a poor prognosis (Wang et al., 2017). Moreover, there is growing evidence that the TME can change in response to cancer cell-derived signals to support tumor growth, invasion and progression (Junttila and de Sauvage, 2013; Quail and Joyce, 2013). In the following sections, we will examine the phenotypic and functional features of cytotoxic effector cells (CTLs and NK cells) and immunosuppressive populations (Tregs, TAMs and MDSCs), the mechanisms employed by immunosuppressive cells to suppress antitumor responses, as well as therapeutic strategies to target the TME.

3.1- $CD8^+$ cytotoxic T lymphocytes, $CD4^+$ T-helper cells and regulatory T cells

$CD8^+$ CTLs are one of the major antitumoral effector cells within the TME and detect antigenic peptide fragments presented by the MHC class I or the human leukocyte antigen (HLA) molecules via a cross-presentation mechanism (Chen and Flies, 2013). To be activated, naïve $CD8^+$ T cells

need to interact with antigen-presenting cells (APCs), specifically with DCs, in a secondary lymphoid organ. Its full activation requires the interaction of the costimulatory receptor CD28 with its ligands CD80 (B7-1) and CD86 (B7-2) expressed by APCs (Appay et al., 2008) (Figure 4). Fully activated $CD8^+$ T cells start proliferating and becoming cytotoxically activated, whereupon they acquire the ability to migrate to peripheral tissues (Figure 4). When CTLs recognize their target cells, the interaction between the T-cell receptor (TCR) and the antigen displayed by the MHC class I/HLA complex produces a stabilization complex, after which lytic granules are secreted (Nikolich-Žugich et al., 2004) (Figure 4). Perforin forms pores in the target cell membrane, which allows granzymes A and B, cathepsin C and granulysin to enter the cytosol and induce apoptosis (Basu et al., 2016; Gordy and He, 2012) (Figure 4). In addition, the interaction between Fas ligand (FasL), which is expressed on $CD8^+$ T cells, and Fas receptors on target cells activates death domains (FADD), which, in turn, activate caspases and endonucleases that lead to DNA fragmentation (Fu et al., 2016). CTLs also secrete interferon (IFN)-γ and tumor necrosis (TNF)-α, which stimulate a pro-inflammatory immune response (Voskoboinik et al., 2015) (Figure 4).

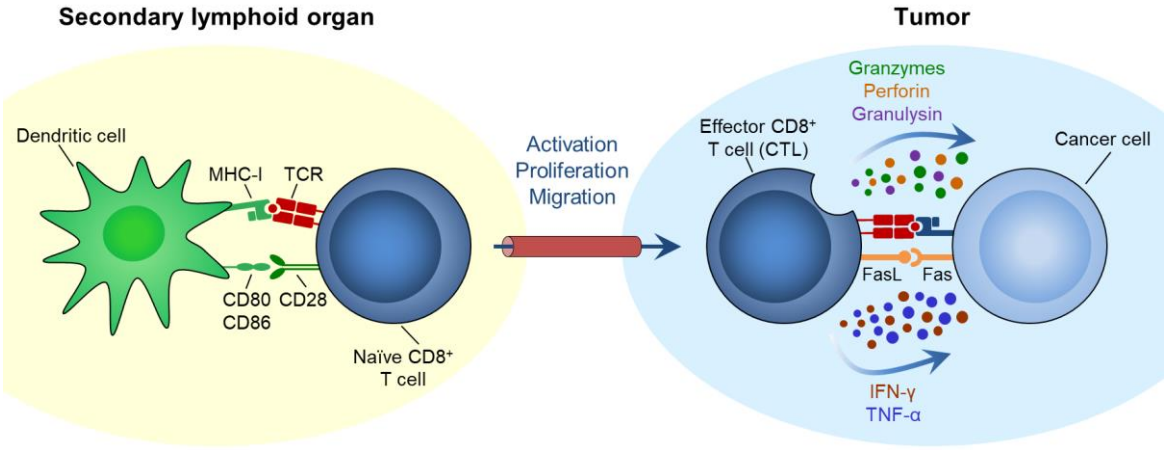

Figure 4. CTL-mediated cytotoxicity (adapted from Drijvers et al., 2020)**.** Naïve $CD8^+$ T cells recognize antigens presented by antigen-presenting cells, such as dendritic cells, in a secondary lymphoid organ. T cells then become activated, proliferate and migrate to the tumor. T cells can mediate an effective antitumoral response through direct cytolytic activity mediated by perforin, granzymes and granulysin, the secretion of cytokines like IFN-γ and TNF-α, and the induction of apoptosis via FasL-Fas interaction.

$CD4^+$ T-helper (Th) cells recognize antigenic peptides presented by MHC class II molecules and coordinate effective adaptive immune responses by producing cytokines (van den Broek et al., 2018). $CD4^+$ Th cells are classed into two main subsets, T-helper 1 (Th1) and T-helper 2 (Th2) cells. $CD4^+$ Th1 cells secrete pro-inflammatory molecules such as IFN-γ, TNF-α and IL-2 (Romagnani, 1997). These cytokines collaborate with the cytotoxic functions of $CD8^+$ T cells and NK cells and can induce the upregulation of antigen processing and the expression of MHC class I and II molecules in APCs (Uzhachenko and Shanker, 2019). $CD4^+$ Th1 cells also promote the activation

of M1-like macrophage activity (DeNardo and Coussens, 2007). In contrast, $CD4^+$ Th2 cells express IL-4, IL-5, IL-6, IL-10 and IL-13, which induce the loss of T-cell cytotoxicity, enhance the humoral immune response (B-lymphocyte functions) and regulate the tumor-promoting activities of M2-like macrophages (DeNardo et al., 2009).

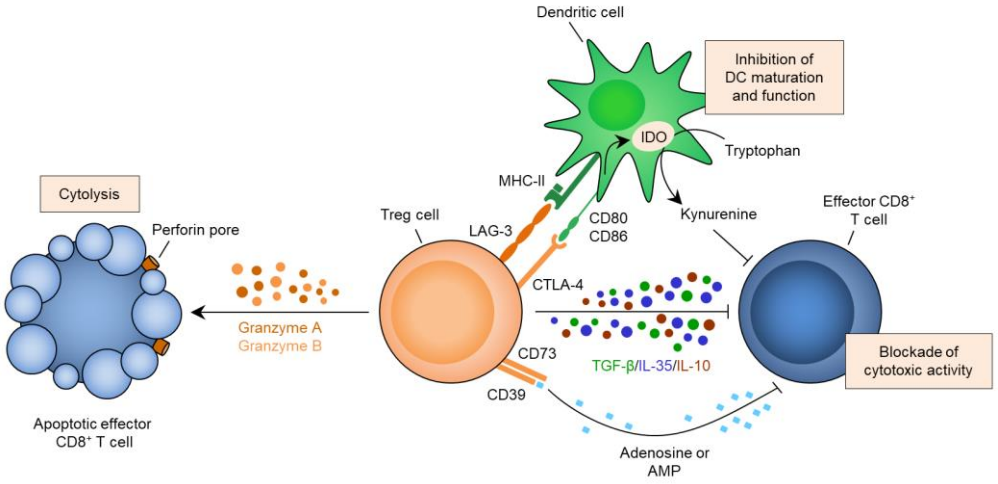

Figure 5. Immunosuppressive Treg mechanisms (adapted from Romano et al., 2019; Vignali et al., 2008)**.** Treg cells produce anti-inflammatory cytokines (TGF-β, IL-35 and IL-10) that block cytotoxic T-cell activity, and can induce T-cell apoptosis in a granzyme- and perforin-dependent manner (cytolysis). Treg cells can also inhibit the maturation and function of DCs, through the interaction between CD80/CD86 and CTLA-4, which induces DCs to express the immunosuppressive molecule IDO, or through the binding of LAG-3 with MHC class II molecules. Finally, Treg cells express CD39 and CD73, which induce metabolic alterations via the generation of adenosine and AMP, molecules that suppress cytotoxic T-cell activity.

Within the general $CD4^+$ T cell population, Treg cells are characterized by the expression of markers such as CD25 (also known as IL-2Rα) and forkhead box P3 (FoxP3), which plays an important role in Treg-cell development and function (Sakaguchi et al., 2010). Under physiological conditions, Treg cells regulate the activation of T and B lymphocytes and maintain the homeostasis of CTLs (Gasteiger et al., 2013). However, it has been described that Treg cells facilitate tumor progression by interfering with the cytotoxic activity of T and NK cells and by suppressing tumor antigen presentation (von Boehmer and Daniel, 2013; Romano et al., 2019; Vignali et al., 2008). In this regard, Treg cells secrete immunosuppressive cytokines (IL-10, IL-35, and TGF-β) that block the cytotoxic activity of T and NK cells (Nikolova et al., 2009; Schmidt et al., 2012), and can induce their apoptosis in a granzyme- and perforin-dependent manner (Cao et al., 2007) (Figure 5). Treg cells also modulate the maturation and function of DCs, which are required for the activation of effector T cells. This process involves the interaction between CD80/CD86 expressed by DCs and the co-stimulatory molecule CTLA-4, which is constitutively expressed by Treg cells (Read et al., 2000) (Figure 5). This interaction conditions DCs to express indoleamine 2,3-dioxygenase (IDO), a molecule that induces the production of pro-apoptotic metabolites such as kynurenine from the

tryptophan catabolism, resulting in the suppression of effector T cells (Figure 5). Other studies have also demonstrated that the expression of LAG-3, a CD4 homologue that binds with high affinity to MHC class II molecules expressed by DCs, suppresses DC maturation and their immunostimulatory capacity (Huang et al., 2004; Liang et al., 2008) (Figure 5). In addition, Treg cells express CD39 and CD73, which induce metabolic alterations via the generation of adenosine and AMP, molecules that suppress cytotoxic T and/or NK cell activities (Bopp et al., 2007; Deaglio et al., 2007) (Figure 5). Finally, Treg cells can sequester IL-2 through the high expression of its receptor CD25 (IL-2Rα), which is a interleukin required for T and NK cell proliferation (Romano et al., 2019; Sojka et al., 2008). Given all these immunosuppressive Treg functions, their increased presence in tumors is often associated with poor patient prognosis (Fridman et al., 2017), as in gastric, esophageal, pancreatic, liver, and breast carcinomas (Bates et al., 2006; Fridman et al., 2017; Fu et al., 2007; Hiraoka et al., 2006; Kobayashi et al., 2007; Kono et al., 2006).

3.2-Natural killer (NK) cells

NK cells are important effector cells of the innate immune system and play critical roles in antitumor host defense (Bald et al., 2020; Chiossone et al., 2018; Muntasell et al., 2017; Vivier et al., 2008). NK cells can modulate the function of DCs, macrophages and T lymphocytes via the production of cytokines, underlying a complex interplay between the innate and the adaptive immunity (Gasteiger and Rudensky, 2014; Schuster et al., 2016). NK cells are defined as $CD3^{-}CD56^{+}$ cells in humans and $CD3^{-}NK1.1^{+}$ cells in mice. Furthermore, cytotoxic human NK cells are defined as $CD56^{dim}CD16^{+}$ cells, are mostly locate in peripheral blood and express high levels of perforin and granzyme B (Moretta et al., 2008). In contrast, immunoregulatory $CD56^{bright}CD16^{-/low}$ cells are mostly found in secondary lymphoid organs and have a great ability to release cytokines such as IFN-γ, TNF-α and IL-10, among others (Baginska et al., 2013; Stiff et al., 2018; Viel et al., 2016). In contrast to T lymphocytes, NK cells use multiple activating and inhibitory receptors to respond to alterations such as cellular stress, cellular transformation, and malignancy (Long et al., 2013). One of the most important mechanisms of NK cells is the identification and elimination of target cells lacking MHC class I expression through a process called 'missing self-recognition' (Figure 6b). The MHC class I inhibitory receptors include the killer immunoglobulin-like receptors (KIRs) in humans, the lectin-like Ly49 dimers in mice, and the lectin-like CD94-NKG2A heterodimers in both species (Parham, 2005; Vivier et al., 2012). Inhibitory KIR and Ly49 receptors recognize self-MHC-I molecules to ensure tolerance to healthy cells while allowing toxicity to cancer cells (Raulet et al., 2001) (Figure 6a). To evade adaptive immunity, cancer cells frequently downregulate classical MHC-I molecules, which renders them susceptible to NK-cell activity. In addition, CD94-NKG2A recognizes non-classical MHC-I molecules, such as HLA-E in humans and Q-1 in mice. But along with the activity of these inhibitory receptors, NK cells are also equipped with activating receptors, which recognize stress-induced ligands to promote the killing of cancer cells (Figure 6c). For instance, natural

cytotoxicity receptors (NCRs) such as NKp30, NKp46 and NKp44 (Barrow et al., 2019), NKG2D, CD16, and DNAX accessory molecule-1 (DNAM-1/CD226) (Martinet et al., 2015) contribute to NK-cell activation and function. Specifically, DNAM-1 promotes NK-cell activation and cytotoxicity upon binding its ligands CD155/PVR or CD112/Nectin 2 (Chan et al., 2014). When activated, NK cells secrete cytotoxic granules such as perforin and granzymes to permeabilize target cells (Moretta et al., 2008; Smyth et al., 1999; Trapani and Smyth, 2002), or induce target cell apoptosis by releasing IFN-γ, TNF-α, FasL and TRAIL (Arase et al., 1995; Kayagaki et al., 1999; Wajant et al., 2003).

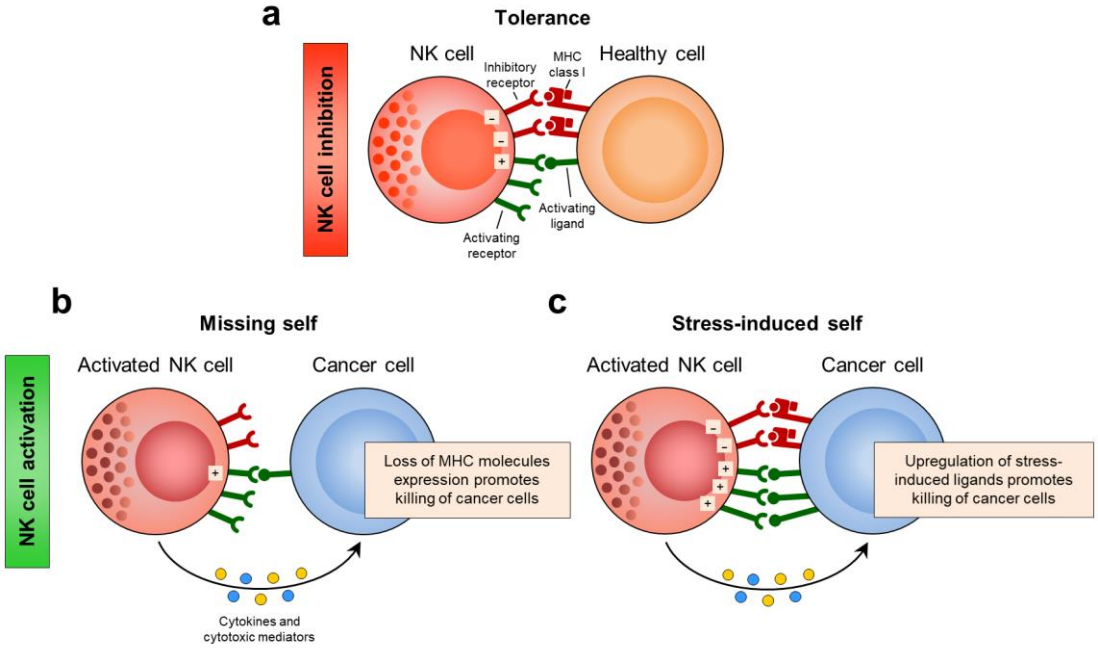

Figure 6. Recognition of cancer cells by NK cells (adapted from Vivier et al., 2012)**. a.** NK cells are tolerant to healthy cells, when the activating signals are suppressed by the engagement of inhibitory receptors. **b.** Cancer cells can lose the expression of MHC class I molecules, which render them susceptible to NK cells through a process known as 'missing-self' activation. **c.** NK cells can be activated by the upregulation of stress-induced ligands, thereby overcoming the inhibitory signals delivered by MHC class I molecules. In both conditions, NK-cell activation leads to cancer-cell elimination through the production of cytotoxic granules and/or pro-inflammatory cytokines.

3.3-T and NK cell exhaustion

CTL and NK-cell activities are tightly regulated to preserve antigenic self-tolerance and prevent autoimmunity. Autoreactive clones are eliminated in the thymus by a process known as central tolerance (Xing and Hogquist, 2012). Also, a peripheral regulation of the cytotoxic response is essential to avoid inappropriate responses to self-antigens. To achieve this, activated CTLs and NK cells upregulate the expression of multiple coinhibitory receptors, known as immune checkpoint (IC) receptors, which ensures a precise regulation of their effector functions (Kim et al., 2016)

(Figure 7). However, tumors co-opt certain IC pathways as a major mechanism of immune resistance (Bi and Tian, 2017; Wherry and Kurachi, 2015). In this regard, tumor-infiltrating lymphocytes (TILs) and NK cells exhibit an enhanced co-expression of IC receptors (Schietinger and Greenberg, 2014), which leads to a state of dysfunction or exhaustion that is characterized by decreased effector functions. This situation induces an immunosuppressive state that promotes cancer-cell proliferation and survival (Joyce and Fearon, 2015; Vodnala et al., 2019; Wherry, 2011). In addition, the persistent exposure of $CD8^+$ T cells to tumor neoantigens can induce the sustained expression of IC molecules (Wherry and Kurachi, 2015). It has been reported that IC ligands are commonly overexpressed on cancer cells and immunosuppressive cells within the TME, thereby avoiding immunosurveillance and allowing tumor progression (Kim et al., 2016) (Figure 7).

Although several IC receptors have been described in the last years, in this Thesis we will focus on the cytotoxic T-lymphocyte-associated molecule 4 (CTLA-4), the programmed cell death protein 1 (PD-1), the lymphocyte activation gene 3 (LAG-3), the T cell immunoglobulin and mucin-containing molecule 3 (TIM-3), and the T cell immunoglobulin and ITIM domain (TIGIT). All these receptors play a key role in controlling CTL and NK cell effector functions. It has been reported that a high and sustained co-expression of IC inhibitory receptors is a hallmark of exhausted T and NK cells (Blackburn et al., 2009). These co-expression patterns are important, as the simultaneous blockade of multiple IC receptors results in synergistic reversal of T and NK cell exhaustion (Melero et al., 2015). In addition, the downregulated expression of certain co-stimulatory receptors, such as 4-1BB, CD28, CD40, OX40, ICOS, CD226/DNAM-1, B7-H3, and NKG2D, among others, are involved in T and NK cell exhaustion (Bi and Tian, 2017; Chen and Flies, 2013; Odorizzi and Wherry, 2012) (Figure 7). Finally, immunosuppressive cytokines such as IL-10, TGF-β, IFN-α/β and IL-6 also regulate T and NK cell activity.

CTLA-4 regulates the amplitude of the early stages of T-cell activation, ensuring tolerance of self-antigens in the lymph nodes. CTLA-4 has a high sequence similarity with the co-activator receptor CD28 and competes, with higher affinity, to bind CD80 and CD86 ligands (Figure 7). In this situation, CTLA-4 acts as a negative regulator of T-cell activation (Leach et al., 1996; Parry et al., 2005; Schneider et al., 2006). Blockade experiments have demonstrated that anti-CTLA-4 treatment enhances T-cell proliferation and stimulates the cytotoxic T-cell response against cancer cells (Pardoll, 2012; Schnell et al., 2020), and its concomitant blockade together with PD-1 further potentiates these effects in preclinical models (Curran et al., 2010). CTLA-4 is also expressed by Treg cells, and its signaling enhances their immunosuppressive functions (Peggs et al., 2009; Wing et al., 2008). The role of CTLA-4 in NK cells remains to be elucidated. However, the *in vivo* blockade of CTLA-4 might enhance NK-cell activity indirectly by inhibiting Treg immunosuppressive activity and enhancing Th1 pro-inflammatory functions (Khan et al., 2020).

In contrast to CTLA-4, the major role of PD-1 is to regulate T-cell activity within peripheral tissues in the latter stages of the immune response (Freeman et al., 2000; Nishimura et al., 1999; Schnell et al., 2020). PD-1 promotes inhibitory signals upon binding PD-L1 and PD-L2 ligands (Ishida et al., 1992a) (Figure 7). Notably, PD-L1 and PD-L2 expression is upregulated in many tumor types and is usually associated with poor patient outcome. High PD-1 levels, concomitantly with other ICs, are detected in TILs and associated with an exhausted phenotype (Ahmadzadeh et al., 2009; Pesce et al., 2017). In addition, PD-1^+ NK cells displayed poor antitumoral activity (Pesce et al., 2017). Similarly to CTLA-4, PD-1 signaling is highly expressed in Treg cells, where it enhances their proliferative and immunosuppressive functions (Francisco et al., 2009; Khan et al., 2020; Pardoll, 2012). It has been demonstrated that PD-1 signaling blockade decreases tumor growth and enhances T and NK antitumoral activity, and PD-1 blockade alongside other ICs has proven increased immune responses (Stecher et al., 2017).

LAG-3 is expressed by $CD8^+$ T cells and NK cells and regulates peripheral tolerance (Triebel et al., 1990). LAG-3 is structurally similar to CD4 and binds to MHC class II molecules, FGL-1, galectin-3 and LSECTin (Baixeras et al., 1992; Kouo et al., 2015; Wang et al., 2019b; Xu et al., 2014) (Figure 7). These ligands are expressed by cancer cells, macrophages and DCs, and participate in immune evasion mechanisms that reduce T and NK cell responses (Anderson et al., 2016). LAG-3 is also expressed by Treg cells and its blockade disrupts their suppressor functions (Camisaschi et al., 2010; Huang et al., 2004). In NK cells, it has been described that LAG-3 may be a negative regulator of pro-inflammatory cytokine production, rather than a modulator of NK-mediated cytotoxicity (Khan et al., 2020; Narayanan et al., 2020). LAG-3 is co-expressed with PD-1 in $CD8^+$ TILs of many mouse and human tumors (Huang et al., 2015a). For that reason, the combinatorial blockade of PD-1 and LAG-3 synergizes to enhance antitumoral activity and reduces tumor growth by enhancing $CD8^+$ TILs and decreasing Treg cells in several cancer types (Burova et al., 2019; Wierz et al., 2018).

TIM-3 acts as a coinhibitory receptor of T cells and is also expressed in Treg cells, NK cells, DCs and macrophages (Anderson, 2012). TIM-3 binds to Galectin-9, phosphatidyl serine (PtdSer), carcinoembryonic antigen cell adhesion molecule 1 (CEACAM-1) and high-mobility group protein 1 (HMGB1) (Chiba et al., 2012; Huang et al., 2015b; Zhu et al., 2005) (Figure 7). TIM-3 ligand expression is upregulated in APCs, endothelial cells, neutrophils and cancer cells, and has been linked to tumor progression. In this sense, TIM-3 blockade downregulates Th2 cell function and increases CTL proliferation and cytokine production (Anderson et al., 2016). Moreover, the combinatorial blockade of PD-1 and TIM-3 further improves T-cell antitumoral functions and reduces tumor growth more effectively (Sakuishi et al., 2010). TIM-3^+ Treg cells increase suppressor functions (Gautron et al., 2014). In NK cells, TIM-3 acts as a negative regulator of NK effector functions, and its expression has been associated with NK exhaustion in cancer (Khan et al., 2020). TIM-3 blockade reversed exhausted NK cells (Khan et al., 2020), and advanced MHC class I-

deficient tumors treated with IL-21 combined with anti-TIM-3 and anti-PD-1 resulted in decreased tumor progression through an enhanced NK-cell antitumoral immunity (Seo et al., 2018). Hence, TIM-3 blockade also boosts NK cytotoxic activity (Khan et al., 2020).

TIGIT is expressed on NK and T cells and acts as an inhibitory receptor by binding to its ligands PVR (CD155) and nectin-2 (CD112) (Yu et al., 2009) (Figure 7). These ligands are expressed in a variety of cancer and immune cells (Bottino et al., 2003). TIGIT signaling reduces NK cytotoxicity and cytokine release by counterbalancing DNAM-1 activation, while in T cells, TIGIT reduces T-cell proliferation and effector functions (Martinet et al., 2015; Sanchez-Correa et al., 2019). The blockade of TIGIT enhances antitumoral CTL responses and prompts tumor regression in a colorectal cancer model, and the dual blockade with PD-1 or TIM-3 has a synergistic action that increases the immune responses (Johnston et al., 2014). The dual blockade of PD-1 and TIGIT also enhances antitumoral responses and increases survival in a mouse glioblastoma model (Hung et al., 2018). Recently, it was demonstrated that TIGIT blockade elicits NK-mediated antitumoral immunity in tumor-bearing mouse models (Khan et al., 2020). TIGIT^{+} Treg cells have great suppressive capacities *in vitro* and selectively suppress the Th1 pro-inflammatory response *in vivo*. The conditional TIGIT KO in Treg cells reduces tumor growth in melanoma mouse model, proving that the TIGIT blockade effect is also mediated by Treg cells (Anderson et al., 2016).

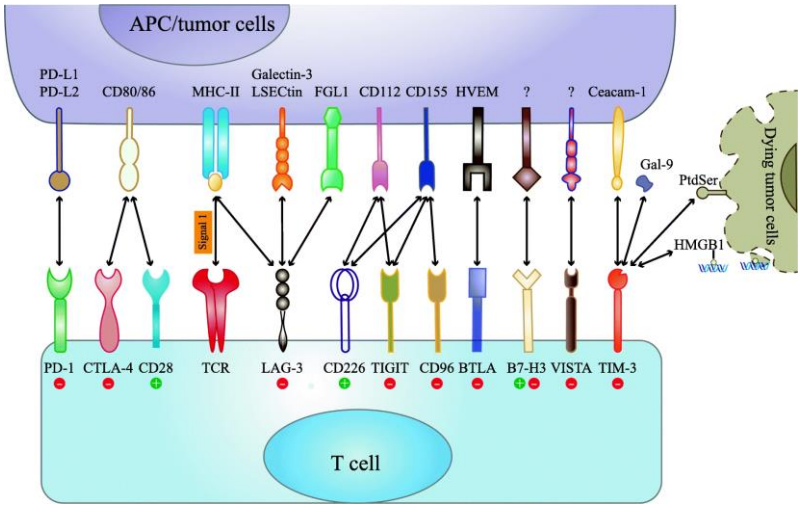

Figure 7. Multiple co-stimulatory and inhibitory interactions regulate T cell responses (Qin et al., 2019)**.** Scheme of several IC receptors expressed on T cells that bound with their respective ligands on APCs and/or tumor cells, triggering a negative (-) or positive (+) response.

Since antitumoral effects have been mainly ascribed to T and NK cells, it is important to understand the mechanisms that regulate their cytotoxic activity to design effective pharmacological strategies against cancer cells. One of these strategies is based on restoring the cytotoxic activity of CTLs and NK cells by blocking the interaction between IC receptors and their ligands (Muntasell et al., 2017; Pardoll, 2012). The most frequent targets of current ICB therapies are CTLA-4 and PD-1 receptors

(Fife and Bluestone, 2008; Zhao et al., 2018), although other IC receptors such as TIM-3, LAG-3 and TIGIT are emerging as targets for immunotherapy (Bejarano et al., 2021). At the same time, the blockade of the IC signaling could also diminish the suppressive functions of Treg cells, which interfere with the cytotoxic activity of CTLs and NK cells and suppress tumor antigen presentation (Romano et al., 2019). Although some ICB-approved drugs have shown a favorable clinical ORR and DCR, an important percentage of patients still shows partial or short-term responses, or are refractory to treatment. Furthermore, late relapses can occur in patients who initially respond to ICB therapies (Jenkins et al., 2018), which has sparked interest in targeting other coinhibitory receptors and finding new therapeutic combinations to treat non-responder patients. There is currently much focus on combining different IC receptors, or their combination with chemotherapy, radiotherapy, targeted therapies, anti-angiogenic agents and partial surgical resections to modulate immune outcomes and to reduce on-target side effects (Melero et al., 2015).

Other strategies are based on the adoptive cell transfer (ACT) of genetically-modified T cells equipped with TCRs or chimeric antigen receptors (CARs) (Waldman et al., 2020). These therapies are based on the ex vivo genetic modification of T cells to recognize tumor-associated antigens and kill target cells expressing these antigens (Labanieh et al., 2018; Rafiq et al., 2020; Tang et al., 2016). TCR T cells can only recognize antigens displayed by MHC/HLA molecules, which is a limitation for eliminating those cancer cells that lose MHC expression (Zhao and Cao, 2019). In contrast, CAR-T cells can recognize target molecules on the surface of cancer cells (Waldman et al., 2020). CAR-T therapy has shown considerable success in treating hematologic malignancies (Zhao and Cao, 2019), but limited efficacy in solid tumors (Tang et al., 2016), except for neuroblastoma (Louis et al., 2011; Park et al., 2007). These observations suggest that the TME may block immune-driven tumor clearance by impairing CAR-T infiltration, activation or survival. Therefore, the removal of TME barriers to immune clearance may improve the efficiency of CAR-T therapies in solid tumors (Newick et al., 2016). Recently, another therapeutic strategy uses armored CAR-T cells, which constitutively express cytokines or ligands to favor effector immune responses (Chang et al., 2018; Hong et al., 2020; Jackson et al., 2016; Lanitis et al., 2020). Indeed, the production of IL-12 by armored CAR-T cells overcomes immunosuppression mediated by Treg cells and myeloid cells, promotes $CD8^+$ T-cell cytotoxic activity (Zhao et al., 2012), and enhances antigen presentation (Chmielewski et al., 2011). Overall, although the use of engineered T cells has been successful in several tumor types, there are several issues to be addressed, such as the toxicity effects, the selection of new antigens, and the re-education of the immunosuppressive TME toward antitumoral activities.

3.4- Tumor-Associated Macrophages (TAMs)

Macrophages are differentiated myeloid cells, whose functions are to eliminate infectious agents, promote wound healing and regulate adaptive immunity (Mosser and Edwards, 2008). In mice,

macrophages are characterized by the expression of markers such as CD11b, F4/80, CD68, and colony-stimulating factor-1 receptor (CSF1R), and low levels of expression of Gr1, whereas, in humans, macrophages are identified by the expression of CD68, CD16, CD14, CD312, CD115, and other markers (Qian and Pollard, 2010). Macrophages have usually been classified into two subtypes. M1 or 'classically activated' macrophages are activated via Th1-derived cytokines and/or bacterial products such as LPS. M1-like macrophages secrete pro-inflammatory cytokines (IL-12, IL-1β, IL-6, IL-23 and TNF-α), generate ROS and nitric oxide (NO) and express high levels of MHC class II molecules. These cells have a tumoricidal function (DeNardo and Ruffell, 2019). By contrast, M2 or 'alternatively activated' macrophages are activated in response to Th2-derived cytokines, such as IL-4, IL-10, IL-13, and glucocorticoid hormones. M2-like macrophages are characterized by high levels of scavenging, mannose and galactose receptors, activation of the arginase (ARG1) pathway, production of IL-10, vascular endothelial growth factor (VEGF), matrix metalloproteinases (MMPs), and these immune cells facilitate tumor progression (Mantovani et al., 2002). Clinical data has indicated that a high frequency of M2-like macrophages is correlated with poor prognosis in a variety of human cancers such as breast, lung, prostate and ovarian cancers (Larionova et al., 2020). Although the M1/M2 nomenclature has been useful for many years, it is known that macrophages can acquire intermediate plastic phenotypes in response to environmental stimuli (Lambrechts et al., 2018; Murray et al., 2014). In this sense, the tissue location, the cancer subtype and the specific microenvironment niche contribute to the intratumoral macrophage heterogeneity. For this reason, it has been proposed that the TAM classification should be based on the anti-tumorigenic or pro-tumorigenic function of macrophages (Qian and Pollard, 2010).

Growing evidences have indicated that TAMs enhance tumor progression by promoting EMT and CSCs properties in cancer cells (Figure 8). Indeed, M2-like TAMs, via IL-10 (Liu et al., 2013), TGF-β1 (Fan et al., 2014) or IL-6 (Wan et al., 2014), can promote EMT and CSC features in pancreatic, hepatocellular and breast carcinomas, respectively. TNF-α secreted by pro-inflammatory TAMs induces a switch from a differentiated to a dedifferentiated phenotype in melanoma cells, which escape immune surveillance and contribute to tumor relapse (Landsberg et al., 2012). Furthermore, mesenchymal-like breast cancer cells induce immunosuppressive TAM activation via GM-CSF. In turn, these activated macrophages secrete CCL18, creating a positive feedback loop that promotes EMT and metastasis (Su et al., 2014) (Figure 8).

Other studies have demonstrated that TAMs support tumor growth and progression (Mantovani et al., 2017; Qian and Pollard, 2010) by promoting angiogenesis (Lin et al., 2006) and enhancing invasion and metastasis (Qian et al., 2009). TAMs produce a plethora of pro-angiogenic factors, including VEGF-A, TNF-α, ADM, PDGF and TGF-β, which promote the formation of a vascular network during the malignant progression (Lin et al., 2006; Linde et al., 2012) (Figure 8). In addition, immunosuppressive TAMs promote cancer-cell invasion and metastasis via the secretion

of MMPs, serine proteases, and cathepsins, which alter the ECM, modify cell-cell contacts and induce basal membrane disruptions (Gocheva et al., 2010; Yan et al., 2016) (Figure 8). CSF1 also promotes the development of invasive and metastatic carcinomas by regulating the recruitment of TAMs at the tumor site (Lin et al., 2001). CSF1R inhibition abrogates TAM infiltration and enhances $CD8^+$ T cell recruitment, reducing cervical and mammary tumor growth and progression (Strachan et al., 2013). However, glioma cell-supplied GM-CSF, IFN-γ, and CXCL10 promote TAM survival upon CSF-1R inhibition, although these TAMs lose M2-like polarization and show enhanced phagocytosis activity, ultimately leading to the regression of established tumors (Pyonteck et al., 2013). Similarly, the inhibition of CCL2-CCR2 signaling specifically blocks macrophage recruitment within breast tumors, which is associated with reduced metastasis and enhanced mouse survival (Qian et al., 2011). A paracrine signaling loop between tumor-derived CSF-1 and macrophage-derived EGF has been linked to increased cancer-cell invasion (Coniglio et al., 2012; Goswami et al., 2005) (Figure 8). Accordingly, M2-polarized TAMs by IL-4 from $CD4^+$ Th2 cells produce high levels of EGF, which enhance cancer-cell invasion, migration and lung metastasis by activating the EGFR signaling in breast cancer cells (DeNardo et al., 2009). Therefore, these studies show that $CD4^+$ T cells can enhance cancer-cell dissemination and metastasis through their ability to regulate the pro-tumorigenic properties of TAMs.

Finally, immunosuppressive M2-like TAMs can subvert antitumoral immunity by eliminating M1-like responses and by impairing T and NK cell activation (DeNardo and Ruffell, 2019) (Figure 8). TAMs can directly inhibit CTL and NK responses through the expression of IC ligands such as PD-L1/PD-L2 and CD80/CD86, the production of immunosuppressive cytokines (IL-10, TGF-β, ARG1, PGE2), the depletion of metabolites (such as L-arginine) and the production of ROS (Figure 8). In addition, TAMs can express PD-1, which is associated with a reduction of their phagocytosis activity. $PD\text{-}1^+$ TAMs have a polarization M2-like and pro-tumorigenic functions, and the blockade of PD-1/PD-L1 increases the phagocytosis activity of these immune cells, reducing tumor growth (Gordon et al., 2017). M2-like TAMs can also inhibit T and NK-cell activity through the recruitment of Treg cells or the inhibition of stimulatory populations such as DCs (DeNardo and Ruffell, 2019).

Several strategies have been developed to therapeutically target TAMs (Cassetta and Pollard, 2018). The main strategies are: (i) CSF1R inhibitors to reduce TAM survival or promote their reeducation into a antitumoral phenotype (such as BLZ945, edicotinib, emactuzumab and PLX7486); (ii) CCL2 or CCR2 inhibitors to prevent TAM recruitment (such as PF-04136309, MLN1202 and TAK202); (iii) CD47 and SIRPα antagonists to enhance TAM phagocytosis (such as CC-90002, ZL-1201, TTI-621 and TTI-622); (iv) CD40 agonists, a TNF receptor superfamily member, to promote antitumoral T-cell responses, activate APCs and reeducate myeloid cells (such as Chi Lob 7/4, CP-870,893 and dacetuzumab); and (v) inhibitors of PI3Kγ (eganelisib) and TREM2 (PY314) to reeducate TAMs toward antitumoral phenotypes (Duan and Luo, 2021; Tang et al., 2021).

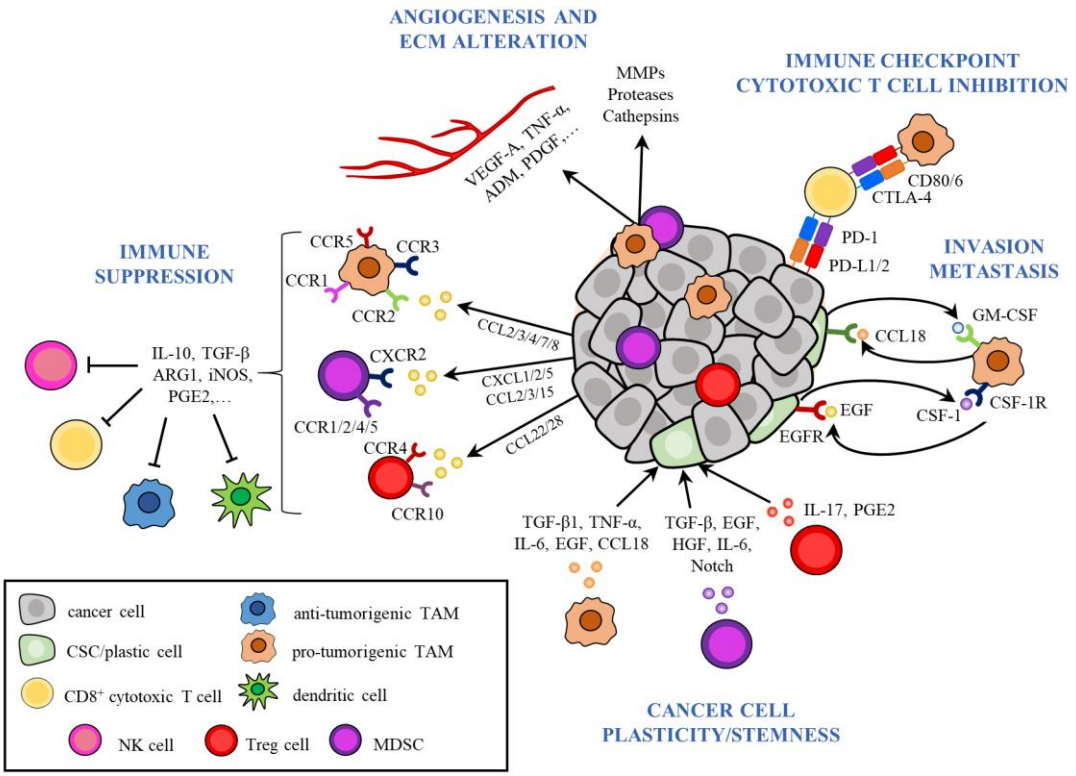

Figure 8. The tumor-immunosuppressive network limits cytotoxic immune-cell responses and promotes cancer-cell plasticity (original figure from Lorenzo-Sanz L, published in Lorenzo-Sanz and Muñoz, 2019)**.** Immune cells, such as TAMs, MDSCs, and Treg cells are recruited into the tumor and become educated by cancer cell-derived cytokines and chemokines to acquire pro-tumorigenic functions. These cancer and immune cells disrupt immune surveillance through multiple mechanisms, including inhibition of antigen presentation by DCs, T-cell proliferation, M1 macrophage polarization and NK-cell cytotoxicity. In addition, cancer cells and immunosuppressive TAMs inhibit cytotoxic T-cell function by activating immune-checkpoint pathways. Immunosuppressive cells support invasion and metastasis by secreting a variety of pro-tumorigenic cytokines and growth factors. Paracrine signal loops between CSCs and TAMs enhance cancer-cell plasticity, immunosuppression and tumor progression. Finally, immunosuppressive TAMs and MDSCs produce pro-angiogenic factors such as VEGF, TNF-α, ADM, PDGF, among others, to promote angiogenesis, or secrete MMPs, serine proteases, and cathepsins, leading to ECM alterations.

3.5- Myeloid derived suppressor cells (MDSCs)

MDSCs play an important role in tumor progression by evading the host's immune response. These immune cells arise as a consequence of the aberrant myelopoiesis associated with cancer, and are functionally defined as immunosuppressive immature myeloid cells (Gabrilovich and Nagaraj, 2009). Two main populations have been described: polymorphonuclear MDSCs (PMN-MDSCs), and monocytic MDSCs (M-MDSCs) (Gabrilovich et al., 2012). PMN-MDSCs share phenotypic features with neutrophils, but are less phagocytic. By contrast, M-MDSCs exhibit a similar phenotype to that of inflammatory monocytes and differentiate into immunosuppressive macrophages and DCs under specific TME signals (Bronte et al., 2016). In mice, PMN-MDSCs are

identified by the expression of $CD11b^{+}Ly6G^{+}Ly6C^{low}$ and M-MDSCs as $CD11b^{+}Ly6G^{-}Ly6C^{high}$. In humans, PMN-MDSCs are $CD11b^{+}CD33^{+}CD14^{-}CD15^{+}$ cells, and M-MDSCs are $CD11b^{+}CD33^{+}$ $CD14^{+}CD15^{-}$ cells. To distinguish PMN-MDSCs from neutrophils, a recent study has shown that the lectin-type oxidized receptor 1 (LOX-1) is overexpressed in PMN-MDSCs while neutrophils do not express it (Condamine et al., 2016). However, its classification as MDSCs is based on their immunosuppressive ability to inhibit immune responses mediated mainly by T and NK cells (Bronte et al., 2016; Veglia et al., 2021). An elevated frequency of MDSCs is positively correlated with advanced disease and poor therapeutic response in patients with a range of cancers, including melanoma, colorectal, breast, bladder, thyroid and NSCL cancers (Almand et al., 2001; Diaz-Montero et al., 2009). It has been reported that PMN-MDSCs are the most prevalent MDSC population in most solid tumors. However, in certain cancers such as melanoma, multiple myeloma and prostate cancers, the M-MDSC population is more prevalent (Solito et al., 2014).

Several studies have shown that MDSCs disrupt immune surveillance mechanisms, such as T-cell activation, antigen presentation, M1-like polarization, and NK-cell cytotoxicity (Groth et al., 2019) (Figure 8). Some of the factors involved in MDSC suppressive activity include: (i) the production of ARG1, which leads to the deprivation of L-arginine, an essential amino acid for T-cell activity and proliferation; (ii) the production of iNOS, which promotes NO synthesis; (iii) the production of ROS; and (iv) the expression of immunosuppressive factors such as COX-2, PGE2, IL-10, and TGF-β, which induce severe anergy of effector T and NK cells. NO and ROS induce T-cell apoptosis and the nitration of cytokines and the TCR, which block T-cell migration and cytotoxic activities against cancer cells. Moreover, MDSCs can induce a Treg expansion and recruitment through the expression of CD40, which also act by suppressing the effector T and NK cells (Bronte et al., 2016; Pan et al., 2010). Lastly, MDSCs upregulate the expression of PD-L1, blocking antitumoral T-cell activity via the interaction with the PD-1 receptor of these cells (Ostrand-Rosenberg, 2010; Zhang et al., 2017). This upregulation has been associated with the S100A9 inflammatory protein and the hypoxia-inducible factor-1α (HIF-1α) (Cheng et al., 2019; Noman et al., 2014).

More recently, other MDSC functions have been described, such as the formation of a pre-metastatic niche (Psaila and Lyden, 2009), the enhancement of tumor growth and invasion, and the stimulation of angiogenesis (Marvel and Gabrilovich, 2015) (Figure 8). These processes are regulated by MDSC-derived factors such as VEGF, basic fibroblast growth factor (bFGF), Bombina variegate peptide 8 (Bv8), and MMP-9, which are essential for tumor angiogenesis and cancer-cell invasion (Bronte et al., 2016). MDSCs are also involved in the regulation of EMT and CSC features (Lorenzo-Sanz and Muñoz, 2019) (Figure 8). Indeed, MDSC-induced EMT occurs through the upregulation of COX-2 and the activation of the β-catenin/TCF4 pathway in nasopharyngeal cells (Li et al., 2015), or through the stimulation of miR-101 expression in ovarian cancer cells (Cui et al., 2013). Furthermore, tumor-infiltrated MDSCs, which show STAT3 signaling activation, promote the

stemness of pancreatic cancer cells by increasing the expression of SNAI1/2, ZEB1, NANOG and OCT-4 (Panni et al., 2014). Other studies based on mouse models of breast cancer implicated MDSC-derived IL-6 in increasing cancer-cell stemness and EMT (Oh et al., 2013; Zhu et al., 2017). Accordingly, MDSCs endow breast cancer cells with stem-like features through IL-6/STAT3 and NO/NOTCH crosstalk signaling (Peng et al., 2016). Although many studies have not distinguished between MDSC populations, a recent report demonstrated that M-MDSCs and PMN-MDSCs have opposite effect on cancer cells. Indeed, tumor-infiltrated M-MDSCs facilitate breast cancer-cell dissemination by inducing EMT/CSC properties. In contrast, pulmonary PMN-MDSCs support metastasis by reverting the EMT phenotype and promoting cancer-cell proliferation (Ouzounova et al., 2017).

Therefore, targeting MDSCs is emerging as an attractive approach for the design of new cancer treatments, as their presence is often associated with resistance against treatments and poor patient outcomes (Gabrilovich et al., 2012; Mantovani, 2010; Messmer et al., 2015). Several strategies have been developed to therapeutically target MDSCs (Law et al., 2020). The main approaches are: (i) tyrosine kinase inhibitors of VEGF and STAT3 to deplete MDSCs (such as sunitinib and ibrutinib); (ii) CCR5 (maraviroc), CXCR2 (AZD5069, reparixin, and SX-682) and CSF1R (plexidartinib) inhibitors to prevent MDSC recruitment into the TME; (iii) COX-2 (celecoxib), PDE5 (tadalafil and sildenafil) and STAT3 (AZD9150) inhibitors to mitigate the immunosuppressive functions of MDSCs by downregulating the expression and generation of ARG1, iNOS, and ROS; and (iv) all-trans-retinoic acid (ATRA), the casein kinase inhibitor tetrabromocinnamic acid or HDAC inhibitors (entinostat) to differentiate MDSCs into an antitumoral phenotype.

Taking altogether, pro-inflammatory states such as $CD4^+$ Th1 and M1-like macrophages, together with cytotoxic $CD8^+$ T cells and NK cells drive an antitumoral immune response against cancer cells. In contrast, anti-inflammatory states such as $CD4^+$ Th2 and M2-like macrophages, together with immunosuppressive Treg cells and MDSCs facilitate tumor progression, angiogenesis and metastasis development, as they downregulate cell-mediated antitumoral responses. This makes it necessary not only to therapeutically restore the effector activity of CTLs and NK cells, but also to reduce the immunosuppressive TME of tumors. Currently, some studies have demonstrated the value of targeting Treg, TAM, and MDSC populations as part of a combinatorial therapy to enhance the potency of IC inhibitors and other immunotherapy strategies (Bejarano et al., 2021).

4- TUMOR RESISTANCE AND IMMUNE EVASION MECHANISMS

Several studies have demonstrated that cancer-cell features can influence the tumor's immune landscape and that cancer cells develop mechanisms to evade the immune attack (Kalbasi and Ribas, 2020; Terry et al., 2017). The most common mechanisms driving immune evasion are neoantigen loss, defects of the antigen processing machinery, abnormal IFN-γ signaling, aberrant oncogenic

signaling, the upregulation of coinhibitory IC pathways, and the generation of an immunosuppressive TME (Aldea et al., 2021; Dongre and Weinberg, 2019) (Figure 9).

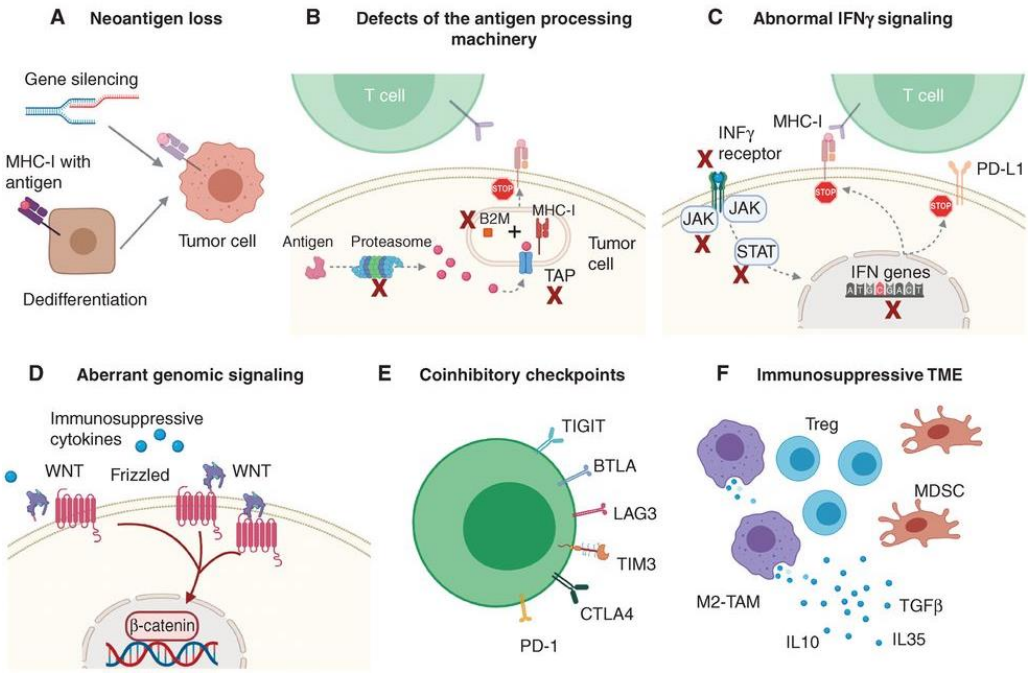

Figure 9. Tumor resistance and immune evasion mechanisms (Aldea et al., 2021)**. a.** Neoantigen loss. **b.** Defects of the antigen processing machinery. **c.** Abnormal IFN-γ signaling. **d.** Aberrant genomic signaling. **e.** Coinhibitory checkpoints. **f.** Immunosuppressive TME.

It is known that tumors that activate a *de novo* antitumor immune response, as a result of increased TMB and antigenicity, are most likely to respond to ICB therapies (Schumacher and Schreiber, 2015). However, loss of genes encoding neoantigens (Anagnostou et al., 2017; Gubin et al., 2014; Lee et al., 2020; Rosenthal et al., 2019) and altered antigen presentation are detected in several cancer types (Aldea et al., 2021; Sucker et al., 2014) (Figures 9a and 9b). Hence, by decreasing the expression of MHC class I molecules, which are required for the presentation of antigens to T cells, cancer cells evade the cytotoxic functions of T cells (Blum et al., 2013; Fruci et al., 2012). Other defects in the antigen-processing machinery are the loss of function (LOF) of beta-2-microglobulin (B2M), which is required for MHC class I folding and transport to the cell surface, the dysregulation of the transporters that pump the antigenic fragments across the endoplasmic reticulum (TAP1, TAP2 and TAPBP), and the disruption of the IFN-γ-JAK-STAT signaling, which promotes MHC-I expression (Campo et al., 2014; Patel et al., 2017; Sade-Feldman et al., 2017). B2M LOF causes acquired resistance to ICB therapies in melanoma, NSCLC, and colorectal cancer (Gettinger et al., 2017; Le et al., 2017), and a reduced expression of several components of the immunoproteasome (PSMB8, PSMB9 and PSMB10) have been observed in NSCLC (Tripathi et al., 2016). In addition, cancer cells lacking sensitivity to IFN-γ signaling have defects on MHC class I antigen presentation, permitting immune escape (Restifo et al., 1993).

Likewise, the IFN-γ signaling pathway has both favorable and adverse effects on antitumoral immune responses (Ikeda et al., 2002; Kaplan et al., 1998; Pardoll, 2012) (Figure 9c). On the one hand, IFN-γ produced by T cells induces an effective antitumoral response through the activation of the JAK-STAT signaling pathway. In turn, this pathway activates the interferon regulatory factor 1 (IRF1), which enhances the expression of MHC-I and PD-L1, and has direct anti-proliferative effects on cancer cells (Figure 9c) (Platanias, 2005). However, a continuous IFN-γ exposure can lead to immunoediting of cancer cells (Benci et al., 2016). In addition, cancer cells can escape the effects of IFN-γ by mutating molecules involved in the IFN-γ pathway such as IFNGR1, IFNGR2, JAK1, JAK2, IRF1, and STAT proteins (Darnell et al., 1994). Supporting this notion, mutations in JAK1 and JAK2 have been detected in melanoma patients with primary or acquired resistance to anti-PD-1 and anti-CTLA-4 therapies, respectively (Gao et al., 2016; Keenan et al., 2019; Sucker et al., 2017; Zaretsky et al., 2016). Mutations in this pathway would also result in lack of adaptive PD-L1 expression upon IFN-γ exposure. In this scenario, blocking PD-L1 or PD-1 would not be therapeutically effective (Shin et al., 2017). Recently, it has been demonstrated that IFN secretion can be regulated by the cyclic GMP-AMP synthase (cGAS), which is a DNA sensor that serves to mount a rapid immune response. Activation of cGAS stimulates the adapter protein STING to trigger IFN signaling (Ishikawa et al., 2009). In this sense, IFN secretion can be impaired when STING and cGAS expression is silenced through epigenetic processes (Kwon and Bakhoum, 2020). In line with this work, EZH2 inhibition activates a STING-IFN response, which upregulates genes involved in antigen presentation, IFN pathway, Th1 chemokine signaling, and PD-L1 expression in prostate cancer models. In addition, EZH2 inhibition increased the presence of activated $CD8^+$ T cells and M1-like macrophages, reversing PD-1 therapy resistance (Morel et al., 2021).

Oncogenic signaling pathways are also relevant to tumor immunity (Spranger and Gajewski, 2018) (Figure 9d). Several pathways play an important role in tumor-intrinsic resistance to ICB therapies, through the generation of immunosuppressive environments that affect T-cell functions. Some of the pathways that have been more extensively studied are the WNT-β-catenin, the cyclin-dependent kinase 4 (CDK4)-CDK6 and the mitogen-activated protein kinase (MAPK) pathways and/or loss of PTEN expression (Kalbasi and Ribas, 2020; Skoulidis et al., 2018; Spranger et al., 2015).

Finally, tumors with hybrid and mesenchymal features are associated with increased vascularity and immunosuppressive immune infiltrates, which leads to an impair cytotoxic function of CTLs and NK cells (Figures 9e and 9f) (Chockley and Keshamouni, 2016; Lou et al., 2016; Murciano-Goroff et al., 2020; Sharma et al., 2017; Thommen et al., 2015). Hence, a comprehensive study that immunophenotyped around 9,000 tumors of 29 solid cancers showed that tumor features influence the characteristics of their immune infiltrate (Tamborero et al., 2018). Tumors that are enriched for the EMT program, focal adhesion, ECM remodeling, angiogenesis, inflammation and hypoxia genes are associated with the infiltration of immunosuppressive cells (Tamborero et al., 2018). In this line,

Dongre et al. showed that epithelial breast tumors contain active cytotoxic $CD8^+$ T cells, which express high levels of perforin, granzyme B and IFN-γ, antitumor M1-like macrophages, and were sensitive to anti-CTLA-4 therapy. In contrast, mesenchymal breast tumors expressed low levels of MHC-I, contained Treg cells, M2-like macrophages, exhausted $CD8^+$ T cells, and were resistance to anti-CTLA-4 therapy (Dongre et al., 2017). These findings indicate that cancer cells with an induced EMT program promote the recruitment of immunosuppressive cells, making mesenchymal tumors resistant to anti-CTLA-4 therapy (Dongre et al., 2017). The same authors have recently demonstrated that the abrogation of the mesenchymal cell-derived factors CD73, CSF1, or SPP1 prevents the generation of an immunosuppressive TME, specifically by decreasing the presence of M2-like macrophages and mobilizing active T cells and DCs into the tumor core (Dongre et al., 2020). This situation sensitizes refractory mesenchymal tumors partially or completely to anti-CTLA-4 therapy (Dongre et al., 2020). Likewise, melanomas that are resistant to anti-PD-1 treatment display a transcriptional signature reminiscent of EMT-related processes, including the downregulation of E-cadherin and the concomitant upregulation of factors involved in ECM remodeling, angiogenesis, and immunosuppression (Hugo et al., 2016). These observations suggest that the mesenchymal and immunosuppressive phenotype is associated with innate anti-PD-1 resistance (Hugo et al., 2016). Recently, Cerezo-Wallis et al. have demonstrated that the cancer-cell secreted-growth factor midkine (MDK) rewires the molecular profile of melanoma cells to promote an immunosuppressive state. In the absence of MDK, this immunosuppressive state shifts to a pro-inflammatory IFN response, characterized by the presence of M1-like macrophages, cytotoxic $CD8^+$ T cells and increased sensitivity to anti-PD-1/PD-L1 treatment (Cerezo-Wallis et al., 2020).

Cancer cells undergoing EMT can also express immunosuppressive cytokines or IC ligands to modulate the efficacy of the immune response (Kim et al., 2016). Among those, TGF-β has been one of the most studied (Massagué, 2008; Scheel et al., 2011). TGF-β can impair maturation, differentiation or activation of NK cells, DCs, macrophages, neutrophils, and $CD4^+$ and $CD8^+$ T cells. In addition, TGF-β can inhibit the cytotoxic T-cell functions by altering the expression of perforin, granzyme B, Fas ligand and IFN-γ (Joffroy et al., 2010; Thomas and Massagué, 2005). In prostate cancer cell lines, TGF-β and EGF led to MHC class I downregulation through upregulation of SNAIL (Chen et al., 2015). In addition, EMT can induce the expression of PD-L1 by cancer cells (Chen et al., 2014; Dongre et al., 2017; Noman et al., 2017). Indeed, ZEB1-mediated EMT in NSCLC cells results in increased tumor PD-L1 expression, thus reducing the activity of tumor-infiltrating $CD8^+$ lymphocytes and increasing metastasis (Chen et al., 2014). Additionally, the EMT signature in patients with NSCLC correlates with increased expression of multiple immune checkpoint proteins and the presence of Treg cells in the primary tumors (Lou et al., 2016). Thus, although epithelial-mesenchymal plasticity is most often associated with pro-invasive and pro-migratory phenotypes, there is increasing evidence of the impact of the induction of the EMT

program in modulating the TME. The precise mechanisms by which EMT mediates such processes and the innate or acquired resistance to immunotherapy (Hugo et al., 2016) represents a great area for future investigation.

In conclusion, it is important to unravel the complex mechanisms used by cancer cells for immune surveillance during cancer initiation, development and metastasis in different tumor types. This will allow the personalized design of therapeutically strategies to improve the survival of those patients who are refractory or show partial or short-term responses to treatments currently under study or approved in the clinic.

Some fragments of this Introduction have been extracted and partially modified from two published reviews that I co-authored (Lorenzo-Sanz and Muñoz, 2019; da Silva-Diz et al., 2018).

Lorenzo-Sanz, L., and Muñoz, P. (2019). Tumor-Infiltrating Immunosuppressive Cells in Cancer-Cell Plasticity, Tumor Progression and Therapy Response. Cancer Microenviron. 12, 119–132.

da Silva-Diz, V., **Lorenzo-Sanz, L.**, Bernat-Peguera, A., Lopez-Cerda, M., and Muñoz, P. (2018). Cancer cell plasticity: Impact on tumor progression and therapy response. Semin. Cancer Biol. 53, 48–58.

HYPOTHESIS AND OBJETIVES

Based in our previous results, we hypothesize that cancer cells show a strong plasticity and the ability to switch from an epithelial to a mesenchymal-like state, increasing their tumor- and metastasis-initiating capabilities and, therefore, promoting SCC progression. We propose that this switch may be induced by the crosstalk between tumor-infiltrating immune cells and cancer cells. In turn, as cancer cells contribute to remodel the tumor microenvironment, alterations in cancer-cell features may impact on the recruitment of tumor-infiltrating immune cells and impair the anti-tumor immune responses mediated by cytotoxic T lymphocytes and natural killer cells. This situation could promote tumor growth, invasion and SCC progression.

The specific aims of this Thesis are:

1. Analyze cancer (stem) cell plasticity and dynamics during SCC progression.
2. Characterize the tumor immune microenvironment and the alterations in the expression profile of cancer-cell immune checkpoint (IC) ligands during mice SCC progression.
3. Characterize cancer-cell features and the recruitment of immune cells in patient skin SCCs at different stages of progression.
4. Determine the effect of blocking different IC pathways to boost the anti-tumor immune response of SCCs.
5. Evaluate the benefits of targeting the immunosuppressive tumor microenvironment to block cancer-cell plasticity and to enhance the anti-tumor immune response of SCCs.

MATERIALS AND METHODS

1. Mouse models and lineages of skin SCC progression

Our group generated mouse models of skin SCC progression based on tumors developed in K14-HPV16$^{Tg/+}$ mice (FVB/C57/Bl6 F1) (Arbeit et al., 1994). These mice express the E6 and E7 viral oncoproteins from HPV16 in basal keratinocytes, and 30% of mice develop spontaneous SCCs in the skin one year after birth. To induce tumor formation, K14-HPV16$^{Tg/+}$ mice were treated with a single dose of 7,12-dimethylbenz(a)anthracene (DMBA; 20 µg in 200 µl of acetone; Sigma) and then twice weekly with 12-O-tetradecanoylphorbol-13-acetate (TPA; 12.5 µg in 200 µl of acetone; Sigma) for 15 weeks. Subsequently, small pieces (2-4 mm^3) of spontaneous or DMBA/TPA-induced tumors were engrafted in the back skin of 6-week-old male immunodeficient mice. Tumor growth was monitored and the volume was calculated ($V = \pi/6 \times L \times W^2$) every 2-3 days. When tumors reached a critical size, they were surgically excised and small pieces were serially engrafted in immunodeficient mice, generating ortho-SCC (OT-SCC) lineages. Resected immunodeficient mice were checked daily until they presented symptoms of poor health, whereupon they were sacrificed and checked for the presence of metastatic lesions.

Cancer cells from WD-SCCs, MD/PD-SCCs and PD/S-SCCs were obtained and isolated using FACS sorting. Then, isolated full epithelial cancer cells from WD-SCCs, epithelial EpCAM$^+$ and mesenchymal-like EpCAM$^-$ cancer cells from MD/PD-SCCs were engrafted in immunodeficient or immunocompetent syngeneic mice in order to generate epithelial (containing >70% EpCAM$^+$ cancer cells), mixed (containing 10-70% EpCAM$^+$ cancer cells), and mesenchymal (containing <10% EpCAM$^+$ cancer cells) SCCs.

Animal housing, handling and all procedures involving mice were approved by the Institutional Animal Care and Use Committee at IDIBELL (Barcelona, Spain), in accordance with the Spanish national guidelines and regulations. Mice were housed at 2-5 animals per cage with a 12h light/dark cycle at constant temperature (23ºC) with ad libitum access to food and water.

2. Patient skin SCC samples

Patient skin SCC samples were supplied by the Plastic Surgery and Pathology Units of the Hospital Universitario de Bellvitge (Barcelona, Spain). The patient samples used in this Thesis, together with their degree of differentiation, are listed in Table 1.

These studies were carried out in compliance with the principles of the Declaration of Helsinki (Fortaleza, 2013). The treatment of the personal data was adjusted to the provisions of the European data protection regulation. The protocol of sample collection was supervised and approved by the Research Ethics Committee of the Hospital Universitario de Bellvitge (Barcelona, Spain). All patients were fully informed about the study before giving their signed consent to be included in it.

		% of the indicated tumor region in overall sample			
Sample	Classification/grade	% WD-SCC	% MD-SCC	% PD-SCC	% spindle SCC
H10	PD-SCC/ G3	5	55	40	0
H11	PD/S-SCC/ G4	0	0	0	100
H14	MD-SCC/ G2	0	80	20	0
H15	PD/S-SCC/ G4	0	0	0	100
H24	WD/MD-SCC/ G2	30	70	0	0
H34	MD/PD-SCC/ G3	0	75	25	0
H41	MD-SCC/ G2	35	65	0	0
H43	PD-SCC/ G3	0	20	80	0
H44	PD-SCC/ G3	0	60	40	0
H45	MD/PD-SCC/ G2	0	85	15	0
H46	MD/PD-SCC/ G3	5	45	50	0
H48	PD/S-SCC/ G4	0	10	20	70
H49	WD/MD-SCC/ G2	40	60	0	0
H54	PD-SCC/ G3	0	0	100	0

Table 1. Features of patient skin SCC samples. As patient samples frequently exhibit intratumoral heterogeneity in the histopathological grade, a pathologist determined the percentage represented by each region in the overall sample.

3. Isolation of SCC cells and flow cytometry (FACS) assays

For flow cytometry analysis and sorting of tumor samples, excised mouse tumors were mechanically minced and incubated in RPMI medium (Life Technologies, 61870044) containing 10% FBS (Life Technologies, 10270106), 20 mM HEPES (Sigma, H3537), 1% Antibiotic-Antimycotic (Biowest, L0010-100), 1600 U/ml collagenase type I (Sigma, C0130) and 70 U/ml dispase (Life Technologies, 17105-041) overnight at 37ºC. Cell suspensions were filtered and then depleted of red blood cells by incubating with ammonium-chloride-potassium (ACK) lysis buffer (Lonza, BP10-548E) for 10 min at room temperature. For endothelial cell depletion, cell suspensions were incubated with a purified Rat anti-mouse CD31 antibody (1:100, BD Bioscience, 550274) for 30 min at 4ºC, and then with Dynabeads anti-rat IgG (1:33, Life Technologies, 11035) for 30 min at 4ºC. For cell surface staining, isolated cells were incubated with cell surface antibodies (Table 2) in blocking buffer (5% FBS in PBS) with 1 mg/mL IgG (Sigma, I5381) for 30 min at 4ºC. Cells were then washed with 0.5% BSA, 2 mM EDTA in PBS, and resuspended in analysis buffer (2% FBS, 2 mM EDTA in PBS). Viability was assessed with DAPI (Thermo Scientific, 62248) staining. For intracellular staining, single-cell suspensions were firstly stimulated in DMEM F-12 medium containing 10 ng/mL phorbol 12-myristate 13-acetate (PMA), 1 µg/mL ionomycin, and 5 µg/mL brefeldin A (Sigma, B6542) (for IFN-γ and CTLA-4) or just 5 µg/mL brefeldin A (for GzmB) for 4h at 37ºC.

Cell suspensions were then incubated with cell surface antibodies (Table 2) for 30 min at 4ºC, fixed with 4% paraformaldehyde (Electron Microscopy Sciences, 15710-S) for 20 min at 4ºC, and permeabilized using Permeabilization Buffer 1X (Life Technologies, 00-8333-56) for 15 min at 4ºC. The intracellular proteins (Table 2) were then stained for 30 min at 4ºC. The LIVE/DEAD Fixable Dead Cell Stain Kit (Life Technologies, L34963) was used to evaluate cell viability.

For flow cytometry analysis of spleen samples, mice were euthanized by CO_2 asphyxiation and the spleen was collected into RPMI medium containing 10% FBS, 1% Non-essential amino acids (Sigma, M7145), 1% Na-Pyruvate (Sigma, S8636), 1% Glutamine, 1% Penicillin/Streptomycin (Biowest, L0022-100), and 1% HEPES. To generate a single-cell suspension, we placed the spleen into a 70 µm cell strainer mesh and mashed it using the plunger of a syringe. Cell suspensions were then depleted of red blood cells by incubating with ACK lysis buffer for 10 min at 4ºC. Isolated spleen cells were incubated with conjugated antibodies (Table 2) in blocking buffer (5% FBS in PBS) with 1 mg/mL IgG for 30 min at 4ºC, then washed with 0.5% BSA, 2 mM EDTA in PBS, and finally resuspended in analysis buffer (2% FBS, 2 mM EDTA in PBS).

Mice blood samples were taken via cardiac puncture and collected in tubes containing heparin, depleted of red blood cells with ACK lysis buffer for 10 min at room temperature, and stained with conjugated antibodies (Table 2) for 30 min at 4ºC. Then, isolated blood cells were washed with 0.5% BSA, 2 mM EDTA in PBS, and resuspended in analysis buffer (2% FBS, 2 mM EDTA in PBS).

All FACS sorting and analysis were carried out with a BD Bioscience Fusion II equipment, and data was analyzed using FlowJo v10.4.2 software.

Antibody	Clone	Dilution	Source	Catalog number
CD11b APC	M1/70	1/250	BioLegend	101212
CD11b PE	M1/70	1/250	BD Bioscience	557397
CD11c PE	N418	1/200	BioLegend	117307
CD140a (PGFRA) PE	APA5	1/100	eBioscience	12-1401-81
CD152 (CTLA-4) PE/Cyanine7	UC10-4B9	1/200	BioLegend	106313
CD155 (PVR) PE/Cyanine7	TX56	1/200	BioLegend	131511
CD206 (MMR) APC	MR6F3	1/100	eBioscience	17-2061-80
CD223 (LAG-3) PE/Cyanine7	C9B7W	1/250	BioLegend	125225
CD226 (DNAM-1) PE/Cyanine7	10E5	1/250	BioLegend	128811
CD274 (B7-H1, PD-L1) PE/Cyanine7	10F.9G2	1/200	BioLegend	124313
CD279 (PD-1) APC/Cyanine7	29F.1A12	1/250	BioLegend	135223
CD3ε APC	145-2C11	1/200	BioLegend	100311
CD31	MEC 13.3	1/100	BD Bioscience	550274
CD326 (EpCAM) APC-eF780	G8.8	1/400	eBioscience	47-5791-82

CD34 eFluor 660	RAM34	1/150	eBioscience	50-0341-82
CD366 (TIM-3) PE/Cyanine7	B8.2C12	1/250	BioLegend	134009
CD4 PE/Cyanine7	RM4-5	1/300	BioLegend	100527
CD45 APC	30-F11	1/200	BioLegend	103112
CD45 PE	30-F11	1/350	TONBO	50-0451-U100
CD47 PE/Cyanine7	Miap301	1/200	BioLegend	127523
CD49f FITC	GoH3	1/10	BD Bioscience	555735
CD8a PE	53-6.7	1/300	BioLegend	100707
CD80 PE/Cyanine7	16-10A1	1/250	BioLegend	104733
CD86 PE	GL-1	1/150	BioLegend	105007
F4/80 APC	BM8	1/200	BioLegend	123115
F4/80 APC/Cyanine7	BM8	1/200	BioLegend	123118
F4/80 PE	BM8	1/200	BioLegend	123110
Galectin-9 PE/Cyanine7	108A2	1/250	BioLegend	137913
Ly-6G/Ly-6C (Gr-1) PE/Cyanine7	RB6-8C5	1/300	BioLegend	108415
Granzyme B PE/Cyanine7	NGZB	1/200	eBioscience	25-8898-82
IFN-γ PE/Cyanine7	XMG1.2	1/200	BioLegend	505825
Ly-6C PE/Cyanine7	HK1.4	1/300	BioLegend	128017
Ly-6G APC	1A8	1/300	BioLegend	127613
H-2K^{b} (MHC-I) PE/Cyanine7	AF6-88.5	1/200	BioLegend	116519
I-A/I-E (MHC-II) PE/Cyanine7	M5/114.15.2	1/400	BioLegend	107629
NK-1.1 PE	PK136	1/200	BioLegend	108707
TIGIT (Vstm3) PE/Cyanine7	1G9	1/250	BioLegend	142107

Table2: Cell surface and intracellular mouse antibodies used in flow cytometry assays.

4. Cell culture

Cancer cells from mouse WD-SCCs (full epithelial cancer cells), MD/PD-SCs (epithelial EpCAM^{+} and mesenchymal-like EpCAM^{-} cancer cells) and PD/S-SCCs (full mesenchymal cancer cells) were isolated using the previously described FACS protocol. These isolated cancer cells were cultured in DMEM-F12 medium (Life Technologies, 31331-093) with 1X B27 (Life Technologies, 17504-044) and 1% Penicillin/Streptomycin (Biowest, L0022-100), and were grown at 37ºC in a humidified 5% CO_2 incubator. These cancer cells were previously transduced with a MSCV-IRES-GFP plasmid, and, therefore, cancer cells can be identified by EGFP expression.

5. Tumor-cell grafting and *in vivo* treatments

To study the immune landscape and cancer-cell features, we generated epithelial (containing >70% EpCAM^{+} cancer cells), mixed (containing 10-70% EpCAM^{+} cancer cells), and mesenchymal (containing <10% EpCAM^{+} cancer cells) SCCs. To do that, isolated GFP^{+} full epithelial cancer cells

from WD-SCCs, GFP^+ epithelial $EpCAM^+$ and GFP^+ mesenchymal-like $EpCAM^-$ cancer cells from MD/PD-SCCs (10,000 cells) were mixed 1:1 with Matrigel Basement Membrane matrix (Corning, 356234), and then subcutaneously engrafted in the back skin of 6–8-week syngeneic males (C57Bl6/FVB F1 background). Tumor growth ($V = \pi/6 \times L \times W^2$) was monitored every 2-3 days and tumors were excised when they reached a critical size for processing by flow cytometry assays.

To determine the effect of anti-PD-L1 therapy on SCC progression, epithelial, mixed and mesenchymal SCCs were generated in immunocompetent syngeneic mice, as described above. When epithelial and mesenchymal tumors were palpable (upon reaching a volume of approximately 113 mm^3), mice were randomly assigned to a control (mouse IgG2b isotype control) or treatment (anti-PD-L1) group (Table 3). Then, mice were administered intraperitoneally 3 days per week with 200 µg/dose. For mixed tumors, all treatments started on day -1, and then mice were administered intraperitoneally 3 times per week with 200 µg/dose. Tumor size was monitored every 2 days in order to determine the effect of the treatment to suppress tumor growth. When mice bearing epithelial or mesenchymal tumors received 9 doses (3 weeks), and mice bearing mixed tumors received 14 doses (5 weeks), tumors were surgically excised. To evaluate if the boost of the anti-tumor immune response after anti-PD-L1 treatment was dependent on the release of the IC PD-1/PD-L1 blockade of cytotoxic T cells, when epithelial tumors were palpable, mice were administered intraperitoneally 3 days per week with an anti-CD8α antibody (300 µg/dose) for CD8 depletion (9 doses, 3 weeks).

To determine the effect of anti-TIGIT therapy on PD/S-SCC tumor growth, GFP^+ mesenchymal-like $EpCAM^-$ cancer cells were engrafted in immunocompetent syngeneic mice. When tumors were palpable (upon reaching a volume of approximately 20 mm^3), mice were randomly assigned to a control (mouse IgG2b isotype control) or treatment (anti-TIGIT) group (Table 3). Then, mice were administered intraperitoneally 3 times per week with 200 µg/dose. Tumor volume was monitored every 2 days and tumors were excised when they reached a critical size (13 doses, 4 weeks). To study if the boost of the anti-tumor immune response after anti-TIGIT treatment was dependent on the release of the IC CD155/TIGIT blockade of cytotoxic T cells, when mesenchymal tumors were palpable, mice were administered intraperitoneally 3 days per week with an anti-CD8α antibody (300 µg/dose) for CD8 depletion (13 doses, 4 weeks).

To study the role of macrophages promoting cancer-cell plasticity and on TME, mice bearing mixed tumors were treated with anti-CSF1R (250 µg/dose) or IgG2b isotype control (200 µg/dose) (Table 3). To study the role of MDSCs promoting cancer-cell plasticity and on TME, mice bearing mixed tumors were treated with anti-Gr1 (200 µg/dose) or IgG2b isotype control (200 µg/dose) (Table 3). In both experiments, mice were administered intraperitoneally on day -1, and then 3 times per week until experimental endpoint (18 doses).

In all *in vivo* experiments, when tumors reached a critical size or the treatment was completed, they were excised and processed by flow cytometry assays. Cryopreserved and paraffin-embedded samples were collected for subsequent immunofluorescence and immunohistochemical analysis.

***InVivo* MAb Antibodies**	**Clone**	**Source**	**Catalog number**
Mouse IgG2b isotype control	MPC-11	BioXCell	BE0086
anti-Mouse CD8α	2.43	BioXCell	BE0061
anti-Mouse CSF1R (CD115)	AFS98	BioXCell	BE0213
anti-Mouse Ly6G/Ly6C (Gr1)	RB6-8C5	BioXCell	BP0075
anti-Mouse PD-L1	10F.9G2	BioXCell	BE0101
anti-Mouse TIGIT	1G9	BioXCell	BE0274

Table3: Anti-mouse antibodies used in *in vivo* treatments.

6. Histology, immunohistochemistry and immunofluorescence assays

Patient and mouse tumor samples were fixed with 4% formaldehyde (PanReac, 252931) overnight at 4ºC, paraffin-embedded, and sectioned at 4 µm. For histopathological analysis, tumor sections were stained with hematoxylin and eosin (H/E). Tumor viability was analyzed with the ImageJ Weka Training Segmentation plugin, which allows the selection of the reference viable and necrotic regions from each tumor section (training), and provides a labeled result for the whole tumor section, from which the percentages of viable and necrotic areas were calculated.

Patient and mouse tumor paraffin-embedded sections were deparaffinized and antigen retrieval was performed using 10 mM sodium citrate (pH 6.0) or 10 mM TRIS/EDTA (pH 9.0), depending on the specifications of the primary antibody supplier. Endogenous peroxidase activity was quenched with 3% hydrogen peroxidase diluted in water (Millipore, 1.07210.1000) for 10 min at room temperature. Tumor sections were then blocked with 5% horse serum (HS, Life Technologies, 16050122) in Tris-buffered saline (TBS) buffer 1X for at least 1h at room temperature, and incubated with primary antibodies diluted with 3% HS in 0.1% Tween20 TBS 1X overnight at 4ºC in a humidified chamber. The mouse and human primary antibodies used are described in Table 4. For immunofluorescence (IF) detection, tumor sections were then incubated with secondary antibodies diluted with 3% HS in 0.1% Tween20 TBS 1X for 1h at room temperature (see Table 5). Nuclei were stained with 4',6-Diamidino-2-phenylindole (DAPI, Life Technologies, D3571) for 10 min at room temperature. Finally, samples were mounted with Vectashield mounting medium (Palex, 416397), and images were captured with a Leica TCS SP5 confocal microscope. For immunohistochemistry (IHC) detection, tumor sections were incubated with secondary anti-mouse EnVision+System-HRP antibody (Dako, K4001) or anti-rabbit EnVision+System-HRP antibody (Dako, K4003) for 1h at room temperature, followed by the 3,3'-Diaminobenzidine (DAB) developing system (Dako, K3468). Samples were then counterstained with hematoxylin, mounted with permanent DPX

mounting medium (Sigma, 06522), and visualized under light microscopy (Nikon Eclipse 80i). All images were analyzed with the ImageJ software.

To visualize EGFP directly in mouse tumor sections, after resection, tumor samples were fixed with 4% formaldehyde for 30 min, washed for 30 min with PBS and then embedded in optimal cutting temperature (OCT) medium. Tumors were maintained at -80ºC and cut by cryostat, sectioning into 4 µm slices. The slices were stored at -20ºC, defrosted at room temperature, and washed with TBS 1X. Then, samples were permeabilized with 0.1% TRITON X-100 (Sigma, 9036-19-5) in TBS 1X for 15 min at room temperature, blocked with 5% HS in TBS 1X for at least 1h, and incubated with primary antibodies diluted with 3% HS in 0.1% Tween20 TBS1X overnight at 4ºC (Table 4). Tumor sections were then labelled with a secondary antibody diluted with 3% HS in 0.1% Tween20 TBS 1X for 1h at room temperature (Table 5). Nuclei were stained with DAPI for 10 min at room temperature and samples were mounted with Vectashield mounting medium. Images were taken with a Leica TCS SP5 confocal microscope and analyzed with the ImageJ software.

Reactivity	Antibody	Host	Source	Catalog no.	Use	Dilution
Mouse	CD163 [EPR19518]	Rb	Abcam	ab182422	IHC	1/50
	CD326 (EpCAM)	Rt	eBioscience	14-5791-85	IF	1/50
	CD4 (D7D2Z)	Rb	Cell Signaling	25229	IHC	1/50
	CD45	Rb	Abcam	ab10558	IF	1/300
	CD68	Rb	Abcam	ab125212	IF	1/200
	CD8α (D4W2Z)	Rb	Cell Signaling	98941	IHC	1/50
	CD80	Gt	R&D systems	AF740	IF	1/100
	FoxP3 (D608R)	Rb	Cell Signaling	12653	IHC	1/50
	Ly6-G/Ly6C (Gr1)	Rt	R&D systems	MAB1037	IF	1/200
	Vimentin [EPR3776]	Rb	Abcam	ab92547	IF	1/100
Human	CD163 [EPR19518]	Rb	Abcam	ab182422	IHC	1/50
	CD68	Ms	Abcam	ab955	IHC	1/150
	CD8α [C8/144B]	Ms	Abcam	ab17147	IF	1/50
	CD80	Rb	Abcam	ab254579	IF	1/50
	E-Cadherin	Ms	BD Bioscience	610182	IF	1/50-100
	FoxP3 (D2W8E)	Rb	Cell Signaling	98377	IHC	1/50
	Galectin-9	Gt	R&D systems	AF2045	IF	1/50
	HLA Class I ABC	Ms	Abcam	ab70328	IF	1/50
	PD-1 [EPR4877(2)]	Rb	Abcam	ab137132	IF	1/100
	Vimentin	Rb	Abcam	ab45939	IF	1/100

Table 4: Primary antibodies used in immunohistochemistry and immunofluorescence mouse and human assays. Gt, Goat; Ms, Mouse; Rb, Rabbit; Rt, Rat. IF, immunofluorescence; IHC, immunohistochemistry.

Antibody	Host	Source	Catalog no.	Use	Dilution
anti-Goat Alexa Fluor 568	Dy	Invitrogen	A-11057	IF	1/50-200
anti-Mouse Alexa Fluor 568	Dy	Invitrogen	A-10037	IF	1/100
anti-Mouse Alexa Fluor 647	Gt	Invitrogen	A-21235	IF	1/100-200
anti-Rabbit Alexa Fluor 568	Dy	Invitrogen	A-10042	IF	1/50-400
anti-Rabbit Alexa Fluor 647	Dy	Invitrogen	A-31573	IF	1/100-300
anti-Rat Alexa Fluor 546	Gt	Invitrogen	A-11081	IF	1/200-400
anti-Rat Alexa Fluor 647	Dy	Invitrogen	A-48272	IF	1/100
anti-Rat Alexa Fluor 647	Gt	Invitrogen	A-21247	IF	1/200
anti-Mouse EnVision+System-HRP	-	Dako	K4001	IHC	-
anti-Rabbit EnVision+System-HRP	-	Dako	K4003	IHC	-

Table 5: Secondary antibodies used in immunohistochemistry and immunofluorescence assays. Dy, Donkey; Gt, Goat. IF, immunofluorescence; IHC, immunohistochemistry.

7. Reverse transcription and quantitative real-time PCR

RNA was extracted from isolated cancer cells by using Trizol Reagent (Invitrogen, 15596026), according to the manufacturer's instructions. Reverse-transcription reactions were carried out with the High-Capacity cDNA Reverse Transcription kit (Applied Biosystems, 4374966). To retro transcribed, we mixed 12.5 µl of 2X RT master mix (2.5 µl 10X RT Buffer, 1 µl 25x dNTP Mix, 2.5 µl 10X RT Random Primers, 1.25 µl MultiScribe Reverse Transcriptase, 1.25 µl RNase inhibitor and 4 µl Nuclease-free H_2O) together with 12.5 µl of RNA sample (1µg RNA diluted in water) into each tube. The reverse-transcription reaction was performed using the conditions below: 25ºC for 10 min, 37ºC for 120 min, 85ºC for 10 min, and 4ºC for 30 min. Alternatively, cDNA amplification by pico profiling was performed in the Functional Genomics Core of IRB Barcelona, as previously described (Gonzalez-Roca et al., 2010). Real-time PCR reactions were performed (three replicates for each sample) on an Applied QuantStudio5 machine, using SYBR Green Mix (Applied Biosystems, 4312704) and the primers described in Table 6. *Gapdh* and *Ppia* were used to normalize the gene expression values for all mouse samples. mRNA levels are shown as fold change (expressed in $\log_2$), in which the mean of mRNA levels relative to two housekeeping genes was calculated.

Gene	Forward (5' - 3')	Reverse (5' - 3')
Arg1	TTTTAGGGTTACGGCCGGTG	CCTCGAGGCTGTCCTTTTGA
Ccl2	GCATCCACGTGTTGGCTCA	CTCCAGCCTACTCATTGGGATCA
Ccl22	ACCTCTGATGCAGGTCCCTA	CTTGCGGCAGGATTTTGAGG
Ccl5	CTCACCATATGGCTCGGACA	CGACTGCAAGATTGGAGCAC
Ccl9	TACTGCCCTCTCCTTCCTCA	CAATTTCAAGCCCTTGCTGT
Ccr2	TGCCATCATAAAGGAGCCAT	TTTGTTTTTGCAGATGATTCAA

Ccr3	CATAGGGTGTGGTCTCAAAGC	AAAGGACTTAGCAAAATTCACCA
Ccr4	GGGTACCAGCAGGAGAAGC	CGACGGCATTGCTTCATAG
Cd163	GTGCTGGATCTCCTGGTTGT	CGTTAGTGACAGCAGAGGCA
Cd4	CTCCTTCGGCTTTCTGGGTT	TGCCTGGCGCTGTTGG
Cd8a	GGATTGGACTTCGCCTGTGA	CTTTCGGCTCCTGTGGTAGC
Cd80	TTCACCTGGGAAAAACCCCC	ACAACGATGACGACGACTGT
Cd86	CAGCACGGACTTGAACAACC	CTCCACGGAAACAGCATCTGA
Cdh1	ATCCTCGCCCTGCTGATT	ACCACCGTTCTCCTCCGTA
Csf1r	TTGCCTTCGTATCTCTCGATG	CTCTGCTGGTGCTACTGCTG
Ctla4	AACTGCAGCTGCCTTCTAGG	GGGTCACCTGTATGGCTTCA
Cxcl10	ATGACGGGCCAGTGAGAATG	TCGTGGCAATGATCTCAACAC
Cxcl9	GCCATGAAGTCCGCTGTTCT	TAGGGTTCCTCGAACTCCACA
Cxcr3	CCCAACCACAAGTGCCAAAG	TCACTAACCTCAAGGTACATGGC
Dnp63	GTACCTGGAAAACAATGCCCAG	CGCTATTCTGTGCGTGGTCTG
Epcam	CCGCGGCTCAGAGAGACT	AGGAAGTACACTGGCATTCACC
Fasl	CTCCGTGAGTTCACCAACCA	TGAGTGGGGGTTCCCTGTTA
Fizz1 (Retnla)	CCTGCTGGGATGACTGCTAC	CAGTGGTCCAGTCAACGAGT
Lgals9	AAGGGGCGCAAACAGAAAAC	GGAGGGATTCCAGGAGTAGAGA
Gapdh	AGGTCGGTGTGAACGGATTTG	TGTAGACCATGTAGTTGAGGTCA
Gas6	GGAGGCCTGCCAGAAGTATC	TGCTTGTACGAGGCCGTATC
Gata3	GCTCCTTGCTACTCAGGTGAT	GGAGGGAGAGAGGAATCCGA
Grhl1	CCTTCACGTGGGACATCAAT	AGCCCTTCACACCCTTCTG
Grhl2	GACAACAAATGCTTCCGACA	GCTGCTCATCTCGGTTTTTG
Gzmb	ACAACACTCTTGACGCTGGG	ATGATCTCCCCTGCCTTTGTC
Ifng	CGGCACAGTCATTGAAAGCC	TGTCACCATCCTTTTGCCAGT
Il10	GGCGCTGTCATCGATTTCTC	ATGGCCTTGTAGACACCTTGG
Il12b	GCACCAAATTACTCCGGACG	TGGTCCAGTGTGACCTTCTC
Il13	ATGGCCTCTGTAACCGCAAG	CTCATTAGAAGGGGCCGTGG
Il18	CCTCTTGGCCCAGGAACAAT	ACAGTGAAGTCGGCCAAAGT
Il1b	TGCCACCTTTTGACAGTGATG	TGATGTGCTGCTGCGAGATT
Il2	CTCTGCGGCATGTTCTGGAT	AATGTGTTGTCAGAGCCCTTT
Il23a	ACCAGCGGGACATATGAATCT	AGACCTTGGCGGATCCTTTG
Il2rA	CGGGCAGAACTGTGTCTGTA	CCGTTCTTGTAGGAGAGGGC
Il5	TGGGGGTACTGTGGAAATGC	CCACACTTCTCTTTTTGGCGG
Il6	ACCAGAGGAAATTTTCAATAGGC	TGATGCACTTGCAGAAAACA
K14	GGCCCAGATCCAGGAGATGAT	CAGGGGCTCTTCCAGCAGTATC
Lag3	CCAGGCCTCGATGATTGCTA	ACGCGGTGAGTTGTAGACAG
Lamp1	GCCCTGGAATTGCAGTTTGG	TGCTGAATGTGGGCACTAGG
Lta	TCTAGGGGCCCAGGGACT	AGGATGCCATGGGTCAAGTG

Ly6c1	ACTGTGCCTGCAACCTTGT	TCCCTGAGCTCTTTCTGCAC
Ly6g	GAGAGGAAGTTTTATCTGTGCAGC	TCAGGTGGGACCCCAATACA
H2-Aa class II	AAGCTTTGACCCCCAAGGTG	GGAGCCTCATTGGTAGCTGG
Nos2	TCCTGGACATTACGACCCCT	CTCTGAGGGCTGACACAAGG
Ovol1	CTCCACGTGCAAGAGGAACT	CTCTGGTTCCCGGTAGGG
Ovol2	GCCAGGTCAAAAATCAAGTTTACCA	AGCTCTTGCCACAAAGGTCA
Pdcd1	ATCTACCTCTGTGGGGCCAT	AGGTCTCCAGGATTCTCTCTGT
Cd274 (Pdl1)	CGCCTGCAGATAGTTCCCAA	AGCCGTGATAGTAAACGCCC
Pdcd1lg2	TGCTGGGTGCTGATATTGACA	GGGGCTGTCACGGTGAATAA
Ppia	GTTCATGCCTTCTTTCACCTTCCC	CAAATGCTGGACCAAACACAAACG
Prf1	TCTTGGTGGGACTTCAGCTTTC	TCTGCTTGCATTCTGACCGA
Snai1	CTTGTGTCTGCACGACCTGT	AGTGGGAGCAGGAGAATGG
Tbx21	ACTAAGCAAGGACGGCGAAT	TAATGGCTTGTGGGCTCCAG
Tgfb1	TGGAGCAACATGTGGAACTC	GTCAGCAGCCGGTTACCA
Tnf	GCCTCTTCTCATTCCTGCTTG	CTGATGAGAGGGAGGCCATT
Twist	AGCTACGCCTTCTCCGTCT	TCCTTCTCTGGAAACAATGACA
Vegfa	GGCCTCCGAAACCATGAACT	CTGGGACCACTTGGCATGG
Vim	AGAGAGAGGAAGCCGAAAGC	TCCACTTTCCGTTCAAGGTC
Zeb1	GCCAGCAGTCATGATGAAAA	TATCACAATACGGGCAGGTG
Zeb2	TCTTATCAATGAAGCAGCCG	TGCGTCCACTACGTTGTCAT

Table 6: Primers for mouse mRNA quantification used in qRT-PCR assays.

8. Phosphoproteomic analysis

To identify kinase-dependent signaling pathways responsible for cancer-cell plasticity during SCC progression, I moved to the OncoProteomics Laboratory (OPL) at the VU University Medical Center (Amsterdam, The Netherlands) under the supervision of Prof. Dr. Connie R. Jimenez. The OPL is an internationally recognized laboratory specialized in (phospho)protein profiling and protein biomarker discovery by mass spectrometry, so the protocols carried out for this study had been previously set up in Dr. Jimenez's laboratory (Beekhof et al., 2019; van der Mijn et al., 2015).

Three biological replicates of cancer cells at each stage of progression (full epithelial, epithelial $EpCAM^+$, mesenchymal-like $EpCAM^-$, and full mesenchymal cancer cells) were grown *in vitro* to 70-80% confluency, washed with PBS, scrapped into the lysis buffer (9 M urea, 20 mM HEPES pH 8.0, 1 mM sodium orthovanadate, 2.5 mM sodium pyrophosphate, 1 mM β-glycerophosphate), and sonicated using a Branson high-intensity cuphorn sonicator (3 cycles of 30 s). Cell lysates were reduced by incubation in 45 mM dithiothreitol (DTT) for 30 min at 55ºC, and alkylated in 110 mM iodoacetamide for 15 min at room temperature in the dark. Subsequently, cell lysates were diluted to 2 M urea using 20 mM HEPES pH 8.0 and digested overnight at room temperature with 5 µg/ml

trypsin (Promega, V542). After acidifying the digests by adding trifluoroacetic acid (TFA) to a final concentration of 1%, tryptic digests were desalted and purified on Sep-Pak C18 columns using a vacuum system, eluted in 50% acetonitrile (ACN) and 0.1% TFA, and lyophilized for at least 48h. For global phosphopeptide analysis, desalted peptides were enriched with titanium dioxide (TiO_2) beads, using aliphatic hydroxy-acid modified metal oxide chromatography (MOAC). For specific enrichment of phosphotyrosine (pTyr)-containing peptides, lyophilized peptides were dissolved in 700 µl immunoprecipitation buffer (20 mM Tris-HCl pH 7.2, 10 mM sodium phosphate, 50 mM NaCl) and transferred at 4ºC to a tube containing 20 µl of a 50% (v/v) slurry of agarose beads harboring P-Tyr-1000 anti-phosphotyrosine monoclonal antibodies (Cell Signaling Technologies, 8803). Following a 2h incubation at 4ºC on a rotator, beads were washed twice with cold PBS, and 3 times with cold Milli-Q water. Bound peptides were eluted with a total of 50 µl 0.15% TFA in two steps. Peptides were desalted with custom-made C18 stage tips, and eluted in 0.1% TFA. Then, peptides were speed-vac dried, solubilized in 20 µl loading solvent (4% ACN in 0.5% TFA), and samples were subjected to LC-MS/MS analysis. Peptides were separated by an Ultimate 3000 nanoLC-MS/MS system (Dionex LC-Packings, The Netherlands), and eluting peptides were ionized at a potential of +2 kV and introduced into a Q Exactive mass spectrometer (Thermo Fisher, Bremen, Germany). Phosphopeptides were relatively quantified by their extracted ion intensities ('Intensity' in MaxQuant). For each sample, the phosphopeptide intensities were normalized on the median intensity of all identified peptides in the sample. Overall kinase phosphorylation was calculated by summing all identified phosphopeptides MS/MS spectra for a kinase (spectral-counting). Normalization, statistical testing, and cluster analysis of differential phosphopeptides were performed in R Studio. Protein–protein interaction networks were retrieved from the STRING v10.0 database and visualized in Cytoscape v3.4. Gene Ontology analysis were performed in DAVID. Their in-house developed kinase-focused pipeline based on kinase-centered phosphorylation analysis (INKA) (Beekhof et al., 2019), the substrate-based motif analysis (NetworKIN) and the PhosphositePlus database were used for integrative inferred kinase activity scoring.

9. Statistical analysis

All statistical tests and graphs were generated using the Prism v5.0 software (GraphPad software, San Diego, CA). Depending on the experimental setup, we used unpaired two-tailed Student's *t*-test or one-way ANOVA followed by Tukey's or Dunnett's multiple comparison test to determine the significance of group differences in each experiment, as detailed in figure legends. Significant differences between tumor growths were analyzed by Repeated Measures ANOVA test. For all graphical analyses, mean ± SD values are represented. No statistical methods were used to predetermine sample size in *in vivo* experiments, which was estimated based on our previous experience and similar experiments reported in literature. The statistical significance of group differences is expressed with asterisks: ns $p>0.05$, *$p\leq0.05$, **$p\leq0.01$, ***$p\leq0.001$, ****$p\leq0.0001$.

RESULTS

CHAPTER 1. ANALYZE CSC PLASTICITY/DYNAMICS DURING SCC PROGRESSION

To determine the mechanisms that promote tumor progression, our group generated mouse models of skin SCC progression based on tumors developed in K14-HPV16 mice. These mice express the E6 and E7 viral oncoproteins from human papillomavirus (HPV16) in basal keratinocytes, which abrogate the function of p53 and Rb family proteins, and 30% of mice developed spontaneous SCCs in the skin one year after birth. To promote SCC development, these mice were treated with 7,12-dimethylbenz(a)anthracene (DMBA)/12-O-tetradecanoyl phorbol-13-acetate (TPA). Subsequently, small pieces from several SCC samples (spontaneous or DMBA/TPA-induced) were orthotopically and serially engrafted in the back skin of immunodeficient mice, generating ortho-SCC lineages (Figure 10a). After serial engraftments, well differentiated SCCs (WD-SCCs) showing epithelial features progressed to moderately differentiated SCCs containing poorly differentiated regions (MD/PD-SCCs), and then to full poorly differentiated and spindle-shaped SCCs (PD/S-SCCs) (Figure 10a). PD/S-SCCs grew significantly faster than their respective WD-SCC precursors in all tumor lineages (Figure 10b). In addition, nude mice carrying PD/S-SCCs showed a reduced survival (Figure 10c) due to more frequent lower-latency metastasis than their respective WD-SCC precursors (Figures 10d and 10e). SCC progression was associated with a dramatic expansion of the CSC population and a strong induction of the EMT program. These results demonstrate that PD/S-SCCs are generated through the malignant advance of WD-SCCs (da Silva-Diz et al., 2016).

Interestingly, the comparative analysis of the whole gene expression profile of α6-integrin^{+}/CD34^{+} CSCs isolated from PD/S-SCCs (late-CSCs; L-CSCs) and from their WD-SCC precursors (early-CSCs; E-CSCs) revealed that CSC features change during SCC progression. Whereas E-CSCs from WD-SCCs expressed epithelial markers (EpCAM, E-cadherin, K14 and p63), L-CSCs from PD/S-SCCs showed a mesenchymal-like phenotype, characterized by a strong expression of EMT-TFs and a downregulation of epithelial differentiation markers. Besides, signaling pathways regulating CSC proliferation, survival and dissemination changed during skin SCC progression to promote the aggressive growth and metastasis of PD/S-SCCs (da Silva-Diz et al., 2016). Specifically, whereas β-catenin and autocrine EGFR signaling controlled proliferation and survival of E-CSCs, these pathways were shut down and autocrine FGFR1 and PDGFRα signaling were strongly induced in L-CSCs. The genetic and pharmacological inhibition of FGFR and PDGFR repressed advanced SCC growth and metastasis, respectively. In accordance, advanced and recurrent patient SCCs showed a strong induction of the EMT program, as well as an overexpression of PDGFRα and FGFR1 (da Silva-Diz et al., 2016). These findings suggest that the regulatory mechanisms controlling CSCs at specific stages of progression may guide the choice of the most suitable therapy for selectively targeting the signaling pathway that regulates this subset of cells. However, given that the activation of these signaling pathways does not promote the progression from E-CSCs to L-CSCs in our SCC model, our group became interested in identifying which mechanisms might be driving this process.

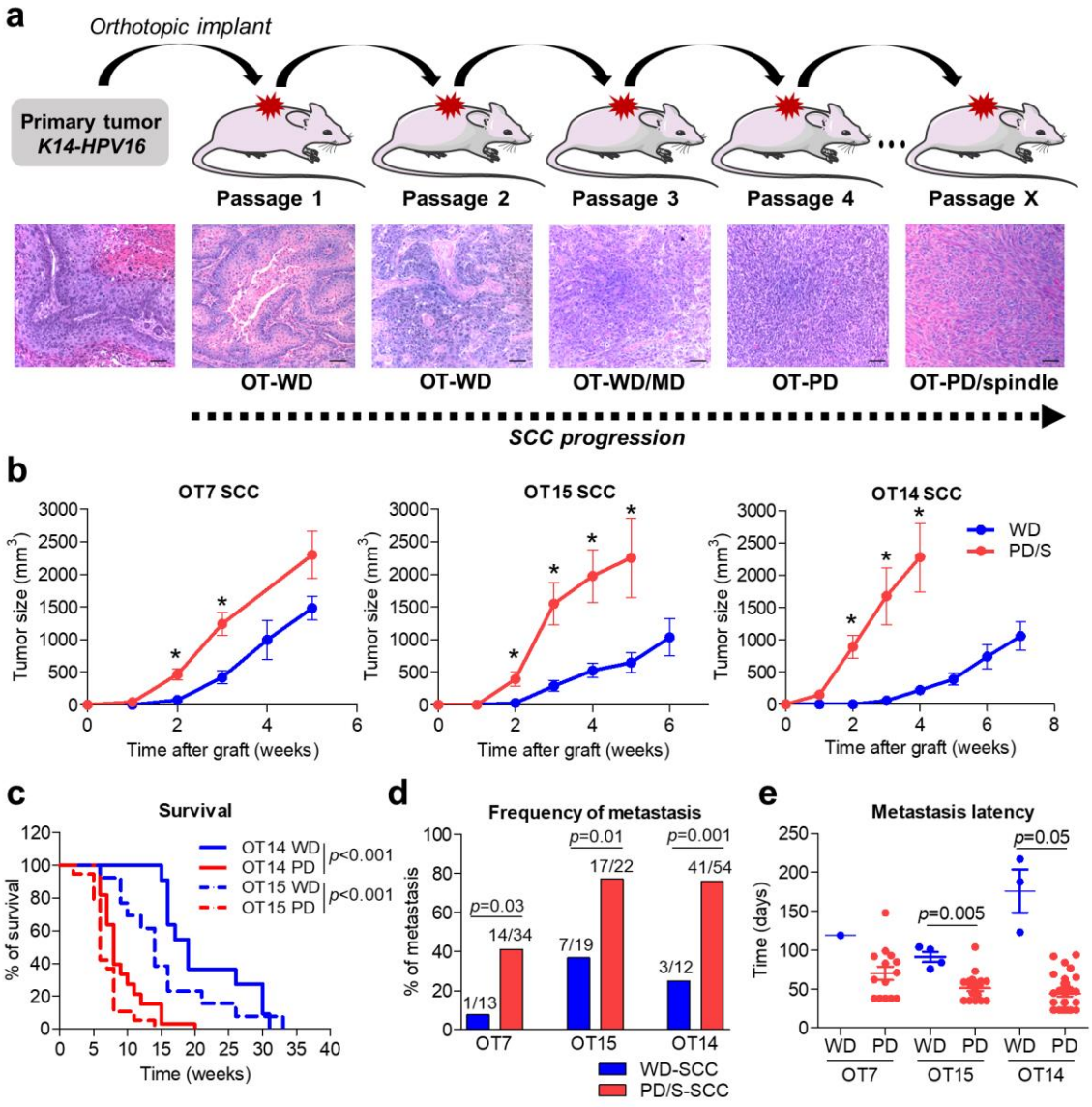

Figure 10. Characterization of ortho-SCCs during tumor progression (da Silva-Diz et al., 2016)**. a.** Scheme for generating lineages with orthotopic skin SCCs. Ortho-SCCs (OT) were serially engrafted to allow tumor progression. Representative H/E images of the different stages of SCC progression are included. Scale bar, 50 µm. **b.** Growth kinetics of PD/S-SCCs and their respective WD-SCC precursors of the indicated lineages. **c.** Kaplan-Meier curves comparing the survival of mice carrying WD-SCCs and PD/S-SCCs. **d.** Percentage of mice developing metastatic lesions (mean) and metastasis frequency out of the total number of mice in each group and lineage (indicated in the fraction number). **e.** Latency time of metastasis development in the indicated groups. All data are presented as mean ± SEM; *p≤0.05; unpaired two-tailed Student's *t*-test.

1.1- Generation of WD-SCCs from single tumor-initiating cells to evaluate their ability to progress toward PD- and mesenchymal-like tumors after serial engraftments

To identify the mechanisms involved in CSC plasticity and in the generation of highly aggressive mesenchymal L-CSCs during SCC progression, together with other lab members, we started from two hypothesis. The first hypothesis was that the changes in CSC features and regulation could be a

consequence of the selection and expansion of a rare population of L-CSCs, already present in WD-SCCs in a very low frequency, after long-term tumor growth. To address this, we analyzed the presence of α6-integrin^{+}/CD34^{+}/EpCAM^{-}/PDGFRα^{high} CSCs (L-CSCs) in a subset of WD-SCCs by flow cytometry. After analyzing different WD-SCCs, we observed that most cancer cells were α6-integrin^{+}/EpCAM^{+}/PDGFRα^{low} (epithelial features, Figure 11a), and α6-integrin^{+}/CD34^{+}/EpCAM^{-}/PDGFRα^{high} (L-CSCs) were practically undetectable in these WD-SCCs (Figure 11a). In addition, we engrafted high amounts of epithelial cancer cells (>10^{6} cells, that could include rare L-CSCs) isolated from WD-SCCs in immunodeficient mice. No PD/S-SCCs were generated from these epithelial cancer cells and we did not detect tumor regions with mesenchymal-like features (Figure 11b). These results indicate that L-CSCs are not present in early WD-SCCs.

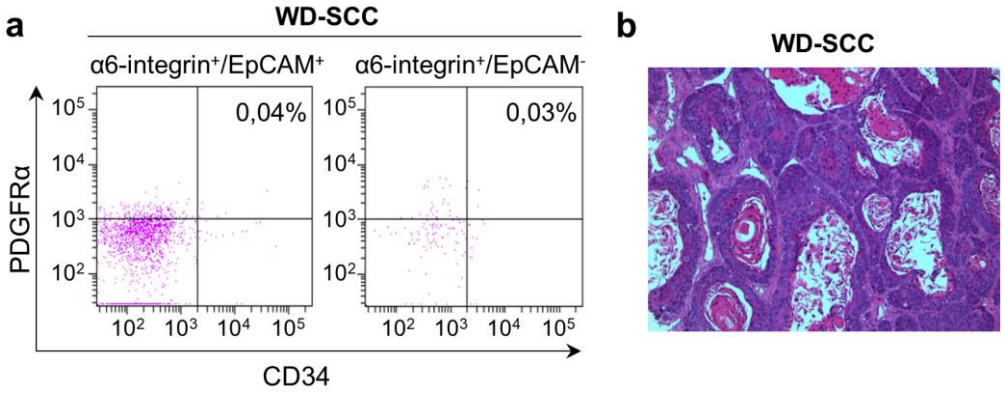

Figure 11. L-CSCs are not detected in early WD-SCCs. a. Representative flow cytometry plots showing the frequency of PDGFRα^{+}/CD34^{+} cancer cells within α6-integrin^{+}/EpCAM^{+} or α6-integrin^{+}/EpCAM^{-} cancer cells isolated from WD-SCCs. **b.** Representative hematoxylin/eosin (H/E) image showing the well-differentiated histopathologic features of tumors generated after the engraftment of high amounts of cancer cells (>10^{6} cells) isolated from WD-SCCs.

Our second hypothesis was whether the transformation or reprogramming of E-CSCs may generate L-CSCs. To tackle this, and having previous information about the frequency of E-CSCs in WD-SCCs (as determined by limiting-dilution assays) (da Silva-Diz et al., 2016), we generated WD-SCCs from a putative single E-CSC by engrafting in immunodeficient mice 10 fold less epithelial cancer cells than the E-CSC frequency (Figure 12a). This strategy was designed to avoid a possible CSC heterogeneity and the initial presence of rare L-CSCs in the parental WD-SCCs. These single-E-CSC-derived WD-SCCs were then serially transplanted in immunodeficient mice, generating different SCC lineages (Figure 12a). The characterization of parental and derived tumors by flow cytometry demonstrated that, whereas early WD-SCCs contained mostly cancer cells with epithelial differentiation traits (α6-integrin^{+}/EpCAM^{+} cancer cells), a mixed population of epithelial α6-integrin^{+}/EpCAM^{+} and mesenchymal-like α6-integrin^{+}/EpCAM^{-} cancer cells was detected in MD/PD-SCCs at intermediate stages of progression (Figure 12b). Furthermore, the subsequent engraftment of these MD/PD-SCCs led to the generation of PD/S-SCCs, which contained only

mesenchymal-like α6-integrin^{+}/EpCAM^{-} cancer cells (Figure 12b). These results indicate that, during SCC progression, epithelial cancer cells acquire a strong plasticity and mesenchymal-like EpCAM^{-} cancer cells are generated by the reprogramming of E-CSCs.

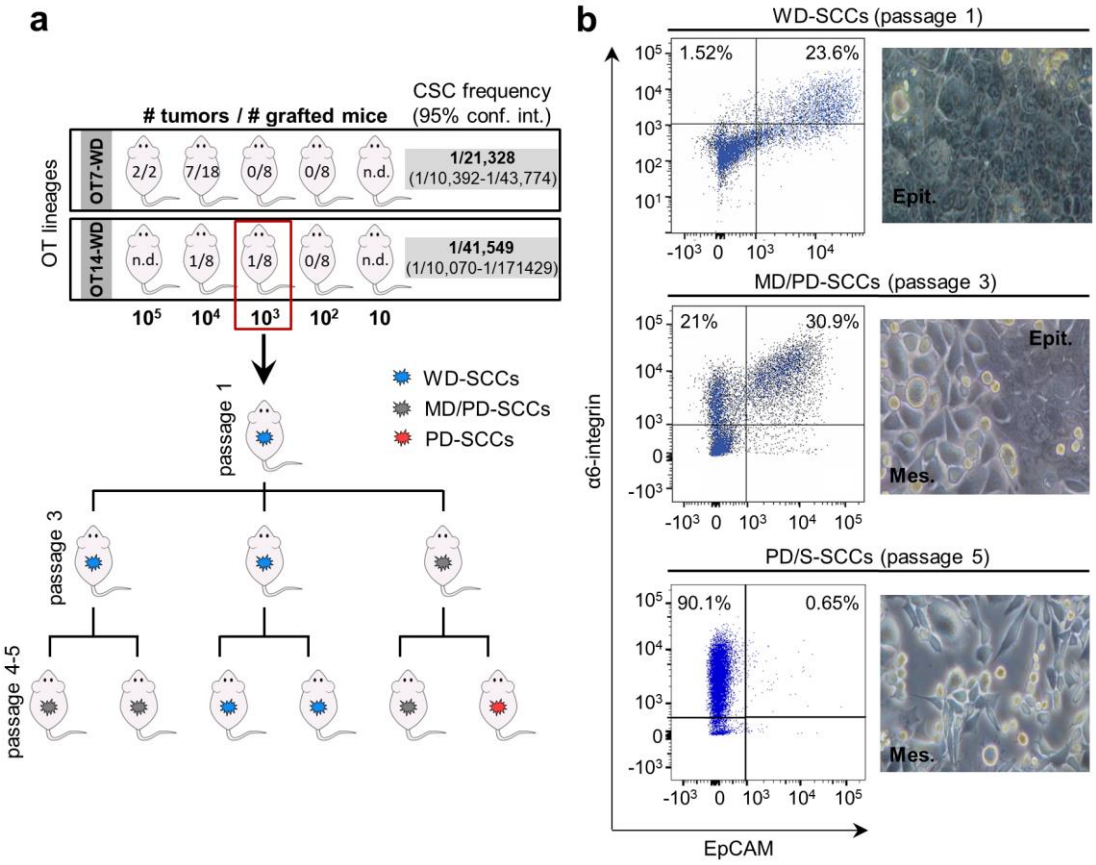

Figure 12. Mesenchymal-like EpCAM^{-} cancer cells are generated by the reprogramming of E-CSCs. a. Serial dilutions of cancer cells isolated from WD-SCCs from the indicated lineages (OT) were injected into immunodeficient mice. The number of tumors generated, frequency of CSCs, and confidence intervals (conf. int.) for each condition are shown (n.d., not determined). Then, WD-SCCs from a putative single E-CSCs were generated and serially transplanted into immunodeficient mice, generating different SCC lineages. **b.** Representative flow cytometry plots showing the frequency of α6-integrin$^{+/}$EpCAM^{+} or EpCAM^{-} cancer cells within WD-SCCs, MD/PD-SCCs, and PD/S-SCCs. Representative cell culture images of cancer cells isolated from WD-SCCs, MD/PD-SCCs, and PD/S-SCCs, indicating cancer cells with epithelial (Epit.) and mesenchymal (Mes.) morphology.

Indeed, we observed that full epithelial cancer cells isolated from WD-SCCs gave rise to full epithelial tumors (mostly containing EpCAM^{+} cancer cells) when they were engrafted in immunodeficient or immunocompetent syngeneic mice, whereas PD/S-SCCs exhibiting mesenchymal traits were generated when EpCAM^{-} cancer cells were engrafted (Figure 13). In contrast, epithelial EpCAM^{+} cancer cells from MD/PD-SCCs gave rise to tumors containing a variable percentage of mesenchymal-like EpCAM^{-} cancer cells, confirming the plastic phenotype of this cancer cell population and suggesting that this variability could be consequence of the strong

heterogeneity present in the EpCAM$^+$ cancer cell population (Figure 13). Furthermore, as this plastic behavior occurs both in T-cell deficient mice and under the pressure of a full immune system in immunocompetent syngeneic mice, these data denote that T cells may not be key drivers to promote this dynamic behavior during SCC progression.

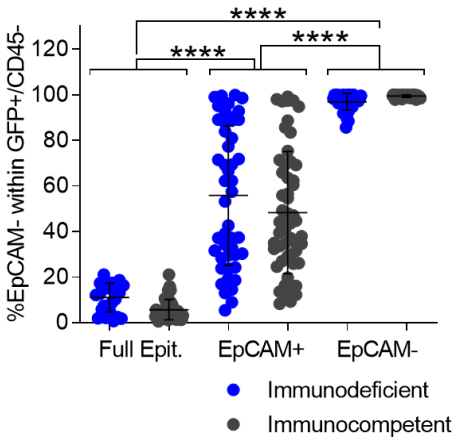

Figure 13. Epithelial EpCAM$^+$ cancer cells from MD/PD-SCCs are a plastic population that show the ability to switch to mesenchymal-like EpCAM$^-$ cancer cells under tumor growth. Percentage of mesenchymal (GFP$^+$/CD45$^-$/EpCAM$^-$) cancer cells in tumors generated after the engraftment in immunodeficient and immunocompetent syngeneic mice of full epithelial (Full Epit.) cancer cells isolated from WD-SCCs, epithelial EpCAM$^+$ and mesenchymal EpCAM$^-$ cancer cells isolated from MD/PD-SCCs, as determined by flow cytometry. Each symbol represents a single tumor and mean ± SD is shown. One-way ANOVA followed by Tukey's multiple comparison test; ****p≤0.0001.

1.2- Characterization of plastic epithelial EpCAM$^+$ cancer cells isolated from MD/PD-SCCs

Given the strong cancer cell heterogeneity generated after the engraftment of epithelial EpCAM$^+$ cancer cells, we characterized this population. Together with another member of the lab (Marta López Cerdá, PhD student), we identified that epithelial EpCAM$^+$ cancer cells were a heterogeneous population, containing cancer cells with a variable expression of the epithelial marker EpCAM.

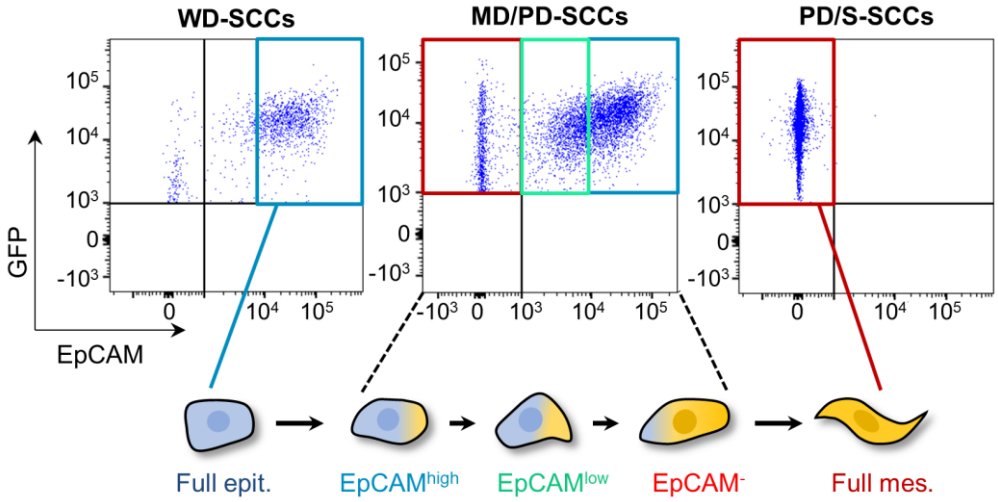

Figure 14. Flow cytometry strategy to isolate cancer cells during SCC progression. Representative flow cytometry plots showing the gating of full epithelial, EpCAM^{high}, EpCAM^{low}, EpCAM^{-} and full mesenchymal cancer cells isolated from WD-SCCs, MD/PD-SCCs and PD/S-SCCs by the intensity of the EpCAM marker.

To characterize them, we isolated full epithelial cancer cells from WD-SCCs, EpCAM^{high}, EpCAM^{low} (epithelial EpCAM^{+} cancer cells) and mesenchymal-like EpCAM^{-} cancer cells from MD/PD-SCCs by FACS sorting (Figure 14), and we grew them in *in vitro* culture during several weeks. We observed that EpCAM^{high}, EpCAM^{low}, and mesenchymal-like EpCAM^{-} cancer cells from MD/PD-SCCs initially had the ability to generate *in vitro* the other cell types during 3-4 weeks after isolation by FACS sorting (Figure 15a). However, this ability was lost after long-term *in vitro* growth, and only EpCAM^{low} cancer cells conserved a strong plasticity to reverse dynamically into EpCAM^{high} and to switch to mesenchymal-like EpCAM^{-} cancer cells (Figure 15a). This ability to switch from an epithelial to a mesenchymal phenotype was never observed in full epithelial cancer cells from WD-SCCs (Figure 15a). In addition, we compared the plasticity of these cancer cell populations *in vivo*. For this purpose, we engrafted full epithelial, EpCAM^{high}, EpCAM^{low}, and mesenchymal-like EpCAM^{-} cancer cells in immunocompetent syngeneic mice. Full epithelial cancer cells gave rise to full epithelial tumors (WD-SCCs), mostly containing epithelial EpCAM^{+} cancer cells (≈70% of EpCAM^{high} and ≈20% of EpCAM^{low} cancer cells), whereas EpCAM^{-} cell-derived tumors were comprised exclusively by mesenchymal-like EpCAM^{-} cancer cells (PD/S-SCCs) (Figure 15b). Interestingly, while EpCAM^{high} cancer cells showed a moderate ability to generate mesenchymal-like EpCAM^{-} cancer cells (MD/PD-SCCs), EpCAM^{low} cell-derived tumors contained about 95% of mesenchymal-like EpCAM^{-} cancer cells (Figure 15b). These results indicate that the presence of plastic epithelial cancer cells at early stages could be a risk factor of SCC progression, as they show a stronger plasticity and ability to progress to mesenchymal-like EpCAM^{-} cancer cells.

a

	Initial isolated cells			3-4 week (NO FACS sorting)			6-8 week (2-3 FACS sorting)		
Tumor cells	Ep. high	Ep. low	Ep. neg	Ep. high	Ep. low	Ep. neg	Ep. high	Ep. low	Ep. neg
Full Epit. 1	100	0	0	99,8	0,2	0	99,9	0,1	0
Full Epit. 2	100	0	0	99,7	0,3	0	99,9	0,1	0
Ep. high 1	100	0	0	5,5	28	61,1	98,9	0,5	0,5
Ep. high 2	100	0	0	4,1	20,7	70,1	99,7	0,3	0
Ep. low 1	0	100	0	2,6	35	58,4	21	24	49
Ep. low 2	0	100	0	9,8	46,7	34,6	16,6	58,4	12,8
Ep. neg 1	0	0	100	1,2	4	93,7	0,6	5,5	92,5
Ep. neg 2	0	0	100	1,5	18,6	76,6	11,7	1,8	85,9

b

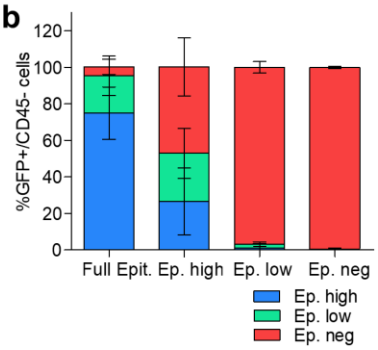

Figure 15. Epithelial EpCAM^{low} cancer cells show a strong plasticity and the ability to progress to mesenchymal-like EpCAM^{-} cancer cells under *in vitro* and *in vivo* growth. a. Percentage of EpCAM^{high} (Ep. high), EpCAM^{low} (Ep. low) and EpCAM^{-} (Ep. neg) cancer cells generated under *in vitro* growth from full epithelial cancer cells (GFP^{+}/CD45^{-}/EpCAM^{high}) isolated from WD-SCCs (n=2), and from GFP^{+}/CD45^{-}/EpCAM^{high}, GFP^{+}/CD45^{-}/EpCAM^{low} and GFP^{+}/CD45^{-}/EpCAM^{-} cancer cells isolated from MD/PD-SCCs (n=2), as determined by flow cytometry. The epithelial or mesenchymal state of these cancer cells was assessed by flow cytometry 3-4 weeks after the initial isolation by FACS sorting. To maintain a more stable phenotype during cell culture, these populations were re-sorted 2-3 times and their ability to dynamically shift continued to be evaluated. **b.** Flow cytometry quantification of GFP^{+}/CD45^{-}/EpCAM^{high}, GFP^{+}/CD45^{-}/EpCAM^{low} and GFP^{+}/CD45^{-}/EpCAM^{-} cancer cells in tumors generated after the engraftment in immunocompetent syngeneic mice of full epithelial cancer cells isolated from WD-SCCs, EpCAM^{high}, EpCAM^{low} and mesenchymal-like EpCAM^{-} cancer cells isolated from MD/PD-SCCs. All data are presented as mean ± SD.

To further characterize the molecular features of these cancer cell populations, we isolated full epithelial cancer cells (GFP^{+}/CD45^{-}/EpCAM^{high}) from WD-SCCs; EpCAM^{high} (GFP^{+}/CD45^{-}/EpCAM^{high}), EpCAM^{low} (GFP^{+}/CD45^{-}/EpCAM^{low}) and mesenchymal-like EpCAM^{-} (GFP^{+}/CD45^{-}/EpCAM^{-}) cancer cells from MD/PD-SCCs; and full mesenchymal cancer cells (GFP^{+}/CD45^{-}/EpCAM^{-}) from PD/S-SCCs by FACS-sorting assays (Figure 14). Then, we obtained RNA from these isolated cancer cells, which was amplified as cDNA by pico profiling assays (Functional Genomics Core, IRB Barcelona). The characterization by qRT-PCR of these populations demonstrated that EpCAM^{high} cancer cells from MD/PD-SCCs start downregulating the expression of some epithelial differentiation genes such as *Ovol1* and *Grhl1*, and slightly induced the expression of the mesenchymal gene *Vimentin* and the EMT-TF *Zeb1* compared to full epithelial cancer cells (Figures 16a to 16c). We also observed that EpCAM^{low} cancer cells further downregulated epithelial differentiation genes (*Cdh1*, *EpCAM*, *Ovol1* and *Ovol2*) and strongly upregulated *Vimentin* and EMT-TFs such as *Snail*, *Twist*, *Zeb1* and *Zeb2* compared to full epithelial and EpCAM^{high} cancer cells (Figures 16a to 16c). However, although this population had a strong expression of mesenchymal genes, the expression of epithelial differentiation genes in EpCAM^{low} cancer cells was still higher than those expressed by mesenchymal-like EpCAM^{-} and full mesenchymal cancer cells (Figures 16a to 16c).

These results indicate that epithelial EpCAM^{high} cancer cells represent an initial plastic state, being the EpCAM^{low} a cell population with hybrid epithelial-mesenchymal features and a strong ability to switch toward the mesenchymal-like state. The identification of this population in our SCC model is important since the presence of hybrid epithelial-mesenchymal cancer cells has been associated with poor patient survival and chemotherapy resistance in other tumor types such as breast, ovarian, HNSCC, pancreatic and prostate cancers (Grosse-Wilde et al., 2015; Puram et al., 2017; Smith and Bhowmick, 2016; Strauss et al., 2009).

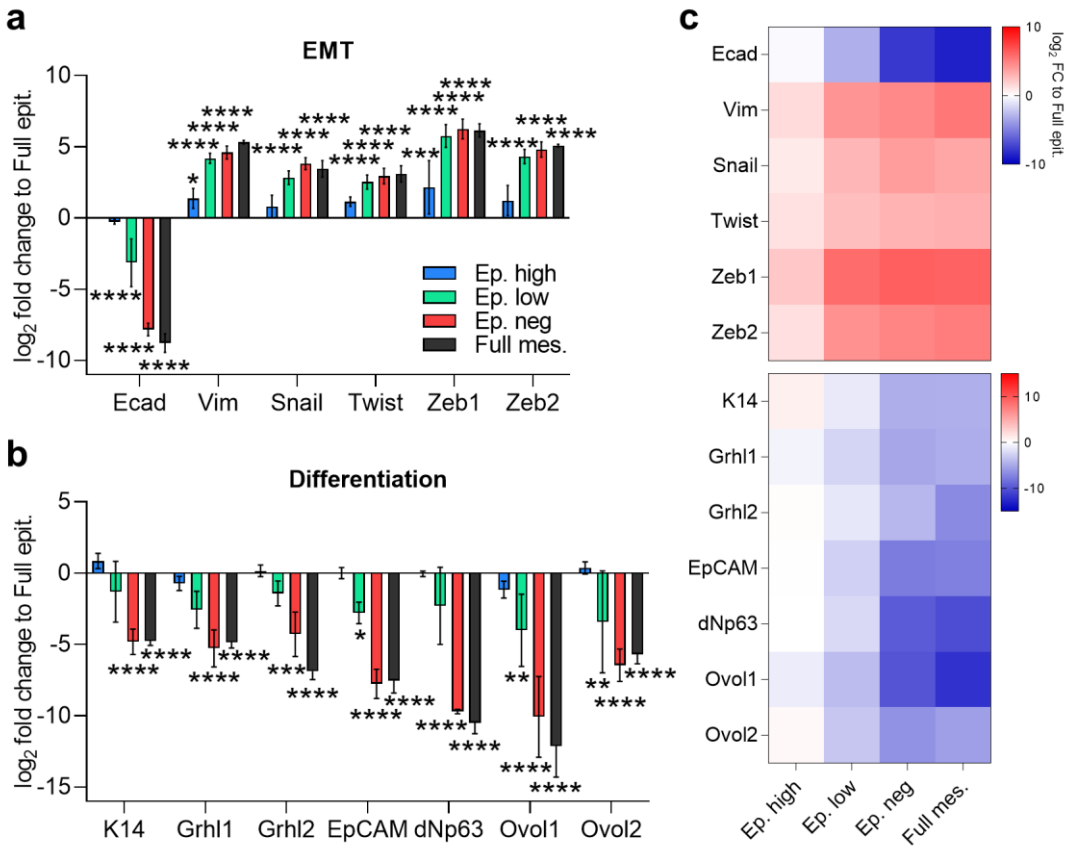

Figure 16. EpCAM^{low} cancer cells show hybrid epithelial-mesenchymal features. Gene expression levels (mean ± SD) of a subset of (**a**) EMT and (**b**) epithelial differentiation genes in EpCAM^{high} (Ep. high), EpCAM^{low} (Ep. low), EpCAM^{-} (Ep. neg) and full mesenchymal (Full mes.) cancer cells represented as the fold change (log_2) relative to full epithelial cancer cells, as quantified by qRT-PCR. mRNA levels of indicated genes were normalized to *Gapdh* and *Ppia* mRNA. **c.** Heat map showing gene expression levels of the indicated genes. Same data that in plots (**a, b**). (**a, b**) One-way ANOVA followed by Dunnett's multiple comparison test; *p≤0.05, **p≤0.01, ***p≤0.001, ****p≤0.0001.

Next, we evaluated whether these hybrid EpCAM^{low} cancer cells (dual EpCAM/Vimentin expression) could be histologically identified at intermediate stages of SCC progression. Immunofluorescence assays were performed to determine the presence of epithelial GFP^{+}/EpCAM^{+}/Vimentin^{-}, hybrid GFP^{+}/EpCAM^{+}/Vimentin^{+} and mesenchymal-like GFP^{+}/EpCAM^{-}/Vimentin^{+} cancer cells in epithelial (WD-SCCs), mixed (MD/PD-SCCs) and mesenchymal tumors (PD/S-SCCs, Figure 17a). We observed that the frequency of epithelial GFP^{+}/EpCAM^{+}/Vimentin^{-} cancer cells per tumor area slightly decreased in mixed tumors as compared to epithelial tumors and disappeared in mesenchymal tumors (Figures 17b and 17e). In addition, whereas the expression of Vimentin was only detected in stromal cells of epithelial tumors, Vimentin expression was increased in a subset of cancer cells in mixed tumors and was highly expressed in most mesenchymal-like EpCAM^{-} cancer cells (Figures 17d and 17e). We also noticed that the frequency of hybrid GFP^{+}/EpCAM^{+}/Vimentin^{+} cancer cells per tumor area specifically increased in mixed tumors,

coinciding with the appearance of hybrid EpCAM^{low} cancer cells at intermediate stages of progression (Figures 17c and 17e). Despite that all epithelial EpCAM^{+} cancer cells showed histopathological similarities, these assays allowed us to discriminate between EpCAM^{high} cancer cells with an epithelial phenotype characterized by single EpCAM expression, and hybrid epithelial-mesenchymal cancer cells at intermediate stages. For all these reasons, another member of the lab (Marta López Cerdá, PhD student) is currently working on demonstrating the potential role of these hybrid epithelial-mesenchymal cancer cells as early prognostic markers of SCC progression, along with other plasticity markers that are under investigation.

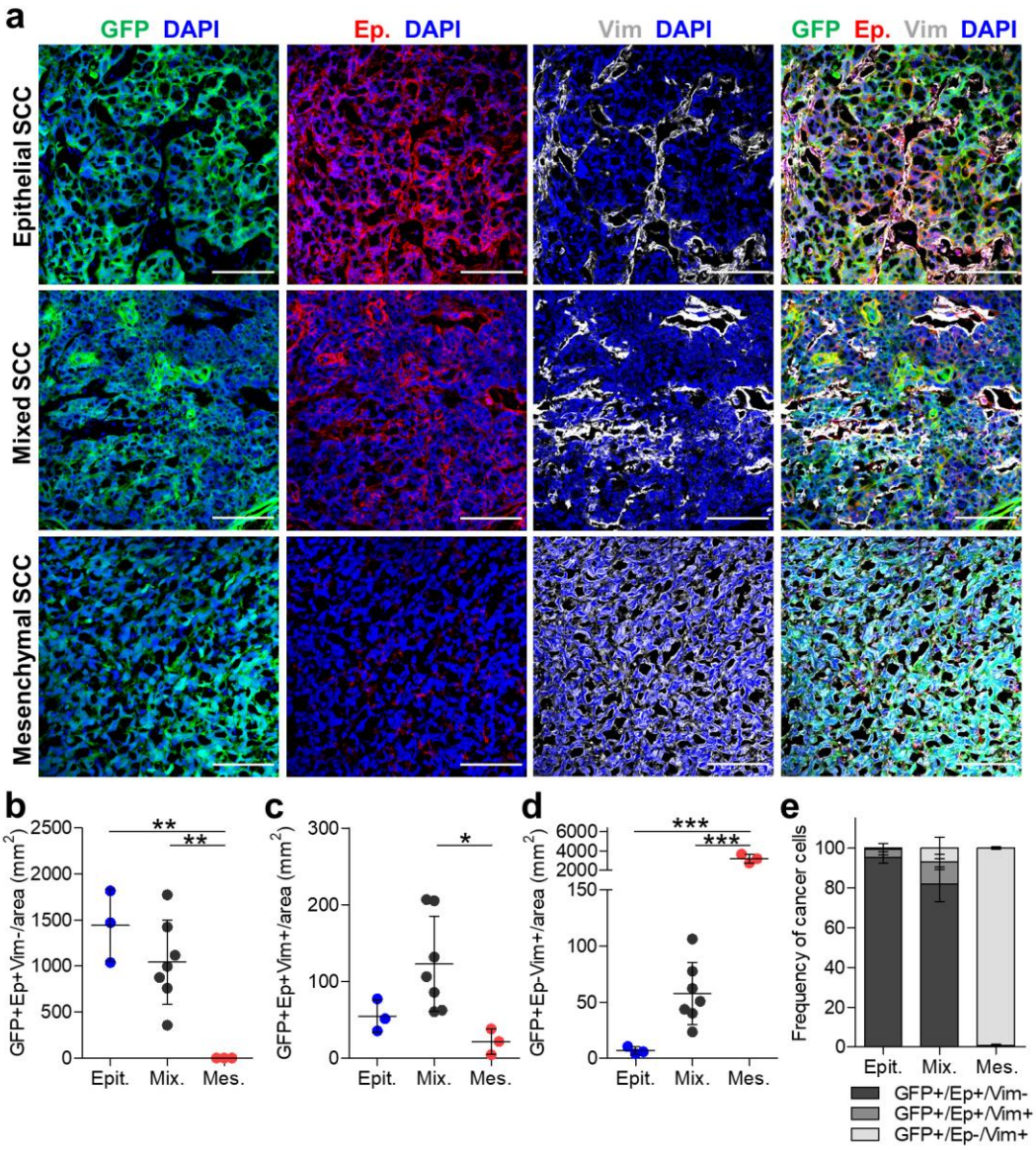

Figure 17. Hybrid cancer cell frequency is increased at intermediate stages of progression. a. Representative immunofluorescence images of GFP^{+}, EpCAM^{+}, Vimentin^{+} cancer cells and DAPI labelled cell nuclei in epithelial, mixed and mesenchymal SCCs. Scale bar: 100 µm. Quantification of the frequency of (**b**) epithelial GFP^{+}/EpCAM^{+}/Vimentin^{-}, (**c**) hybrid GFP^{+}/EpCAM^{+}/Vimentin^{+}, and (**d**) mesenchymal GFP^{+}/EpCAM^{-}/Vimentin^{+} cancer cells per tumor area (mm^{2}) in epithelial (n=3), mixed (n=7) and mesenchymal (n=3) tumors. At least 8 fields of different regions were quantified in each tumor. Each symbol

represents a single tumor and mean ± SD for each group is shown. **e**. Percentage (mean ± SD) of $GFP^+/EpCAM^+/Vimentin^-$, $GFP^+/EpCAM^+/Vimentin^+$, and $GFP^+/EpCAM^-/Vimentin^+$ cancer cells relative to total cancer cells in the indicated tumors. (**b-d**) One-way ANOVA followed by Tukey's multiple comparison test; *p≤0.05, **p≤0.01, ***p≤0.001.

1.3- Identification of signaling pathways regulating cancer-cell plasticity and SCC progression

Given the importance of elucidating the mechanisms contributing to cancer-cell plasticity during SCC progression, we decided to identify kinase-dependent signaling pathways responsible of these processes via phosphoproteomic analysis. These analyses were important because, by focusing on activated cell circuitry, we gained insights into cancer-cell regulation not available at the transcriptional level. To tackle this project, I moved during 3 months to the OncoProteomics Laboratory at the VU University Medical Center (Amsterdam, The Netherlands) under the supervision of Prof. Dr. Connie R. Jimenez (EMBO Short-Term stay). In this highly specialized phosphoproteomic laboratory, we compared the large-scale and phospho-tyrosine phospho-proteomes by mass spectrometry-based profiling of full epithelial cancer cells isolated from WD-SCCs, epithelial $EpCAM^+$ and mesenchymal-like $EpCAM^-$ cancer cells isolated from MD/PD-SCCs, and full mesenchymal cancer cells isolated from PD/S-SCCs.

To obtain an overview of SCC progression, we performed cluster analysis of differential phosphorylation at serine (Ser, S), threonine (Thr, T) and tyrosine (Tyr, Y) residues, which revealed that the phospho-proteome of each population clustered closely and was distinct from other stages (Figures 18a and 18b). With all this information, we characterize the proteome profile of epithelial $EpCAM^+$ cancer cells, since as previously mentioned, they showed the ability to switch to mesenchymal $EpCAM^-$ cancer cells during SCC progression. The phosphoproteomic comparison between full epithelial and epithelial $EpCAM^+$ cancer cells identified a total of 366 phosphosites that were differentially phosphorylated (FDR $p<0.05$, Figure 18a). Among these differentially identified phosphosites, 152 enriched phosphopeptides belonged to 132 unique proteins, and 214 lost phosphopeptides belonged to 158 unique proteins (Figure 18a). These differentially phosphorylated proteins were then categorized using Gene Ontology (GO) analysis to identify processes and pathways activated or inhibited specifically in epithelial $EpCAM^+$ cancer cells as compared to full epithelial cancer cells. The identified enriched phosphoproteins in epithelial $EpCAM^+$ cancer cells were involved in GO biological process such as cytoskeleton organization, cell division, cell cycle, cell migration, response to growth factors, cellular response to stress and immune system development, among others (Figure 18c). Conversely, a decrease in the phosphorylation of proteins in $EpCAM^+$ cancer cells was mainly observed in those involved in cellular, cytoskeleton and organelle organization, cell junction assembly, epithelial cell differentiation and cell proliferation, among others (Figure 18d). These results also revealed some pathways that could be involved in the acquisition of the plastic phenotype such as mTOR, ErbB,

PI3K-Akt, integrin-mediated and insulin signaling pathways. In addition, using GSEA analysis, we identified several kinases that were hyperphosphorylated in epithelial EpCAM$^+$ cancer cells as compared to full epithelial cancer cells, including ARAF, AXL, CDC42BPA, CDK12, DYRK1A, IGF-1R, MAP3K3, PKN2, PTK2, TRIM28 and WNK1. These results suggest that the activation of some of these kinases or pathways could lead to the acquisition of cancer-cell plasticity during SCC progression.

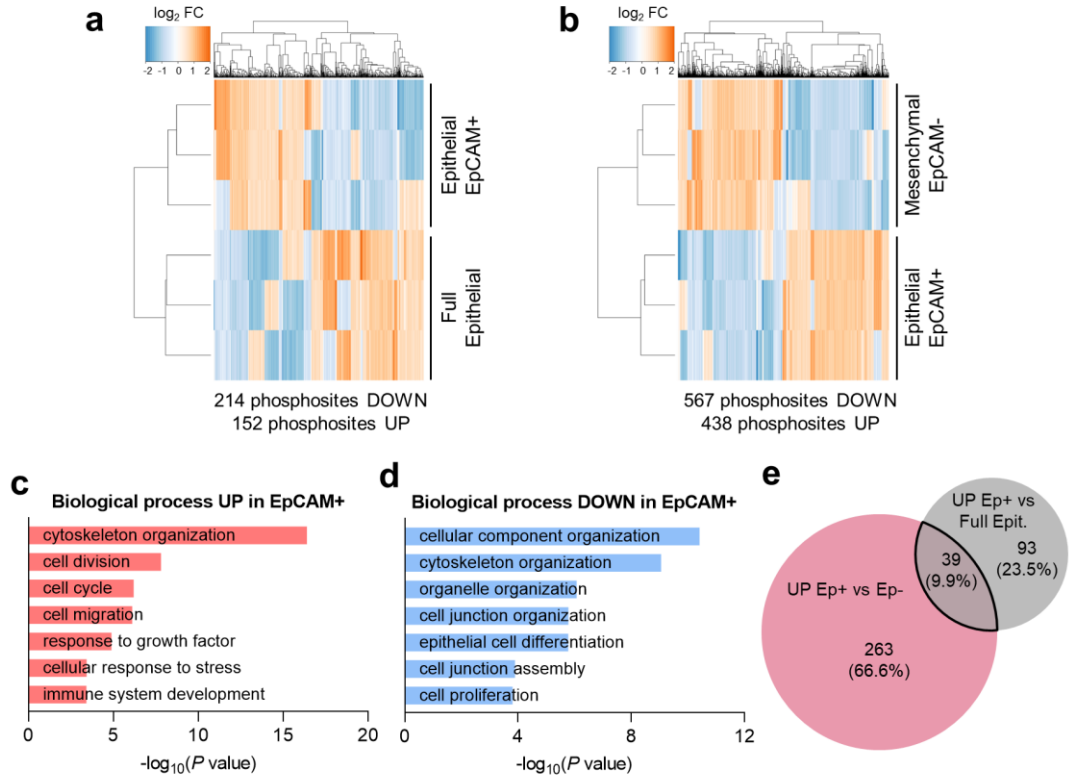

Figure 18. Phospho-proteome profile changes in cancer cells during SCC progression. Supervised hierarchical cluster analysis of differentially phosphorylated peptides (FDR p<0.05, columns) between (**a**) full epithelial and epithelial EpCAM$^+$ cancer cells and between (**b**) epithelial EpCAM$^+$ and mesenchymal-like EpCAM$^-$ cancer cells isolated from mouse skin SCCs (three samples per group, rows). Gene ontology (GO) analysis of (**c**) enriched (UP) or (**d**) less abundant (DOWN) proteins in EpCAM$^+$ cancer cells as compared to full epithelial cancer cells. **e.** Venn diagram showing the overlap of proteins from the unique EpCAM$^+$ signature vs full epithelial or mesenchymal-like EpCAM$^-$ cancer cells.

To study the relevance of these kinases and pathways in the acquisition of cancer-cell plasticity, we studied if the activation of some of them could be specific of epithelial EpCAM$^+$ cancer cells. To address this, we focused on those phosphorylations that were specifically acquired in epithelial EpCAM$^+$ cancer cells in comparison to full epithelial cancer cells, and that were lost during the switch toward mesenchymal-like EpCAM$^-$ cancer cells (Figures 18a and 18b). We identified 39 common proteins (9.9%) enriched in epithelial EpCAM$^+$ cancer cells (Figure 18e, AEBP2, ANO1, ARHGAP18, ARHGEF2, ATXN2L, BCAR1, BCAR3, CHAMP1, CSRP1, EEF1A1, EPHA2,

GTF3C1, HNRNPA3, IER3, IGF-1R, KDF1, MARCKS, MARCKSL1, NECTIN1, NEDD9, NIPAL4, OTUD4, PCNT, PHACTR4, PLEC, PLEKHG3, PRAG1, RALY, RPL15, SEPT9, SHB, SON, SREK1IP1, SRRM2, STMN1, TANC1, TCF20, TJP2, TLN1). Among the previously listed proteins, we focused our attention in the insulin-like growth factor 1 receptor (IGF-1R), as it is a tyrosine kinase receptor involved in cell growth and survival, and it is crucial for tumor transformation and survival of malignant cells (Zha and Lackner, 2010). In this regard, we observed that IGF-1R was hyperphosphorylated in the residues Y1167 and Y1168 in epithelial EpCAM$^+$ cancer cells and its phosphorylation levels decreased in the residues Y1163, Y1167 and Y1168 in mesenchymal-like EpCAM$^-$ cancer cells during SCC progression. The phosphorylation of these three tyrosine residues is necessary to facilitate the stabilization of the kinase activation loop (A-loop) in a position that promotes catalysis and the subsequent phosphorylation of several substrates (PhosphositePlus database). Specifically, the phosphorylation of IGF-1R leads to the activation of two main signaling pathways: the PI3K-AKT/PKB pathway and the Ras-MAPK pathway, which were also identified as being involved in the acquisition of the plastic EpCAM$^+$ phenotype by GO analysis. The result of MAPK pathway activation is an increase in cellular proliferation, whereas the activation of the PI3K pathway triggers anti-apoptotic effects through the inactivation of BAD/Bcl2 and stimulates protein synthesis through mTOR activation (Iams and Lovly, 2015). The phosphorylation of these residues specifically in EpCAM$^+$ cancer cells highlight the important role that these signaling pathways may play in epithelial EpCAM$^+$ cancer cells. Altogether, these results reveal that IGF-1R pathway is induced specifically in epithelial EpCAM$^+$ cancer cells, being a good candidate to regulate the acquisition of cancer-cell plasticity and the switch between the epithelial and the mesenchymal-like phenotype.

From all these data that I generated, another member of the lab (Marta López Cerdá, PhD student) is currently evaluating the potential role of IGF-1R signaling pathway, among other kinases, on promoting cancer-cell plasticity and the acquisition of the mesenchymal-like state in epithelial EpCAM^{high} and EpCAM^{low} cancer cells. These studies have been the starting point to explore the impact of these kinases and pathways on cancer-cell plasticity and SCC progression, and they are key to design novel targeted therapies that specifically target those molecules to suppress SCC growth and metastasis development.

Summary Chapter 1: Cancer-cell features change during SCC progression

The results presented in Chapter 1 demonstrate that cancer-cell features change during SCC progression. We observed that early WD-SCCs conserve epithelial differentiation traits, as the expression of EpCAM and E-cadherin markers, among others. After serial engraftments in mice, WD-SCCs evolve into MD/PD-SCCs, which are formed by a mixed population of epithelial EpCAM$^+$ and mesenchymal-like EpCAM$^-$ cancer cells. The subsequent engraftment of these mixed

MD/PD-SCCs give rise to PD/S-SCCs, which are comprised exclusively by mesenchymal-like EpCAM^{-} cancer cells. Interestingly, during this dynamic progression of cancer cells toward the mesenchymal-like state, we detected the appearance of EpCAM^{low} cancer cells in MD/PD-SCCs at intermediate stages of progression. This population shows a hybrid epithelial-mesenchymal phenotype, as it expresses low levels of epithelial markers such as EpCAM, E-cadherin and K14, but also upregulates the expression of mesenchymal markers such as Vimentin and EMT-inducer TFs (*Snail*, *Twist*, *Zeb1*, and *Zeb2*). In addition, these hybrid EpCAM^{low} cancer cells comprise a population of highly plastic cancer cells, which evolve into mesenchymal-like EpCAM^{-} cancer cells after its engraftment in immunodeficient and immunocompetent syngeneic mice. These results demonstrate the potential role of these hybrid epithelial-mesenchymal cancer cells as early prognostic markers of SCC progression. Since the progression to the mesenchymal-like state was enhanced during tumor growth, our results also indicate that signals provided by the TME could promote cancer-cell plasticity and SCC progression. Furthermore, large-scale and phospho-tyrosine phospho-proteome analysis of full epithelial, epithelial EpCAM^{+}, mesenchymal-like EpCAM^{-} and full mesenchymal cancer cells reveal some kinases and pathways that could lead to the acquisition of cancer-cell plasticity and which are currently under investigation in our group. In particular, IGF-1R pathway is induced specifically in epithelial EpCAM^{+} cancer cells, being a good candidate to understand the switch toward the mesenchymal-like phenotype.

CHAPTER 2. CHARACTERIZATION OF TUMOR IMMUNE MICROENVIRONMENT ALTERATIONS RESPONSIBLE OF PROMOTING CANCER-CELL PLASTICITY AND SCC PROGRESSION

Since the progression from epithelial to mesenchymal-like cancer cells was preferentially enhanced during tumor growth in immunodeficient and immunocompetent syngeneic mice (Figure 13), our results suggest that TME signals could promote the plasticity of epithelial cancer cells to acquire the mesenchymal-like state during SCC progression. In this regard, the comparison of gene expression profile of stromal fibroblasts (α6-integrin$^-$/CD31$^-$/CD45$^-$ cells, Figure 19a) and tumor-infiltrating immune cells (α6-integrin$^-$/CD31$^-$/CD45$^+$ cells, Figure 19b) isolated from full epithelial WD-SCCs and from mixed MD/PD-SCCs generated in immunodeficient mice showed significant changes in the TME profile during SCC progression.

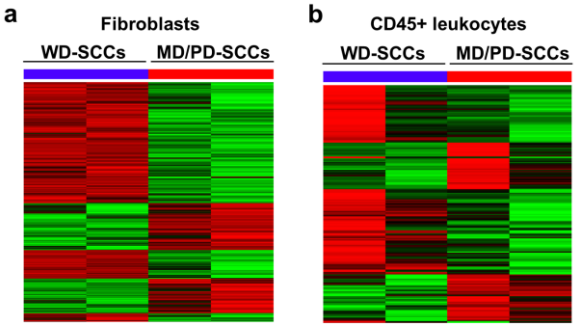

Figure 19. Tumor microenvironment profile changes during SCC progression. Hierarchical cluster analysis of differentially expressed genes (log_2 FC ≥ 1; FDR p<0.05) between (**a**) stromal fibroblasts (α6-integrin$^-$/CD31$^-$/CD45$^-$ cells) and (**b**) tumor-infiltrating immune cells (α6-integrin$^-$/CD31$^-$/CD45$^+$ cells) isolated by FAS-sorter from MD/PD-SCCs and their respective WD-SCC precursors (three sample per group), as detected by microarray assays.

The comparison of stromal fibroblasts indicated that the expression of *Bmp2*, *Clcf1*, *G-Csf*, *Cx3cl1*, *Cxcl14*, *Cxcl7*, *Igf2* and *Osteopontin* were significantly induced in fibroblasts of MD/PD-SCCs, as compared to those from WD-SCCs. Some of these cytokines have been previously related to EMT induction and migration (BMP2, CX3CL1, Osteopontin and IGF2) and in the recruitment and polarization of macrophages to M2 subtype (CX3CL1, CSF3/G-CSF, and Osteopontin) in other tumor types (Griffith et al., 2014). In this regard, *Igf2* upregulation further strengthens our hypothesis about the potential impact of TME signals on the regulation of the IGF-1R pathway and the acquisition of cancer-cell plasticity. In contrast, the comparison of tumor-infiltrating immune cells did not reveal major changes in the cytokine profile between the two stages of progression. We thought this might be because these microarray analyses were performed on samples isolated from immunodeficient mice, and these mice do not have a full immune system because they are deficient in T lymphocytes. However, we found that the expression of *Cxcl7* was induced in tumor-infiltrating immune cells of MD/PD-SCCs. CXCL7 is a platelet-derived growth factor that functions as a potent

chemoattractant and activator of neutrophils through binding to its receptor CXCR2 (Griffith et al., 2014). CXCL7/CXCR2 axis has been described to play an important role in tumor growth in several types of cancer (Nagarsheth et al., 2017). In addition, the expression of the macrophage scavenger receptor and cluster of differentiation 204 (CD204), a M2-like marker (Aras and Zaidi, 2017; Sainz et al., 2016), was also induced in tumor-infiltrating immune cells of MD/PD-SCCs. Clinical data has indicated that a high frequency of M2-like macrophages is correlated with poor prognosis in a variety of human cancers such as breast, lung, prostate, ovarian and cervical cancers (Larionova et al., 2020). These results indicate that the cytokine-mediated crosstalk between cancer cells and the TME may play a relevant role in SCC progression, showing a possible relevance of fibroblasts, neutrophils and M2-like macrophages as inducers of cancer-cell plasticity. Therefore, we wonder whether the tumor immune microenvironment changes accordingly with cancer-cell features.

2.1- Changes in the frequency and features of tumor and immune cell components are observed during SCC progression

To characterize how tumor cell components change during SCC progression, we analyzed cancer-cell features and the immune cells recruited to WD-SCCs, MD/PD-SCCs and PD/S-SCCs by flow cytometry. To address this, WD-SCCs, MD/PD-SCCs and PD/S-SCCs were generated after engrafting full epithelial, epithelial EpCAM^{+} and mesenchymal-like EpCAM^{-} cancer cells in immunocompetent syngeneic mice, respectively. These tumors were then classified accordingly to the presence of epithelial EpCAM^{+} cancer cells, as: epithelial SCCs (Epit.; containing >70% EpCAM^{+} cancer cells), mixed SCCs (Mix.; containing 10-70% EpCAM^{+} cancer cells) and mesenchymal SCCs (Mes.; containing <10% EpCAM^{+} cancer cells) (Figure 20a). As it was described in the Chapter 1, epithelial tumors contained mainly EpCAM^{high} cancer cells (≈70%), followed by 20% of EpCAM^{low} and 10% of mesenchymal-like EpCAM^{-} cancer cells (Figures 20b to 20d). In mixed tumors, EpCAM^{high} cancer cells decreased to 20% (Figure 20b), due to the significant appearance of EpCAM^{low} cancer cells (Figure 20c) and the generation of mesenchymal-like EpCAM^{-} cancer cells (Figure 20d). Hence, there was a higher percentage of EpCAM^{low} (≈40%) and mesenchymal-like EpCAM^{-} cancer cells (≈40%) than EpCAM^{high} cancer cells (≈20%) at intermediate stages of progression (Figures 20b to 20d). In contrast, mesenchymal tumors were mostly composed of mesenchymal-like EpCAM^{-} cancer cells (Figure 20d).

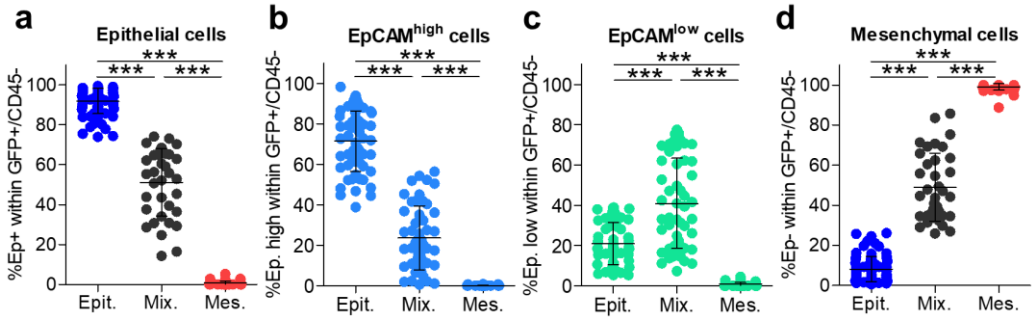

Figure 20. Cancer-cell features change during SCC progression. Percentage of (**a**) epithelial ($GFP^+/CD45^-/EpCAM^+$), (**b**) $EpCAM^{high}$ ($GFP^+/CD45^-/EpCAM^{high}$), (**c**) $EpCAM^{low}$ ($GFP^+/CD45^-/EpCAM^{low}$), and (**d**) mesenchymal ($GFP^+/CD45^-/EpCAM^-$) cancer cells in epithelial (n=79), mixed (n=36) and mesenchymal (n=59) tumors, as determined by flow cytometry. Each symbol represents a single tumor and mean ± SD for each group is shown. (**a-d**) One-way ANOVA followed by Tukey's multiple comparison test; ***p≤0.001.

The characterization of the growth kinetics of these tumors showed that epithelial tumors grew faster than mixed and mesenchymal tumors in immunocompetent syngeneic mice (Figure 21a). However, mice bearing mesenchymal tumors showed more frequent metastasis, occurring mainly in the lungs and regional lymph nodes, than mice bearing epithelial and mixed tumors (Figure 21b), and no significant differences were detected in the metastasis latency (Figure 21c). Nevertheless, the overall frequency of metastasis was lower in immunocompetent than in immunodeficient mice (Figure 10d). Consequently, the presence of a full immune system in immunocompetent syngeneic mice could play a key role blocking the process of cancer-cell invasion and metastasis development, as previously reported (Granot et al., 2011; Hanahan and Weinberg, 2011; Maimon et al., 2021).

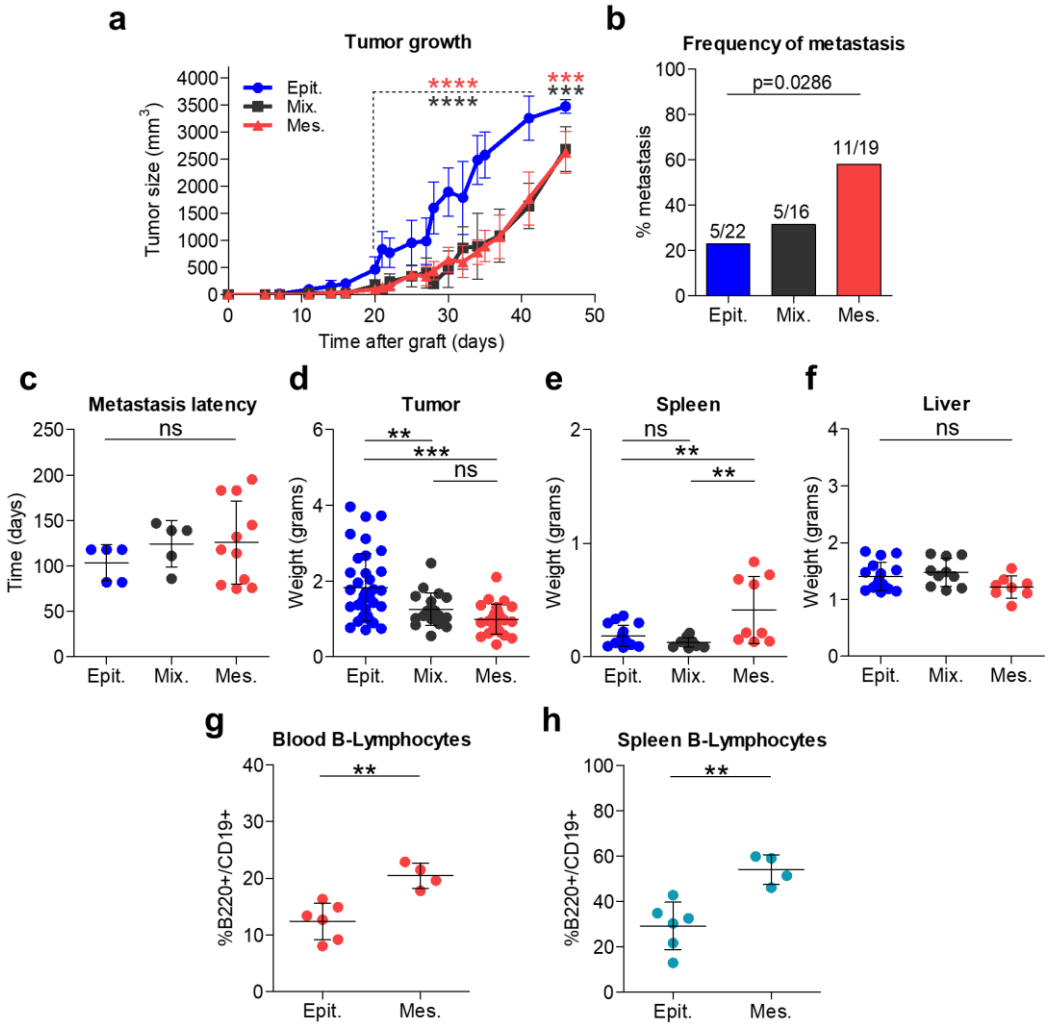

Figure 21. Characterization of skin SCCs generated in immunocompetent syngeneic mice. **a.** Growth kinetics of tumors generated after engrafting full epithelial (Epithelial, Epit.; n=79), epithelial $EpCAM^+$

(Mixed, Mix.; n=48) and mesenchymal-like EpCAM$^-$ cancer cells (Mesenchymal, Mes.; n=59). **b.** Percentage of mice developing metastatic lesions (mean) and metastasis frequency out of the total number of mice in each group (indicated in the fraction number). **c.** Latency time of metastasis development in the indicated groups. Weigh of (**d**) tumor, (**e**) spleen and (**f**) liver in the indicated groups. Percentage of (**g**) blood or (**h**) spleen B lymphocytes (B220$^+$/CD19$^+$ cells) in mice bearing epithelial (n=6) or mesenchymal (n=4) tumors. Each symbol represents a single mouse (**c**, **e**, **f**, **g**, **h**) or tumor (**d**), and mean ± SD for each group is shown. (**a**) Repeated Measures ANOVA test, where significance differences in tumor growth between epithelial and mixed tumors are indicated with grey *, and between epithelial and mesenchymal tumors with red *, (**b**) Fisher's exact test, (**c-f**) one-way ANOVA followed by Tukey's multiple comparison test, and (**g, h**) unpaired two-tailed Student's *t*-test; ns p>0.05, **p≤0.01, ***p≤0.001, ****p≤0.0001.

We also observed a reduction in the weight of mixed and mesenchymal tumors as compared to epithelial tumors (Figure 21d), and no changes in liver weight were detected (Figure 21f). Surprisingly, the spleen weight was significantly increased in mice bearing mesenchymal tumors compared to mice bearing epithelial or mixed tumors, reflecting the development of splenomegaly (Figure 21e), which might be associated with an increased workload of the spleen (Mackay, 1965). It is known that the spleen serves as a secondary lymphoid organ and it is the site for maturation and storage of T and B lymphocytes (Lewis et al., 2019). For that reason, we suggest that this splenomegaly might be related to the increased percentage of B lymphocytes (B220$^+$/CD19$^+$ cells) observed in the blood and spleen of mice bearing mesenchymal tumors (Figures 21g and 21h).

To assess whether we could detect changes in the cell components among these epithelial, mixed and mesenchymal tumors, we analyzed the presence of cancer cells (GFP$^+$/CD45$^-$ cells), fibroblasts (GFP$^-$/CD45$^-$ cells), and leukocytes (CD45$^+$ cells) by flow cytometry. Mesenchymal tumors contained a higher percentage of cancer cells (≈90%) than epithelial and mixed tumors, which correlates with the high viability and aggressiveness of these tumors (Figure 22a). In addition, fibroblast frequency was significantly reduced in mesenchymal tumors as compared to epithelial and mixed tumors (Figure 22b). Interestingly, epithelial tumors contained a high infiltrate of CD45$^+$ leukocytes, which was slightly reduced in mixed tumors and dramatically diminished in mesenchymal tumors (Figure 22c). The percentage of these immune cells did not change in the blood of mice bearing epithelial or mesenchymal tumors (Figure 22d), suggesting that the reduction of CD45$^+$ cells was specific to tumor-infiltrating leukocytes. After this interesting observation, we evaluated the differences in the recruitment and distribution of CD45$^+$ leukocytes in epithelial and mesenchymal tumors by immunofluorescence assays (Figure 22e). Importantly, in mouse epithelial SCCs, tumor regions were characterized by the presence of cancer cells in enclosed areas, which allows their clear distinction from stromal regions. Nevertheless, in mesenchymal SCCs it was not possible to differentiate intratumoral from stromal areas due to the higher invasion and presence of cancer cells (Figure 22e). Consistent with FACS analysis, a significant decreased of the frequency of CD45$^+$ leukocytes per tumor area was detected in mesenchymal tumors (Figures 22e and 22f).

We also observed that CD45$^+$ leukocytes were principally located in the stromal region of epithelial tumors, whereas a reduced percentage of these cells (≈20%) were located in intratumoral areas (Figure 22g). Contrarily, CD45$^+$ leukocytes were proximal to cancer cells (intratumoral areas) in mesenchymal tumors (Figure 22g).

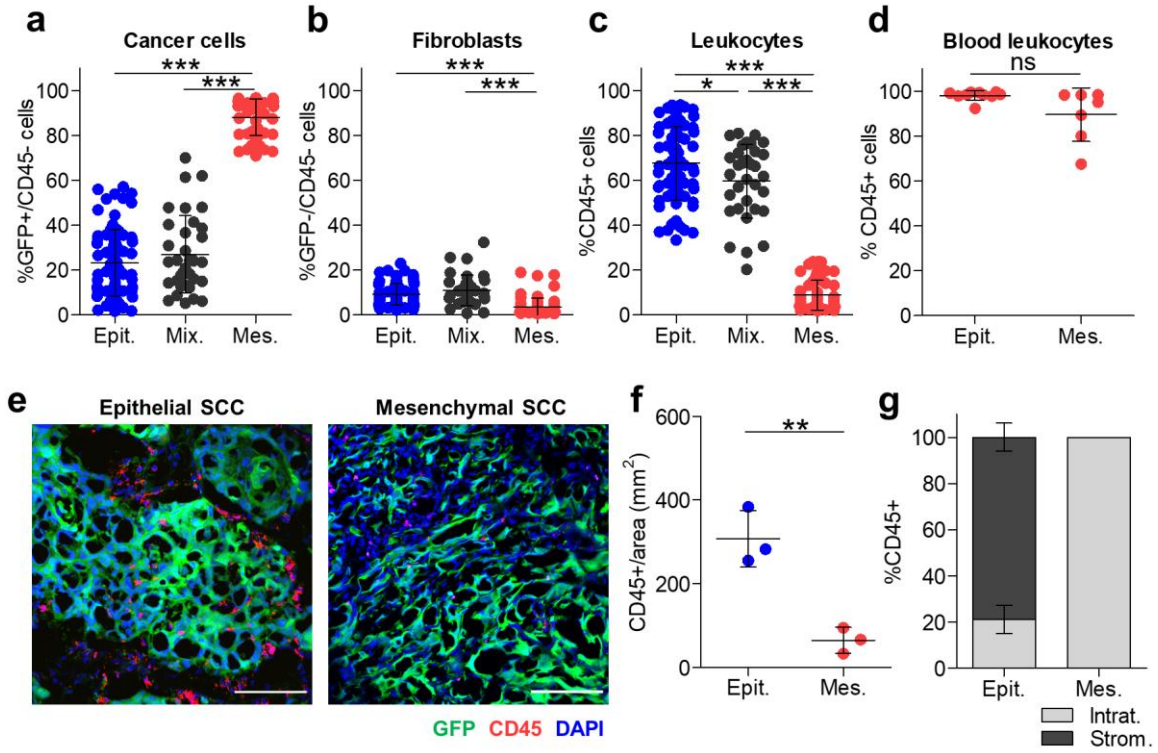

Figure 22. Tumor cell components change during SCC progression. Percentage of (**a**) cancer cells (GFP$^+$/CD45$^-$ cells), (**b**) fibroblasts (GFP$^-$/CD45$^-$ cells) and (**c**) leukocytes (CD45$^+$ cells) in epithelial (n=79), mixed (n=36) and mesenchymal (n=59) tumors, as determined by flow cytometry. **d**. Percentage of blood CD45$^+$ leukocytes in mice bearing epithelial (n=10) or mesenchymal (n=7) tumors. **e**. Representative immunofluorescence images of GFP$^+$ cancer cells, CD45$^+$ immune cells and DAPI labelled cell nuclei in epithelial and mesenchymal SCCs. Scale bar: 100 µm. **f**. Quantification of CD45$^+$ cells per tumor area (mm^2) in epithelial and mesenchymal SCCs (n=3). At least 5 fields of different regions were quantified in each tumor. Each symbol represents a single tumor and mean ± SD for each group is shown. **g**. Percentage (mean ± SD) of intratumoral or stromal CD45$^+$ cells relative to total CD45$^+$ leukocytes in the indicated tumors. (**a-c**) One-way ANOVA followed by Tukey's multiple comparison test, and (**d**, **f**) unpaired two-tailed Student's *t*-test; ns p>0.05, *p≤0.05, **p≤0.01, ***p≤0.001.

Subsequently, we quantified the percentage of necrotic areas, identified histologically by nuclear fragmentation, of different hematoxylin/eosin (H/E) sections of epithelial, mixed and mesenchymal SCCs (Figure 23a). It was consistent across the different tumor samples that epithelial and mixed tumors presented larger necrotic regions (30-60% of tumor area) than mesenchymal tumors (5-10% of tumor area) (Figure 23b), in accordance with the high cancer-cell viability observed by flow cytometry in mesenchymal tumors (Figure 22a). In addition, a strong CD45$^+$ leukocyte recruitment

was observed in the necrotic areas of epithelial and mixed tumors, which were infrequent in mesenchymal SCCs. Hence, our results suggest that the differences in the frequency of recruited $CD45^+$ leukocytes to epithelial, mixed and mesenchymal tumors may be due to a distinct ratio of necrotic regions between the indicated tumor types. In accordance, we observed that some immune cells such as $CD68^+$ macrophages and $Gr1^+$ MDSCs were mainly recruited to these necrotic areas (Figures 23c and 23d), possibly with the aim of eliminating dead cells. $CD8^+$ T lymphocytes and $CD163^+$ M2-like macrophages were excluded from these areas (Figures 23e and 23f).

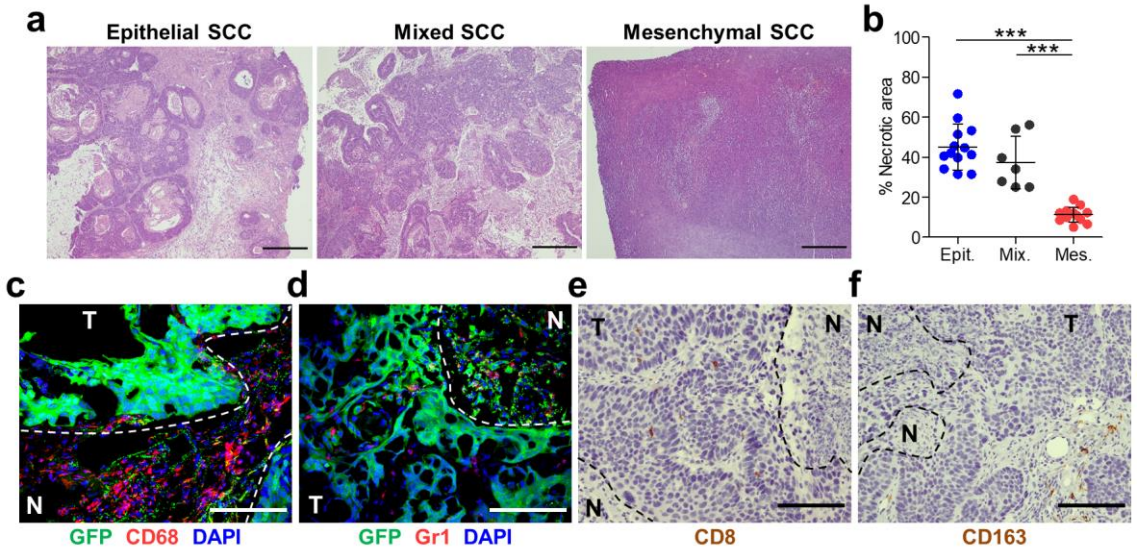

Figure 23. Epithelial and mixed tumors exhibit extensive necrotic areas compared to mesenchymal tumors. a. Representative hematoxylin/eosin (H/E) images of epithelial, mixed and mesenchymal SCCs. Scale bar: 100 µm. **b.** Percentage of necrotic areas relative to total tumor area in different sections of epithelial (n=13), mixed (n=7) and mesenchymal (n=13) tumors. Each symbol represents a single tumor and mean ± SD for each group is shown. Representative immunofluorescence images of GFP^+ cancer cells, (**c**) $CD68^+$ or (**d**) $Gr1^+$ immune cells and DAPI labelled cell nuclei, and immunohistochemistry images of (**e**) $CD8^+$ and (**f**) $CD163^+$ immune cells in SCCs. (T) indicates tumor region and (N) indicates necrotic areas. Scale bar: 100 µm. (**b**) One-way ANOVA followed by Tukey's multiple comparison test; ***$p \leq 0.001$.

Since in our SCC progression model the expression of E6/E7 oncogenes was under the control of the K14 promoter, whose expression was strongly reduced in PD/S-SCCs (Coussens et al., 1996; da Silva-Diz et al., 2016), we hypothesized that the differences in $CD45^+$ leukocyte frequency between epithelial and mesenchymal tumors might be due to a difference in E6/E7 expression. To study that, DMBA-TPA-derived epithelial (PB and MSC11B9) and mesenchymal (CarB and CarC) SCC cells were engrafted in immunodeficient mice. These cells were kindly provided by Dr. Miguel Quintanilla from the Instituto de Investigaciones Biomédicas "Alberto Sols" (IIBM, Madrid, Spain). Mesenchymal-derived tumors (CarB and CarC) grew faster than epithelial-derived tumors (PB and MSC11B9), corroborating the aggressiveness of mesenchymal tumors (Figure 24a). In addition, a significant increase in the weight of the spleen and the liver was detected in mice bearing

mesenchymal tumors as compared to mice bearing epithelial tumors (Figures 24b and 24c). PB and MSC11B9 SCC cells gave rise to epithelial tumors, which mainly contained epithelial EpCAM^{+} cancer cells and a small percentage of mesenchymal-like EpCAM^{-} cancer cells (Figure 24g). Focusing on epithelial cancer cells, PB-derived tumors contained approximately 80% of EpCAM^{high} and 20% of EpCAM^{low} cancer cells, showing WD-SCCs characteristics, whereas MSC11B9-derived tumors contained 60% of EpCAM^{high} and 40% of EpCAM^{low} cancer cells (showing WD/MD-SCCs features, Figures 24e and 24f). In contrast, CarB and CarC-derived tumors were comprised exclusively by mesenchymal-like EpCAM^{-} cancer cells (PD/S-SCCs, Figure 24g). According to our SCC progression model based on tumors developed in K14-HPV16 mice, the generated DMBA-TPA-derived mesenchymal tumors exhibited a similar CD45^{+} leukocyte reduction as compared to epithelial tumors (Figure 24h). The percentage of these immune cells did not change significantly in the blood of mice bearing epithelial or mesenchymal tumors, suggesting that the reduction of CD45^{+} cells was specific to tumor-infiltrating leukocytes (Figure 24d). These results indicate that the drastic decrease of tumor-infiltrating CD45^{+} leukocytes does not depend of the expression of E6/E7 viral oncoproteins on cancer cells during SCC progression.

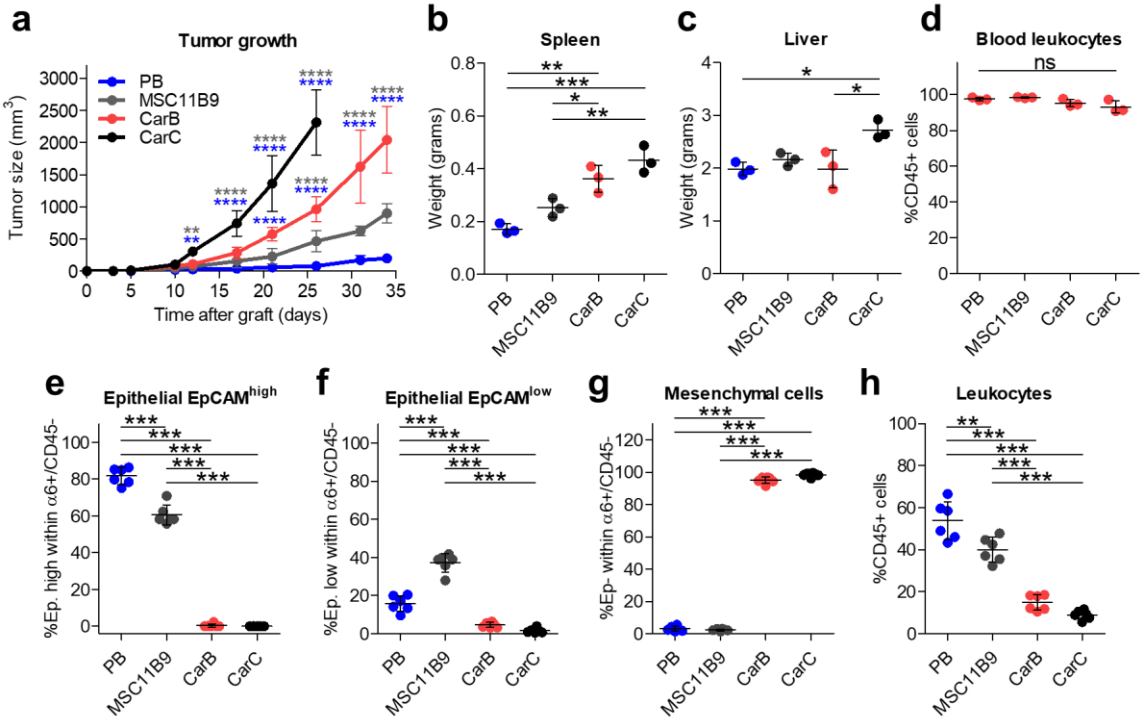

Figure 24. Characterization of DMBA-TPA-derived SCCs. a. Growth kinetics of tumors generated (n=6 tumors per cell type) after engrafting PB, MSC11B9, CarB and CarC SCC cells in immunodeficient mice. Weigh of (**b**) spleen and (**c**) liver of mice bearing the indicated tumors. **d**. Percentage of blood CD45^{+} leukocytes in mice bearing the indicated tumors (n=3). Percentage of (**e**) EpCAM^{high} (α6-integrin^{+}/CD45^{-} /EpCAM^{high} cancer cells), (**f**) EpCAM^{low} (α6-integrin^{+}/CD45^{-}/EpCAM^{low} cancer cells), (**g**) mesenchymal-like EpCAM^{-} cancer cells (α6-integrin^{+}/CD45^{-}/EpCAM^{-} cancer cells), and (**h**) leukocytes (CD45^{+} cells) in the indicated tumor groups, as determined by flow cytometry. Each symbol represents a single mouse (**b-d**) or

tumor (**e-h**), and mean ± SD for each group is shown. (**a**) Repeated Measures ANOVA test, where significance differences in tumor growth between CarB or CarC and PB tumors are indicated with blue *, and between CarB or CarC and MSC11B9 tumors with grey *, and (**b-h**) one-way ANOVA followed by Tukey's multiple comparison test; ns p>0.05, *p≤0.05, **p≤0.01, ***p≤0.001, ****p≤0.0001.

2.2- Mesenchymal SCCs exhibit an increased infiltration of exhausted T cells and immunosuppressive Treg cells

To evaluate whether the frequency of different immune cell populations change within the $CD45^+$ leukocyte compartment during SCC progression, we analyzed the presence of T lymphocytes ($CD45^+/CD11b^-/CD3^+$ cells) in epithelial, mixed, and mesenchymal SCCs by flow cytometry. This analysis showed an increased recruitment of $CD3^+$ T lymphocytes in mesenchymal tumors compared to epithelial and mixed tumors (Figure 25a). Furthermore, T lymphocytes did not change in the blood and spleen of mice bearing epithelial and mesenchymal tumors (Figures 25b and 25c), indicating that the increase of $CD3^+$ cells was specific to tumor-infiltrating T lymphocytes and dependent of the cancer-cell features.

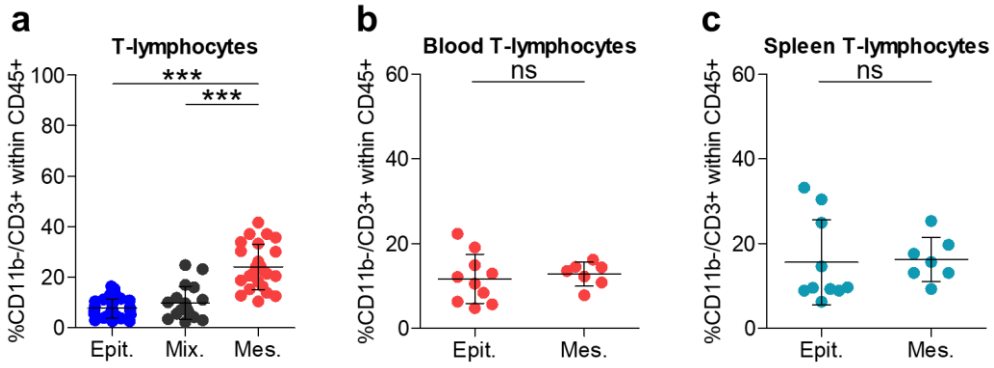

Figure 25. $CD3^+$ T lymphocyte population increases in mesenchymal tumors. a. Percentage of $CD3^+$ T lymphocytes ($CD45^+/CD11b^-/CD3^+$ cells) in epithelial (n=32), mixed (n=18) and mesenchymal (n=25) tumors, as determined by flow cytometry. Percentage of (**b**) blood or (**c**) spleen $CD3^+$ T lymphocytes in mice bearing epithelial (n=10) or mesenchymal (n=7) tumors. Each symbol represents a single tumor (**a**) or mice (**b, c**), and mean ± SD for each group is shown. (**a**) One-way ANOVA followed by Tukey's multiple comparison test, and (**b**, **c**) unpaired two-tailed Student's *t*-test; ns p>0.05, ***p≤0.001.

To assess the composition of T-cell compartment, we analyzed the presence of cytotoxic $CD8^+$ T lymphocytes (CTLs) and $CD4^+$ T-helper (Th) cells in epithelial, mixed, and mesenchymal SCCs. It has been described that CTLs recognize target cells via the interaction between polyclonally rearranged TCR with a peptide/MHC class I complex, and are responsible for immunosurveillance and eliminating target cells (Chen and Flies, 2013; Zhang and Bevan, 2011). In contrast, $CD4^+$ Th cells recognize peptides presented by MHC class II molecules and regulate effective immune responses (Borst et al., 2018; Chen and Flies, 2013). FACS analysis showed that mixed tumors presented a higher infiltration of $CD4^+$ T lymphocytes ($CD3^+/CD4^+/CD8^-$ cells) than epithelial

tumors, and this population then decreased in mesenchymal tumors (Figure 26a). Furthermore, a higher percentage of $CD8^+$ T lymphocytes ($CD3^+/CD4^-/CD8^+$ cells) was observed in mesenchymal tumors (Figure 26c). No changes in $CD4^+$ T lymphocytes were detected in the blood of mice bearing epithelial and mesenchymal tumors (Figure 26b), whereas $CD8^+$ T lymphocytes also increased in the blood of mice bearing mesenchymal tumors (Figure 26d). Surprisingly, the high infiltration of cytotoxic $CD8^+$ T lymphocytes detected in mesenchymal tumors was contradictory with the high cancer-cell viability and the aggressive growth of these tumors. These observations suggested that mesenchymal cancer cells could evade immunosurveillance through several mechanisms that we tackle later in this Thesis. Some of the mechanisms we have explored are (i) an impaired interaction between cancer and immune cells due to their different spatial location within the tumor; (ii) the action of infiltrating immunosuppressive cells; (iii) the activation of immune checkpoint pathways that suppress cytotoxic immune responses; or (iv) the expression of low levels of MHC molecules, thus becoming invisible to T cells. It is known that immunosuppressive immune cells, including M2-like macrophages, MDSCs and Treg cells, may block the cytolytic activity of CTLs and NK cells by releasing soluble factors and/or expressing immune checkpoint (IC) ligands that interact with CTLs and NK cell co-inhibitory receptors (Kim et al., 2016). Furthermore, cancer cells can also upregulate the expression of IC ligands that, when interacting with their respective IC receptors expressed by CTLs and NK cells, contribute to a dysfunctional state of these immune cells known as exhaustion (Wherry, 2011; Wherry and Kurachi, 2015). In this regard, it was previously reported that tumors with a strong immunosuppressive TME are associated with impaired immune cytotoxicity, are more aggressive and have a poor prognosis (Wang et al., 2017).

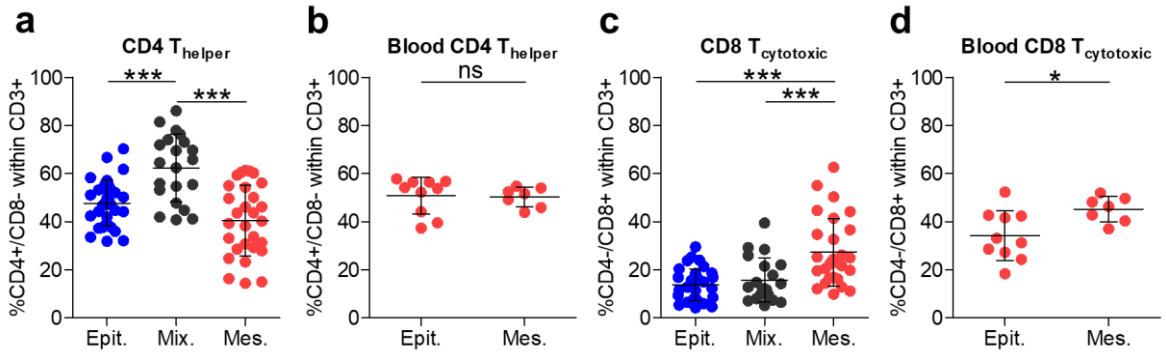

Figure 26. Tumor-infiltrating $CD4^+$ and $CD8^+$ cell populations change during SCC progression. Percentage of (**a**) $CD4^+$ T lymphocytes ($CD3^+/CD4^+/CD8^-$ cells) and (**c**) $CD8^+$ T lymphocytes ($CD3^+/CD4^-/CD8^+$ cells) in epithelial (n=35), mixed (n=21) and mesenchymal (n=32) tumors, as determined by flow cytometry. Percentage of blood (**b**) $CD4^+$ T lymphocytes and (**d**) $CD8^+$ T lymphocytes in mice bearing epithelial (n=10) or mesenchymal (n=7) tumors. Each symbol represents a single tumor (**a, c**) or mice (**b, d**), and mean ± SD for each group is shown. (**a**, **c**) One-way ANOVA followed by Tukey's multiple comparison test, and (**b**, **d**) unpaired two-tailed Student's *t*-test; ns $p>0.05$, *$p\leq0.05$, ***$p\leq0.001$.

To evaluate the spatial distribution of T lymphocytes within the tumor, we performed immunohistochemistry analysis of $CD8^+$ T lymphocytes and $CD4^+$ T lymphocytes in epithelial and mesenchymal SCCs (Figures 27a to 27f). A significant increase of the $CD8^+$ T lymphocyte frequency per tumor area was detected in mesenchymal tumors (Figures 27a and 27b). This was accompanied by no changes of $CD4^+$ T lymphocytes per tumor area in mesenchymal tumors (Figures 27d and 27e). These cells were mainly located in stromal regions of epithelial tumors, whereas they were fully located in intratumoral areas of mesenchymal tumors (Figures 27c and 27f). These results indicate that there was no impaired interaction between cancer cells and $CD8^+$ T lymphocytes in mesenchymal tumors. Still, this could not explain the high viability of these tumors. Furthermore, we analyzed the presence of Treg immunosuppressive cells by the expression of FoxP3 marker (Figure 27g). Given that Treg cells facilitate tumor progression by interfering with the cytotoxic activity of T and NK cells (von Boehmer and Daniel, 2013), we evaluated the presence of this population in our SCCs. As we expected, a significant increase of $FoxP3^+$ Treg lymphocytes per tumor area was detected in mesenchymal tumors (Figures 27g and 27h), being mainly located in the stromal regions of epithelial tumors and fully located in intratumoral areas of mesenchymal tumors (Figure 27i). These results indicate that mesenchymal tumors exhibit a high infiltration of immunosuppressive Treg cells, which could interfere with the cytotoxic activity of $CD8^+$ and NK cells and favor the aggressive growth of advanced SCCs.

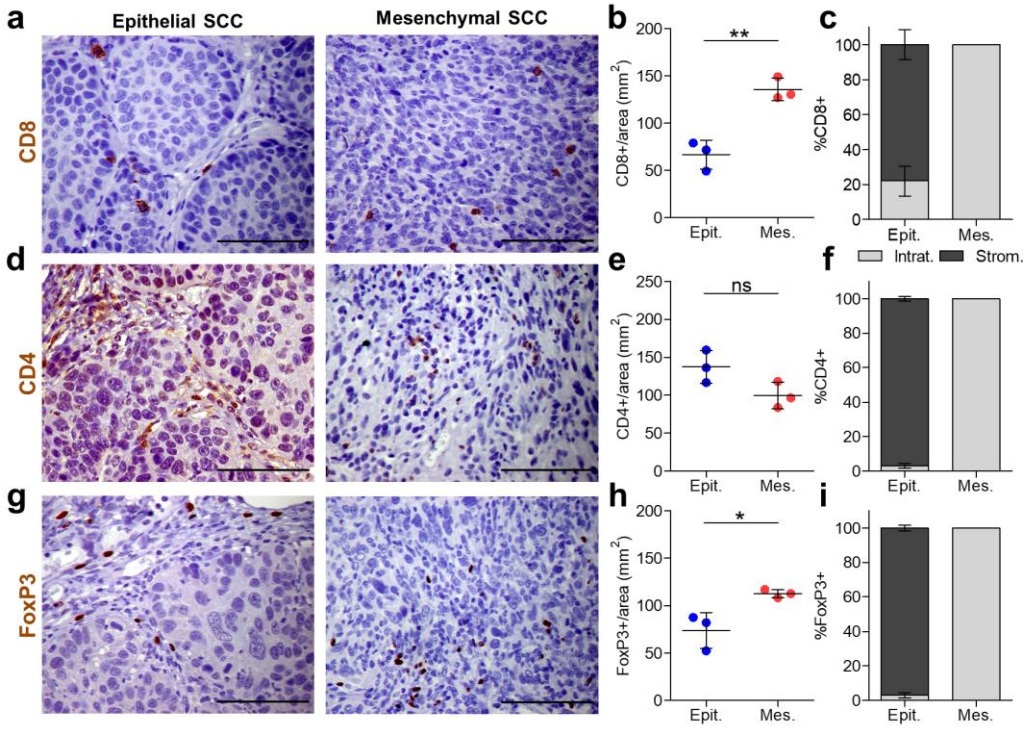

Figure 27. Frequency and distribution of $CD8^+$, $CD4^+$ and Treg lymphocytes at different stages of SCC progression. Representative immunohistochemistry images of (**a**) $CD8^+$, (**d**) $CD4^+$, and (**g**) $FoxP3^+$ immune cell detection in epithelial and mesenchymal SCCs. Scale bar: 100 µm. Quantification of the frequency of (**b**) $CD8^+$, (**e**) $CD4^+$, and (**h**) $FoxP3^+$ cells per tumor area (mm^2) in epithelial and mesenchymal tumors (n=3). At

least 7 fields of different regions were quantified in each tumor. Each symbol represents a single tumor and mean ± SD for each group is shown. Percentage (mean ± SD) of intratumoral or stromal (**c**) $CD8^+$ cells relative to total $CD8^+$ T lymphocytes, (**f**) $CD4^+$ cells relative to total $CD4^+$ T lymphocytes, and (**i**) $FoxP3^+$ cells relative to total $FoxP3^+$ T regulatory lymphocytes in the indicated tumors. (**b, e, h**) Unpaired two-tailed Student's *t*-test; ns $p>0.05$, *$p\leq0.05$, **$p\leq0.01$.

To further characterize the molecular features of these immune cell populations, we isolated $CD4^+$ T lymphocytes ($CD3^+/CD4^+/CD8^-$ cells) and $CD8^+$ T lymphocytes ($CD3^+/CD4^-/CD8^+$ cells) from WD-SCCs and PD/S-SCCs by FACS sorting. The gene expression profile of these immune cell populations demonstrated that $CD8^+$ T lymphocytes isolated from PD/S-SCCs showed a stronger expression of some co-inhibitory receptors such as PD-1, CTLA-4, and LAG-3 compared to $CD8^+$ cells isolated from WD-SCCs, which indicated the exhausted state of these lymphocytes (Figure 28a). Although no significant changes in the expression of some effector cytokines and lytic molecules such as *Ifn-γ*, *Tnf-α* and *GzmB* were detected, we also observed a strong downregulation of perforin (*Prf1*) and *Lt-α* that could impair the lytic-mediated apoptosis and the stimulation of a pro-inflammatory immune response, respectively (Figure 28a). These results indicate that mesenchymal tumors exhibit a high infiltration of exhausted $CD8^+$ T lymphocytes, characterized by the expression of some IC receptors and by an impaired capability to execute a cytotoxic response. Furthermore, $CD4^+$ T lymphocytes isolated from PD/S-SCCs showed a downregulation of some Th1 pro-inflammatory cytokines (*Il12b* and *Il2*), a slight induction of the expression of Th2 and Treg immunosuppressive cytokines such as *Il5*, *Il13*, *Gata3*, and *Tgf-β1*, as well as an upregulation of *Ccr3* (Figure 28b) compared to $CD4^+$ cells isolated from WD-SCCs. The receptor CCR3 is important for the recruitment of Th2 cells and the amplification of polarized Th2 responses following the release of cytokines such as CCL17, CCL22, and CCL24 by M2-like macrophages (Griffith et al., 2014). These results suggest that mesenchymal tumors exhibit a high infiltration of $CD4^+$ Th2 and Treg cells, which may secrete immunosuppressive cytokines to block T and NK-cell activity.

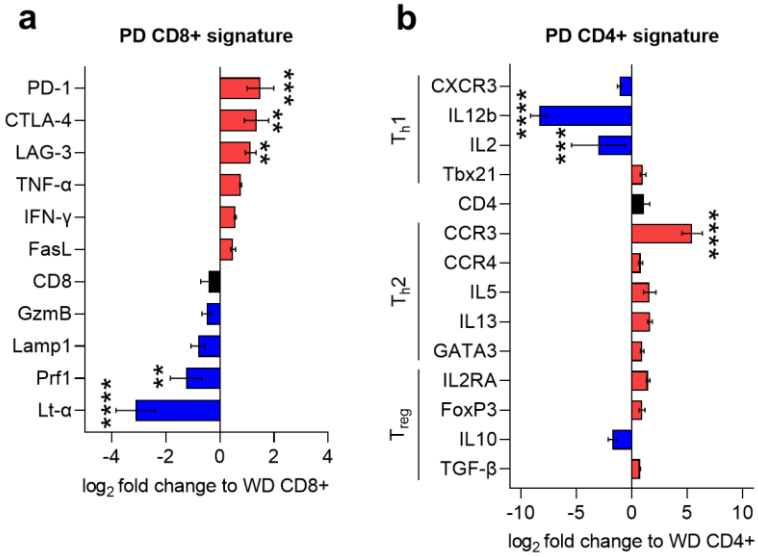

Figure 28. Characterization of CD8$^+$ and CD4$^+$ T lymphocyte signature in epithelial and mesenchymal SCCs. Gene expression levels (mean ± SD) of the indicated genes in (**a**) CD8$^+$ T lymphocytes (CD3$^+$/CD4$^-$/CD8$^+$ cells) and (**b**) CD4$^+$ T lymphocytes (CD3$^+$/CD4$^+$/CD8$^-$ cells) isolated by FACS-sorting from PD/S-SCCs represented as the fold change (expressed in $\log_2$) relative to those isolated from WD-SCCs, as quantified by qRT-PCR. One-way ANOVA followed by Dunnett's multiple comparison test; **p≤0.01, ***p≤0.001, ****p≤0.0001.

To validate these results, we analyzed the expression of the IC inhibitory receptors PD-1, LAG-3, TIM-3, CTLA-4, and TIGIT, as well as the activating receptor DNAM-1, in CD8$^+$ T lymphocytes from epithelial, mixed, and mesenchymal SCCs by flow cytometry. Our results showed that the percentage of PD-1$^+$ cells within CD11b$^-$/CD8$^+$ T lymphocytes increased during SCC progression (Figure 29a). However, most of these immune cells were also co-expressing LAG-3, TIM-3, and TIGIT (Figures 29b, 29c and 29e), which are markers of exhausted T cells (He and Xu, 2020; Kim et al., 2016). By contrast, the expression of CTLA-4 was reduced in mesenchymal tumors (Figure 29d). Given that T-cell exhaustion has been correlated with the increasing expression of these inhibitory receptors, our data indicate that most cytotoxic CD8$^+$ T lymphocytes found in mesenchymal tumors are in an exhausted state. Moreover, given that CTLA-4 was more co-expressed in epithelial tumors, while LAG-3, TIM-3, and TIGIT were more co-expressed in mesenchymal tumors, these data suggest that IC mechanisms might be different depending on the cancer-cell features. Interestingly, the expression of the activating receptor DNAM-1 was significantly induced in mesenchymal tumors (Figure 29f). It has been described that the regulation of T cells by DNAM-1 and TIGIT receptors is achieved by complex interactions that, depending on their binding affinity for the ligands CD155 and CD112, will counteract or not the activation signals mediated through the DNAM-1 receptor (Chauvin and Zarour, 2020; Sanchez-Correa et al., 2019). Studies on the affinity of these receptors for their ligands show that TIGIT has a higher affinity than DNAM-1 for CD155 and competes for binding to CD155, which interrupts the activation mediated by DNAM-1 and delivers an inhibitory signal to T cells (Stanietsky et al., 2009; Tahara-Hanaoka et al., 2004; Yu et al., 2009). These results suggest that, even with an increase of DNAM-1$^+$ T cells in mesenchymal tumors (Figure 29f), TIGIT recognition of the ligands CD155 and CD112 could be stronger and might exert an inhibitory effect on T cell-mediated cytotoxicity. Hence, we hypothesized that this axis represents a promising target for cancer immunotherapy, blocking TIGIT recognition of CD155 or CD112 and activating the recognition of these ligands by DNAM-1 to potentiate T cell-mediated cytotoxicity. Finally, the intracellular expression of IFN-γ and GzmB significantly decreased in T lymphocytes during SCC progression as determined by FACS analysis (Figures 30a and 30b), although no significant changes were observed in gene expression (Figure 28a). This result confirms the impaired lytic-mediated apoptosis and the stimulation of a pro-inflammatory immune response by CD8$^+$ T lymphocytes in mesenchymal tumors. Altogether, these results indicate that mesenchymal tumors exhibit a higher infiltration of exhausted CD8$^+$ T

lymphocytes and immunosuppressive Treg cells than epithelial and mixed tumors, which may favor the aggressive growth of advanced SCCs.

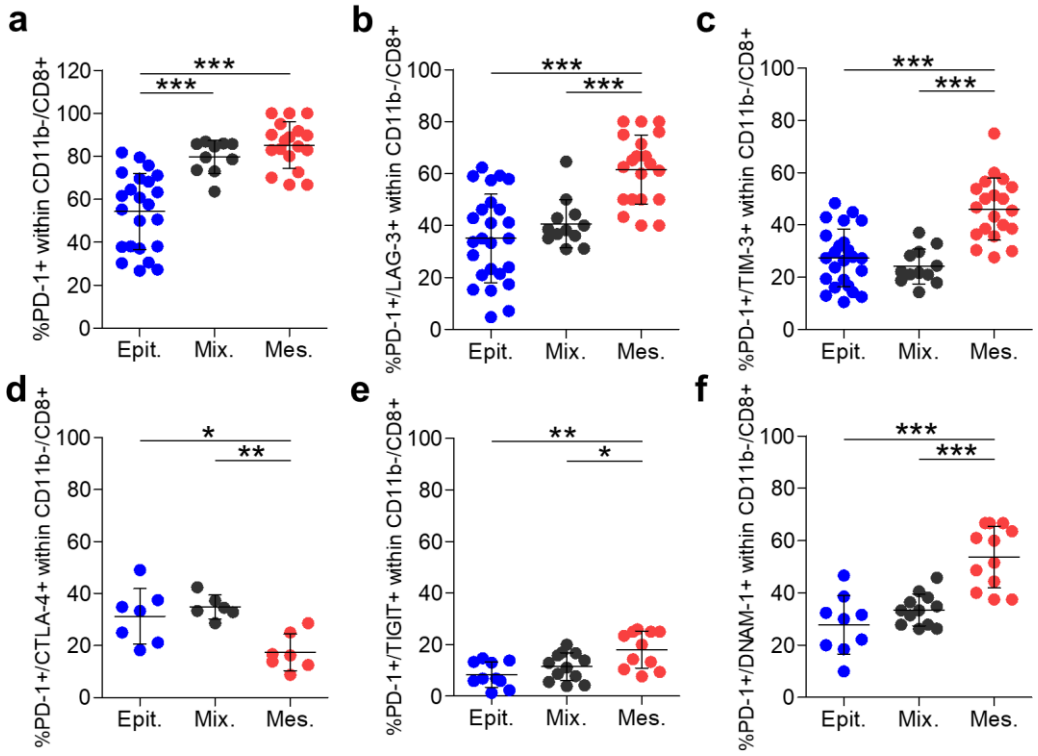

Figure 29. Activated/exhausted state of tumor-infiltrating CD8$^+$ T lymphocytes during SCC progression. Percentage of (**a**) PD-1$^+$, (**b**) PD-1$^+$/LAG-3$^+$, (**c**) PD-1$^+$/TIM-3$^+$, (**d**) PD-1$^+$/CTLA-4$^+$, (**e**) PD-1$^+$/TIGIT$^+$, and (**f**) PD-1$^+$/DNAM-1$^+$ cells within CD8$^+$ T lymphocyte population (CD11b$^-$/CD8$^+$ cells) in epithelial (n≥7), mixed (n≥7) and mesenchymal (n≥8) tumors, as determined by flow cytometry. Each symbol represents a single tumor and mean ± SD for each group is shown. (**a-f**) One-way ANOVA followed by Tukey's multiple comparison test; *p≤0.05, **p≤0.01, ***p≤0.001.

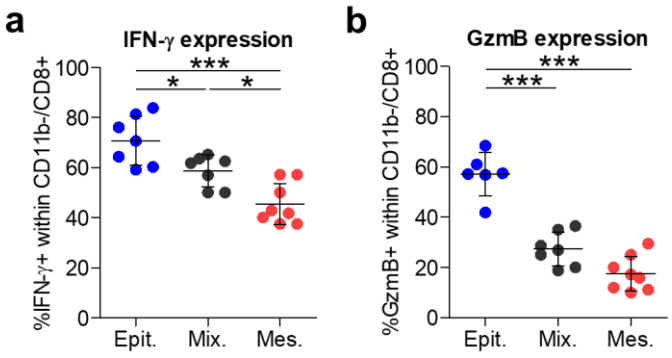

Figure 30. IFN-γ and GzmB expression is reduced in CD8$^+$ T lymphocytes during SCC progression. Percentage of (**a**) IFN-γ or (**b**) GzmB expressing cells within CD8$^+$ T lymphocyte population (CD11b$^-$/CD8$^+$ cells) in epithelial (n=7), mixed (n=7) and mesenchymal (n=8) tumors, as determined by flow cytometry. Each symbol represents a single tumor and mean ± SD for each group is shown. (**a, b**) One-way ANOVA followed by Tukey's multiple comparison test; *p≤0.05, ***p≤0.001.

2.3- Mesenchymal SCCs exhibit an increased infiltration of exhausted NK cells

Subsequently, we evaluated the frequency of NK cells during SCC progression. NK cells are part of the innate immune system and, as CTLs, are responsible for immunosurveillance and for eliminating target cells (Moretta et al., 2008). NK cells can target cells lacking MHC expression and without antigen presentation (Voskoboinik et al., 2015). Flow cytometry assays showed that NK cells ($CD11b^+/CD3^-/NK\text{-}1.1^+$ cells) increased in mixed tumors, and were higher recruited to mesenchymal tumors compared to epithelial tumors (Figure 31a). In addition, NK-cell frequency did not change in the blood and spleen of mice bearing epithelial and mesenchymal tumors (Figures 31b and 31c), indicating that the increase of NK cells was specific in the tumor compartment. This observation was again contradictory with the aggressive growth of mesenchymal tumors, since if NK cells were activated, they would stimulate a pro-inflammatory immune response to block tumor growth. As this situation did not occur, we hypothesized that these NK cells might express multiple co-inhibitory receptors, downregulating their cytotoxic activity by binding to their IC ligands.

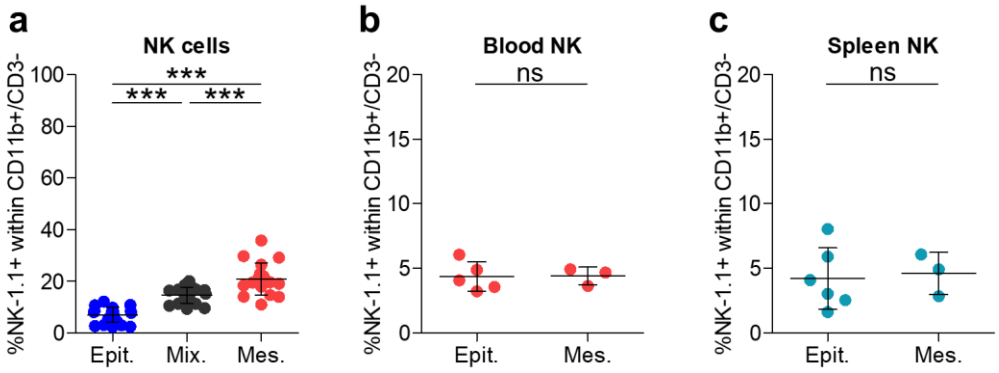

Figure 31. Tumor-infiltrating NK cells increase during SCC progression. a. Percentage of NK cells ($CD11b^+/CD3^-/NK\text{-}1.1^+$ cells) in epithelial (n=23), mixed (n=21) and mesenchymal (n=18) tumors, as determined by flow cytometry. Percentage of (**b**) blood or (**c**) spleen NK cells in mice bearing epithelial (n=5) or mesenchymal (n=3) tumors. Each symbol represents a single tumor (**a**) or mice (**b, c**), and mean ± SD for each group is shown. (**a**) One-way ANOVA followed by Tukey's multiple comparison test, and (**b**, **c**) unpaired two-tailed Student's *t*-test; ns $p>0.05$, ***$p\leq0.001$.

To confirm this hypothesis, we analyzed the expression of the IC inhibitory receptors PD-1, LAG-3, TIM-3, and TIGIT, and the activating receptor DNAM-1, in NK cells from epithelial, mixed and mesenchymal SCCs by flow cytometry. Our results revealed that the percentage of NK cells co-expressing PD-1 together with LAG-3, TIM-3, and TIGIT slightly increased in mixed tumors, and dramatically incremented in mesenchymal tumors (Figures 32a to 32c), which confirm their exhausted state. In addition, the expression of the activating receptor DNAM-1 was greatly induced during SCC progression (Figure 32d), which suggest that it could enhance NK cell-mediated cytotoxicity against a wide range of cancer cells. However, given that TIGIT recognition of the ligands CD155 and CD112 is stronger than DNAM-1, we hypothesized that this situation might

exert an inhibitory effect on NK cells by diminishing IFN-γ production and NK cell-mediated cytotoxicity (Sanchez-Correa et al., 2019). These results indicate that mesenchymal tumors have a large infiltration of exhausted NK cells, as it happens with CTLs. At this point, we evaluated which cancer or immune cell populations were upregulating the expression of some IC ligands, which might be involved in the dysfunctional cytolytic activity of CTLs and NK cells.

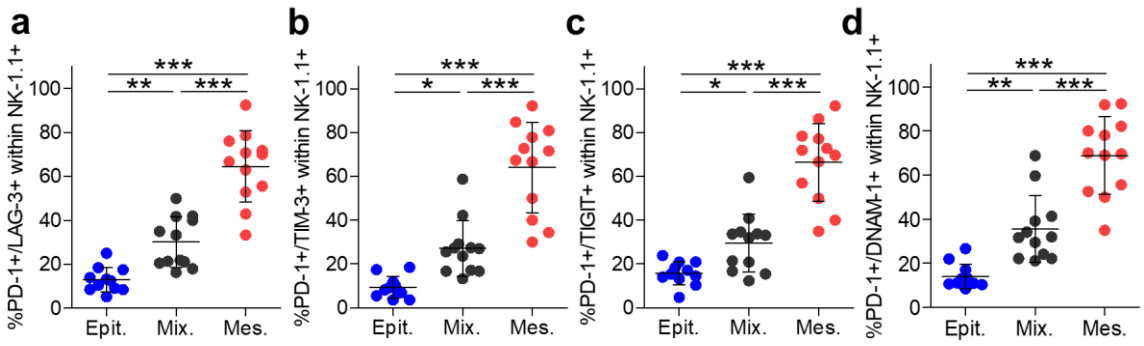

Figure 32. Activated/exhausted state of tumor-infiltrating NK cells during SCC progression. Percentage of (**a**) PD-1$^+$/LAG-3$^+$, (**b**) PD-1$^+$/TIM-3$^+$, (**c**) PD-1$^+$/TIGIT$^+$, and (**d**) PD-1$^+$/DNAM-1$^+$ cells within NK (CD11b$^+$/CD3$^-$/NK-1.1$^+$ cells) cell population in epithelial, mixed and mesenchymal tumors (n=12), as determined by flow cytometry. Each symbol represents a single tumor and mean ± SD for each group is shown. (**a-d**) One-way ANOVA followed by Tukey's multiple comparison test; *p≤0.05, **p≤0.01, ***p≤0.001.

2.4- Mesenchymal SCCs exhibit an increased infiltration of macrophages and a decreased infiltration of MDSCs

To compare the frequency of myeloid cells in SCCs at different stages of progression, we analyzed the presence of CD45$^+$/CD11b$^+$/CD3$^-$ cells in epithelial, mixed, and mesenchymal SCCs by flow cytometry. This analysis showed a significant reduction of myeloid cells in mesenchymal tumors compared to epithelial and mixed tumors (Figure 33a). Furthermore, myeloid cells presented a similar frequency in the blood of mice bearing epithelial and mesenchymal tumors (Figure 33b), whereas they decreased in the spleen of mice bearing mesenchymal tumors (Figure 33c).

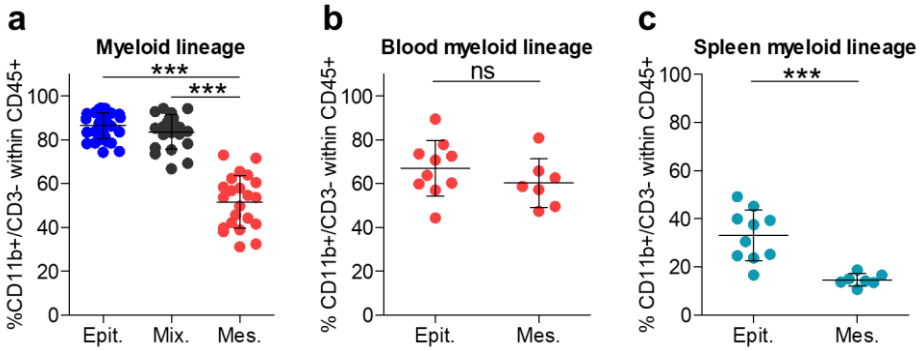

Figure 33. Tumor-infiltrating myeloid cells decrease during SCC progression. a. Percentage of myeloid cells (CD45$^+$/CD11b$^+$/CD3$^-$ cells) in epithelial (n=32), mixed (n=21) and mesenchymal (n=22) tumors, as determined by flow cytometry. Percentage of (**b**) blood or (**c**) spleen myeloid cells in mice bearing epithelial

(n=10) or mesenchymal (n=7) tumors. Each symbol represents a single tumor (**a**) or mice (**b, c**), and mean ± SD for each group is shown. (**a**) One-way ANOVA followed by Tukey's multiple comparison test, and (**b**, **c**) unpaired two-tailed Student's *t*-test; ns p>0.05, ***p≤0.001.

We then evaluated whether there were changes within the different myeloid cell populations, in particular MDSCs and macrophages, during SCC progression. In mice, macrophages are characterized by the expression of markers such as CD11b, F4/80, CD68, and CSF1R, and low levels of Gr1, whereas MDSCs are identified as cells that co-express CD11b and Gr1 (Gabrilovich et al., 2012; Qian and Pollard, 2010). We showed that MDSCs are the most frequent tumor-infiltrating myeloid cell, independently of the epithelial or mesenchymal features of the tumors (Figure 34a). However, we observed that epithelial and mixed tumors presented a higher infiltration of MDSCs ($CD11b^+/Gr1^+$ cells) than mesenchymal tumors (Figure 34a), whereas a higher percentage of macrophages ($CD11b^+/F4\text{-}80^+/Gr1^-$ cells) was observed in advanced mesenchymal tumors compared to epithelial or mixed SCCs (Figure 34c). In addition, no significant changes in MDSCs were observed in the blood of mice bearing epithelial and mesenchymal tumors (Figure 34b), whereas macrophages increased in the blood of mice bearing mesenchymal tumors (Figure 34d).

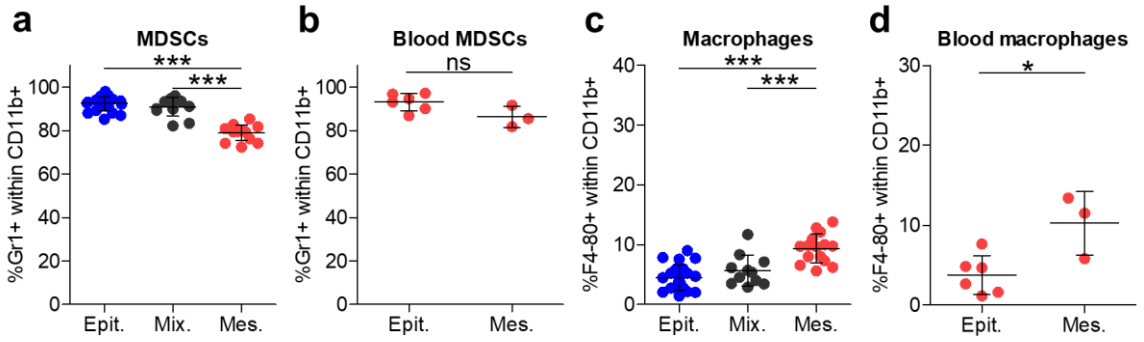

Figure 34. Tumor-infiltrating MDSCs decrease and macrophages increase during SCC progression. Percentage of (**a**) MDSCs ($CD11b^+/Gr1^+$ cells) and (**c**) macrophages ($CD11b^+/F4\text{-}80^+/Gr1^-$ cells) within myeloid cell population in epithelial (n=25), mixed (n=12) and mesenchymal (n=15) tumors, as determined by flow cytometry. Percentage of blood (**b**) MDSCs and (**d**) macrophages in mice bearing epithelial (n=6) or mesenchymal (n=3) tumors. Each symbol represents a single tumor (**a, c**) or mice (**b, d**), and mean ± SD for each group is shown. (**a**, **c**) One-way ANOVA followed by Tukey's multiple comparison test, and (**b**, **d**) unpaired two-tailed Student's *t*-test; ns p>0.05, *p≤0.05, ***p≤0.001.

Although flow cytometry data illustrate about the relative abundance of myeloid infiltrates, this method does not provide insights on their spatial location and distribution within the tumor. We therefore performed immunofluorescence assays at different stages of SCC progression with an α-CD68 antibody, which recognize both M1- and M2-like macrophages (Figure 35a), and with an α-Gr1 antibody, which recognize both polymorphonuclear and monocytic MDSC subtypes (Figure 35d). In these assays, we observed a significant increase of $CD68^+$ macrophages per tumor area in mixed tumors, which then subsequently increased in mesenchymal tumors (Figures 35a and 35b).

Along with this increase in the frequency of macrophages, we observed that the frequency of $Gr1^+$ MDSCs per tumor area significantly decreased during SCC progression (Figures 35d and 35e). In addition, about 90% of $CD68^+$ macrophages were located in the stroma of epithelial tumors (Figure 35c). In mixed tumors, there was a shift in the localization of $CD68^+$ macrophages toward the intratumoral areas, but still maintaining 60% of them in the stromal area, to finally be localized in the intratumoral area of mesenchymal tumors (Figure 35c). We also detected a similar distribution trend of $Gr1^+$ MDSCs during SCC progression, although the tumor-infiltrating capabilities of these immune cells were higher than that of macrophages in viable regions (Figure 35f). In this regard, 30% of MDSCs were detected in intratumoral areas of epithelial tumors, and this increased to almost 70% in mixed tumors (Figure 35f). Overall, the distribution of these immune cells was coincidental with that observed for $CD8^+$ T cells (Figure 27c). However, it remained unclear if these MDSCs correspond to PMN-MDSCs or M-MDSCs, and whether these macrophages were anti-tumorigenic M1-like or immunosuppressive M2-like according to their functional role.

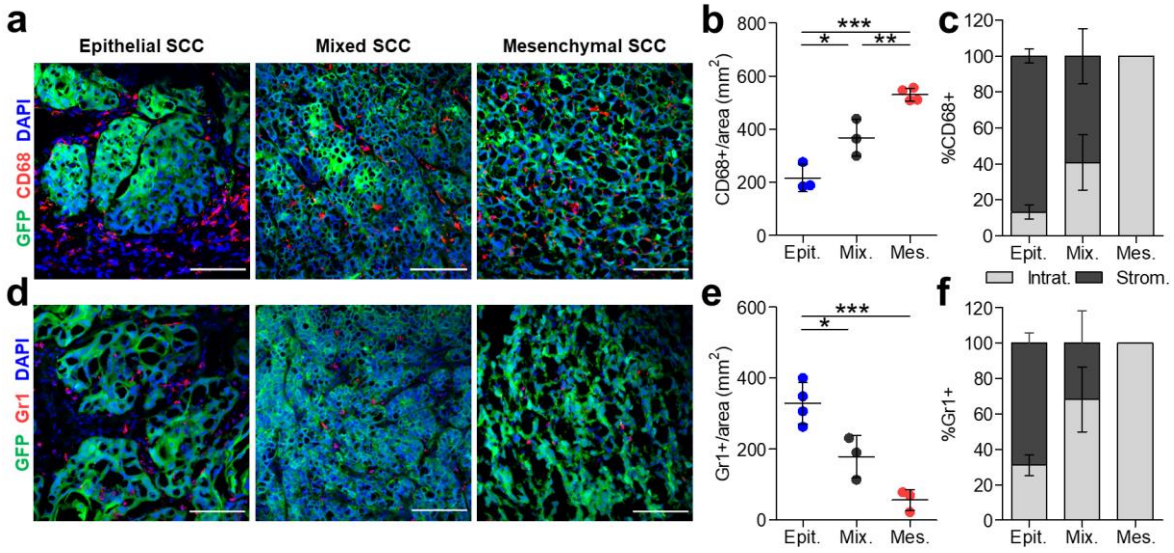

Figure 35. Tumor-infiltrating MDSCs decrease and macrophages increase during SCC progression. Representative immunofluorescence images of GFP^+ cancer cells, (**a**) $CD68^+$ or (**d**) $Gr1^+$ immune cells and DAPI labelled cell nuclei detected in epithelial, mixed, and mesenchymal SCCs. Scale bar: 100 µm. Quantification of the frequency of (**b**) $CD68^+$ cells and (**e**) $Gr1^+$ cells per tumor area (mm^2) in epithelial (n=3), mixed (n=3) and mesenchymal (n=3) tumors. At least 7 fields of different regions were quantified in each tumor. Percentage (mean ± SD) of intratumoral or stromal (**c**) $CD68^+$ cells relative to total $CD68^+$ macrophages and (**f**) $Gr1^+$ cells relative to total $Gr1^+$ MDSCs in the indicated tumors. Each symbol represents a single tumor and mean ± SD for each group is shown. (**b, e**) One-way ANOVA followed by Tukey's multiple comparison test; *p≤0.05, **p≤0.01, ***p≤0.001.

To address this, we analyzed the presence of PMN-MDSCs, which share phenotypic features with neutrophils but are less phagocytic, and M-MDSCs, which exhibit a similar phenotype to inflammatory monocytes and differentiate into immunosuppressive M2-like macrophages and DCs

under specific TME signals (Gabrilovich et al., 2012), in epithelial, mixed and mesenchymal SCCs by flow cytometry. Epithelial and mixed tumors had a higher infiltration of PMN-MDSCs ($CD11b^+/Ly6C^+/Ly6G^+$ cells) than mesenchymal tumors (Figure 36a), whereas a higher percentage of M-MDSCs ($CD11b^+/Ly6C^+/Ly6G^-$ cells) was observed in mesenchymal tumors (Figure 36c). This data suggest that within the PMN-MDSCs detected in epithelial and mixed tumors we might be considering tumor-associated neutrophils (TANs), which are phenotypically similar to PMN-MDSCs and their anti-tumor or pro-tumoral activity is modulated by distinct TME signals (Brandau et al., 2013; Mantovani et al., 2011; Shaul and Fridlender, 2019). In this sense, we hypothesized that TANs in epithelial and mixed tumors may have mostly anti-tumor activity, as previously reported in colorectal cancer (Droeser et al., 2013; Sconocchia et al., 2011). In recent years, it has been demonstrated that the pro-tumorigenic and immunosuppressive activity of TANs could be in fact attributed to PMN-MDSCs (Brandau et al., 2013). For that reason, we hypothesized that mesenchymal tumors might recruit mainly immunosuppressive PMN-MDSCs, which could interfere with the cytotoxic activity of T and NK cells, as well as play an essential role in tumor development and progression, as previously described (Condamine et al., 2015; Umansky et al., 2016). In addition, the higher recruitment of M-MDSCs in mesenchymal tumors could led to a higher generation of M2-like macrophages and DCs. No changes in the frequency of PMN-MDSCs and M-MDSCs were detected in the blood of mice bearing epithelial and mesenchymal tumors (Figures 36b and 36d).

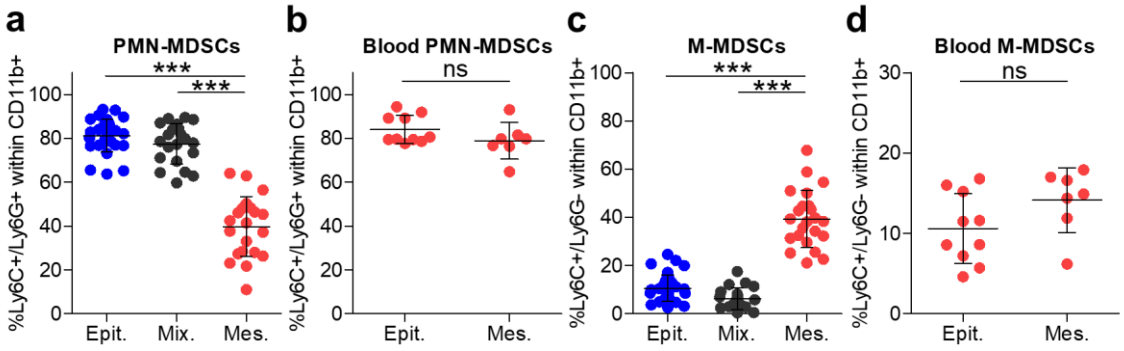

Figure 36. Epithelial SCCs present a high infiltration of PMN-MDSCs, whereas a high percentage of M-MDSCs is observed in mesenchymal SCCs. Percentage of (**a**) PMN-MDSCs ($CD11b^+/Ly6C^+/Ly6G^+$ cells) and (**c**) M-MDSCs ($CD11b^+/Ly6C^+/Ly6G^-$ cells) in epithelial (n=33), mixed (n=21) and mesenchymal (n=23) tumors, as determined by flow cytometry. Percentage of blood (**b**) PMN-MDSCs and (**d**) M-MDSCs in mice bearing epithelial (n=10) or mesenchymal (n=7) tumors. Each symbol represents a single tumor (**a, c**) or mice (**b, d**), and mean ± SD for each group is shown. (**a**, **c**) One-way ANOVA followed by Tukey's multiple comparison test, and (**b**, **d**) unpaired two-tailed Student's *t*-test; ns $p>0.05$, ***$p\leq0.001$.

We then analyzed the presence of M1-like ($CD11b^+/F4\text{-}80^+/Gr1^-/CD206^-$ cells) and M2-like macrophages ($CD11b^+/F4\text{-}80^+/Gr1^-/CD206^+$ cells) in epithelial, mixed, and mesenchymal SCCs by flow cytometry. It has been described that M1-like macrophages are anti-tumorigenic and are

involved in cancer control by directly killing cancer cells, producing pro-inflammatory cytokines or stimulating anti-tumor T cell responses (Murray, 2017). Conversely, M2-like macrophages enhance tumor growth by producing some factors and cytokines that favor cancer-cell survival, proliferation, migration, invasion and metastasis (Lorenzo-Sanz and Muñoz, 2019; Murray, 2017). M2-like macrophages can also blunt anti-tumor immunity by eliminating M1-like macrophages and by impairing T cell functions through direct interaction with these immune cells or by secreting immunosuppressive cytokines (Qian and Pollard, 2010). In particular, a reduction of anti-tumorigenic M1-like macrophages and an increase of immunosuppressive M2-like macrophages were observed during SCC progression (Figures 37a and 37c), which was consistent with the aggressiveness of mesenchymal tumors. No changes in the frequency of these populations were detected in the blood of mice bearing epithelial and mesenchymal tumors (Figures 37b and 37d).

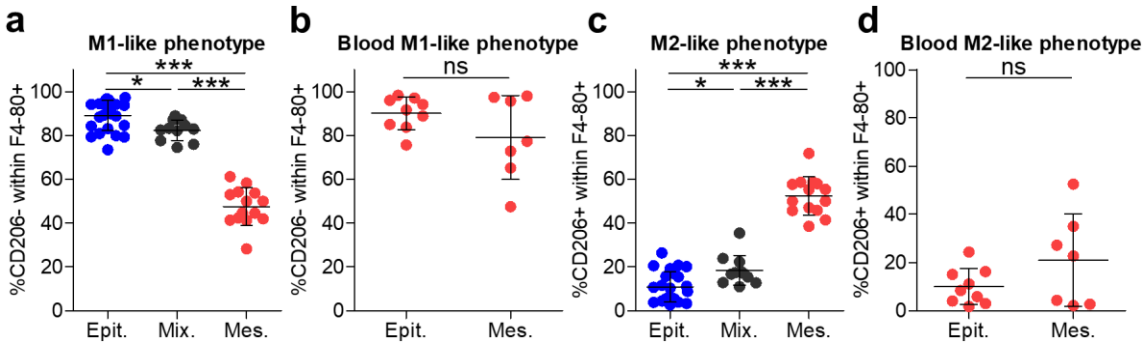

Figure 37. Epithelial SCCs present a high infiltration of M1-like macrophages, whereas a high percentage of M2-like macrophages is observed in mesenchymal SCCs. Percentage of (**a**) M1-like macrophages ($CD11b^+/F4\text{-}80^+/Gr1^-/CD206^-$ cells) and (**c**) M2-like macrophages ($CD11b^+/F4\text{-}80^+/Gr1^-/CD206^+$ cells) in epithelial (n=24), mixed (n=11) and mesenchymal (n=14) tumors, as determined by flow cytometry. Percentage of blood (**b**) M1-like and (**d**) M2-like macrophages in mice bearing epithelial (n=9) or mesenchymal (n=7) tumors. Each symbol represents a single tumor (**a**, **c**) or mice (**b, d**), and mean ± SD for each group is shown. (**a**, **c**) One-way ANOVA followed by Tukey's multiple comparison test, and (**b**, **d**) unpaired two-tailed Student's *t*-test; ns $p>0.05$, *$p\leq0.05$, ***$p\leq0.001$.

To complete these studies, we performed immunohistochemistry assays with an α-CD163 antibody (M2-like marker, (Lau et al., 2004)) in epithelial and mesenchymal SCCs (Figure 38a). These results indicated that, similarly to that reported for Treg cells (Figure 27h), the frequency of immunosuppressive $CD163^+$ M2-like macrophages was increased in mesenchymal tumors (Figures 38a and 38b). Almost all $CD163^+$ M2-like macrophages were located in the stroma of epithelial tumors (Figure 38c), indicating that most of $CD68^+$ macrophages infiltrating the epithelial tumor core may be anti-tumorigenic M1-like macrophages (Figure 35c). However, M2-like macrophages were in close proximity to cancer cells (intratumoral areas) in mesenchymal tumors (Figure 38c). Altogether, these results indicate that epithelial and mixed tumors contain a high infiltration of anti-tumorigenic M1-like macrophages and PMN-MDSCs, possibly of the neutrophil subtype, whereas

mesenchymal tumors exhibit a high infiltration of immunosuppressive M2-like macrophages and M-MDSCs. This situation might generate a tumor-promoting local environment that could negatively influence the immunotherapy response of mesenchymal tumors.

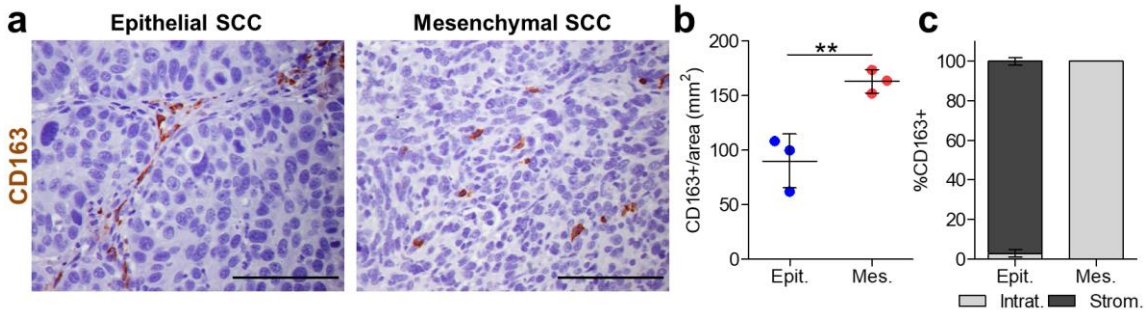

Figure 38. Frequency of immunosuppressive CD163$^+$ M2-like macrophages increase during SCC progression. a. Representative immunohistochemistry images of CD163$^+$ cells detected in epithelial and mesenchymal SCCs. Scale bar: 100 µm. **b.** Quantification of CD163$^+$ cells per tumor area (mm^2) in epithelial and mesenchymal tumors (n=3). At least 6 fields of different regions were quantified in each tumor. **c.** Percentage (mean ± SD) of intratumoral or stromal CD163$^+$ cells relative to total CD163$^+$ M2-like macrophages in the indicated tumors. Each symbol represents a single tumor and mean ± SD for each group is shown. (**b**) Unpaired two-tailed Student's *t*-test; **p≤0.01.

With all the previous information, we characterized these immune populations to test the relevance of some cytokines and growth factors provided by these immune cells in regulating cancer-cell plasticity, immune evasion, and tumor progression. To tackle this, we isolated M1-like macrophages (F4-80$^+$/Gr1$^-$/CD206$^-$ cells), M2-like macrophages (F4-80$^+$/Gr1$^-$/CD206$^+$ cells), and M-MDSCs (CD11b$^+$/Ly6C$^+$/Ly6G$^-$ cells) from WD-SCCs and PD/S-SCCs by FACS-sorting assays (3 different biological samples for each population). M1-like macrophages isolated from PD/S-SCCs downregulated the expression of MHC-II, which is required for the presentation of tumor-specific antigens, the expression of some M1-like pro-inflammatory cytokines (*Il23a*, *Tnf-α*, *Il12b*, *Il18*, *Il1β*), and the expression of *iNOS*, which is involved in the production of reactive nitrogen and oxygen intermediates (Chanmee et al., 2014; Lorenzo-Sanz and Muñoz, 2019) compared to M1-like macrophages isolated from WD-SCCs (Figure 39a). A downregulation of some Th1 cell-attracting chemokines such as *Cxcl9* and *Cxcl10*, which drive the polarization and recruitment of Th1 cells, thereby amplifying a type 1 response (Griffith et al., 2014), was also observed in M1-like macrophages from PD/S-SCCs. Interestingly, an upregulated expression of *Ccl2* provided by M1-like macrophages in mesenchymal tumors could be involved in the high recruitment of M2-like macrophages and M-MDSCs to the mesenchymal tumor core (Figure 39a), as previously described (Griffith et al., 2014; Murray and Wynn, 2011; Qian et al., 2011). In addition, *Il6* expression was increased in M1-like macrophages isolated from PD/S-SCCs compared to those isolated from WD-SCCs (Figure 39a). It has been described that IL-6 secretion promotes tumor growth and immunosuppression in the TME of various cancer types (Chanmee et al., 2014), and foster the

recruitment of MDSCs (Marvel and Gabrilovich, 2015), stimulating their inhibitory activity toward cytotoxic T cells (Groth et al., 2019). In addition, TAM-derived IL-6 induces STAT3-mediated expression of stem cell-related genes in breast, liver and pancreatic cancer cells, promoting the CSC state (Yang et al., 2013; Wan et al., 2014; Yin et al., 2017). These results demonstrate that M1-like macrophages of PD/S-SCCs have less pro-inflammatory and tumoricidal functions than those isolated from WD-SCCs.

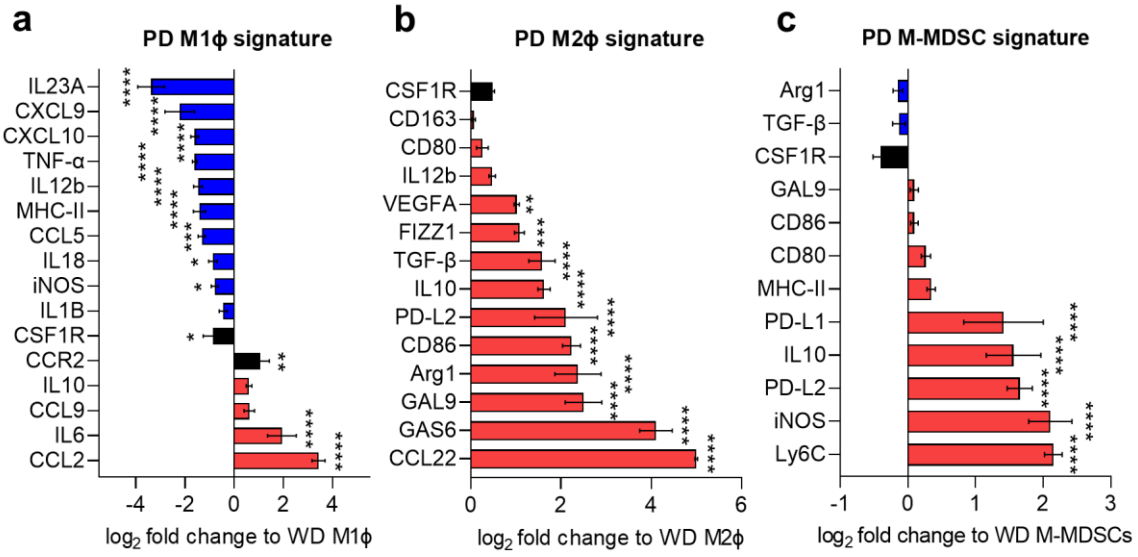

Figure 39. Characterization of M1-like, M2-like and M-MDSC signatures in epithelial and mesenchymal SCCs. Gene expression levels (mean ± SD) of the indicated genes in (**a**) M1-like macrophages (F4-80$^+$/Gr1$^-$/CD206$^-$ cells), (**b**) M2-like macrophages (F4-80$^+$/Gr1$^-$/CD206$^+$ cells), and (**c**) M-MDSCs (CD11b$^+$/Ly6C$^+$/Ly6G$^-$ cells) isolated from PD/S-SCCs, represented as the fold change (expressed in $\log_2$) relative to those expressed in cells isolated from WD-SCCs, as quantified by qRT-PCR. (**a-c**) One-way ANOVA followed by Dunnett's multiple comparison test; *p≤0.05, **p≤0.01, ***p≤0.001, ****p≤0.0001.

Subsequently, the characterization of M2-like macrophages isolated from PD/S-SCCs showed that this immune population exhibits a stronger immunosuppressive signature compared to those isolated from WD-SCCs (Figure 39b). This signature was characterized by an increased expression of some immunosuppressive cytokines such as *Tgf-β* and *Il10*, which facilitate tumor progression (Chanmee et al., 2014). In addition, an increased production of *Arg1*, which impairs T-cell proliferation and IFN-γ production, and *Vegfa*, a pro-angiogenic factor that promotes angiogenesis, was also observed in M2-like macrophages from PD/S-SCCs (Figure 39b). Interestingly, an upregulated expression of *Ccl22* provided by M2-like macrophages in mesenchymal tumors could be involved in the recruitment of Th2 and Treg cells through its binding to CCR3 or CCR4 receptors, as previously described (Röhrle et al., 2020a; Wang et al., 2019a). These results are consistent with the fact that CD4$^+$ T lymphocytes isolated from PD/S-SCCs upregulate the expression of CCR3 (Figure 28b). Furthermore, some T-cell inhibitory ligands such as *Cd80*, *Pdl2*, *Cd86*, and *Gal9* were also induced in M2-like macrophages isolated from mesenchymal tumors, which could explain the inhibition of

T and NK cell cytotoxic functions in these tumors (Figure 39b). Finally, M-MDSCs isolated from PD/S-SCCs were characterized by an increased expression of *iNOS*, which promotes NO synthesis, *Il10*, which promotes severe anergy of effector immune cells, and *Pdl1/Pdl2*, which could block anti-tumor T of NK cell-mediated activity via interaction with the PD-1 receptor of these immune cells (Figure 39c) (Ostrand-Rosenberg, 2010). Altogether, these results indicate that M2-like macrophages and M-MDSCs could subvert anti-tumor immunity in mesenchymal tumors. This anti-tumor immunity effect could be mediated (i) by eliminating M1-like immune responses, (ii) by impairing $CD8^+$ T cell or NK activation through direct interaction with these immune cells or (iii) by inducing the expression of some immunosuppressive cytokines and IC ligands.

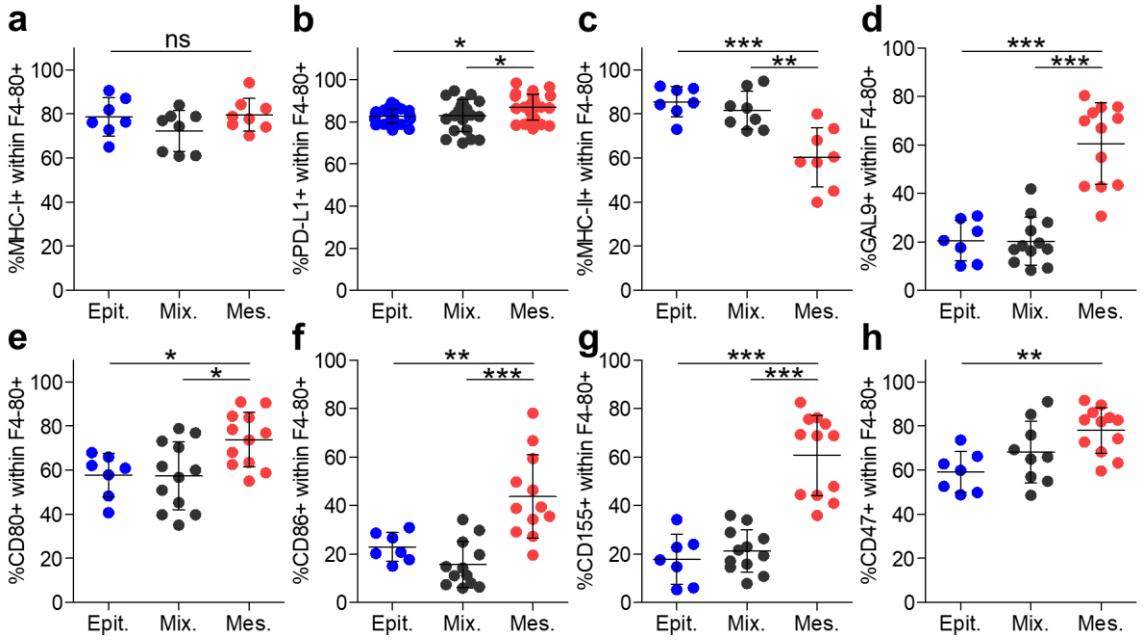

Figure 40. The expression of IC ligands by macrophages changes during SCC progression. Percentage of (**a**) MHC-I^+, (**b**) PD-$L1^+$, (**c**) MHC-II^+, (**d**) $Gal9^+$, (**e**) $CD80^+$, (**f**) $CD86^+$, (**g**) $CD155^+$, and (**h**) $CD47^+$ cells within macrophage population ($CD11b^+$/F4-80^+/$Gr1^-$ cells) that are infiltrating epithelial (n≥7), mixed (n≥8), and mesenchymal (n≥8) tumors, as determined by flow cytometry. Each symbol represents a single tumor and mean ± SD for each group is shown. (**a-h**) One-way ANOVA followed by Tukey's multiple comparison test; ns $p>0.05$, *$p\leq0.05$, **$p\leq0.01$, ***$p\leq0.001$.

At this point, to corroborate these observations, we evaluated the expression of IC ligands in macrophages during SCC progression. To tackle this, we analyzed the expression of PD-L1, MHC-II, Gal9, CD80/CD86, and CD155, which are ligands of the IC receptors PD-1, LAG-3, TIM-3, CTLA-4, and TIGIT, respectively, in macrophages ($CD11b^+$/F4-80^+/$Gr1^-$ cells) from epithelial, mixed, and mesenchymal SCCs. In accordance with gene expression data (Figures 39a and 39b), FACS analysis showed that the percentage of macrophages expressing PD-L1, Gal9, CD80, CD86, and CD155 increased in mesenchymal tumors compared to epithelial and mixed tumors (Figures 40b, 40d to 40g). These results indicate that IC ligands expressed by macrophages might be involved

in the dysfunctional cytolytic activity of CTLs and NK cells when interacting with their co-inhibitory receptors in mesenchymal tumors. As no changes were detected in the expression of MHC class I molecule (Figure 40a), no differences should be expected in the process of antigen presentation by macrophages during SCC progression. In addition, macrophages in mesenchymal tumors reduced the expression of MHC class II (Figure 40c), confirming the loss of the M1-like phenotype toward an M2-like phenotype. Furthermore, they slightly induced the expression of CD47 compared to epithelial and mixed tumors (Figure 40h). CD47 activation in immune cells has been linked to tumor immune evasion, decreased antigen-presentation cell function, and impaired effector functions of NK and T cells (Veillette and Chen, 2018). Furthermore, CD47 also serves as an anti-phagocytic signal for macrophages upon binding to SIRPα (van den Berg and Valerius, 2019). These results indicate that a high activation of CD47 could be blocking macrophage-mediated phagocytosis and antigen presentation in mesenchymal tumors, even observing a similar MHC-I expression during SCC progression, which could interfere the priming of CTLs against tumor antigens, as previously described (Liu et al., 2015; Veillette and Chen, 2018).

2.5- Mesenchymal SCCs exhibit an increased infiltration of DCs

Finally, we analyzed the presence of tumor-infiltrating DCs ($CD45^+/CD11c^+/F4\text{-}80^-/Gr1^-$ cells) in epithelial, mixed, and mesenchymal SCCs by flow cytometry. This analysis showed a significant increase of DCs in mesenchymal tumors compared to epithelial and mixed tumors (Figure 41a). In addition, DC frequency did not change in the blood and spleen of mice bearing epithelial and mesenchymal tumors (Figures 41b and 41c), indicating that the increase of DCs was specific in the tumor core.

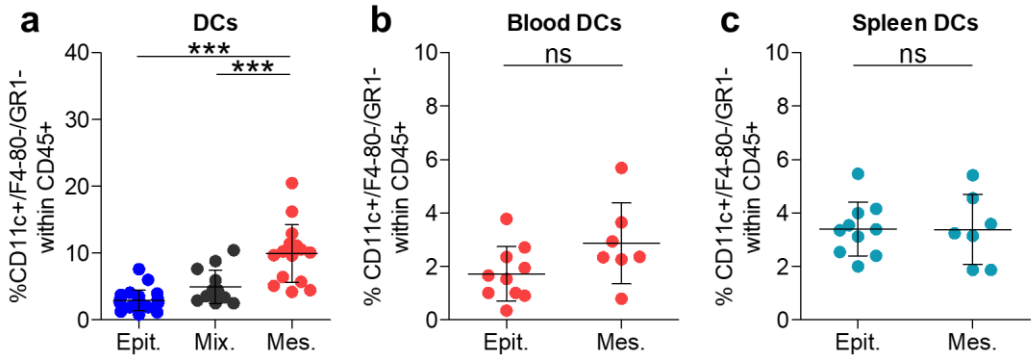

Figure 41. Tumor-infiltrating DCs increase during SCC progression. a. Percentage of DCs ($CD45^+/CD11c^+/F4\text{-}80^-/Gr1^-$ cells) that are infiltrating epithelial (n=23), mixed (n=14) and mesenchymal (n=16) tumors, as determined by flow cytometry. Percentage of (**b**) blood or (**c**) spleen DCs in mice bearing epithelial (n=10) or mesenchymal (n=7) tumors. Each symbol represents a single tumor (**a**) or mice (**b, c**), and mean ± SD for each group is shown. (**a**) One-way ANOVA followed by Tukey's multiple comparison test, and (**b**, **c**) unpaired two-tailed Student's *t*-test; ns $p>0.05$, ***$p\leq0.001$.

Given that this increase in DCs could lead to a higher tumor antigen presentation environment and an effective anti-tumor immunity, we analyzed the expression of MHC-I, PD-L1, MHC-II, Gal9, CD80, CD155, and CD47 in DCs from epithelial, mixed and mesenchymal tumors, as different studies have shown that DCs also represent a critical source of IC ligands (Oh et al., 2020). This analysis showed that the percentage of DCs expressing MHC-I, PD-L1, Gal9, CD80, CD155, and CD47 increased in mesenchymal tumors compared to epithelial and mixed tumors (Figures 42a to 42g). In addition, as no changes were detected in the expression of MHC class II molecule (Figure 42c), no differences should be expected in the process of antigen presentation by DCs during SCC progression. These results indicate that IC ligands expressed by DCs could lead to T and NK cell exhaustion, limiting costimulatory signaling and T cell and NK cell activation (Wculek et al., 2020).

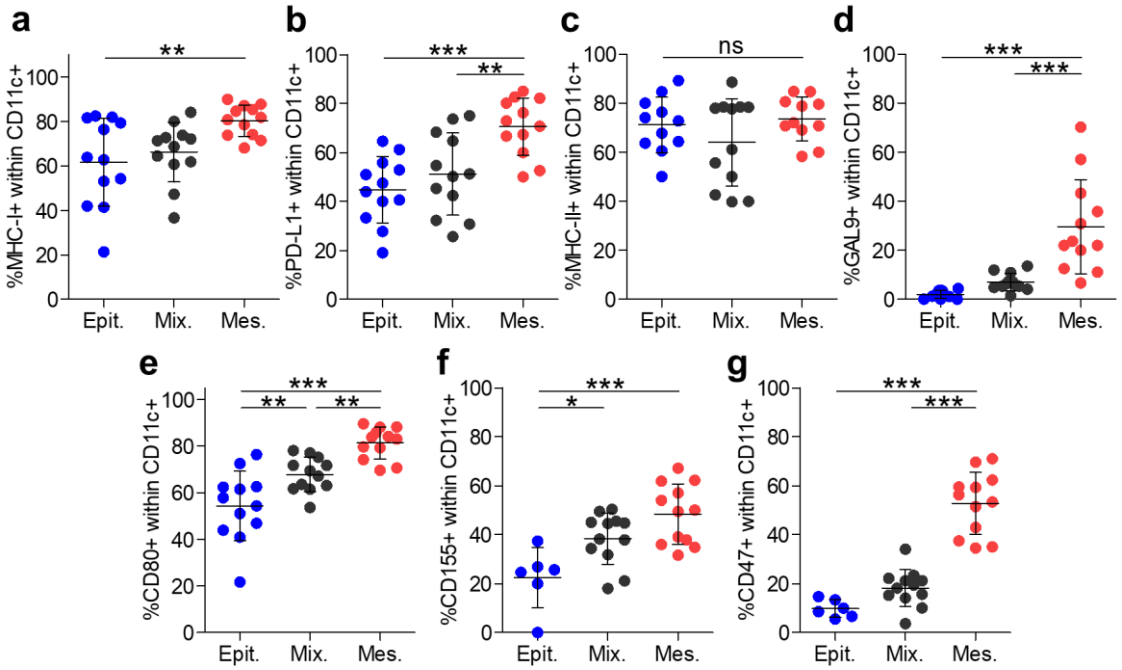

Figure 42. The expression of IC ligands by DCs changes during SCC progression Percentage of (**a**) MHC-I$^+$, (**b**) PD-L1$^+$, (**c**) MHC-II$^+$, (**d**) Gal9$^+$, (**e**) CD80$^+$, (**f**) CD155$^+$, and (**g**) CD47$^+$ cells within DC population (CD11c$^+$/F4-80$^-$/Gr1$^-$ cells) in epithelial (n≥6), mixed (n=12), and mesenchymal (n=12) tumors, as determined by flow cytometry. Each symbol represents a single tumor and mean ± SD for each group is shown. (**a-g**) One-way ANOVA followed by Tukey's multiple comparison test; ns p>0.05, *p≤0.05, **p≤0.01, ***p≤0.001.

Summary Chapter 2: Immune landscape changes during mouse SCC progression, concomitantly with the acquisition of cancer-cell plasticity and mesenchymal-like cell traits

The results presented in Chapter 2 demonstrate that tumor immune microenvironment changes accordingly with cancer-cell features. In this regard, the characterization of immune cells recruited during SCC progression showed that epithelial and mixed tumors present a high infiltration of Th1 CD4$^+$ T lymphocytes, active CTLs and pro-inflammatory M1-like macrophages, which correlates with lower tumor viability. Furthermore, within the high recruitment of PMN-MDSCs detected in

epithelial and mixed tumors, we hypothesized that we could be considering TANs, which are phenotypically similar to PMN-MDSCs but could have anti-tumor activity in these tumors. By contrast, a significant enrichment of M-MDSCs, Th2 $CD4^+$ T lymphocytes, Treg cells and M2-like macrophages is observed in advanced mesenchymal SCCs, which may favor the growth and progression of these tumors. Given the aggressiveness of mesenchymal tumors, it was surprising to observe that the recruitment of $CD8^+$ T lymphocytes and NK cells was higher in these tumors. However, the enhanced co-expression of PD-1 together with LAG-3, TIM-3 and TIGIT in $CD8^+$ and NK cell populations, as well as a significant decrease of the expression of IFN-γ and GzmB in $CD8^+$ T cells, indicate that most of these cytotoxic immune cells are inactive or exhausted in mesenchymal tumors. Finally, the increased secretion of immunosuppressive cytokines and the expression of IC ligands by M2-like macrophages, M-MDSCs and DCs might be also involved in the blockade of the cytolytic activity of CTLs and NK cells in mesenchymal tumors. Altogether, our data demonstrate that the tumor immune microenvironment switches from a pro-inflammatory to a pro-tumoral and immunosuppressive state, concomitantly with the acquisition of mesenchymal-like features in cancer cells. This immunosuppressive TME might favor the aggressive tumor growth and enhance metastasis of advanced mouse SCCs.

CHAPTER 3. CHARACTERIZATION OF THE EXPRESSION PROFILE OF IMMUNE CHECKPOINT LIGANDS IN CANCER CELLS DURING SCC PROGRESSION

In the Chapter 2, we demonstrated that the presence of an immunosuppressive TME could preclude the activation of effector T and NK cells and favor the exclusion of cytotoxic immune cells from the tumor core. Therefore, we next wanted to determine whether cancer cells might also be evading immune responses by expressing IC ligands, as well as corrupting antigen presentation to avoid T cell recognition.

3.1- IC ligand expression changes depending on the epithelial or mesenchymal characteristics of cancer cells

To study whether IC ligand expression changes depending on the characteristics of cancer cells, we analyzed the expression of MHC-I, PD-L1, MHC-II, Gal9, CD80, CD86, and CD155 in full epithelial $GFP^+/CD45^-/EpCAM^+$ cancer cells isolated from epithelial tumors (WD-SCCs) and mesenchymal-like $GFP^+/CD45^-/EpCAM^-$ cancer cells isolated from mesenchymal tumors (PD/S-SCCs). Specifically, PD-L1 is the ligand of PD-1, MHC-II of LAG-3, Gal9 of TIM-3, CD80/CD86 of CTLA-4, and CD155 of TIGIT (Qin et al., 2019). The first interesting observation was that whereas 50% of full epithelial cancer cells expressed MHC-I, the expression of this complex was dramatically reduced in mesenchymal-like $EpCAM^-$ cancer cells (Figures 43a and 43b). MHC-I is responsible for the presentation of peptide antigens to the cell surface for recognition by specific $CD8^+$ T cells (Davis et al., 1998; Festenstein and Garrido, 1986). For this reason, the loss of MHC-I expression in mesenchymal-like $EpCAM^-$ cancer cells (Figure 43b) might impair T-cell recognition and activation, compromising anti-tumor immune activities in mesenchymal tumors. This result again supports the fact that mesenchymal SCCs are highly aggressive and metastatic. However, although these mesenchymal-like $EpCAM^-$ cancer cells could be targeted by NK cells, as they perform recognition of cells lacking MHC-I molecules (Voskoboinik et al., 2015), we previously observed that they were exhausted in mesenchymal tumors (Figures 32a to 32d). This means that NK cells also fail for eliminating the mesenchymal cancer cell population.

Furthermore, FACS analysis indicated that whereas PD-L1 is the IC ligand most predominantly expressed by full epithelial cancer cells (≈40-60% of cancer cells within this population, Figures 43c and 43d), followed by MHC-II (Figures 43e and 43f), Gal9 (Figures 43g and 43h), and CD80/CD86 (Figures 43i to 43l), mesenchymal-like $EpCAM^-$ cancer cells strongly downregulated PD-L1 expression (Figures 43c and 43d) and upregulated a different repertoire of IC ligands. In particular, mesenchymal-like $EpCAM^-$ cancer cells significantly induced the expression of CD80 and CD155, ligands of CTLA-4 and TIGIT IC receptors, respectively (Figures 43i, 43j, 43m and 43n). These IC ligands could be key for preventing the cytolytic activity of T and NK cells in mesenchymal tumors. In addition, we previously observed that the expression of CD80 and CD155

was also induced in infiltrating M2-like macrophages (Figures 40e and 40g) and DCs (Figures 42e and 42f) of mesenchymal tumors, which could impair T and NK cell activity to unleash anti-tumor responses. Taken together, these results demonstrate that epithelial and mesenchymal SCCs have evolved different mechanisms to attenuate the effectiveness of T and NK cells during tumor progression. Specifically, full epithelial cancer cells could do so through PD-L1, MHC-II, Gal9, and CD80/CD86 expression, whereas mesenchymal-like EpCAM^{-} cancer cells could do so through the expression of CD80 and CD155. These results indicate the relevance of different IC pathways induced by cancer and immunosuppressive cells, and inform us about which combinatory ICB therapies could more efficiently boost the adaptive and innate anti-tumor immune response depending on cancer-cell features, as reported in other studies (Pardoll, 2012; Wei et al., 2018).

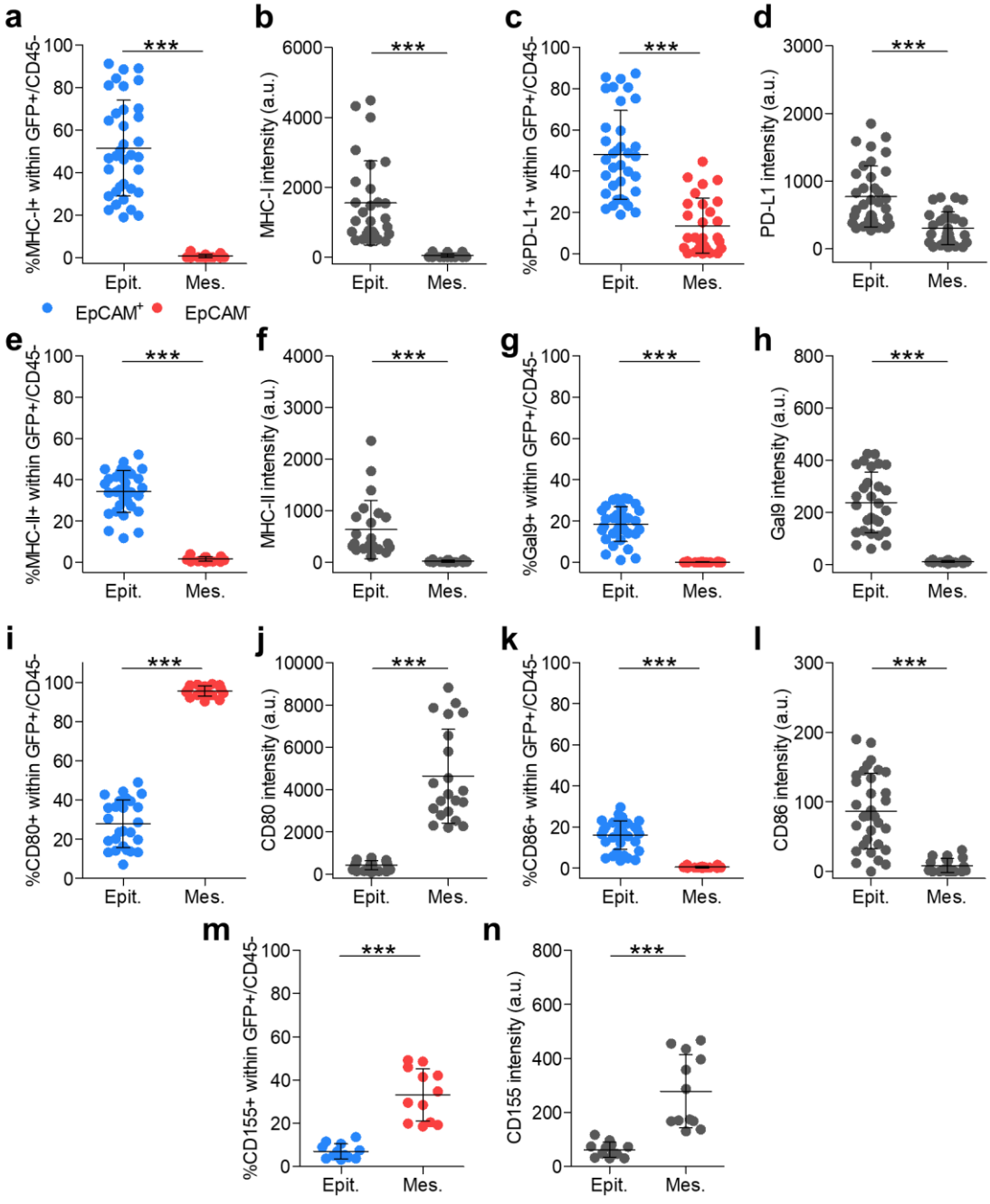

Figure 43. Immune-checkpoint ligand expression changes depending on the epithelial or mesenchymal features of cancer cells. Percentage of (**a**) MHC-I$^+$, (**c**) PD-L1$^+$, (**e**) MHC-II$^+$, (**g**) Gal9$^+$, (**i**) CD80$^+$, (**k**) CD86$^+$, and (**m**) CD155$^+$ cancer cells within epithelial EpCAM$^+$ (GFP$^+$/CD45$^-$/EpCAM$^+$) or mesenchymal-like EpCAM$^-$ (GFP$^+$/CD45$^-$/EpCAM$^-$) cancer cells in epithelial (n≥12) and mesenchymal (n≥12) tumors, as determined by flow cytometry. Intensity of expression of (**b**) MHC-I, (**d**) PD-L1, (**f**) MHC-II, (**h**) Gal9, (**j**) CD80, (**l**) CD86, and (**n**) CD155 in cancer cells of epithelial and mesenchymal tumors. Each symbol represents a single tumor and mean ± SD for each group is shown. (**a**-**n**) Unpaired two-tailed Student's *t*-test; ***p≤0.001.

3.2- Epithelial EpCAM^{low} cancer cells show a similar IC ligand profile to that of mesenchymal-like EpCAM$^-$ cancer cells

We then analyzed the expression of some IC ligands in MD/PD-SCCs, which contained a mixed population of epithelial EpCAM$^+$ (EpCAM^{high} and EpCAM^{low} cancer cells) and mesenchymal-like EpCAM$^-$ cancer cells. We observed that, although the percentage of full epithelial and EpCAM^{high} cancer cells positive for MHC-I, PD-L1, MHC-II, Gal9, and CD86 was similar between both cancer cell populations (Figures 43a, 43c, 43e, 43g, 43k, 44a, 44c, 44e, 44g, and 44k), the intensity of these ligands was lower in EpCAM^{high} than in full epithelial cancer cells (Figures 43b, 43d, 43f, 43h, 43l, 44b, 44d, 44f, 44h and 44l). Furthermore, the expression of these ligands was higher in EpCAM^{high} cancer cells than in EpCAM^{low} and mesenchymal-like EpCAM$^-$ cancer cells from MD/PD-SCCs (Figures 44a to 44h, 44k and 44l). Interestingly, MHC-I expression in EpCAM^{low} and mesenchymal-like EpCAM$^-$ cancer cells from MD/PD-SCCs (Figure 44a and 44b) was higher than the expressed by mesenchymal-like EpCAM$^-$ cancer cells in PD/S-SCCs (Figures 43a and 43b). These results indicate that, during the progression from the epithelial to the mesenchymal state, the loss of MHC-I expression is progressive. Therefore, some EpCAM^{low} and mesenchymal-like EpCAM$^-$ cancer cells from MD/PD-SCCs may still be recognized and killed by T cells in contrast to mesenchymal-like EpCAM$^-$ cancer cells from PD/S-SCCs.

The other interesting result was that the expression of CD80 slightly increased in EpCAM^{low} cancer cells, and significantly incremented in mesenchymal-like EpCAM$^-$ cancer cells as compared to EpCAM^{high} cancer cells (Figures 44i and 44j). However, the expression of CD80 by EpCAM^{low} and mesenchymal-like EpCAM$^-$ cancer cells from MD/PD-SCCs was lower than those expressed by mesenchymal-like EpCAM$^-$ cancer cells in PD/S-SCCs (Figure 43j). These results indicate that the induction of CD80 expression could be associated with the acquisition of cancer-cell plasticity and increased during SCC progression. In addition, CD80 could impede the cytolytic activity of T and NK cells through its binding to CTLA-4 in mixed and mesenchymal tumors. Finally, the expression of CD155 was specifically induced in mesenchymal-like EpCAM$^-$ cancer cells from MD/PD-SCCs compared to EpCAM^{high} and EpCAM^{low} cancer cells (Figures 44m and 44n). This result indicates that the expression of CD155 by mesenchymal-like EpCAM$^-$ cancer cells from MD/PD-SCCs or PD/S-SCCs could be responsible for preventing the cytolytic activity of T and NK cells thorough its

binding to TIGIT. Altogether, our results suggest that ICB therapies should be selected taking into account cancer-cell features. In addition, alterations in the IC ligand expression are observed from the appearance of plastic cancer cells at intermediate stages of SCC progression, indicating that the acquisition of cancer-cell plasticity might impact on tumor immune evasion. As a result, this work brings to the forefront the possibility of using the epithelial, hybrid and mesenchymal phenotypic states of cancer cells as an important marker to predict responses to ICB therapies.

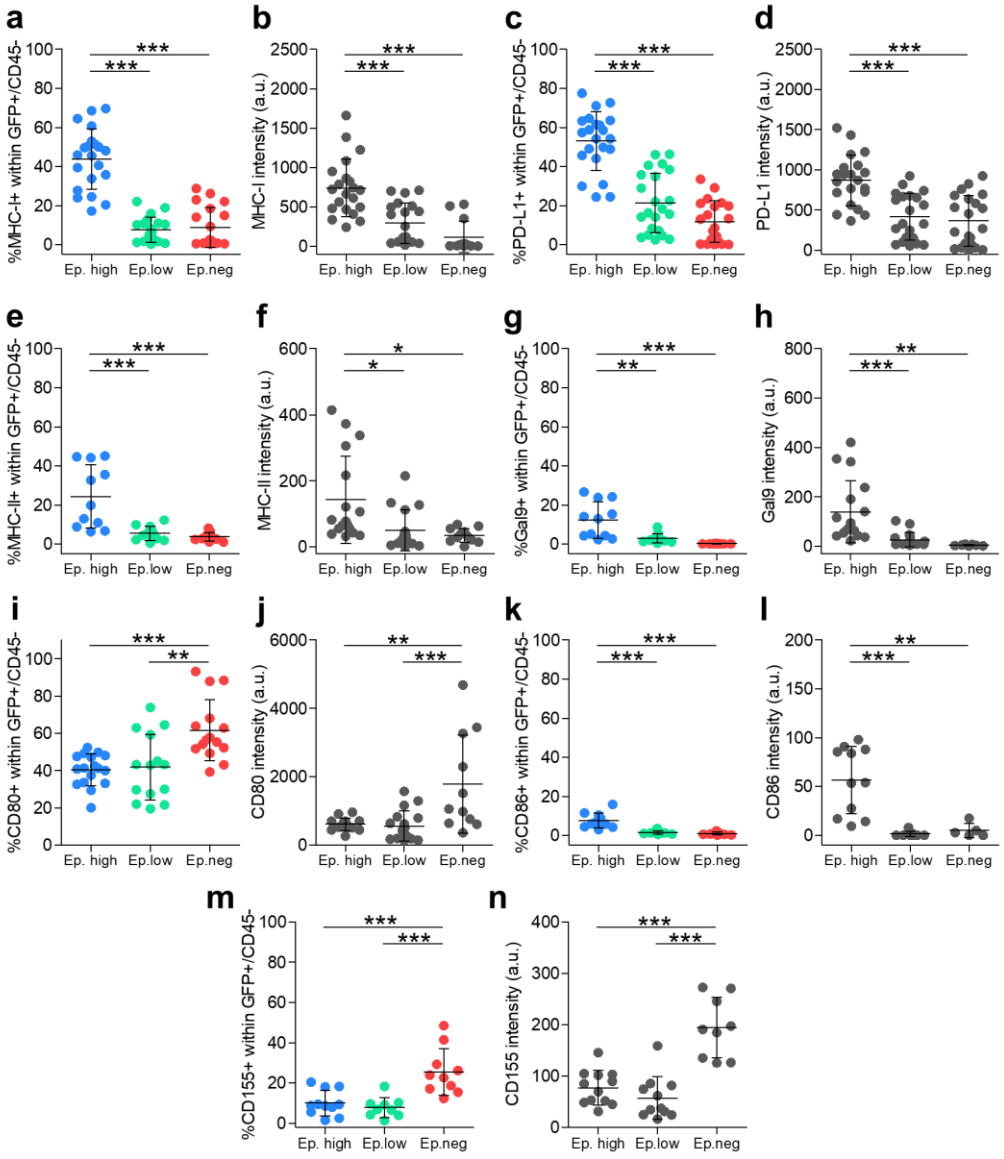

Figure 44. Characterization of immune-checkpoint ligand expression in different cancer cell populations in mixed SCCs. Percentage of (**a**) MHC-I^{+}, (**c**) PD-L1^{+}, (**e**) MHC-II^{+}, (**g**) Gal9^{+}, (**i**) CD80^{+}, (**k**) CD86^{+}, and (**m**) CD155^{+} cancer cells within Ep. high (GFP^{+}/CD45^{-}/EpCAM^{high}), Ep. low (GFP^{+}/CD45^{-}/EpCAM^{low}), or Ep. neg (GFP^{+}/CD45^{-}/EpCAM^{-}) cancer cell populations present in mixed tumors (n≥12), as determined by flow cytometry. Intensity of expression of (**b**) MHC-I, (**d**) PD-L1, (**f**) MHC-II, (**h**) Gal9, (**j**) CD80, (**l**) CD86, and (**n**) CD155 in EpCAM^{high}, EpCAM^{low} and EpCAM^{-} cancer cells. Each symbol represents a single tumor and mean ± SD for each group is shown. (**a-n**) One-way ANOVA followed by Tukey's multiple comparison test; *p≤0.05, **p≤0.01, ***p≤0.001.

3.3- CD80 can be used as a marker of hybrid/plastic cancer cells

Subsequently, we determined whether the induction of CD80 could be identified in a subset of cancer cells at intermediate stages of progression and be associated with the acquisition of cancer-cell plasticity. To do so, we performed immunofluorescence assays to evaluate the presence of $GFP^+/CD80^-/EpCAM^+$, $GFP^+/CD80^+/EpCAM^+$ and $GFP^+/CD80^+/EpCAM^-$ cancer cells in epithelial, mixed and mesenchymal SCCs (Figure 45a). The frequency of epithelial $GFP^+/CD80^-/EpCAM^+$ cancer cells per tumor area decreased in mixed tumors as compared to epithelial tumors, and dramatically disappeared in mesenchymal tumors (Figure 45b). In addition, mesenchymal $GFP^+/CD80^+/EpCAM^-$ cancer cells slightly increased in mixed tumors and highly increased in mesenchymal tumors (Figure 45d). The frequency of $GFP^+/CD80^+/EpCAM^+$ cancer cells per tumor area specifically increased in mixed tumors, this being the main population in these tumors (Figure 45c). These results demonstrate that $GFP^+/CD80^+/EpCAM^+$ cancer cells appear for the first time at intermediate stages of progression, suggesting that the induction of CD80 expression could be associated with the acquisition of cancer-cell plasticity.

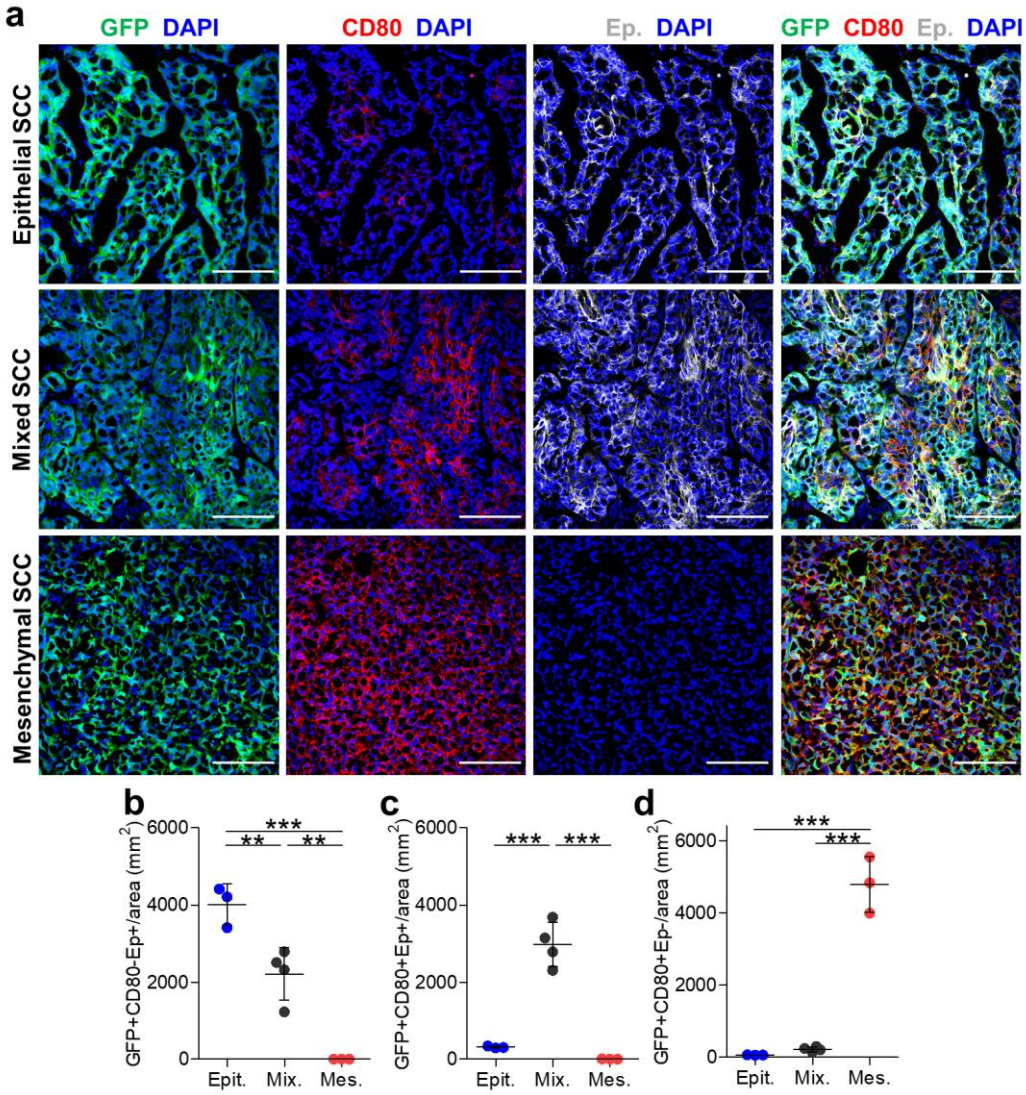

Figure 45. CD80 expression is induced in a population of EpCAM$^+$ cancer cells from mixed tumors and fully expressed by mesenchymal-like EpCAM$^-$ cancer cells. a. Representative immunofluorescence images of GFP$^+$, CD80$^+$, EpCAM$^+$ cancer cells and DAPI labelled cell nuclei in epithelial, mixed and mesenchymal SCCs. Scale bar: 100 µm. Quantification of the frequency of (**b**) GFP$^+$/CD80$^-$/EpCAM$^+$, (**c**) GFP$^+$/CD80$^+$/EpCAM$^+$, and (**d**) GFP$^+$/CD80$^+$/EpCAM$^-$ cancer cells per tumor area (mm^2) in epithelial (n=3), mixed (n=4) and mesenchymal (n=3) tumors. At least 9 fields of different regions were quantified in each tumor. Each symbol represents a single tumor and mean ± SD for each group is shown. (**b-d**) One-way ANOVA followed by Tukey's multiple comparison test; **p≤0.01, ***p≤0.001.

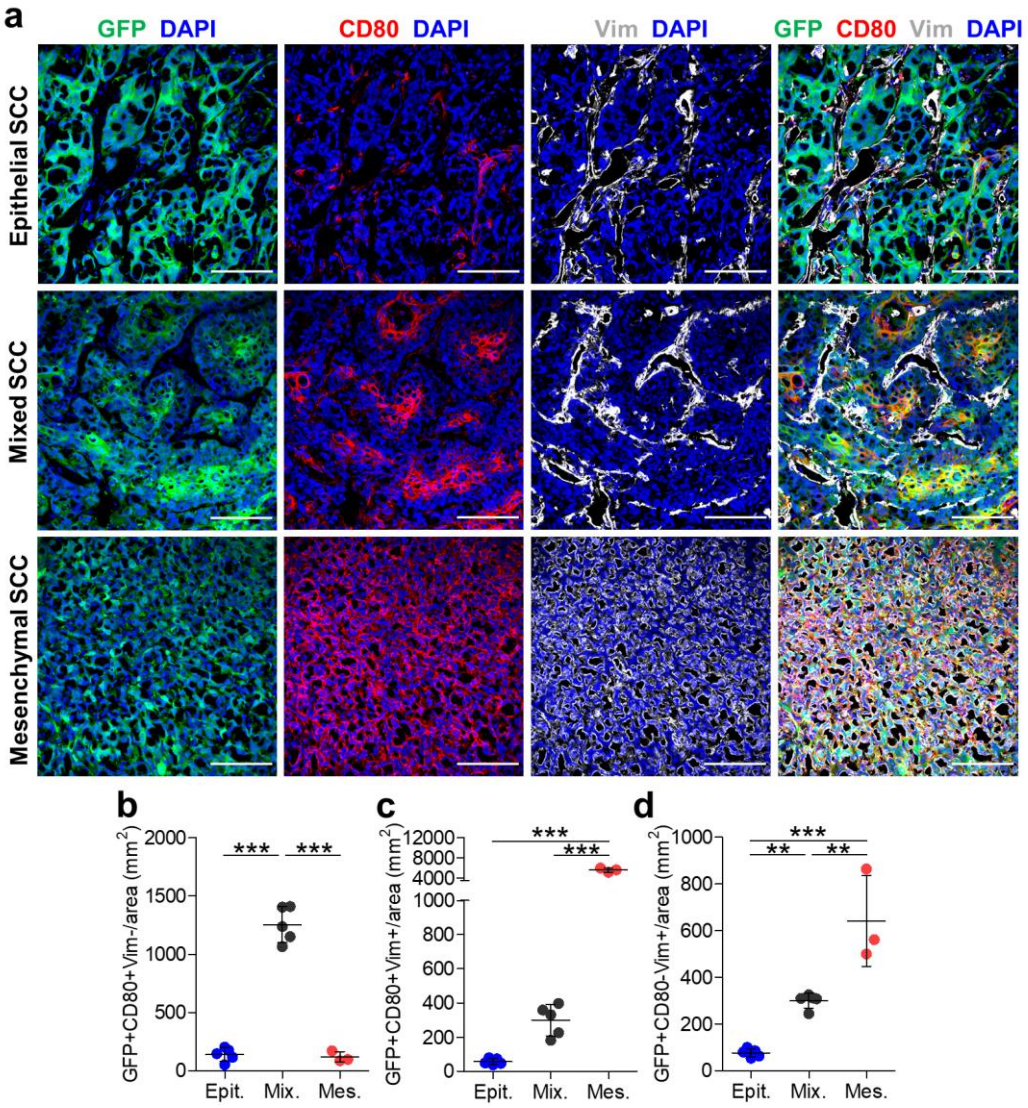

Figure 46. CD80 expression is upregulated in hybrid and mesenchymal cancer cells. a. Representative immunofluorescence images of GFP$^+$, CD80$^+$, Vimentin$^+$ cancer cells and DAPI labelled cell nuclei in epithelial, mixed and mesenchymal SCCs. Scale bar: 100 µm. Quantification of the frequency of (**b**) GFP$^+$/CD80$^+$/Vimentin$^-$, (**c**) GFP$^+$/CD80$^+$/Vimentin$^+$, and (**d**) GFP$^+$/CD80$^-$/Vimentin$^+$ cancer cells per tumor area (mm^2) in epithelial (n=5), mixed (n=5) and mesenchymal (n=3) tumors. At least 9 fields of different regions were quantified in each tumor. Each symbol represents a single tumor and mean ± SD for each group is shown. (**b-d**) One-way ANOVA followed by Tukey's multiple comparison test; **p≤0.01, ***p≤0.001.

To further evaluate whether within these $GFP^+/CD80^+/EpCAM^+$ cancer cells we could find $EpCAM^{low}$ cancer cells (hybrid epithelial-mesenchymal cells), we performed immunofluorescence assays to evaluate the expression of the mesenchymal marker Vimentin (Figure 46a). The identification of $EpCAM^{low}$ cancer cells is of utmost importance because, together with another member of the lab (Marta López Cerdá, PhD student), we demonstrated that hybrid epithelial-mesenchymal cancer cells show a strong plasticity and the ability to switch toward the mesenchymal-like state. We observed that whereas the expression of Vimentin was mostly detected in stromal cells of epithelial tumors, the frequency of $GFP^+/CD80^-/Vimentin^+$ cancer cells increased in mixed tumors, and further increased in mesenchymal tumors (Figure 46d). We also noticed that the frequency of $GFP^+/CD80^+/Vimentin^-$ cancer cells per tumor area specifically increased in mixed tumors (Figure 46b), which would be related to the specific increase in the frequency of epithelial $GFP^+/CD80^+/EpCAM^+$ cancer cells previously detected (Figure 45c). In addition, the frequency of $GFP^+/CD80^+/Vimentin^+$ cancer cells per tumor area slightly increased in mixed tumors, following a similar profile than $EpCAM^{low}$ cancer cells, and dramatically increased in mesenchymal tumors (Figure 46c). Altogether, these results indicate that mesenchymal tumors are mainly composed of $GFP^+/CD80^+/Vimentin^+$ cancer cells, followed by mesenchymal $GFP^+/CD80^-/Vimentin^+$ cancer cells. In contrast, epithelial tumors are composed mainly of cancer cells that could be identified as $GFP^+/CD80^-/EpCAM^+/Vimentin^-$ cancer cells. In addition, the initial induction of CD80 expression in cancer cells happens at intermediate stages of progression, concomitantly with the acquisition of cancer-cell plasticity, and mesenchymal-like $EpCAM^-$ cancer cells strongly induced the expression of CD80. Taken together, these results suggest that CD80 could impede the cytolytic activity of T and NK cells through its binding to CTLA-4 in mixed and mesenchymal tumors, protecting plastic/hybrid and mesenchymal cancer cells of the anti-tumor immune response.

Summary Chapter 3: The characterization of cancer-cell features could be used to predict responses to ICB therapies

All the results presented in Chapter 3 demonstrate that epithelial, mixed and mesenchymal SCCs have different immune evasion mechanisms to attenuate the effectiveness of T and NK cells. This is achieved by a change in IC ligand expression during SCC progression, as well as corrupting antigen presentation to avoid T-cell recognition. Our results demonstrate that during the progression from the epithelial to the mesenchymal state, cancer cells loss progressively the expression of MHC-I, which might lead to an impaired T-cell recognition and activation. In addition, whereas PD-L1, MHC-II, Gal9, and CD86 are mostly expressed by epithelial cancer cells, mesenchymal cancer cells strongly downregulate their expression and upregulate a different repertoire of IC ligands. In particular, mesenchymal cancer cells significantly induce the expression of CD80 and CD155, ligands of CTLA-4 and TIGIT IC receptors, respectively. These results suggest that SCCs containing mostly epithelial differentiation features (WD-SCCs) might respond to ICB therapies based on

monotherapy with anti-PD-1/PD-L1 antibodies, as well as in combination with anti-LAG-3, anti-TIM-3, or anti-CTLA-4. On the other hand, mixed and mesenchymal tumors (PD/S-SCCs) might be refractory to anti-PD-1/PD-L1 therapies, and the blockade of other IC receptors such as CTLA-4 and TIGIT should be tested to enhance anti-tumor responses. Altogether, our data indicate the relevance of different IC pathways induced by cancer and immunosuppressive cells, and inform us about which combinatory ICB therapies could more efficiently boost the adaptive and innate anti-tumor immune response depending on cancer-cell features.

CHAPTER 4. CHARACTERIZATION OF CANCER-CELL FEATURES AND TUMOR-INFILTRATING IMMUNE CELLS IN PATIENT SKIN SCCs AT DIFFERENT STAGES OF PROGRESSION

Previous studies indicated that cancer-cell features may dictate the immune landscape of tumors, and in turn, these immune cells may play an important role in promoting tumor progression and metastasis (Coussens et al., 2013; Dongre et al., 2017; Lu et al., 2014; Tamborero et al., 2018). However, limited information is available about the immune landscape of patient skin SCCs (Bottomley et al., 2019; Ji et al., 2020), or if the tumor immune microenvironment switches from a pro-inflammatory to a pro-tumoral and immunosuppressive state, concomitantly with the loss of epithelial differentiation traits and the acquisition of hybrid and mesenchymal features. To determine the clinical relevance of our findings (Chapters 1 to 3), we examined whether cancer and immune alterations described in mouse mesenchymal tumors were also associated with progression in patient skin SCCs. To address this, we performed immunofluorescence and immunohistochemistry assays in a subset of patient skin SCCs (Table 1). Given that the histopathologic grade of patient samples frequently showed intratumoral heterogeneity, these samples were classified according to their main stage of progression and the percentage that this region represented in the overall sample (Table 1). These samples included two WD/MD-SCCs (G2 grade: H49 and H24), five MD/PD-SCCs (G2/G3 grade: H14, H34, H41, H45, and H46), five PD-SCCs (G3/G4 grade: H10, H43, H44, H48 and H54) and two undifferentiated PD/S-SCCs (G4 grade: H11 and H15). Subsequently, these samples were classified into three groups according to their cancer-cell features (see the next section): epithelial WD/MD-SCCs (H14, H24, H41 and H49), mixed MD/PD-SCCs (H10, H34, H43, H44, H46, and H48), and mesenchymal PD/S-SCCs (H11, H15, H45 and H54).

4.1- Characterization of cancer-cell features of patient skin SCCs at different stages of progression

To determine the epithelial, hybrid or mesenchymal features of cancer cells, we analyzed the expression of E-cadherin and Vimentin by immunofluorescence assays in different patient SCC samples (Figure 47). Furthermore, we determined the frequency of epithelial E-cadherin^{+}/Vimentin^{-}, hybrid E-cadherin^{+}/Vimentin^{+} and mesenchymal E-cadherin^{-}/Vimentin^{+} cancer cells per tumor area in these samples (Figures 48a to 48d). Given that most SCCs showed a strong intratumoral heterogeneity, the presence of epithelial, hybrid and mesenchymal cancer cells changed considerably in the different regions of each sample. Therefore, to perform these analyses, we captured multiple representative images of different tumor regions to recapitulate the heterogeneity of each sample. We observed that the frequency of epithelial E-cadherin^{+}/Vimentin^{-} cancer cells per tumor area slightly decreased in G3 SCCs (H46, H34, H48, H43, H10 and H44) as compared to G2 SCCs (H49, H24, H14 and H41), and disappeared in advanced G3/G4 SCCs (H11, H15, H45 and

H54) (Figures 47, 48a and 48d). In addition, whereas the expression of Vimentin was only detected in stromal cells of epithelial G2 SCCs, its expression was slightly induced in cancer cells from G3 SCCs and was highly expressed in cancer cells from G3/G4 SCCs (Figures 47, 48c and 48d). We also noticed that the frequency of hybrid E-cadherin^{+}/Vimentin^{+} cancer cells per tumor area specifically increased in G3 SCCs (Figures 47, 48b and 48d), coinciding with our previously described appearance of hybrid epithelial-mesenchymal cancer cells at intermediate stages of mouse SCC progression (Figure 17c). Altogether, in accordance to our mouse model results, epithelial G2 SCCs are composed mainly of epithelial cancer cells that could be identified as E-cadherin^{+}/Vimentin^{-} cancer cells (Figure 48d). As tumors progress to a moderate differentiated phenotype (G3 SCCs), we can detect 3 different populations: epithelial E-cadherin^{+}/Vimentin^{-}, hybrid E-cadherin^{+}/Vimentin^{+} and mesenchymal E-cadherin^{-}/Vimentin^{+} cancer cells (Figure 48d), and these tumors were classed as mixed SCCs. Finally, advanced G3/G4 SCCs are composed almost exclusively of mesenchymal E-cadherin^{-}/Vimentin^{+} cancer cells (Figure 48d), and these tumors were classed as mesenchymal SCCs. As a result, these studies bring to the forefront the possibility of using the epithelial, hybrid and mesenchymal phenotypic states of cancer cells as an important marker to predict responses to ICB therapies.

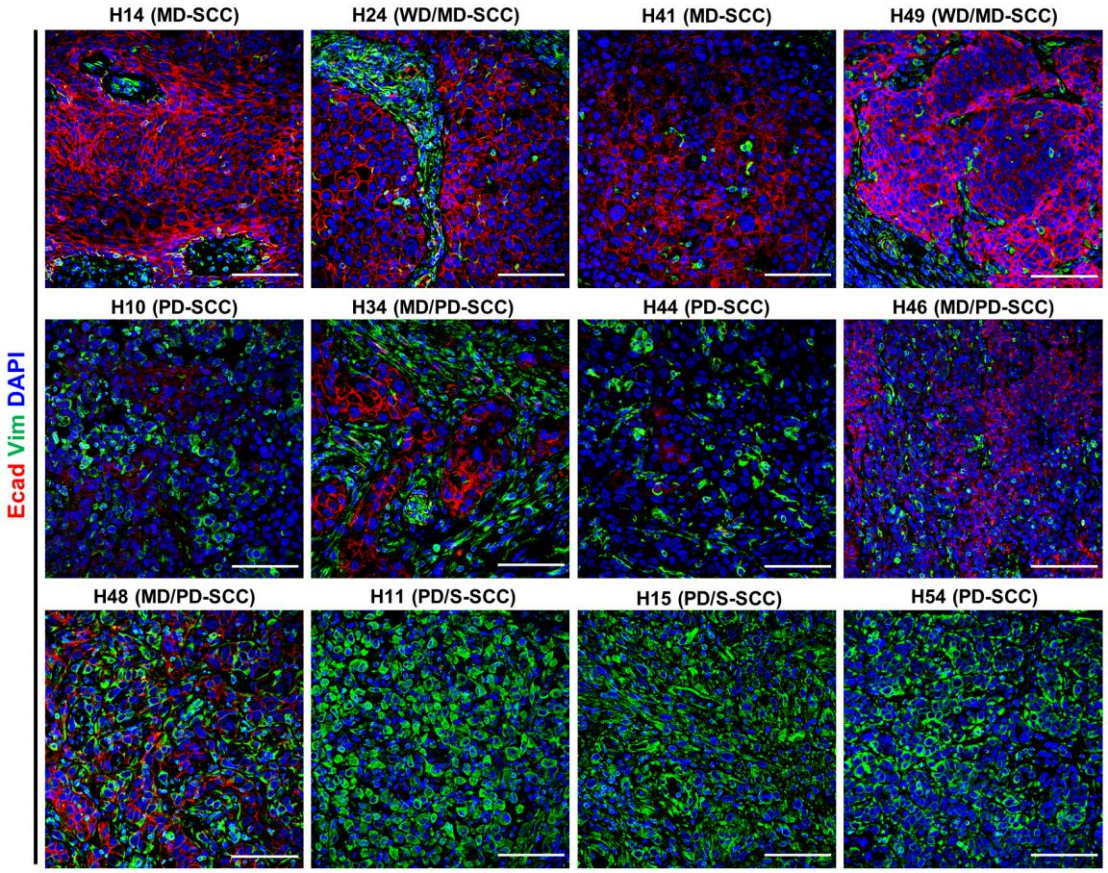

Figure 47. E-cadherin/Vimentin expression in cancer cells from patient SCCs at different stages of progression. Representative immunofluorescence images of E-cadherin^{+}, Vimentin^{+} cells and DAPI labelled cell nuclei in the indicated patient SCC samples. Scale bar: 100 µm.

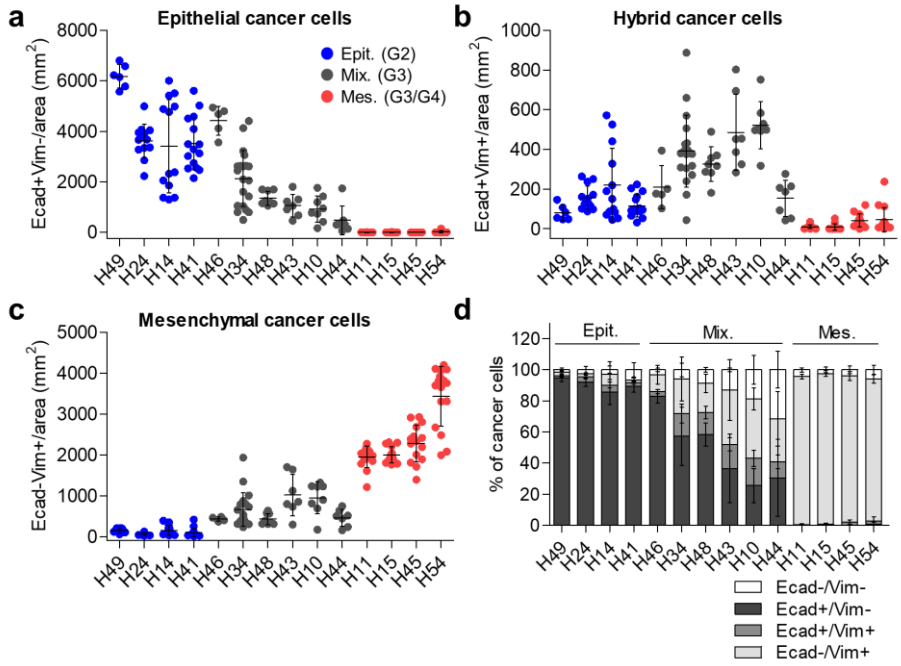

Figure 48. Frequency of epithelial, hybrid and mesenchymal cancer cells in patient SCC samples. Quantification of the frequency of (**a**) epithelial E-cadherin$^+$/Vimentin$^-$, (**b**) hybrid E-cadherin$^+$/Vimentin$^+$, and (**c**) mesenchymal E-cadherin$^-$/Vimentin$^+$ cancer cells per tumor area (mm^2) in the indicated patient SCC samples. At least 8 fields of different regions were quantified in each tumor. Each symbol represents a single tumor region (image) and mean ± SD for each tumor is shown. **d**. Percentage (mean ± SD) of E-cadherin$^-$/Vimentin$^-$, E-cadherin$^+$/Vimentin$^-$, E-cadherin$^+$/Vimentin$^+$, and E-cadherin$^-$/Vimentin$^+$ cancer cells relative to total cancer cells in the indicated tumors.

4.2- Characterization of immune checkpoint ligand profile of patient skin SCCs at different stages of progression

Our previous studies in mouse models demonstrated that, during the progression from the epithelial to the mesenchymal state, cancer cells loss progressively the expression of MHC-I, which might lead to an impaired T-cell recognition. In addition, whereas PD-L1, MHC-II, Gal9 and CD86 were mostly expressed by epithelial cancer cells, mesenchymal cancer cells strongly downregulated their expression and upregulated the expression CD80 and CD155. In this sense, we hypothesized that the response to ICB therapies may be conditioned by the downregulation of MHC-I expression and by the upregulation of a repertoire of IC ligands in cancer cells that may activate different IC pathways to those mostly used in current ICB therapies (anti-PD-1/PD-L1 or anti-CTLA-4 therapy). For this reason, we evaluated whether advanced patient SCCs recapitulate the IC ligand alterations described in mouse mesenchymal tumors. To do this, we performed immunofluorescence assays using the antibodies α-HLA/MHC-I (Figure 49a), α-Galectin-9 (Figure 49b), and α-CD80 (Figure 49c) in different patient SCC samples. These assays showed that epithelial SCCs (H49, H14 and H41) and mixed SCCs (H46, H48 and H44) contained a higher frequency of HLA$^+$ cancer cells than mesenchymal SCCs (H11, H15, and H54; Figures 49a and 50a). In addition, we noticed that HLA

expression was mostly identified in Vimentin$^-$ cancer cells in epithelial and mixed SCCs (Figure 50d), which might correspond to cancer cells that retained E-cadherin expression in these tumors (Figure 48d). Contrarily, mesenchymal SCCs were mostly formed by mesenchymal HLA$^-$/Vimentin$^+$ cancer cells and by a low percentage of HLA$^+$/Vimentin$^+$ cancer cells (Figure 50d). Therefore, these results indicate that advanced patient SCCs formed mostly by mesenchymal Vimentin$^+$ cancer cells, which lose HLA expression, may become invisible to the recognition and attack of cytotoxic CD8$^+$ T lymphocytes and could be resistant to ICB therapies.

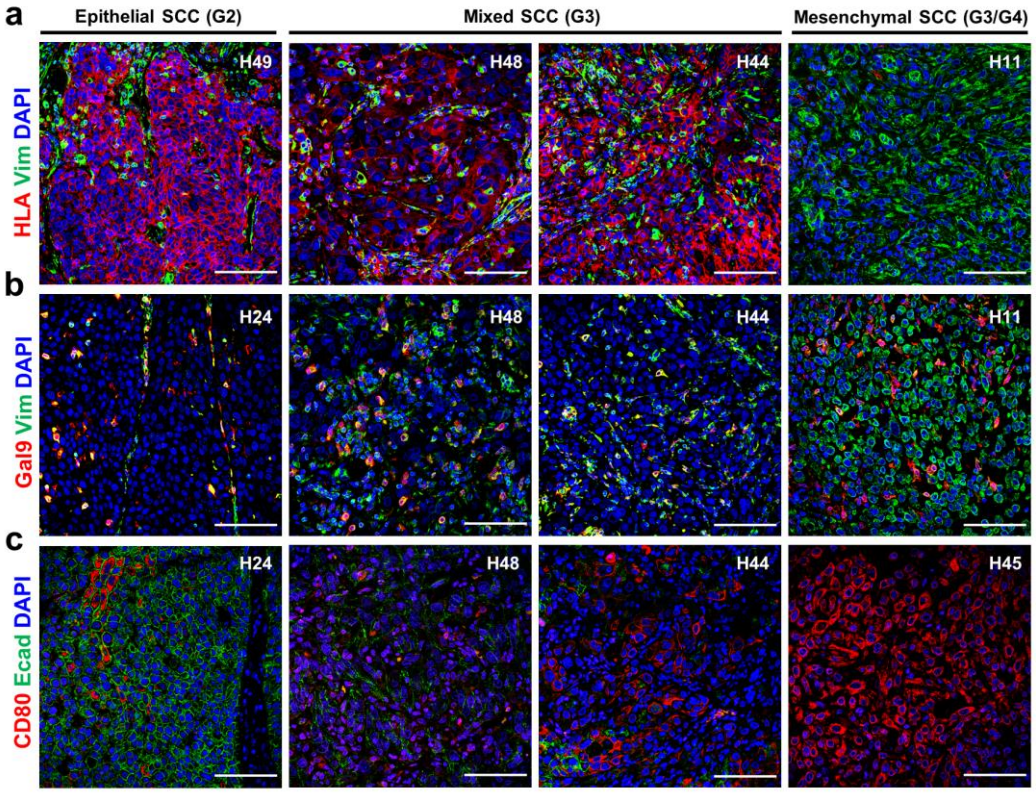

Figure 49. Identification and localization of HLA$^+$, Gal9$^+$, and CD80$^+$ cells in patient SCC samples. Representative immunofluorescence images of (**a**) HLA$^+$, (**b**) Gal9$^+$, (**c**) CD80$^+$, (**a, b**) Vimentin$^+$, (**c**) E-cadherin$^+$ cells and DAPI labelled cell nuclei in the indicated patient SCC samples. Scale bar: 100 µm.

On the other hand, the analysis of the expression of Galectin-9 (ligand of TIM-3) showed that mixed SCCs (H46, H48 and H44) contained a higher frequency of Gal9$^+$ cancer cells than epithelial SCCs (H49, H24 and H14), and its expression increased a bit more in cancer cells from mesenchymal SCCs (H11, H15, H45 and H54) (Figures 49b and 50b). However, focusing on all cancer cell populations found within a tumor, we noticed that the majority of Gal9$^+$ cancer cells express Vimentin, although the frequency of these cancer cells represents only 5-10% of all cancer cells (Figure 50e). These results suggest that Gal9 expression could be associated the acquisition of with hybrid and mesenchymal features (Figure 50e). In this regard, mixed SCCs showed a higher percentage of Gal9$^+$/Vimentin$^+$ cancer cells than epithelial SCCs, which probably correspond to hybrid cancer cells that induced Gal9 expression while showing epithelial-mesenchymal features

(Figure 50e). Furthermore, as we described in mouse models, full mesenchymal Vimentin$^+$ cancer cells from mesenchymal SCCs strongly downregulated Gal9 expression (Figure 50e), since most cancer cells that form these tumors were Gal9$^-$/Vimentin$^+$ cancer cells. We also observed an increased Gal9 expression within tumor-infiltrating immune cells of mixed and mesenchymal SCCs as compared to epithelial SCCs (Figure 50g), indicating the presence of immunosuppressive immune cells that could inactivate the cytotoxic function of CD8$^+$ and NK cells in these tumors.

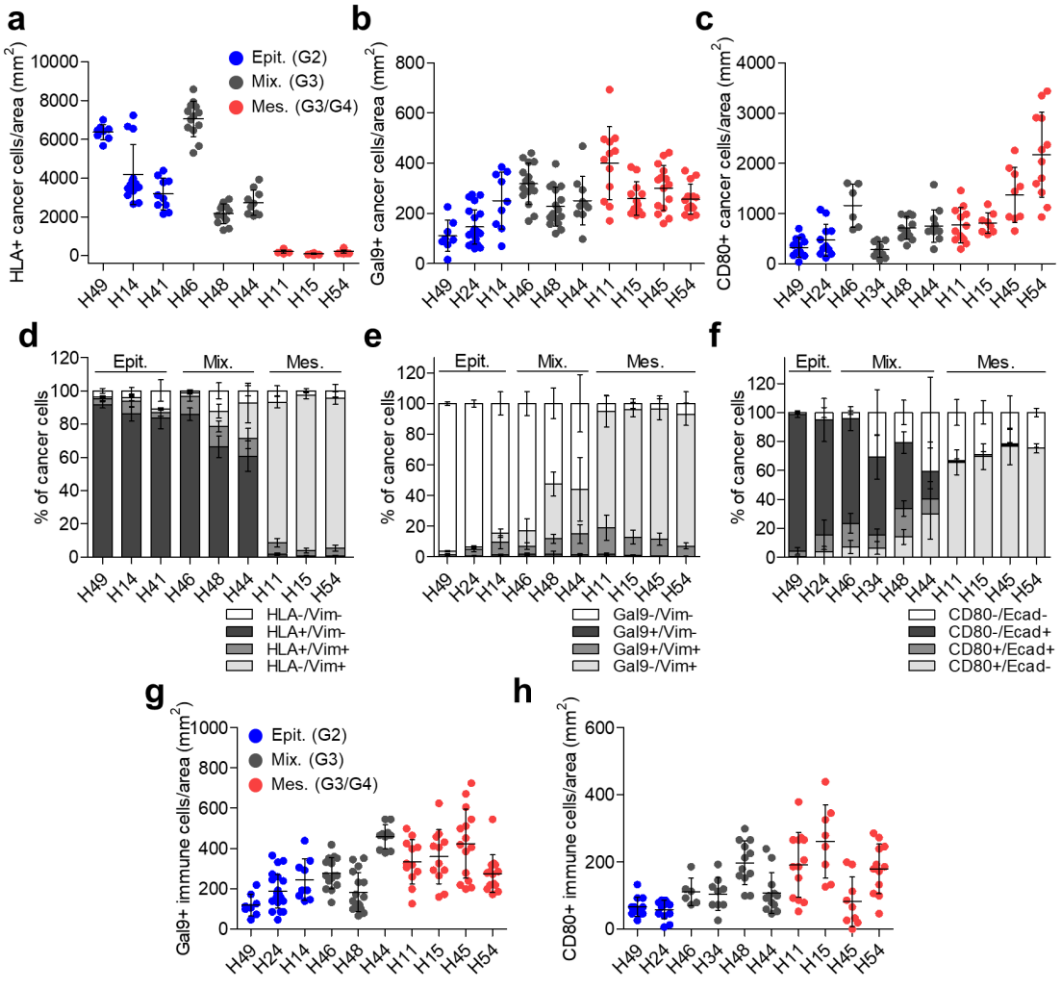

Figure 50. Frequency of HLA$^+$, Gal9$^+$, and CD80$^+$ cancer and immune cells in patient SCC samples. Quantification of the frequency of (**a**) HLA$^+$, (**b**) Gal9$^+$, and (**c**) CD80$^+$ cancer cells or (**g**) Gal9$^+$ and (**h**) CD80$^+$ immune cells per tumor area (mm^2) in the indicated patient SCC samples. At least 9 fields of different regions were quantified in each tumor. Each symbol represents a single tumor region (image) and mean ± SD for each tumor is shown. **d**. Percentage (mean ± SD) of HLA$^-$/Vimentin$^-$, HLA$^+$/Vimentin$^-$, HLA$^+$/Vimentin$^+$, and HLA$^-$/Vimentin$^+$ cancer cells relative to total cancer cells in the indicated tumors. **e**. Percentage (mean ± SD) of Gal9$^-$/Vimentin$^-$, Gal9$^+$/Vimentin$^-$, Gal9$^+$/Vimentin$^+$, and Gal9$^-$/Vimentin$^+$ cancer cells relative to total cancer cells in the indicated tumors. **f**. Percentage (mean ± SD) of CD80$^-$/E-cadherin$^-$, CD80$^-$/E-cadherin$^+$, CD80$^+$/E-cadherin$^+$, and CD80$^+$/E-cadherin$^-$ cancer cells relative to total cancer cells in the indicated tumors.

Finally, the quantification of CD80 expression (ligand of CTLA-4) showed that the frequency of CD80$^+$ cancer cells per tumor area was significantly increased in mesenchymal SCCs (H11, H15,

H45 and H54) (Figures 49c and 50c), and CD80 expression was mostly observed on cancer cells that have lost E-cadherin expression (Figure 50f). In particular, the frequency of mesenchymal CD80^{+}/E-cadherin^{-} cancer cells slightly increased in a subset of cancer cells in mixed SCCs and was highly increased in mesenchymal SCCs (Figure 50f). Of special interest was that the frequency of CD80^{+}/E-cadherin^{+} cancer cells specifically increased in mixed SCCs (Figure 50f). These results suggest that the induction of CD80 could be associated with the acquisition of cancer-cell plasticity, as previously reported during mouse SCC progression in this Thesis. In addition, we observed a higher CD80 expression within tumor-infiltrating immune cells of mixed SCCs and mesenchymal SCCs as compared to epithelial SCCs (Figure 50h). Altogether, these results indicate that IC ligand expression changes depending on the epithelial, hybrid or mesenchymal features of cancer cells of patient SCCs, which could lead these cancer cells to evade immune responses through different IC pathways. Given the importance of having a comprehensive information of all IC ligands expressed by cancer cells at different stages of human progression, we will evaluate in future experiments the expression of PD-L1, MHC-II and CD155, ligands of PD-1, LAG-3 and TIGIT, respectively.

4.3- Advanced and mesenchymal SCCs exhibit an increased infiltration of exhausted T cells and immunosuppressive Treg cells

Our previous studies in mice demonstrated that the presence of hybrid and mesenchymal cancer cells was associated with an increased infiltration of exhausted T lymphocytes (Figures 29a to 29e), which are characterized by an increased expression of some IC receptors such as PD-1, CTLA-4, TIM-3, LAG-3, and TIGIT, among others (Pardoll, 2012; Wherry and Kurachi, 2015). For this reason, we evaluated the frequency, spatial distribution and activation status of CD8^{+} T lymphocytes at different stages of patient SCC progression. To tackle this, we performed immunofluorescence assays using an α-CD8 antibody in epithelial, mixed, and mesenchymal SCCs (Figure 51a).

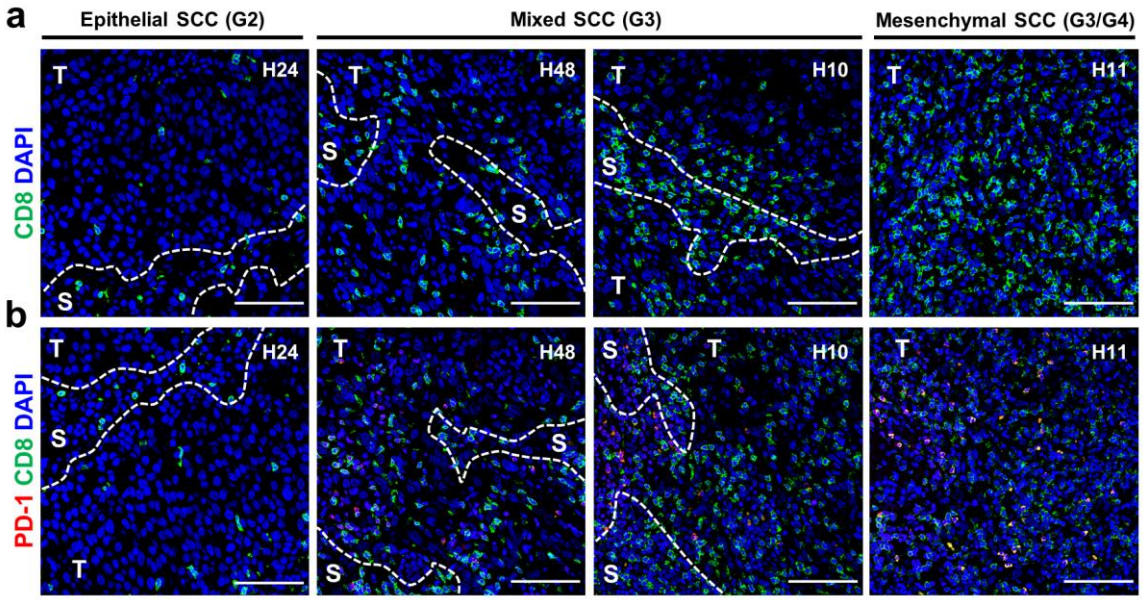

Figure 51. Localization of CD8$^+$ T lymphocytes, with or without PD-1 expression, in patient SCC samples. a-b. Representative immunofluorescence images of CD8$^+$ and PD-1$^+$ cells and DAPI labelled cell nuclei in the indicated patient SCC samples. (T) indicates tumor regions, and (S) indicates stromal regions. Scale bar: 100 µm.

These studies showed that the frequency of CD8$^+$ T cells per tumor area was higher in mixed SCCs (H46, H34, H48, H43, H10 and H44) than in epithelial SCCs (H49, H24, H14 and H41), and further increased in mesenchymal SCCs (H11, H15, H45 and H54) (Figures 51a, 52a and 52b), in agreement with our results in mouse mesenchymal tumors (Figures 27a and 27b). Moreover, whereas CD8$^+$ T cells were mainly located in stromal regions of epithelial SCCs, these immune cells showed a greater capacity to infiltrate the tumor core of mixed SCCs and were totally located in close proximity to cancer cells (intratumoral areas) in mesenchymal SCCs (Figure 52c).

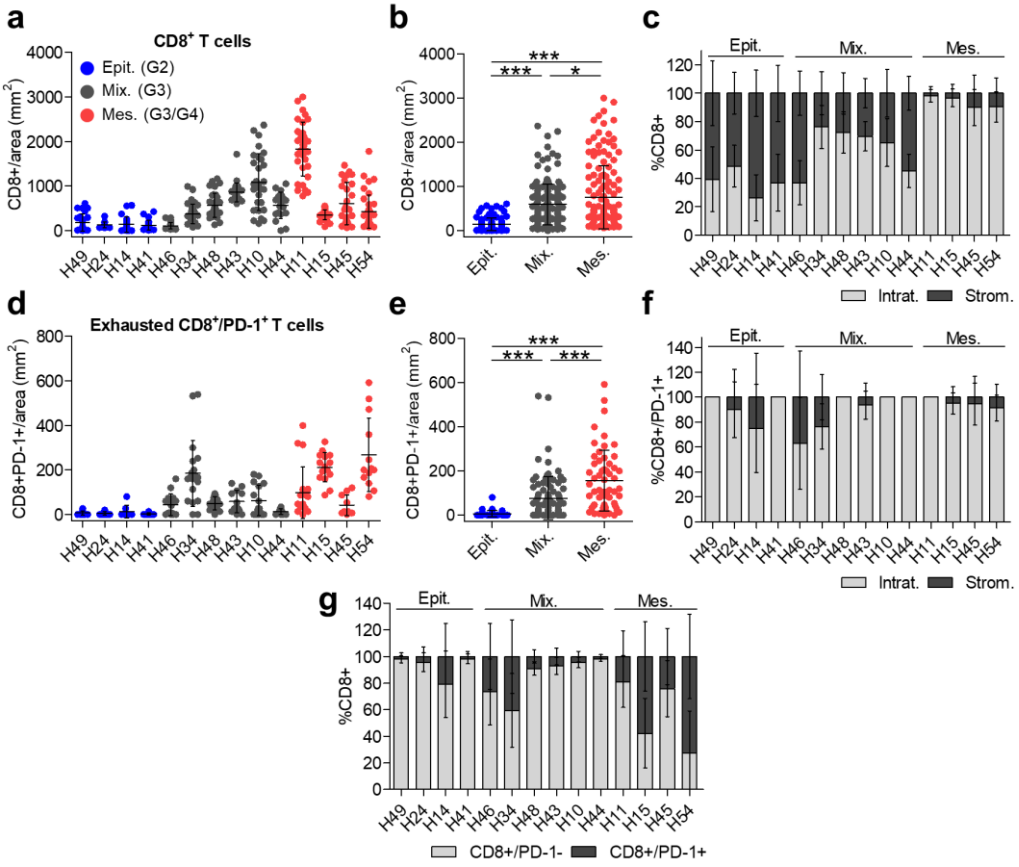

Figure 52. Frequency, localization and active state of CD8$^+$ T cells in patient SCC samples. Quantification of the frequency of (**a**, **b**) CD8$^+$, and (**d**, **e**) CD8$^+$/PD-1$^+$ T cells per tumor area (mm^2) in the indicated patient SCC samples or SCC groups. At least 10 fields of different regions were quantified in each tumor. Each symbol represents a single tumor region (image) and mean ± SD for each tumor or SCC group is shown. Percentage (mean ± SD) of intratumoral or stromal (**c**) CD8$^+$ and (**f**) CD8$^+$/PD-1$^+$ T cells relative to total CD8$^+$ T lymphocytes in the indicated tumors. **g.** Percentage (mean ± SD) of CD8$^+$/PD-1$^-$ and CD8$^+$/PD-1$^+$ T cells relative to total CD8$^+$ T lymphocytes in the indicated tumors. (**b**, **e**) One-way ANOVA followed by Tukey's multiple comparison test; *p≤0.05, ***p≤0.001.

Subsequently, we analyzed the expression of the IC receptor PD-1 within $CD8^+$ T lymphocytes in epithelial, mixed and mesenchymal SCCs by immunofluorescence assays (Figure 51b). This analysis showed that the frequency of $CD8^+/PD\text{-}1^+$ T cells was significantly higher in mixed SCCs (H46, H34, H48, H43, H10 and H44) and mesenchymal SCCs (H11, H15, H45 and H54) than in epithelial SCCs (H49, H24, H14 and H41) (Figures 52b, 52d, and 52e), indicating that a high proportion of $CD8^+$ T cells infiltrating mixed and mesenchymal SCCs might be in an exhausted state (Figure 52g). Furthermore, exhausted $CD8^+/PD\text{-}1^+$ T cells, regardless of tumor differentiation features, were mainly located in close proximity to cancer cells (intratumoral areas), with the exception of patients H14, H46 and H34, in which we detected about 20-40% of them in stromal areas (Figure 52f). Taken together, these results indicate that mixed and mesenchymal SCCs are infiltrated by exhausted cytotoxic $CD8^+$ T lymphocytes, which would be unable to attack cancer cells. Given the importance of having a comprehensive information of all IC receptors expressed by $CD8^+$ T and NK cells at different stages of patient SCC progression, we will evaluate in future experiments the co-expression of LAG-3, TIM-3, CTLA-4 and TIGIT in $CD8^+$ and NK cells to uncover which IC pathways may be being blocked.

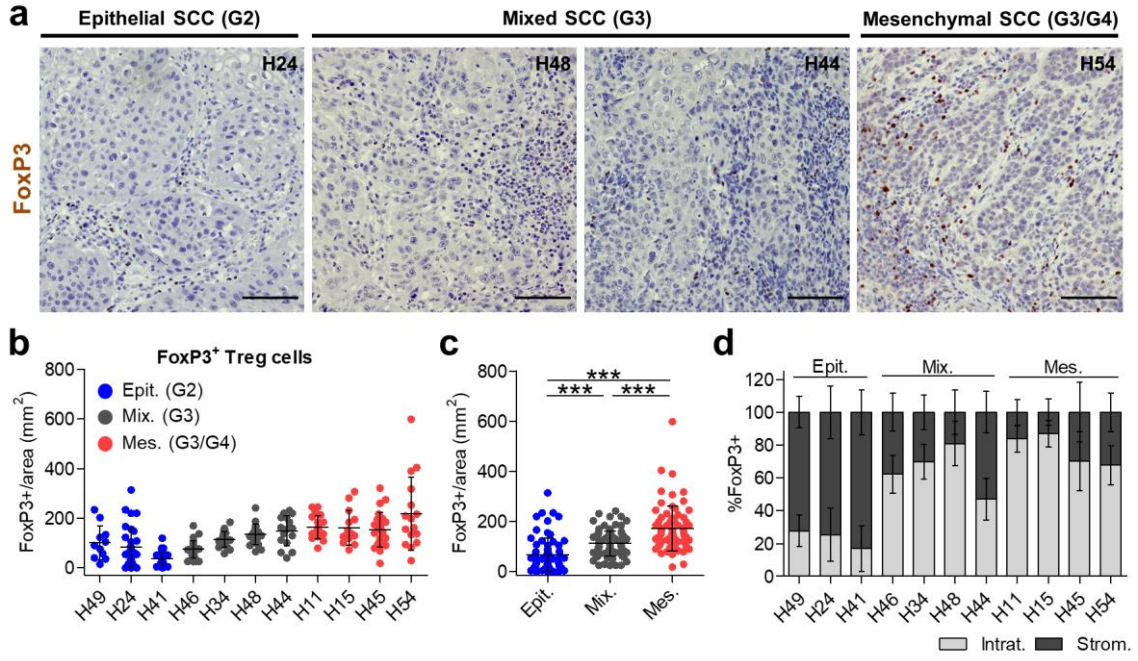

Figure 53. Localization and frequency of $FoxP3^+$ Treg lymphocytes in patient SCC samples. a. Representative immunohistochemistry images of $FoxP3^+$ cells in the indicated patient SCC samples. Scale bar: 100 µm. **b, c.** Quantification of the frequency of $FoxP3^+$ cells per tumor area (mm^2) in the indicated patient SCC samples or SCC groups. At least 11 fields of different regions were quantified in each tumor. Each symbol represents a single tumor region (image) and mean ± SD for each tumor or SCC group is shown. **d.** Percentage (mean ± SD) of intratumoral or stromal $FoxP3^+$ Treg cells relative to total $FoxP3^+$ T regulatory lymphocytes in the indicated tumors. (**c**) One-way ANOVA followed by Tukey's multiple comparison test; ***$p \leq 0.001$.

Given that our studies in mouse models indicated that the presence of hybrid and mesenchymal cancer cells correlates with an increased infiltrate of immunosuppressive Treg cells (Figures 27g and 27h), we analyzed the presence of this immune cell population by the expression of FoxP3 marker in patient SCC samples at different stage of progression, (Figure 53a). As we expected, a significant increase of $FoxP3^+$ Treg lymphocytes per tumor area was detected in mixed SCCs (H46, H34, H48 and H44) and further increased in mesenchymal SCCs (H11, H15, H45 and H54) as compared to epithelial SCCs (H49, H24 and H41) (Figures 53a to 53c). This immune cell population was mainly located in the stromal regions of epithelial SCCs (≈80%), whereas only 20% of them were detected in intratumoral areas (Figure 53d). In mixed SCCs, there was a shift in the location of $FoxP3^+$ cells toward the intratumoral areas, but still maintaining 20-40% of them in the stromal area (Figure 53d). Finally, $FoxP3^+$ cells were fully located in close proximity to cancer cells (intratumoral areas) in mesenchymal SCCs (Figure 53d). These results demonstrate that mixed and mesenchymal SCCs exhibit a high infiltration of immunosuppressive Treg cells into the tumor core that could interfere with the cytotoxic activity of $CD8^+$ and NK cells. Altogether, these results indicate that mesenchymal SCCs exhibit a higher infiltration of exhausted $CD8^+$ T lymphocytes and immunosuppressive Treg cells than epithelial and mixed SCCs, which may favor the aggressive growth of advanced SCCs.

4.4- Advanced and mesenchymal SCCs exhibit an increased infiltration of immunosuppressive macrophages

Finally, we performed immunohistochemistry assays with an α-CD68 antibody, which recognize both M1- and M2-like macrophages, and with an α-CD163 antibody, which recognize M2-like macrophages, in patient samples at different stages of SCC progression (Figures 54a and 54b). In accordance to our results in mouse models (Figures 35a and 35b), we observed a significant increase in the frequency of $CD68^+$ macrophages per tumor area in mixed SCCs (H48 and H10) compared to epithelial SCCs (H49, H24 and H14). This frequency was further increased in mesenchymal SCCs (H11, H15, H45 and H54) (Figures 54a, 55a and 55b). In addition, we detected that about 80% of $CD68^+$ macrophages were located in the stroma of epithelial and mixed SCCs (Figure 55c) and were located in close proximity to cancer cells (intratumoral area) in mesenchymal SCCs (Figure 55c). Furthermore, similarly to that reported for Treg cells (Figures 53a to 53c), a significant increase in the frequency of immunosuppressive $CD163^+$ M2-like macrophages per tumor area was detected in mixed SCCs (H46, H34, H48 and H10), which further increased in mesenchymal SCCs (H11, H15, H45 and H54) in comparison to epithelial SCCs (H49, H24, H14 and H41) (Figures 54b, 55d and 55e). Almost all $CD163^+$ M2-like macrophages were located in the stroma of epithelial SCCs (Figure 55f), indicating that most of $CD68^+$ macrophages infiltrating the epithelial tumor core may be anti-tumorigenic M1-like macrophages (Figure 55c). In mixed SCCs, there was a shift in the location of $CD163^+$ M2-like macrophages toward the intratumoral areas, but still maintaining 40-60% of them

in the stromal area, to finally be located mostly in the intratumoral area of mesenchymal SCCs (Figure 55f). Altogether, these results indicate that advanced and mesenchymal SCCs exhibit a higher infiltration of CD68$^+$ macrophages than epithelial and mixed SCCs, mainly due to an increase in CD163$^+$ M2-like macrophages. This situation might generate a tumor-promoting local environment that could negatively influence the immunotherapy response of advanced and mesenchymal SCCs.

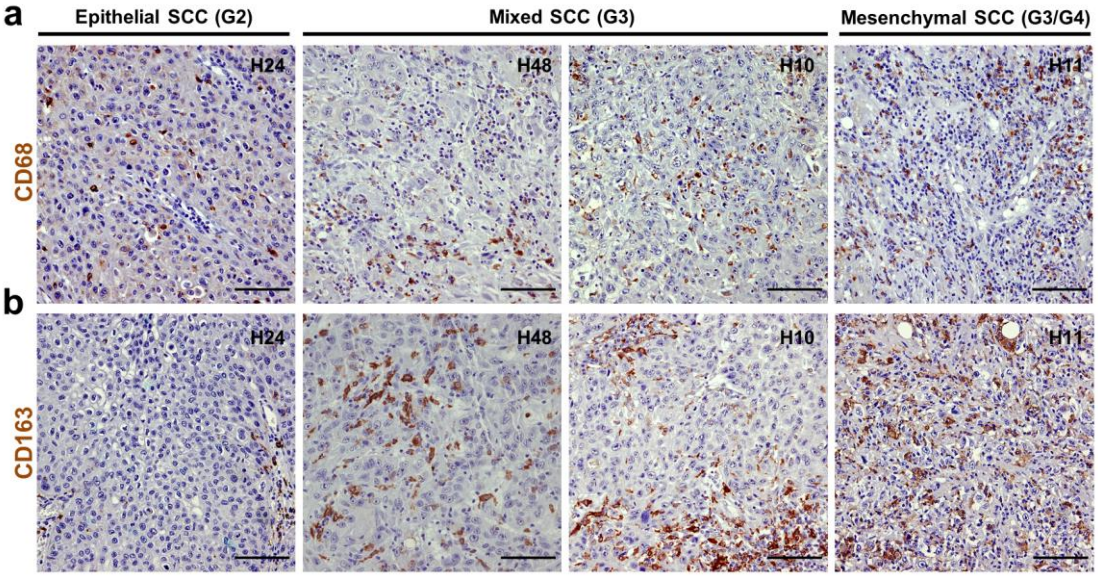

Figure 54. Localization of CD68$^+$ and CD163$^+$ macrophages in patient SCC samples. Representative immunohistochemistry images of (**a**) CD68$^+$ and (**b**) CD163$^+$ immune cells in the indicated patient SCC samples. Scale bar: 100 µm.

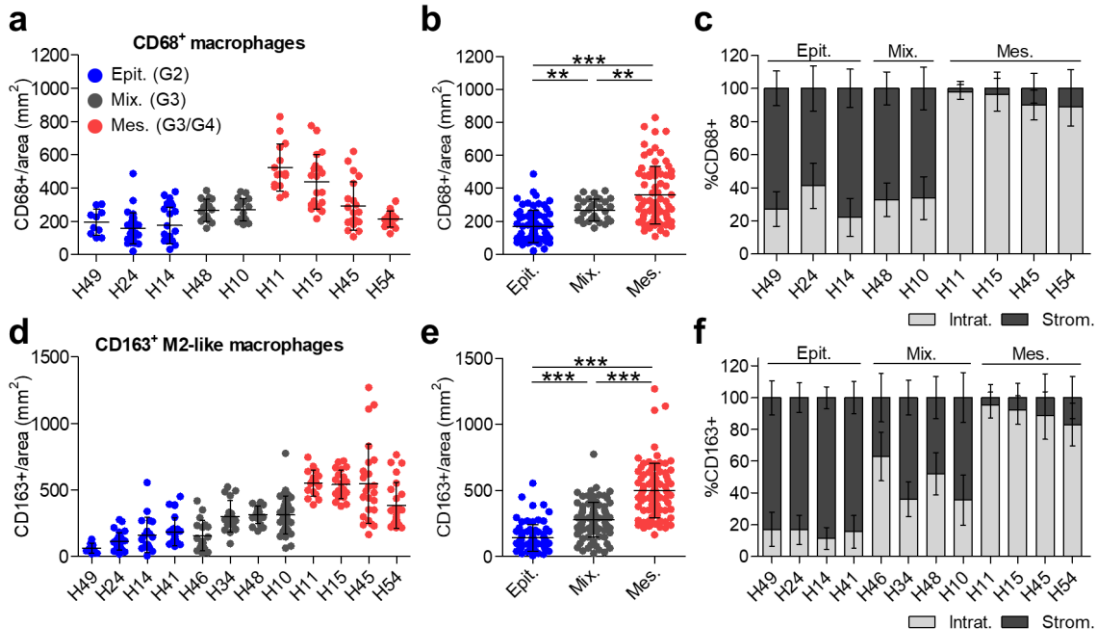

Figure 55. Frequency of tumor-infiltrating CD68$^+$ and CD163$^+$ macrophages in patient SCC samples at different stages of progression. Quantification of the frequency of (**a, b**) CD68$^+$ and (**d, e**) CD163$^+$ cells per

tumor area (mm^2) in the indicated patient SCC samples or SCC groups. At least 15 fields of different regions were quantified in each tumor. Each symbol represents a single tumor region (picture) and mean ± SD for each tumor or SCC group is shown. Percentage (mean ± SD) of intratumoral or stromal (**c**) $CD68^+$ cells relative to total $CD68^+$ macrophages and (**f**) $CD163^+$ cells relative to total $CD163^+$ M2-like macrophages in the indicated tumors. (**b, e**) One-way ANOVA followed by Tukey's multiple comparison test; **$p \leq 0.01$, ***$p \leq 0.001$.

Summary Chapter 4: Immune landscape changes during patient SCC progression, concomitantly with the acquisition of cancer-cell plasticity and mesenchymal-like cancer cell traits

Our results of Chapter 4 demonstrate that, similarly to our studies in mouse models, the frequency and distribution of immune cells change during patient SCC progression. In this sense, patient SCCs with a high content of hybrid and mesenchymal cancer cells might be resistant to ICB therapies because these cancer cells lose the expression of HLA, which is necessary for cancer-cell recognition by $CD8^+$ T cells. These hybrid and mesenchymal cancer cells may have additional mechanisms to evade T cell attack by expressing different IC ligands such as CD80. In addition, a stronger recruitment of Treg cells, exhausted CTLs and $CD163^+$ M2-like macrophages is observed in mesenchymal SCCs, coinciding with the higher frequency of mesenchymal cancer cells, as compared to epithelial SCCs, mostly comprised by epithelial cancer cells. This infiltrate of immunosuppressive immune cells associated with the presence of hybrid and mesenchymal cancer cells could also contribute to the lack response to ICB therapies observed in advanced SCC patients. An important conclusion derived from these studies is that the number of factors that can influence the response to ICB therapies is very broad. Therefore, the characterization of cancer cell and immune infiltrate features in patient SCCs is important in order to design therapeutic strategies that target immunosuppressive immune cells, which may increase the efficiency of ICB therapies and overcome the primary or acquired resistance to this treatment.

CHAPTER 5. EFFECT OF BLOCKING DIFFERENT IMMUNE CHECKPOINT PATHWAYS TO BOOST THE ANTI-TUMOR IMMUNE RESPONSE IN MOUSE SKIN SCCs

Our previous results demonstrated that most patient SCCs show a strong heterogeneity and present plastic cancer cells, which have the ability to progress from an epithelial to a hybrid/mesenchymal phenotype. This situation could lead to the generation of different cancer-cell populations within the tumor that might use different immune evasion mechanisms. In this sense, we hypothesized that the resistance or short-term response of advanced SCC patients to ICB therapies could be consequence of cancer-cell plasticity. Moreover, not only the recruitment of immunosuppressive immune cells, but also the expression of a different repertoire of IC ligands in mesenchymal SCCs could activate immune evasion mechanisms different from those in epithelial and mixed SCCs. In order to test the relevance of the IC ligands expressed by cancer and immune cells in SCC immune evasion, we blocked different IC pathways to boost the anti-tumor immune response (Ishida et al., 1992b; Leach et al., 1996; Pardoll, 2012). We evaluated the impact of the release of the IC blockade on the activation of cytotoxic T and NK cells and in the recruitment of immunosuppressive immune cells, as well as on tumor size.

5.1- Immunotherapy based on anti-PD-L1 antibodies blocks the growth of epithelial skin SCCs

Given that we previously demonstrated that PD-L1 is the most expressed IC ligand by epithelial cancer cells (≈40-60% of cancer cells, Figures 44c and 44d), but also by some tumor-infiltrating immune cells such as macrophages (Figure 40b) and DCs (Figure 42b), we hypothesized that PD-1/PD-L1 pathway might be responsible for impeding the cytolytic activity of T and NK cells in tumors with epithelial features. We treated immunocompetent syngeneic mice carrying detectable epithelial tumors with IgG2b control and anti-PD-L1 antibodies during 21 days (9 doses, Figure 56a). Interestingly, anti-PD-L1 treatment delayed epithelial tumor growth from day 14 onwards compared to IgG2b control tumors (Figure 56b), which was associated with a mild decrease in the weight of anti-PD-L1-treated tumors (Figure 56c). In addition, no changes in spleen and liver weights were detected between the two treatment groups (Figures 56d and 56e). Subsequently, to assess whether the significant reduction in epithelial growth kinetics was associated with a reduced cancer-cell viability, we quantified the percentage of necrotic areas relative to total tumor area of tumors from both treatment groups (Figures 56f and 56g, in collaboration with Adrià Archilla, PhD student). We observed that anti-PD-L1-treated tumors presented bigger necrotic areas (≈50% of tumor area) as compared to IgG2b controls (Figures 56f and 56g). These observations demonstrate that PD-L1/PD-1 signaling blockade decreases epithelial tumor growth and suggest that the lower viability of anti-PD-L1-treated tumors could be mediated by the boost of $CD8^+$ and/or NK cell cytotoxic activity.

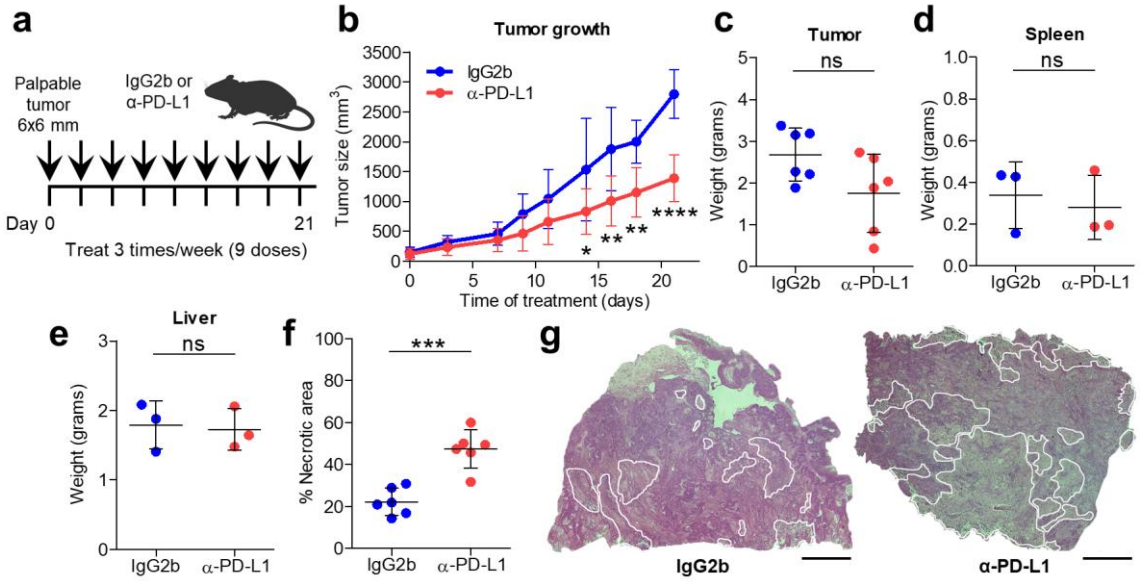

Figure 56. Immunotherapy based on anti-PD-L1 antibodies blocks the growth of epithelial SCCs. a. Experimental scheme for the treatment of epithelial tumors with mouse IgG2b isotype control or anti-PD-L1 antibodies. All treatments started when engrafted tumors reached a volume of approximately 113 mm^3 (6x6 mm), and mice were administered intraperitoneally 3 days per week with 200 µg/dose (9 doses). **b.** Growth kinetics of IgG2b control and anti-PD-L1-treated tumors (n=6). Weight of (**c**) tumor, (**d**) spleen and (**e**) liver in the indicated groups. **f.** Percentage of necrotic areas relative to total tumor area in the indicated groups (n=6). **g**. Representative hematoxylin/eosin (H/E) section of an epithelial tumor treated with IgG2b control or anti-PD-L1 antibodies, where necrotic areas are marked with white lines. Scale bar: 100 µm. Each symbol represents a single mouse (**d**, **e**) or tumor (**c, f**), and mean ± SD for each group is shown. (**b**) Repeated Measures ANOVA test, (**c-f**) unpaired two-tailed Student's *t*-test; ns $p>0.05$, *$p\leq0.05$, **$p\leq0.01$, ***$p\leq0.001$, ****$p\leq0.0001$.

To obtain a more detailed view of cancer and immune cell components within IgG2b control and anti-PD-L1-treated epithelial tumors, we implemented flow cytometry assays to study the abundance of some key populations. As expected from growth kinetics results, anti-PD-L1-treated tumors contained a lower percentage of cancer cells ($GFP^+/CD45^-$ cells) than IgG2b control tumors (Figure 57a), which correlates with the low viability of cancer cells upon anti-PD-L1 treatment (Figure 56f). In addition, although the frequency of fibroblasts ($GFP^-/CD45^-$ cells) remained unchanged between the two treatment groups (Figure 57b), a higher $CD45^+$ leukocyte recruitment was observed in anti-PD-L1-treated tumors (Figure 57c). This increase in the $CD45^+$ leukocyte recruitment could be related to the presence of more necrotic areas (Figures 56f and 56g) or to an increase in the leukocyte proliferation within the tumor, as they could be more active after anti-PD-L1 treatment. Subsequently, we evaluated whether cancer-cell features changed after anti-PD-L1 treatment by FACS analysis. Although a reduction of cancer-cell frequency was detected after anti-PD-L1 treatment (Figure 57a), no changes in the total content of epithelial $EpCAM^+$, $EpCAM^{high}$, $EpCAM^{low}$ and mesenchymal-like $EpCAM^-$ cancer cells were observed between the two treatment

groups (Figures 57d to 57g). These results indicate that tumors remaining after anti-PD-L1-treatment continue to maintain epithelial differentiation features (WD-SCCs), and there were no changes neither in cancer-cell features nor in progression. Therefore, these results suggest that the good response of epithelial tumors (WD-SCCs) could be related to the presence of large numbers of EpCAM^{high} cancer cells, which are the main source of PD-L1 in these tumors.

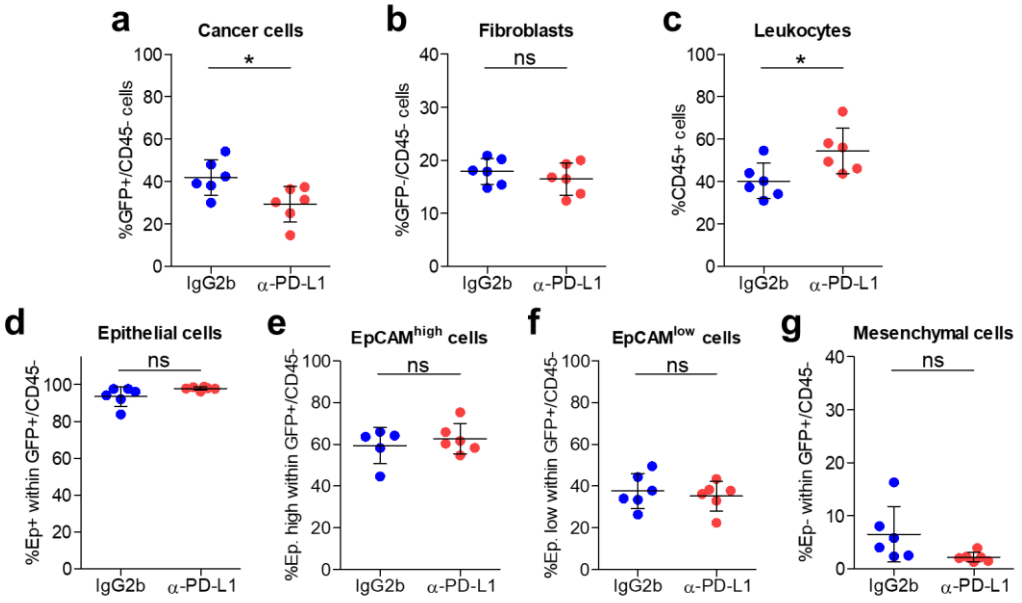

Figure 57. Tumor cell components change in epithelial SCCs after anti-PD-L1 treatment. Percentage of (**a**) cancer cells (GFP$^+$/CD45$^-$ cells), (**b**) fibroblasts (GFP$^-$/CD45$^-$ cells), (**c**) leukocytes (CD45$^+$ cells), (**d**) epithelial (GFP$^+$/CD45$^-$/EpCAM$^+$ cancer cells), (**e**) EpCAM^{high} (GFP$^+$/CD45$^-$/EpCAM^{high} cancer cells), (**f**) EpCAM^{low} (GFP$^+$/CD45$^-$/EpCAM^{low} cancer cells), and (**g**) mesenchymal cancer cells (GFP$^+$/CD45$^-$/EpCAM$^-$ cancer cells) in IgG2b control and anti-PD-L1-treated tumors (n=6), as determined by flow cytometry. Each symbol represents a single tumor and mean ± SD for each group is shown. (**a-g**) Unpaired two-tailed Student's *t*-test; ns $p>0.05$, *$p\leq0.05$.

To study whether T and/or NK cells were responsible for the changes observed after anti-PD-L1 treatment, we analyzed the presence of CD3$^+$ T lymphocytes (CD45$^+$/CD11b$^-$/CD3$^+$ cells), CD4$^+$ T lymphocytes (CD3$^+$/CD4$^+$/CD8$^-$ cells), CD8$^+$ T lymphocytes (CD3$^+$/CD4$^-$/CD8$^+$ cells) and NK cells (CD11b$^+$/CD3$^-$/NK-1.1$^+$ cells) in IgG2b control and anti-PD-L1-treated tumors by FACS assays. We observed that the percentage of CD3$^+$ T cells, and specifically of CD8$^+$ but not CD4$^+$ T cells, increased after anti-PD-L1 treatment (Figures 58a to 58c). In addition, a significant increase of NK cells was observed in anti-PD-L1-treated tumors (Figure 58d), which could mediate the elimination of those epithelial cancer cells that do not express MHC-I. These results support the idea that the boost of anti-tumor responses after anti-PD-L1 treatment could be mediated by the reactivation of cytotoxic CD8$^+$ and NK cells in epithelial tumors and prompted us to investigate the activation status of these populations. To this end, we evaluated by flow cytometry assays the expression of the inhibitory receptors PD-1, TIM-3 and LAG-3 in CD3$^+$/CD8$^+$ T cells. In addition, we quantified the

expression of IFN-γ and GzmB, which are considered to be an indicator of the cytotoxic activity of T cells. We observed that the percentage of PD-1$^+$ cells within CD11b$^-$/CD8$^+$ T lymphocyte population was significantly increased in anti-PD-L1-treated epithelial tumors compared to IgG2b control tumors (Figure 58e). In addition, the percentage of PD-1$^+$/TIM-3$^+$ and PD-1$^+$/LAG-3$^+$ T cells decreased in anti-PD-L1-treated tumors as compared to their respective IgG2b control tumors (Figures 58f and 58g). These results point toward the idea that CD8$^+$ cells found in anti-PD-L1-treated tumors are less exhausted/inactive and could mediate a pro-inflammatory immune response. Accordingly, the percentage of IFN-γ$^+$ and GzmB$^+$ cells within CD3$^+$/CD8$^+$ T lymphocyte population was significantly increased in epithelial tumors that were treated with anti-PD-L1 antibodies (Figures 58h and 58i). Therefore, these results indicate that anti-PD-L1 therapy induces an increase CTL infiltration and the reactivation of CD8$^+$ T-cell activity in epithelial tumors, in accordance with the good response observed on epithelial tumor growth (Figure 56b). At this point, we considered important to evaluate what happened with the activation state of NK cells, so these assays are deferred to future experiments.

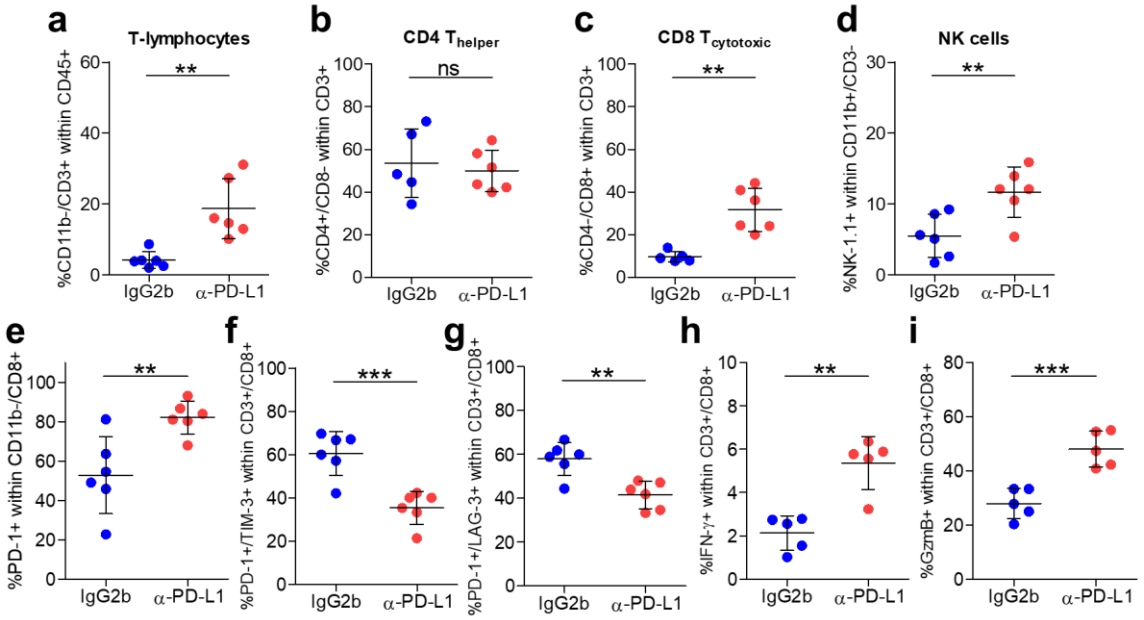

Figure 58. The boost of the anti-tumor immune response could be mediated by the reactivation of cytotoxic T and NK cells in epithelial SCCs after anti-PD-L1 treatment. Percentage of (**a**) CD3$^+$ T lymphocytes (CD45$^+$/CD11b$^-$/CD3$^+$ cells), (**b**) CD4$^+$ T lymphocytes (CD3$^+$/CD4$^+$/CD8$^-$ cells), (**c**) CD8$^+$ T lymphocytes (CD3$^+$/CD4$^-$/CD8$^+$ cells), and (**d**) NK cells (CD11b$^+$/CD3$^-$/NK-1.1$^+$ cells) in IgG2b control and anti-PD-L1-treated tumors (n=6), as determined by flow cytometry. Percentage of (**e**) PD-1$^+$, (**f**) PD-1$^+$/TIM-3$^+$, (**g**) PD-1$^+$/LAG-3$^+$, (**h**) IFN-γ$^+$, and (**i**) GzmB$^+$ cells within CD11b$^-$/CD8$^+$ T lymphocyte population in the indicated groups (n=6). Each symbol represents a single tumor and mean ± SD for each group is shown. (**a-i**) Unpaired two-tailed Student's *t*-test; ns $p>0.05$, $^{**}p\leq0.01$, $^{***}p\leq0.001$.

Next, we evaluated whether the reactivation of CD8$^+$ activity might also be associated with a reduced immunosuppressive cell recruitment in anti-PD-L1-treated epithelial tumors. In particular, we

studied whether there were changes within the frequency of myeloid cells (macrophages and MDSCs) and DCs. FACS analysis showed a significant reduction of the frequency of myeloid cells ($CD45^+/CD11b^+/CD3^-$ cells) in anti-PD-L1-treated tumors (Figure 59a). In addition, a significant increase in the total frequency of macrophages ($CD11b^+/F4\text{-}80^+/Gr1^-$ cells) was observed after anti-PD-L1 treatment (Figure 59b). This was accompanied by no detectable changes in MDSCs ($CD11b^+/Gr1^+$ cells) and DCs ($CD45^+/CD11c^+/F4\text{-}80^-/Gr1^-$ cells) after anti-PD-L1 treatment (Figures 59c and 59d). Interestingly, anti-PD-L1-treated tumors presented a higher infiltration of M1-like macrophages ($CD11b^+/F4\text{-}80^+/Gr1^-/CD206^-$ cells) and a lower percentage of M2-like macrophages ($CD11b^+/F4\text{-}80^+/Gr1^-/CD206^+$ cells) than IgG2b control tumors (Figures 59e and 59f). This change in the polarization phenotype of tumor-infiltrating macrophages was also corroborated by the reduced frequency of $PD\text{-}L1^+$ cells within the macrophage population in anti-PD-L1-treated tumors (Figure 59g). These results indicate that the low PD-L1 expression by macrophages after anti-PD-L1 treatment could also help the recovery of T-cell cytotoxic function in epithelial SCCs. In addition, an increase of PMN-MDSCs ($CD11b^+/Ly6C^+/Ly6G^+$ cells) and a reduction of M-MDSCs ($CD11b^+/Ly6C^+/Ly6G^-$ cells) were detected in anti-PD-L1-treated tumors (Figures 59h and 59i). Taken together, these results demonstrate that anti-PD-L1 treatment leads to a reduction of the immunosuppressive microenvironment (M2-like macrophages and M-MDSCs) that could favor the reactivation of $CD8^+$ T cells and the good response of epithelial SCCs to this therapy.

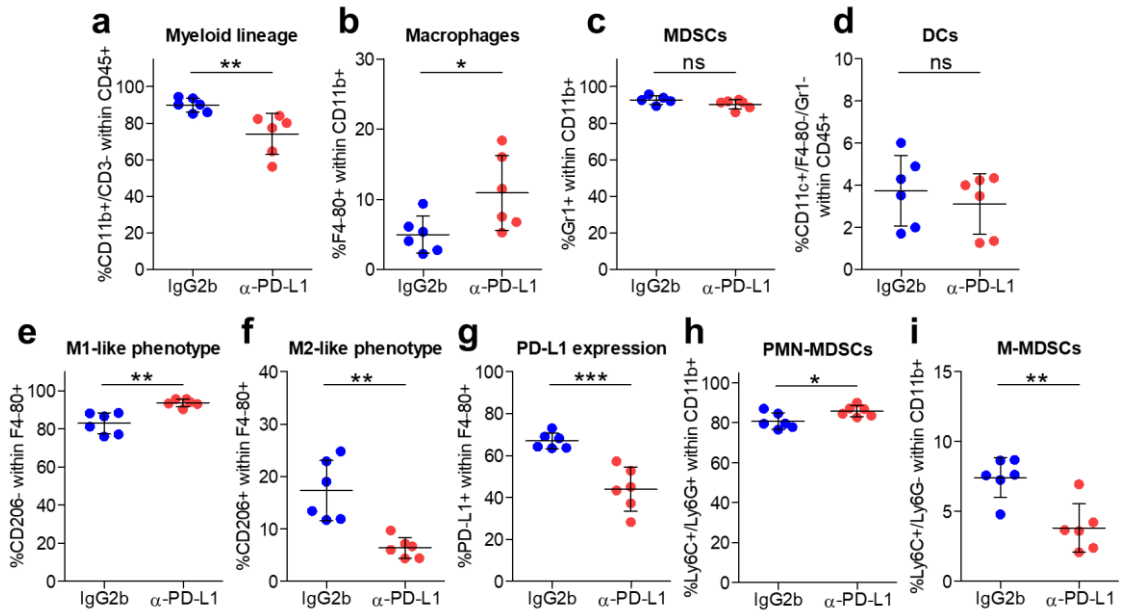

Figure 59. Anti-PD-L1 treatment leads to a reduced recruitment of immunosuppressive cells in epithelial SCCs. Percentage of (**a**) myeloid cells ($CD45^+/CD11b^+/CD3^-$ cells), (**b**) macrophages ($CD11b^+/F4\text{-}80^+/Gr1^-$ cells), (**c**) MDSCs ($CD11b^+/Gr1^+$ cells), (**d**) DCs ($CD45^+/CD11c^+/F4\text{-}80^-/Gr1^-$ cells), (**e**) M1-like macrophages ($CD11b^+/F4\text{-}80^+/Gr1^-/CD206^-$ cells), (**f**) M2-like macrophages ($CD11b^+/F4\text{-}80^+/Gr1^-/CD206^+$ cells), (**g**) $PD\text{-}L1^+$ cells within $F4/80^+$ macrophage population, (**h**) PMN-MDSCs ($CD11b^+/Ly6C^+/Ly6G^+$ cells), and (**i**) M-MDSCs ($CD11b^+/Ly6C^+/Ly6G^-$ cells) in IgG2b control and anti-PD-L1-treated tumors (n=6),

as determined by flow cytometry. Each symbol represents a single tumor and mean ± SD for each group is shown. (**a-i**) Unpaired two-tailed Student's *t*-test; ns $p>0.05$, *$p\leq0.05$, **$p\leq0.01$, ***$p\leq0.001$.

Since we previously demonstrated in Chapter 2 that epithelial tumors exclude most immune populations from the tumor core, we then studied whether anti-PD-L1 therapy could facilitate the entry of these immune populations to the intratumoral area and, thus, the direct contact with cancer cells. To do that, we performed immunohistochemistry and immunofluorescence assays of CD8 (T cytotoxic lymphocytes), FoxP3 (Treg cells), CD68 (M1-like and M2-like macrophages), CD163 (M2-like macrophages), and Gr1 (PMN-MDSCs and M-MDSCs) markers in IgG2b control and anti-PD-L1-treated epithelial tumors (Figures 60a, 60d, 60g, 60j and 60m). We observed a significant increase in the frequency of $CD8^+$ cells (Figures 60a and 60b, in collaboration with Adrià Archilla, PhD student) and $Gr1^+$ MDSCs (Figures 60m and 60n, in collaboration with Adrià Archilla, PhD student) per tumor area in anti-PD-L1-treated tumors as compared to IgG2b control tumors. In addition, we observed a significant increase in the frequency of $CD68^+$ macrophages (Figures 60j and 60k), as previously detected by FACS analysis (Figure 59b), and a slightly decrease in the frequency of $CD163^+$ M2-like macrophages per tumor area after anti-PD-L1 treatment (Figures 60g and 60h). These results suggest that the increase in $CD68^+$ cells may be due to an increase of antitumoral M1-like macrophages (Figure 59e).

Along with these changes, we observed that there was a shift in the location of $CD8^+$ T lymphocytes, $CD68^+$ macrophages and $Gr1^+$ MDSCs, possibly of the neutrophil phenotype, toward the intratumoral areas, but still maintaining an important percentage of them in the stromal area (Figures 60c, 60l and 60o). Probably, this increase of cytotoxic $CD8^+$ T cells and M1-like macrophages in the tumor core, whose main function is to eliminate cancer cells, was in line with the reduced cancer-cell viability and the decreased tumor growth of anti-PD-L1-treated tumors. Interestingly, we noticed that $CD163^+$ M2-like macrophages were totally located in the stromal regions of IgG2b control and anti-PD-L1-treated tumors (Figure 60i), suggesting that this population would not be favoring the formation of an immunosuppressive environment within the tumor core. In addition, this population could be forming a barrier in the stromal area to prevent the entry of cytotoxic immune populations, for example through the expression of PD-L1. This event could be bypassed with the anti-PD-L1 therapy, as we detected a reduction of PD-L1 expression in macrophages associated with the loss of the M2-like phenotype (Figure 59g) and an increased entry of cytotoxic populations to the tumor core. No changes in the frequency of immunosuppressive $FoxP3^+$ Treg cells were detected after anti-PD-L1 treatment (Figures 60d and 60e), even though these immune cells were more located in the intratumoral area of anti-PD-L1-treated tumors (Figure 60f). All these results suggest that tumors showing mainly epithelial differentiation features (WD-SCCs) respond to anti-PD-L1 therapy due to a reactivation of T lymphocytes and a less infiltration of immunosuppressive immune cells (M-MDSCs and M2-like macrophages).

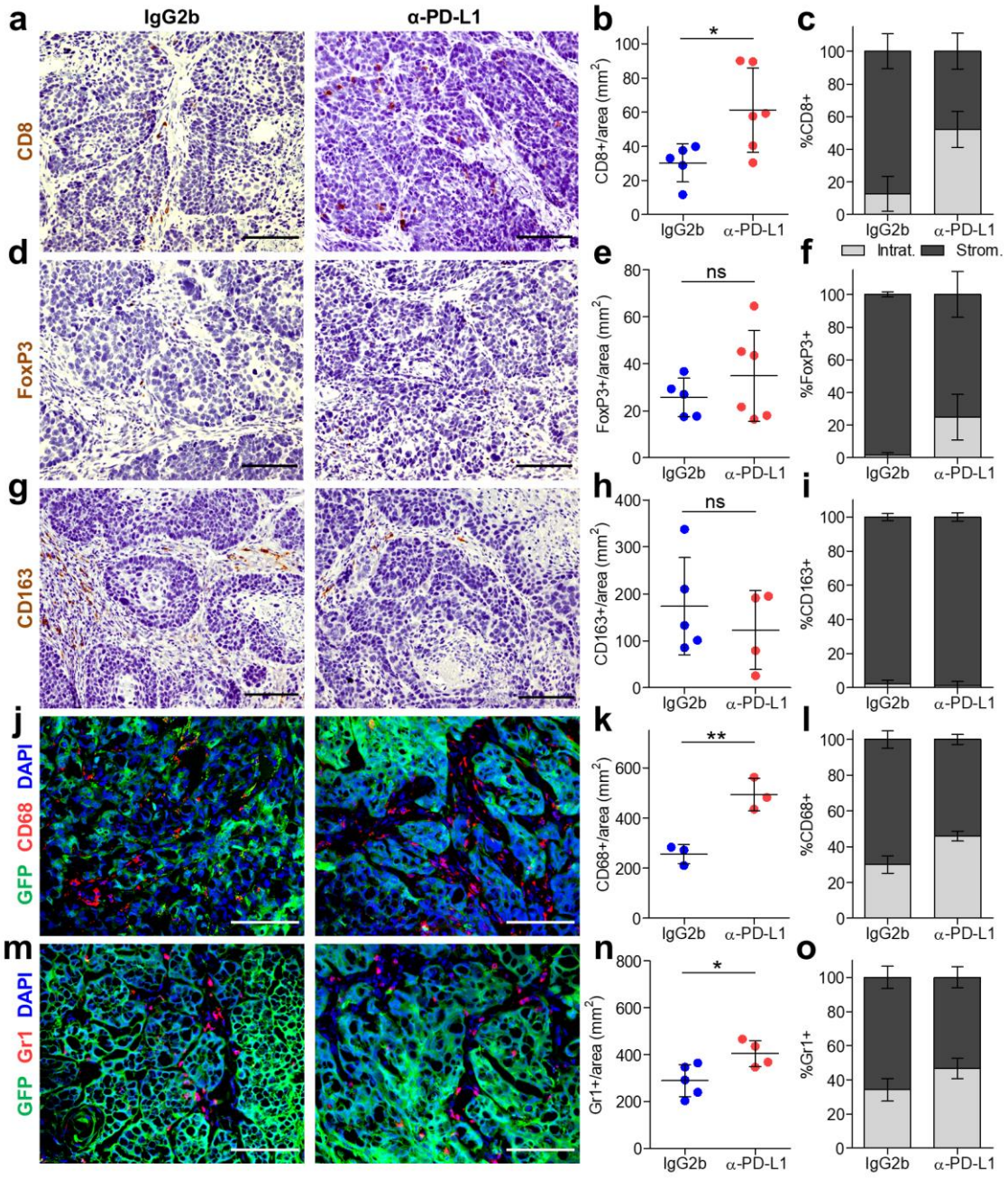

Figure 60. Anti-PD-L1 treatment promotes the infiltration of CD8⁺ T lymphocytes, M1-like macrophages and Gr1⁺ MDSCs into the tumor core of epithelial SCCs. Representative immunohistochemistry images of (**a**) $CD8^+$, (**d**) $FoxP3^+$, and (**g**) $CD163^+$ cells in IgG2b control and anti-PD-L1-treated tumors. Scale bar: 100 µm. Representative immunofluorescence images of GFP^+ cancer cells, (**j**) $CD68^+$ or (**m**) $Gr1^+$ immune cells and DAPI labelled cell nuclei in IgG2b control and anti-PD-L1-treated tumors. Scale bar: 100 µm. Quantification of the frequency of (**b**) $CD8^+$, (**e**) $FoxP3^+$, (**h**) $CD163^+$, (**k**) $CD68^+$, and (**n**) $Gr1^+$ cells per tumor area (mm^2) in IgG2b control and anti-PD-L1-treated tumors ($n \geq 3$ tumors per group). At least 6 fields of different regions were quantified in each tumor. Each symbol represents a single tumor and mean ± SD for each group is shown. Percentage (mean ± SD) of intratumoral or stromal (**c**) $CD8^+$, (**f**) $FoxP3^+$, (**i**) $CD163^+$, (**l**) $CD68^+$, and (**o**) $Gr1^+$ cells in the indicated tumors. (**b, e, h, k, n**) Unpaired two-tailed Student's *t*-test; ns $p>0.05$, *$p\leq0.05$, **$p\leq0.01$.

Finally, to determine if the boost of the anti-tumor immune response after anti-PD-L1 treatment was dependent of the release of the IC PD-1/PD-L1 blockade of cytotoxic $CD8^+$ T cells in epithelial SCCs, we treated immunocompetent mice carrying detectable epithelial tumors with IgG2b control, anti-PD-L1, anti-CD8, and anti-PD-L1/CD8 antibodies during 24 days (10 doses, Figure 61a). As we previously observed (Figure 56b), anti-PD-L1 treatment significantly delayed epithelial tumor growth from day 14 onwards compared to IgG2b control tumors (Figure 61b), which was associated with a significant decrease in the weight of anti-PD-L1-treated tumors (Figure 61c). Interestingly, this effect on tumor growth was abrogated with the administration of anti-CD8 antibodies in anti-PD-L1/CD8-treated tumors, suggesting that the tumor growth reduction was mainly mediated by the reactivation of $CD8^+$ T cells (Figure 61b). No changes in spleen and liver weights were detected between the different treatment groups (Figures 61d and 61e). As expected, anti-PD-L1-treated tumors contained a lower percentage of cancer cells ($GFP^+/CD45^-$ cells) than IgG2b control tumors (Figure 61f). In accordance to the similar growth kinetics curves, IgG2b control, anti-CD8, and anti-PD-L1/CD8-treated tumors contained a comparable percentage of cancer cells (Figure 61f). In addition, although the frequency of fibroblasts ($GFP^-/CD45^-$ cells) remained unchanged between the different treatment groups (Figure 61g), a higher $CD45^+$ leukocyte recruitment was only observed in anti-PD-L1-treated tumors (Figure 61h), which was blocked by the concomitant treatment with anti-CD8/PD-L1 (Figure 61h). This increase in the $CD45^+$ leukocyte recruitment could be related to the presence of more necrotic areas in anti-PD-L1-treated tumors (as we observed previously, Figures 56f and 56g), or to an increase in the leukocyte proliferation within the tumor, although this remains to be analyzed in this experiment.

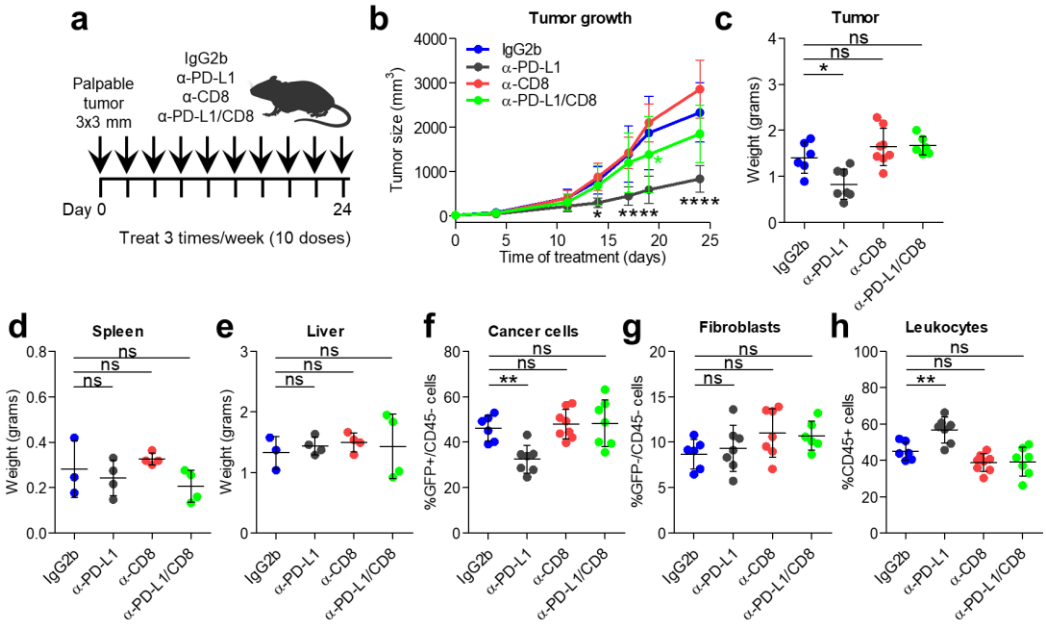

Figure 61. Immunotherapy based on anti-PD-L1 antibodies blocks the growth of epithelial SCCs through the action of $CD8^+$ T lymphocytes. a. Experimental scheme for the treatment of epithelial tumors with mouse IgG2b isotype control, anti-PD-L1, and anti-CD8 antibodies. All treatments started when

engrafted tumors reached a volume of approximately 20 mm^3 (3x3 mm), and mice were administered intraperitoneally three days per week with 200 µg/dose (IgG2b control and anti-PD-L1) or 300 µg/dose (anti-CD8) during 24 days (10 doses). **b.** Growth kinetics of IgG2b control, anti-PD-L1, anti-CD8, and anti-PD-L1/CD8-treated tumors (n=8). Weight of (**c**) tumor, (**d**) spleen and (**e**) liver in the indicated groups. Percentage of (**f**) cancer cells ($GFP^+/CD45^-$ cells), (**g**) fibroblasts ($GFP^-/CD45^-$ cells), and (**h**) leukocytes ($CD45^+$ cells) in the indicated groups, as determined by flow cytometry. Each symbol represents a single mouse (**d**, **e**) or tumor (**c, f-h**), and mean ± SD for each group is shown. (**b**) Repeated Measures ANOVA test, where significance differences in tumor growth between anti-PD-L1 and IgG2b tumors are indicated with grey *, and between anti-PD-L1/CD8 and IgG2b tumors with green *, (**c-h**) one-way ANOVA followed by Dunnett's multiple comparison test; ns $p>0.05$, *$p\leq0.05$, **$p\leq0.01$, ****$p\leq0.0001$.

In addition, we are currently in the process of analyzing more extensively the immune infiltrate and the IC ligand expression profile of cancer cells in this experiment. In this sense, we are studying the reactivation of not only $CD8^+$ T lymphocytes but also NK cells, through the loss of the expression of some IC receptors such as PD-1, TIM-3, LAG-3, and TIGIT. Our idea is to evaluate which IC receptors may be still highly expressed after anti-PD-L1 treatment, which may indicate alternative IC pathways acting in the blockade of the cytotoxic action of T and NK cells in anti-PD-L1-treated epithelial tumors. Furthermore, complementing the previous idea, we are evaluating whether cancer cells remaining in the tumor induce the expression of IC ligands other than PD-L1 such as MHC-II, CD80, CD86, Gal9, CD155 and CD47. We believe that these results will be very important since they may indicate which combinatorial therapies could have more clinical benefits to completely reduce the tumor growth and the immunosuppressive immune infiltrate in epithelial SCCs.

5.2- Immunotherapy based on anti-PD-L1 antibodies does not block the growth of mesenchymal skin SCCs

Our previous results indicate that mesenchymal SCCs may be refractory to most common ICB therapies (anti-PD-1 and anti-PD-L1 antibodies) due to the high frequency of tumor-infiltrating immunosuppressive cells, the loss of MHC-I expression, and the change in the IC ligand expression by cancer and immune cells associated with cancer-cell plasticity. To confirm our hypothesis, we treated immunocompetent syngeneic mice carrying detectable mesenchymal SCCs with IgG2b control and anti-PD-L1 antibodies during 21 days (9 doses, Figure 62a). As predicted, our analysis did not show any significant difference in mesenchymal tumor growth between IgG2b control and anti-PD-L1-treated tumors (Figure 62b), which correlates with no changes in tumor weight between them (Figure 62c). No changes in spleen and liver weights were detected between the two treatment groups (Figures 62d and 62e). Furthermore, the percentage of necrotic areas relative to total tumor area of IgG2b control and anti-PD-L1-treated tumors were similar in both groups (Figures 62f and 62g, in collaboration with Adrià Archilla, PhD student), indicating that anti-PD-L1 treatment did not affect the viability of mesenchymal-like $EpCAM^-$ cancer cells.

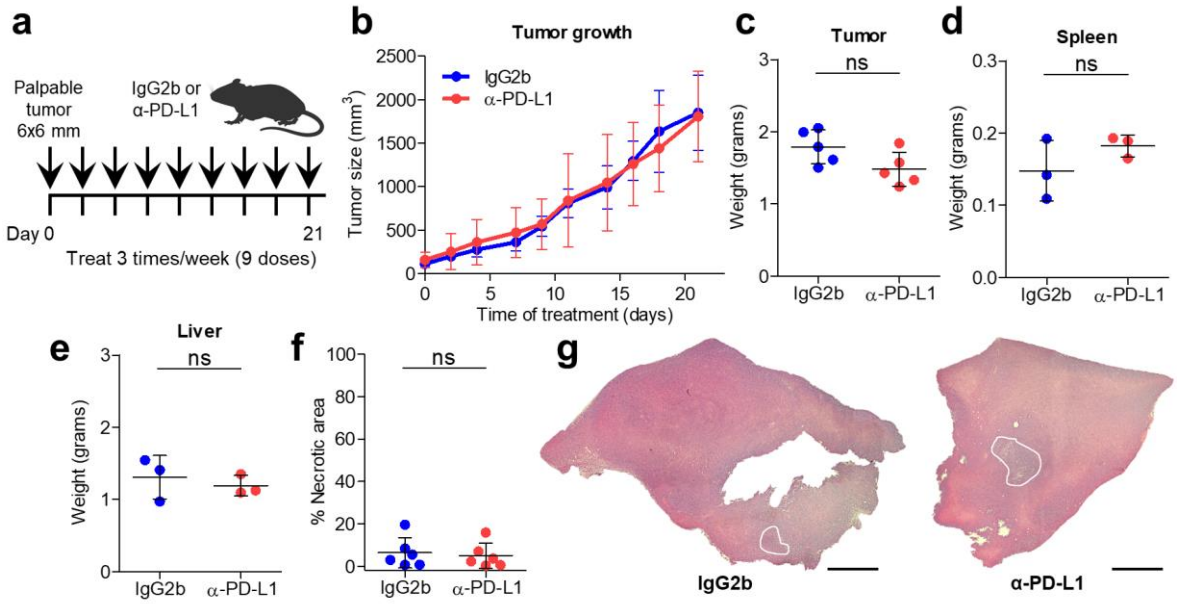

Figure 62. Immunotherapy based on anti-PD-L1 antibodies does not block the growth of mesenchymal SCCs. a. Experimental scheme for the treatment of mesenchymal tumors with mouse IgG2b isotype control or anti-PD-L1 antibodies. All treatments started when engrafted tumors reached a volume of approximately 113 mm^3 (6x6 mm), and mice were administered intraperitoneally three days per week with 200 µg/dose (9 doses). **b.** Growth kinetics of IgG2b control and anti-PD-L1-treated tumors (n=6). Weight of (**c**) tumor, (**d**) spleen and (**e**) liver in the indicated groups. **f.** Percentage of necrotic areas relative to total tumor area in the indicated groups (n=6). **g**. Representative hematoxylin/eosin (H/E) section of a mesenchymal tumor treated with IgG2b control or anti-PD-L1 antibody, where necrotic areas are marked with white lines. Scale bar: 100 µm. Each symbol represents a single mouse (**d**, **e**) or tumor (**c, f**), and mean ± SD for each group is shown. (**b**) Repeated Measures ANOVA test, (**c-f**) unpaired two-tailed Student's *t*-test; ns p>0.05.

This observation was also corroborated because no changes in the frequency of cancer cells (epithelial $EpCAM^+$ and mesenchymal-like $EpCAM^-$ cancer cells), neither fibroblasts ($GFP^-/CD45^-$ cells), nor leukocytes ($CD45^+$ cells) were detected between IgG2b control and anti-PD-L1-treated tumors (Figures 63a to 63e). It is important to note that both treated groups contained a very high percentage of cancer cells (≈90% of $GFP^+/CD45^-$ cancer cells, Figure 63a) and a low frequency of $CD45^+$ immune cells (≈5%, Figure 63c), which may be associated with the high aggressiveness and poor prognosis of mesenchymal SCCs.

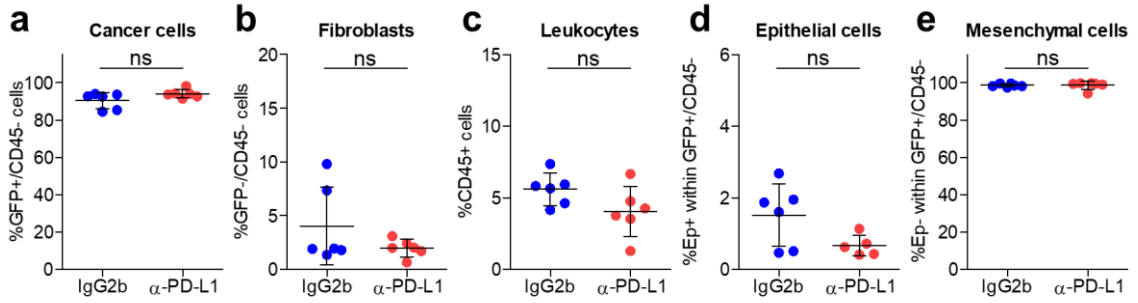

Figure 63. Tumor cell components do not change in mesenchymal SCCs after anti-PD-L1 treatment. Percentage of (**a**) cancer cells ($GFP^+/CD45^-$ cells), (**b**) fibroblasts ($GFP^-/CD45^-$ cells), (**c**) leukocytes ($CD45^+$ cells), (**d**) epithelial ($GFP^+/CD45^-/EpCAM^+$ cancer cells), and (**e**) mesenchymal cancer cells ($GFP^+/CD45^-/EpCAM^-$ cancer cells) in IgG2b control and anti-PD-L1-treated tumors (n=6), as determined by flow cytometry. Each symbol represents a single tumor and mean ± SD for each group is shown. (**a-e**) Unpaired two-tailed Student's *t*-test; ns p>0.05.

Subsequently, we studied whether the anti-PD-L1 therapy had worked by activating the cytotoxic activity of T and NK cells, even though it was not sufficiently effective in eliminating mesenchymal-like $EpCAM^-$ cancer cells. We observed that the percentage of $CD3^+$ T cells, $CD8^+$ and $CD4^+$ T lymphocytes, and NK cells ($CD11b^+/CD3^-/NK\text{-}1.1^+$ cells) did not change between IgG2b control and anti-PD-L1-treated tumors (Figures 64a to 64d). In addition, the frequency of $PD\text{-}1^+$ cells within $CD11b^-/CD8^+$ T lymphocytes, which was very high in IgG2b control mesenchymal tumors, was not further increased after the treatment (Figure 64e). We then evaluated the activation status of $CD8^+$ T lymphocytes. FACS analysis showed that the frequency of exhausted $PD\text{-}1^+/LAG\text{-}3^+$ T cells decreased in mesenchymal tumors that received anti-PD-L1 therapy compared to their respective control tumors (Figure 64g), but no changes were observed in $PD\text{-}1^+/TIM\text{-}3^+$ cells (Figure 64f). Furthermore, whereas the percentage of IFN-γ^+ cells was increased in anti-PD-L1 treated tumors (Figure 64h), no differences were noticed in the expression of GzmB (Figure 64i). Therefore, these results indicate that $CD8^+$ T-cell activity was not completely recovered and a high percentage of exhausted T cells were still present upon anti-PD-L1 treatment, in accordance with the poor response observed on mesenchymal tumor growth (Figure 62b). Moreover, these results suggest that the immune checkpoint blockade might be induced by alternative IC ligands in mesenchymal SCCs and/or that the activity of cytotoxic T cells may be impaired by a highly immunosuppressive environment that hinders the response to immunotherapy.

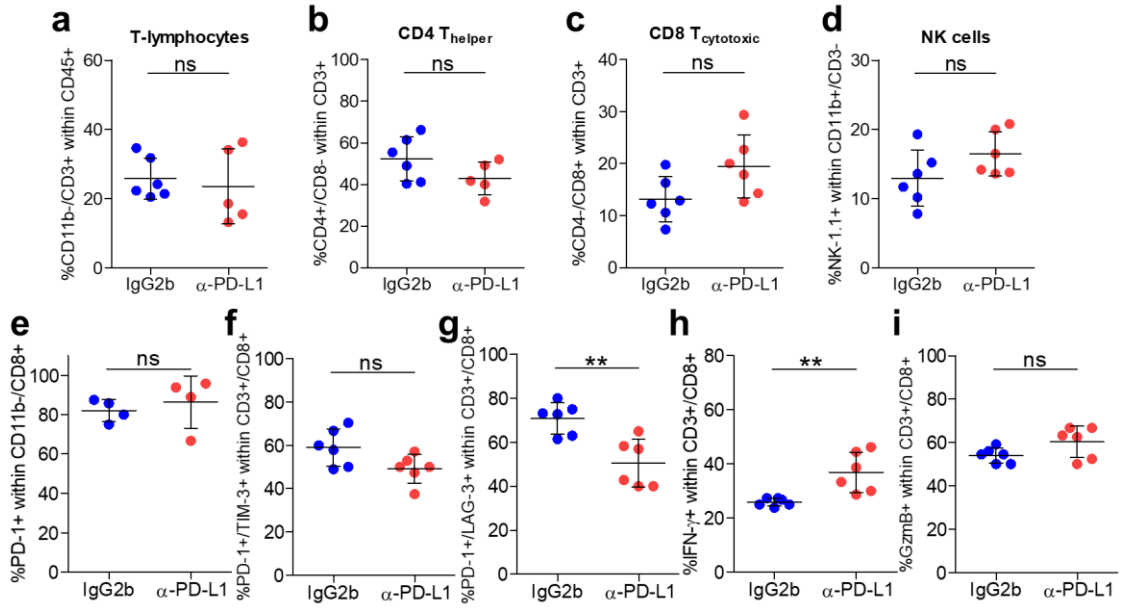

Figure 64. CD8$^+$ T-cell activity is not completely recovered and a high percentage of exhausted T cells are still present upon anti-PD-L1 treatment. Percentage of (**a**) CD3$^+$ T lymphocytes (CD45$^+$/CD11b$^-$/CD3$^+$ cells), (**b**) CD4$^+$ T lymphocytes (CD3$^+$/CD4$^+$/CD8$^-$ cells), (**c**) CD8$^+$ T lymphocytes (CD3$^+$/CD4$^-$/CD8$^+$ cells), and (**d**) NK cells (CD11b$^+$/CD3$^-$/NK-1.1$^+$ cells) in IgG2b control and anti-PD-L1-treated tumors (n=6), as determined by flow cytometry. Percentage of (**e**) PD-1$^+$, (**f**) PD-1$^+$/TIM-3$^+$, (**g**) PD-1$^+$/LAG-3$^+$, (**h**) IFN-γ$^+$, and (**i**) GzmB$^+$ cells within CD3$^+$/CD8$^+$ T lymphocyte population in the indicated groups (n=6). Each symbol represents a single tumor and mean ± SD for each group is shown. (**a-i**) Unpaired two-tailed Student's *t*-test; ns p>0.05, **p≤0.01.

The latter hypothesis was confirmed because no changes in the composition of total myeloid cells (CD45$^+$/CD11b$^{+/}$CD3$^-$ cells), macrophages (CD11b$^+$/F4-80$^+$/Gr1$^-$ cells), MDSCs (CD11b$^+$/Gr1$^+$ cells), and DCs (CD45$^+$/CD11c$^+$/F4-80$^-$/Gr1$^-$ cells) were observed between IgG2b control and anti-PD-L1-treated tumors (Figures 65a to 65d). In addition, anti-PD-L1 treatment did not change the percentage of CD206$^-$ M1-like macrophages, CD206$^+$ M2-like macrophages, PMN-MDSCs, and M-MDSCs compared to IgG2b control tumors, neither PD-L1 expression by macrophages (Figures 65e to 65i). These results demonstrate that anti-PD-L1 therapy is not able to reduce the high immunosuppressive cell recruitment observed in mesenchymal SCCs.

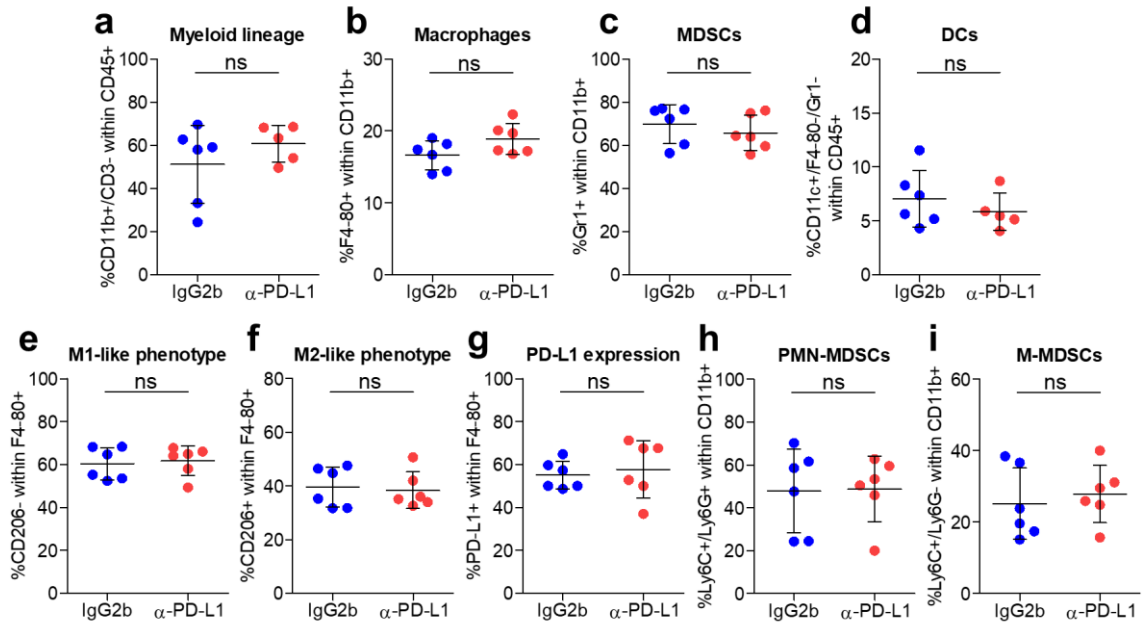

Figure 65. No changes in the immunosuppressive cell recruitment are detected in anti-PD-L1-treated mesenchymal SCCs. Percentage of (**a**) myeloid cells (CD45$^+$/CD11b$^+$/CD3$^-$ cells), (**b**) macrophages (CD11b$^+$/F4-80$^+$/Gr1$^-$ cells), (**c**) MDSCs (CD11b$^+$/Gr1$^+$ cells), (**d**) DCs (CD45$^+$/CD11c$^+$/F4-80$^-$/Gr1$^-$ cells), (**e**) M1-like macrophages (CD11b$^+$/F4-80$^+$/Gr1$^-$/CD206$^-$ cells), (**f**) M2-like macrophages (CD11b$^+$/F4-80$^+$/Gr1$^-$/CD206$^+$ cells), (**g**) PD-L1$^+$ cells within F4/80$^+$ macrophage population, (**h**) PMN-MDSCs (CD11b$^+$/Ly6C$^+$/Ly6G$^+$ cells), and (**i**) M-MDSCs (CD11b$^+$/Ly6C$^+$/Ly6G$^-$ cells) in IgG2b control and anti-PD-L1-treated tumors (n=6), as determined by flow cytometry. Each symbol represents a single tumor and mean ± SD for each group is shown. (**a-i**) Unpaired two-tailed Student's *t*-test; ns p>0.05.

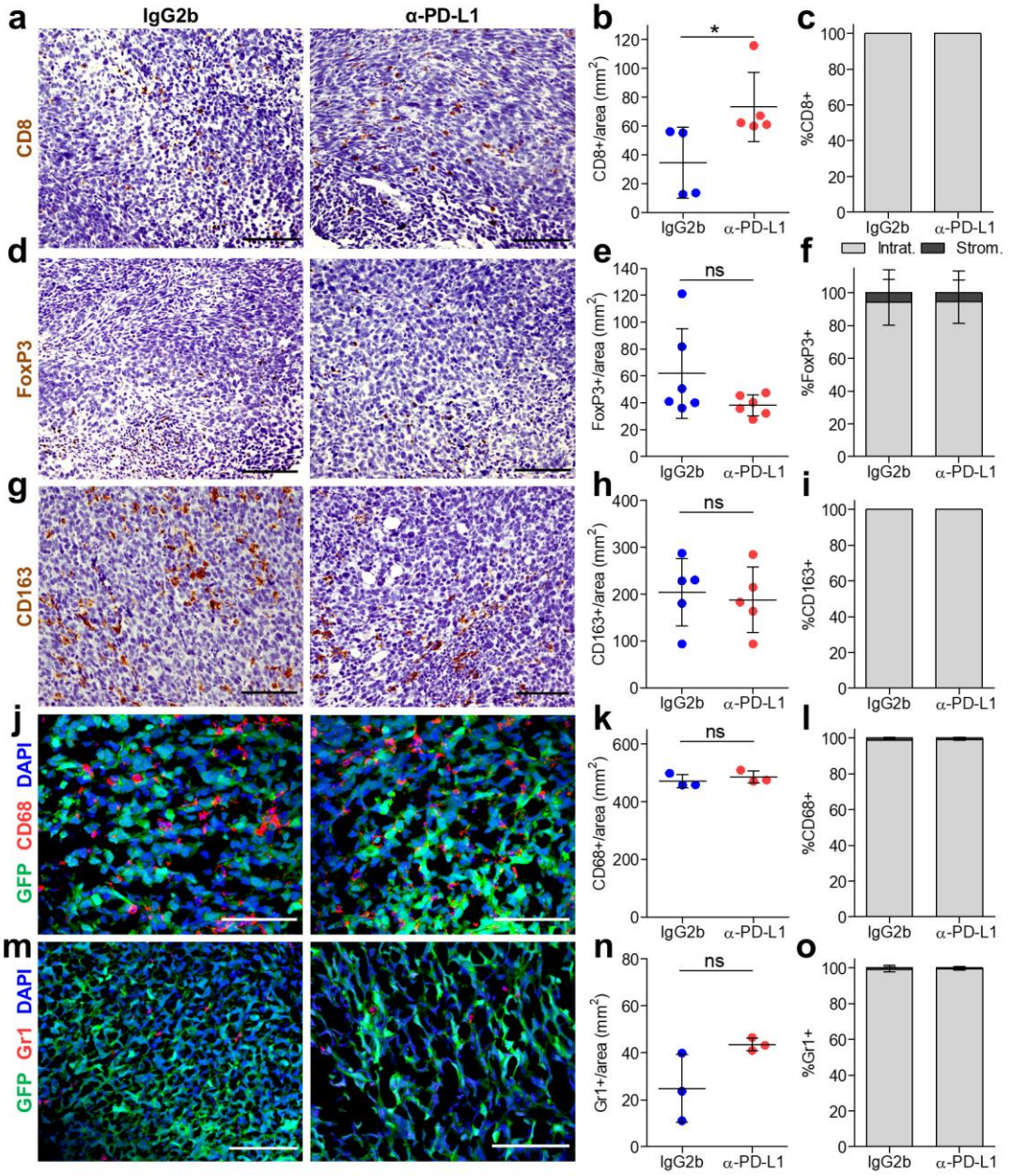

Figure 66. Anti-PD-L1 treatment does not affect the location of different immune cell populations in mesenchymal SCCs. Representative immunohistochemistry images of (**a**) $CD8^+$, (**d**) $FoxP3^+$, and (**g**) $CD163^+$ immune cells in IgG2b control and anti-PD-L1-treated tumors. Scale bar: 100 µm. Representative immunofluorescence images of GFP^+ cancer cells, (**j**) $CD68^+$ or (**m**) $Gr1^+$ immune cells and DAPI labelled cell nuclei in IgG2b control and anti-PD-L1-treated tumors. Scale bar: 100 µm. Quantification of the frequency of (**b**) $CD8^+$, (**e**) $FoxP3^+$, (**h**) $CD163^+$, (**k**) $CD68^+$, and (**n**) $Gr1^+$ immune cells per tumor area (mm^2) in IgG2b control and anti-PD-L1-treated tumors (n≥3 tumors per group). At least 6 fields of different regions were quantified in each tumor. Each symbol represents a single tumor and mean ± SD for each group is shown. Percentage (mean ± SD) of intratumoral or stromal (**c**) $CD8^+$, (**f**) $FoxP3^+$, (**i**) $CD163^+$, (**l**) $CD68^+$, and (**o**) $Gr1^+$ immune cells in the indicated tumors. (**b, e, h, k, n**) Unpaired two-tailed Student's *t*-test; ns $p>0.05$, *$p\leq0.05$.

Finally, we performed immunohistochemistry and immunofluorescence assays in order to evaluate where the different immune populations were located in IgG2b control and anti-PD-L1-treated

mesenchymal SCCs (Figures 66a, 66d, 66g, 66j and 66m). Contrary to FACS results (Figure 64c), we observed a significant increase of $CD8^+$ T cells per tumor area in anti-PD-L1-treated tumors (Figures 66a and 66b; in collaboration with Adrià Archilla, PhD student). However, given that the status of these lymphocytes was still exhausted, this increase into the tumor core did not translate into a reduced cancer-cell viability. Furthermore, no changes in the frequency of immunosuppressive $FoxP3^+$ (Figures 66d and 66e), $CD163^+$ M2-like cells (Figures 66g and 66h), $CD68^+$ macrophages (Figures 66j and 66k), and $Gr1^+$ MDSCs (Figures 66m and 66n) per tumor area were observed between IgG2b control and anti-PD-L1-treated tumors. These analyses also showed that all immune cells were located in close proximity to cancer cells (intratumoral areas) in IgG2b control and anti-PD-L1-treated tumors, generating a highly immunosuppressive microenvironment (Figures 66c, 66f, 66i, 66l and 66o). To sum up, our work has led us to conclude that advanced SCCs containing mesenchymal-like cancer cells (PD/S-SCCs) are refractory to anti-PD-L1 therapy. This means that SCC patients with tumors containing a high content of mesenchymal-like $EpCAM^-$ cancer cells should not be treated with immunotherapy based on PD-1/PD-L1 blocking antibodies. In addition, our results suggest that PD-L1 expression by cancer cells or immune cells located in the TME are not the only responsible for interfering with the cytotoxic activity of T and NK cells. Therefore, it will be necessary to perform further studies in order to determine the mechanisms involved in the resistance to inhibitors of the immune checkpoint in mesenchymal SCCs.

5.3- Combinatorial therapies are necessary to target both epithelial and mesenchymal components of mixed SCCs

Once we demonstrated that epithelial tumors (WD-SCCs) showed a good response to anti-PD-L1 treatment, and that mesenchymal tumors (PD/S-SCCs) were refractory to it, we evaluated what happened with tumors containing both epithelial $EpCAM^+$ and mesenchymal-like $EpCAM^-$ cancer cells (MD/PD-SCCs), as it is a frequent scenario in patient skin SCCs. Most SCC patients showed MD/PD-SCCs histopathological features and it would be interesting to evaluate if anti-PD-L1 therapy is suitable for them. In this case, we not only studied the response to anti-PD-L1 therapy on tumor growth and immunosuppressive cell recruitment, but also if the acquisition of cancer-cell plasticity and the switch toward the mesenchymal phenotype were slowed down. For that, we engrafted epithelial $EpCAM^+$ cancer cells into immunocompetent syngeneic mice to generate mixed SCCs. It is important to highlight that these treatments started the day before the engraftment of epithelial $EpCAM^+$ cancer cells, and then mice were treated 3 days per week during 32 days (14 doses, Figure 67a), to also evaluate the impact of the therapy on cancer-cell plasticity. Interestingly, anti-PD-L1 treatment significantly delayed mixed tumor growth from day 25 onwards compared to IgG2b control tumors (Figure 67b), but this reduction was not associated with a decrease in the weight of anti-PD-L1-treated tumors (Figure 67c). In addition, no changes in spleen and liver weights were detected between the two treatment groups (Figures 67d and 67e). To assess whether

the significant reduction in growth kinetics was associated with a reduced cancer-cell viability, we quantified the percentage of necrotic areas relative to total tumor area in both treatment groups (Figures 67f and 67g; in collaboration with Adrià Archilla, PhD student). Surprisingly, IgG2b control and anti-PD-L1-treated tumors showed no significant differences in the percentage of necrotic areas (Figure 67f). These observations demonstrate that PD-L1/PD-1 signaling blockade decreases mixed tumor growth, but this reduction was not associated with a low viability of anti-PD-L1-treated mixed tumors.

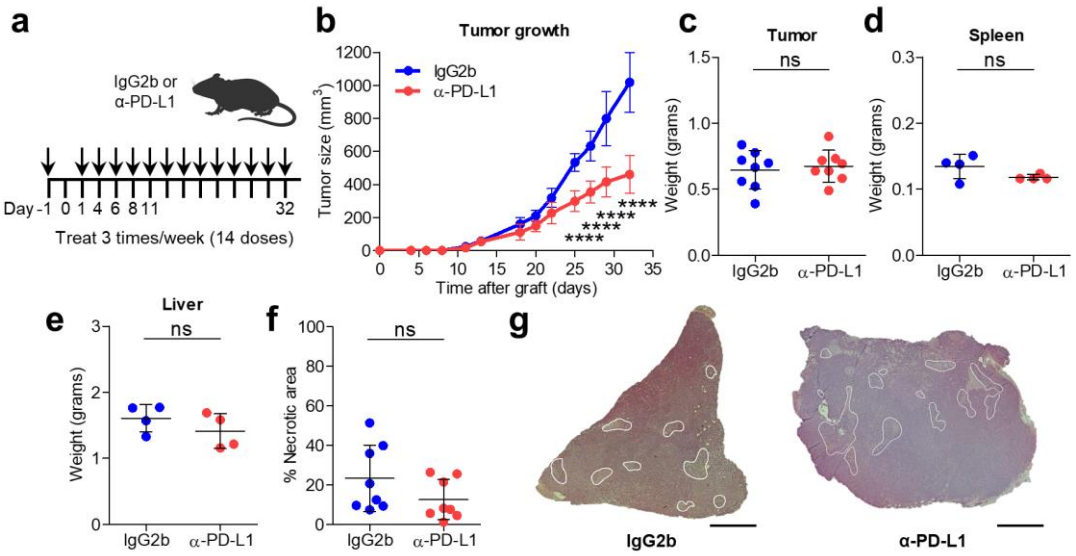

Figure 67. Immunotherapy based on anti-PD-L1 antibodies blocks the growth of mixed SCCs. a. Experimental scheme for the treatment of mixed tumors with mouse IgG2b isotype control or anti-PD-L1 antibodies. All treatments started on day -1, and then mice were administered intraperitoneally three days per week with 200 µg/dose until experimental endpoint (14 doses). **b.** Growth kinetics of IgG2b control and anti-PD-L1-treated tumors (n=8). Weight of (**c**) tumor, (**d**) spleen and (**e**) liver in the indicated groups. **f.** Percentage of necrotic areas relative to total tumor area in the indicated groups (n=8). **g**. Representative hematoxylin/eosin (H/E) section of a mixed tumor treated with IgG2b control or anti-PD-L1 antibodies, where necrotic areas are marked with white lines. Scale bar: 100 µm. Each symbol represents a single mouse (**d**, **e**) or tumor (**c, f**), and mean ± SD for each group is shown. (**b**) Repeated Measures ANOVA test, (**c-f**) unpaired two-tailed Student's *t*-test; ns $p>0.05$, ****$p\leq0.0001$.

Then, we analyzed the frequency of different tumor cell components in control and anti-PD-L1 treated SCCs through FACS analysis. The first interesting observation was that no significant changes were detected in the total frequency of cancer cells ($GFP^+/CD45^-$ cells), fibroblasts ($GFP^-/CD45^-$ cells) and $CD45^+$ leukocytes (Figures 68a to 68c) between IgG2b control and anti-PD-L1-treated tumors. These results supported the fact that anti-PD-L1-treated mixed tumors did not show a change in the percentage of viable and necrotic areas in accordance to the lack of effect of anti-PD-L1 treatment on cancer-cell viability (Figure 68a). Remarkably, these analyses showed that while a reduction in the percentage of epithelial $EpCAM^+$ cancer cells was observed in anti-PD-L1-

treated tumors (Figure 68d), a mild increase in mesenchymal-like EpCAM$^-$ cancer cells was detected upon anti-PD-L1 treatment (Figure 68g). Specifically, the decrease in the epithelial component was due to a reduction in the frequency of EpCAM^{high} cancer cells and not hybrid EpCAM^{low} cancer cells (Figures 68e and 68f). These results indicate that epithelial EpCAM^{high} cancer cells may be the preferred cancer-cell population eliminated after anti-PD-L1 therapy in mixed SCCs and that this population could block the action of cytotoxic T and NK cells through the expression of PD-L1. It is noteworthy that this, in turn, induces a mild enrichment of the mesenchymal-like EpCAM$^-$ cancer cell component of these tumors, which could lead to a subsequent resistance or short-term response to this therapy, even with a very significant decrease in tumor growth after the treatment. Considering all the above, we suggest that the decrease in tumor growth of anti-PD-L1-treated tumors (Figure 67b) is due to the fact that these tumors are acquiring plasticity and have more mesenchymal component. This is confirmed by the fact that anti-PD-L1-treated tumors follow a similar growth kinetics to those observed in the aggressive and mesenchymal SCCs (Figure 21a).

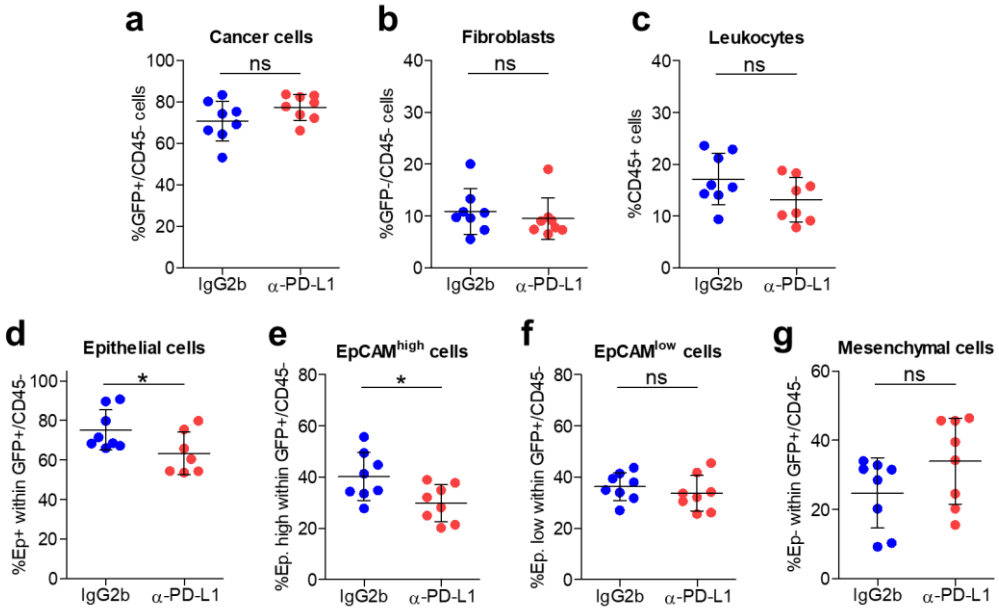

Figure 68. The frequency of epithelial EpCAM^{high} cancer cells is reduced after anti-PD-L1 therapy in mixed SCCs. Percentage of (**a**) cancer cells (GFP$^+$/CD45$^-$ cells), (**b**) fibroblasts (GFP$^-$/CD45$^-$ cells), (**c**) leukocytes (CD45$^+$ cells), (**d**) epithelial (GFP$^+$/CD45$^-$/EpCAM$^+$ cancer cells), (**e**) EpCAM^{high} (GFP$^+$/CD45$^-$/EpCAM^{high} cancer cells), (**f**) EpCAM^{low} (GFP$^+$/CD45$^-$/EpCAM^{low} cancer cells) and (**g**) mesenchymal (GFP$^+$/CD45$^-$/EpCAM$^-$ cancer cells) cancer cells in IgG2b control and anti-PD-L1-treated tumors (n=8), as determined by flow cytometry. Each symbol represents a single tumor and mean ± SD for each group is shown. (**a-g**) Unpaired two-tailed Student's *t*-test; ns $p>0.05$, *$p\leq0.05$.

Subsequently, we analyzed the presence of CD3$^+$ T lymphocytes (CD45$^+$/CD11b$^-$/CD3$^+$ cells), CD4$^+$ T lymphocytes (CD3$^+$/CD4$^+$/CD8$^-$ cells), CD8$^+$ T lymphocytes (CD3$^+$/CD4$^-$/CD8$^+$ cells) and NK cells (CD11b$^+$/CD3$^-$/NK-1.1$^+$ cells) in IgG2b control and anti-PD-L1-treated tumors by FACS assays. As we described in epithelial WD-SCCs, we observed that the percentage of CD3$^+$ T cells,

and specifically of $CD8^+$ but not $CD4^+$ T cells, increased after anti-PD-L1 treatment (Figure 69a to 69c). However, a significant decrease of NK cells was observed in anti-PD-L1-treated tumors (Figure 69d). This could affect the elimination of those cells that do not express MHC-I and, thus, the amplification of therapy-resistant cancer cells. To investigate the activation status of CTLs, we evaluated the expression of the inhibitory receptors PD-1, TIM-3 and LAG-3 in $CD3^+/CD8^+$ T cells, as well as the intracellular production of IFN-γ and GzmB. We observed that the percentage of PD-1^+ cells within $CD11b^-/CD8^+$ T lymphocytes did not change in anti-PD-L1-treated mixed tumors compared to IgG2b control tumors (Figure 69e). In addition, the percentage of PD-1^+/TIM-3^+ and PD-1^+/LAG-3^+ T cells decreased upon anti-PD-L1 treatment (Figures 69f and 69g). This indicates that $CD8^+$ T cells found in anti-PD-L1-treated tumors are less exhausted and could mediate an anti-tumor immune response. Accordingly, the percentage of IFN-γ^+ and $GzmB^+$ cells within $CD3^+/CD8^+$ T lymphocytes was significantly increased in mixed tumors that were treated with anti-PD-L1 antibodies (Figures 69h and 69i). Therefore, these results indicate that anti-PD-L1 therapy induces an increase CTL infiltration and the reactivation of $CD8^+$ T cell activity in mixed SCCs. However, the boost of $CD8^+$ activity may be only effective to eliminate epithelial $EpCAM^{high}$ cancer cells. These results also open the door to evaluate the action of other IC receptors in T cells, as well as the role of NK cells, to combat the hybrid and mesenchymal-like $EpCAM^-$ cancer cells.

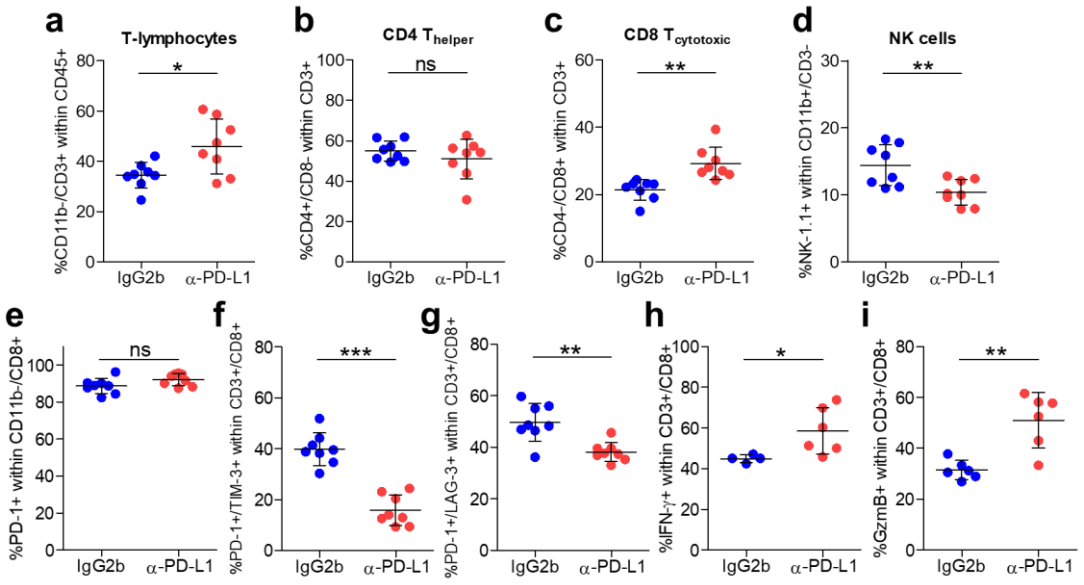

Figure 69. The boost of the anti-tumor immune response could be mediated by the reactivation of cytotoxic T cells in mixed SCCs treated with anti-PD-L1 antibodies. Percentage of (**a**) $CD3^+$ T lymphocytes ($CD45^+/CD11b^-/CD3^+$ cells), (**b**) $CD4^+$ T lymphocytes ($CD3^+/CD4^+/CD8^-$ cells), (**c**) $CD8^+$ T lymphocytes ($CD3^+/CD4^-/CD8^+$ cells), and (**d**) NK cells ($CD11b^+/CD3^-$/NK-1.1^+ cells) in IgG2b control and anti-PD-L1-treated tumors (n=8), as determined by flow cytometry. Percentage of (**e**) PD-1^+, (**f**) PD-1^+/TIM-3^+, (**g**) PD-1^+/LAG-3^+, (**h**) IFN-γ^+, and (**i**) $GzmB^+$ cells within $CD3^+/CD8^+$ T lymphocyte population in the indicated groups (n≥4). Each symbol represents a single tumor and mean ± SD for each group is shown. (**a-i**) Unpaired two-tailed Student's *t*-test; ns $p>0.05$, *$p\leq0.05$, **$p\leq0.01$, ***$p\leq0.001$.

Next, we evaluated whether the reactivation of $CD8^+$ activity might also be associated with a reduced immunosuppressive cell recruitment in anti-PD-L1-treated mixed tumors. FACS analysis showed a reduction of the frequency of myeloid cells ($CD45^+/CD11b^+/CD3^-$ cells) in anti-PD-L1-treated tumors (Figure 70a). In addition, we observed a higher percentage of macrophages ($CD11b^+/F4\text{-}80^+/Gr1^-$ cells, Figure 70b) and a lower frequency of MDSCs ($CD11b^+/Gr1^+$ cells, Figure 70c) in anti-PD-L1-treated tumors compared to IgG2b control tumors, while no changes were detected in DCs ($CD45^+/CD11c^+/F4\text{-}80^-/Gr1^-$ cells, Figure 70d). Interestingly, anti-PD-L1-treated tumors presented a higher infiltration of M1-like macrophages ($CD11b^+/F4\text{-}80^+/Gr1^-/CD206^-$ cells) and a lower percentage of M2-like macrophages ($CD11b^+/F4\text{-}80^+/Gr1^-/CD206^+$ cells) than IgG2b control tumors (Figures 70e and 70f), suggesting that anti-PD-L1 treatment could affect the polarity of macrophages. This change in the polarization phenotype of tumor-infiltrating macrophages was also corroborated by a reduced PD-L1 macrophage expression in anti-PD-L1-treated tumors (Figure 70g), which could also help the recovery of T cell cytotoxic function in mixed SCCs (Figures 69f to 69i). A reduction of PMN-MDSCs ($CD11b^+/Ly6C^+/Ly6G^+$ cells) and an increase of M-MDSCs ($CD11b^+/Ly6C^+/Ly6G^-$ cells) were also detected upon anti-PD-L1 treatment (Figures 70h and 70i). We though this could be triggered by the increase presence of mesenchymal-like $EpCAM^-$ cancer cells in anti-PD-L1-treated tumors. Taken together, these results demonstrate that anti-PD-L1 treatment leads to a reduction of immunosuppressive M2-like macrophages and their expression of PD-L1, which could favor the reactivation of $CD8^+$ T cells toward $EpCAM^{high}$ cancer cells of mixed SCCs. However, the enrichment of cancer cells with mesenchymal-like features upon anti-PD-L1 treatment could lead to an increased recruitment of immunosuppressive M-MDSCs into the tumor core, which could result in these tumors showing a short-term response or a possible resistance to this therapy. These results also indicate that it is important to find combinatorial therapies to attack both the epithelial and the mesenchymal tumor components, as well as to act against the large immunosuppressive infiltrate that mixed SCCs have.

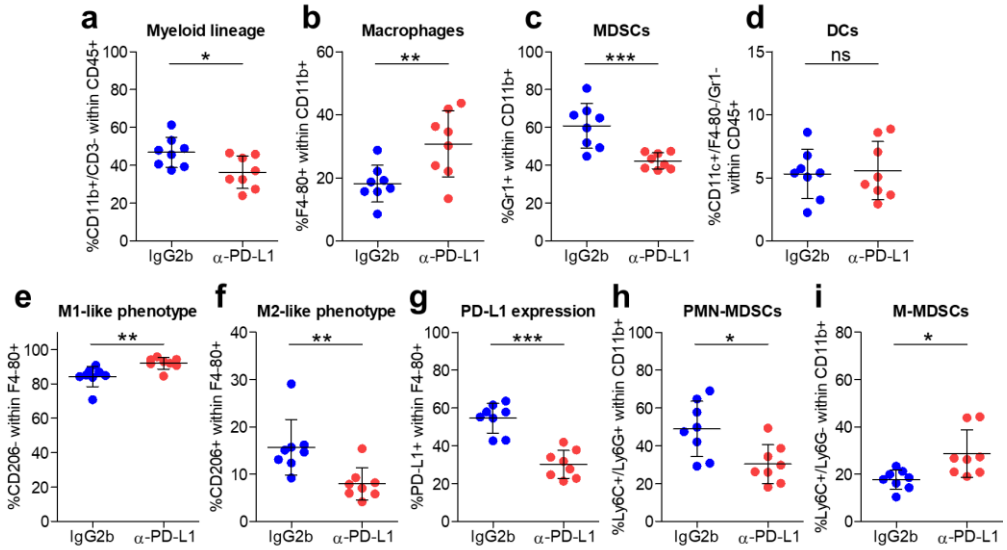

Figure 70. Anti-PD-L1 treatment leads to a reduced recruitment of immunosuppressive M2-like macrophages and increased frequency of M-MDSCs in mixed SCCs. Percentage of (**a**) myeloid cells ($CD45^+/CD11b^+/CD3^-$ cells), (**b**) macrophages ($CD11b^+/F4\text{-}80^+/Gr1^-$ cells), (**c**) MDSCs ($CD11b^+/Gr1^+$ cells), (**d**) DCs ($CD45^+/CD11c^+/F4\text{-}80^-/Gr1^-$ cells), (**e**) M1-like macrophages ($CD11b^+/F4\text{-}80^+/Gr1^-/CD206^-$ cells), (**f**) M2-like macrophages ($CD11b^+/F4\text{-}80^+/Gr1^-/CD206^+$ cells), (**g**) PD-$L1^+$ cells within $F4/80^+$ macrophage population, (**h**) PMN-MDSCs ($CD11b^+/Ly6C^+/Ly6G^+$ cells), and (**i**) M-MDSCs ($CD11b^+/Ly6C^+/Ly6G^-$ cells) in IgG2b control and anti-PD-L1-treated tumors (n=8), as determined by flow cytometry. Each symbol represents a single tumor and mean ± SD for each group is shown. (**a-i**) Unpaired two-tailed Student's *t*-test; ns $p>0.05$, *$p\leq0.05$, **$p\leq0.01$, ***$p\leq0.001$.

Finally, together with other lab members, we investigated whether anti-PD-L1 therapy could facilitate the infiltration of some immune populations to the intratumoral area of mixed tumors and, thus, the direct contact with cancer cells. To address that, we performed immunohistochemistry and immunofluorescence assays of CD8 (T cytotoxic lymphocytes), FoxP3 (Treg cells), CD163 (M2-like macrophages), and CD68 (M1-like and M2-like macrophages) markers in IgG2b control and anti-PD-L1-treated tumors (Figures 71a, 71d, 71g and 71j). In these assays, in accordance with FACS results (Figures 69c and 70b), we observed a significant increase of $CD8^+$ T cells (Figures 71a and 71b) and $CD68^+$ macrophages (Figures 71j and 71k) per tumor area in anti-PD-L1-treated tumors compared to IgG2b control tumors. Furthermore, we observed that there was a shift in the location of these immune populations toward the intratumoral areas (Figures 71c and 71l). This increase of cytotoxic $CD8^+$ T cells and $CD68^+$ macrophages in the tumor core, whose main function is to eliminate cancer cells, was in line with the reduced growth of anti-PD-L1-treated tumors (Figure 67b). In addition, these results suggest that these immune populations may be mainly responsible to the attack of epithelial $EpCAM^+$ cancer cells in mixed SCCs. No changes were detected in the frequency of immunosuppressive $FoxP3^+$ Treg cells after anti-PD-L1 treatment (Figures 71d and 71e), even though these immune cells were more located in the stromal area of anti-PD-L1-treated tumors (Figure 71f). Finally, a reduction of $CD163^+$ M2-like macrophages per tumor area was observed in anti-PD-L1-treated tumors compared to IgG2b controls (Figures 71g and 71h). Interestingly, we noticed that $CD163^+$ M2-like macrophages were more identified in the stromal regions of anti-PD-L1-treated tumors compared to IgG2b control tumors (Figure 71i), suggesting that there might be a partial reduction of the immunosuppressive environment in the tumor core.

All these results suggest that tumors showing moderate differentiation features (MD/PD-SCCs) may have an initial good respond to anti-PD-L1 therapy due to a reactivation of $CD8^+$ T lymphocytes, the elimination of epithelial $EpCAM^{high}$ cancer cells and a less infiltration of immunosuppressive M2-like macrophages. However, the subsequent enrichment of hybrid and mesenchymal-like $EpCAM^-$ cancer cells, concomitantly with the increase of immunosuppressive M-MDSCs, makes it necessary to search for alternative therapies to treat these mixed SCCs.

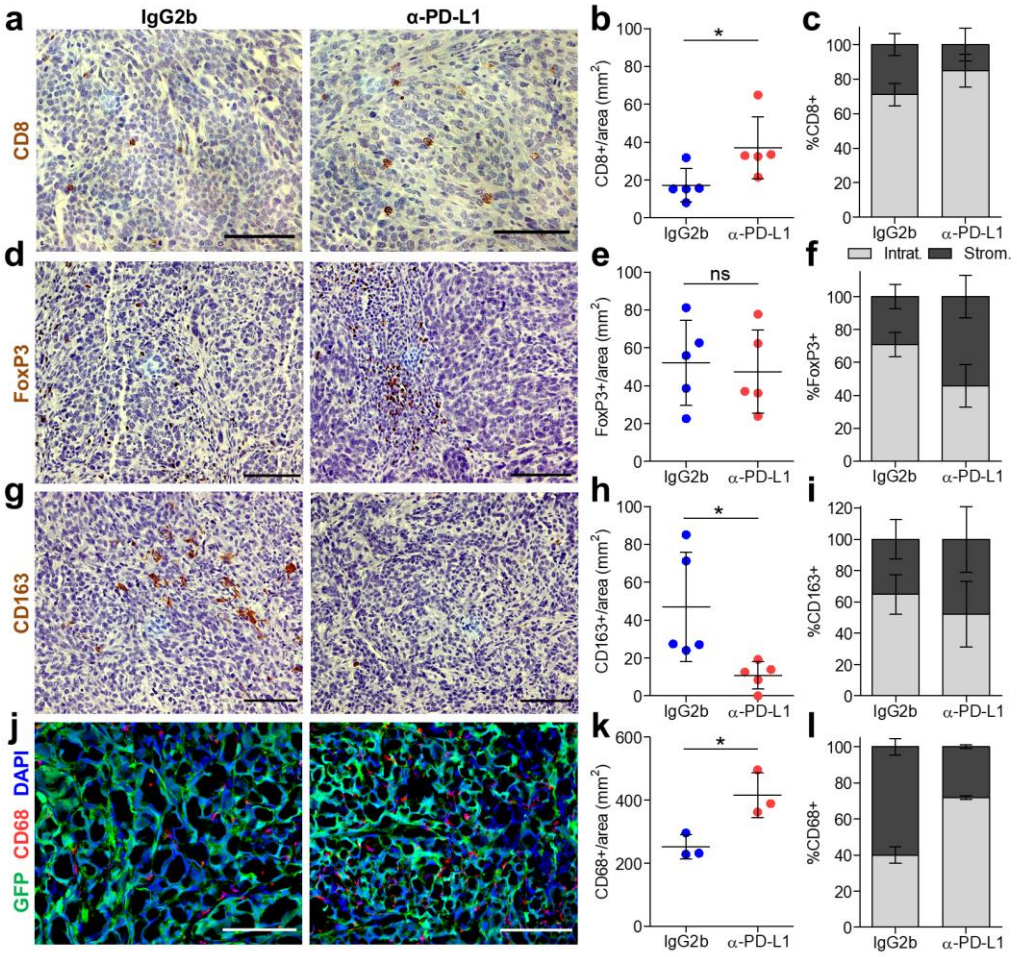

Figure 71. Anti-PD-L1 treatment affects the location of different immune populations in mixed SCCs. Representative immunohistochemistry images of (**a**) $CD8^+$, (**d**) $FoxP3^+$, and (**g**) $CD163^+$ cells in IgG2b control and anti-PD-L1-treated tumors. Scale bar: 100 µm. **j.** Representative immunofluorescence images of GFP^+ cancer cells, $CD68^+$ immune cells and DAPI labelled cell nuclei in IgG2b control and anti-PD-L1-treated tumors. Scale bar: 100 µm. Quantification of (**b**) $CD8^+$, (**e**) $FoxP3^+$, (**h**) $CD163^+$, and (**k**) $CD68^+$ immune cells per tumor area (mm^2) in IgG2b control and anti-PD-L1-treated tumors ($n \geq 3$). At least 8 fields of different regions were quantified in each tumor. Each symbol represents a single tumor and mean ± SD for each group is shown. Percentage (mean ± SD) of intratumoral or stromal (**c**) $CD8^+$, (**f**) $FoxP3^+$, (**i**) $CD163^+$, and (**l**) $CD68^+$ immune cells in the indicated tumors. (**b, e, h, k**) Unpaired two-tailed Student's *t*-test; ns $p>0.05$, *$p \leq 0.05$.

5.4- Immunotherapy based on anti-TIGIT antibodies blocks the growth of mesenchymal skin SCCs

In the Chapter 3, we demonstrated that mesenchymal-like $EpCAM^-$ cancer cells significantly induced the expression of CD155 (Figures 43m and 43n), which is the ligand of the IC receptor TIGIT. For that reason, we hypothesized that mesenchymal tumors (PD/S-SCCs) might be refractory to anti-PD-1/PD-L1 therapies (as we demonstrated in the section 5.2), and that the blockade of TIGIT in T and NK cells could enhance the anti-tumor immune response. We also thought that NK cells may play an important role due to their ability to lyse transformed cells without

antigen-specificity, which makes them unique candidates for killing mesenchymal-like EpCAM$^-$ cancer cells (Sanchez-Correa et al., 2019). To test these hypotheses, we treated immunocompetent syngeneic mice carrying detectable mesenchymal tumors with IgG2b control and anti-TIGIT antibodies during 34 days (13 doses, Figure 72a). Contrary to what we observed after anti-PD-L1 therapy (Figure 62b), the anti-TIGIT treatment significantly delayed mesenchymal tumor growth from day 21 onwards compared to IgG2b control tumors (Figure 72b), which was associated with a decrease in the weight of anti-TIGIT-treated tumors (Figure 72c). In addition, no changes in the spleen weight were detected between the different treatment groups (Figure 72d).

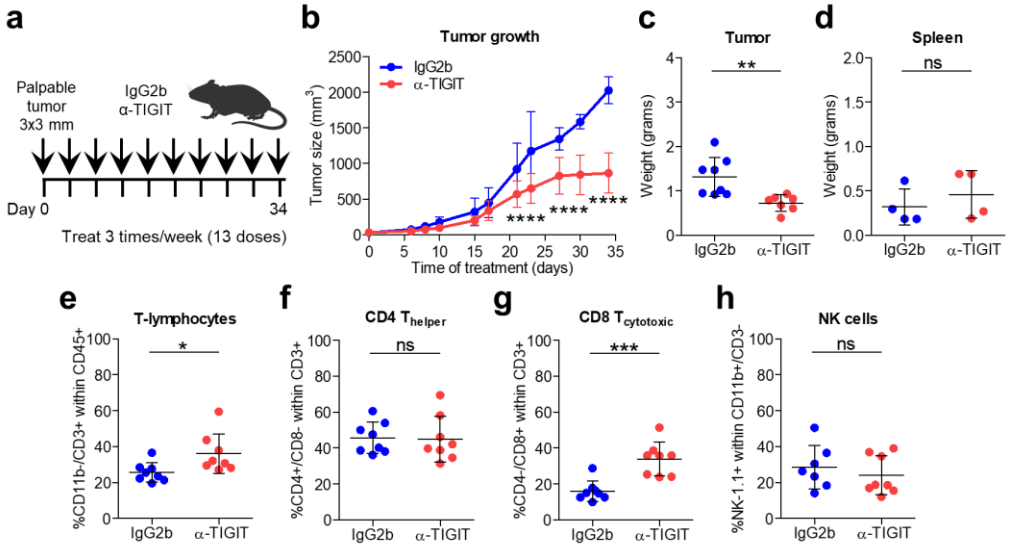

Figure 72. Immunotherapy based on anti-TIGIT antibodies blocks the growth of mesenchymal SCCs. **a.** Experimental scheme for the treatment of mesenchymal tumors with mouse IgG2b isotype control and anti-TIGIT antibodies. All treatments started when engrafted tumors reached a volume of approximately 20 mm^3 (3x3 mm), and mice were administered intraperitoneally three days per week with 200 µg/dose (13 doses). **b.** Growth kinetics of IgG2b control and anti-TIGIT-treated tumors (n=8). Weight of (**c**) tumor and (**d**) spleen in the indicated groups. Percentage of (**e**) CD3$^+$ T lymphocytes (CD45$^+$/CD11b$^-$/CD3$^+$ cells), (**f**) CD4$^+$ T lymphocytes (CD3$^+$/CD4$^+$/CD8$^-$ cells), (**g**) CD8$^+$ T lymphocytes (CD3$^+$/CD4$^-$/CD8$^+$ cells), and (**h**) NK cells (CD11b$^+$/CD3$^-$/NK-1.1$^+$ cells) in IgG2b control and anti-TIGIT-treated tumors (n=8), as determined by flow cytometry. Each symbol represents a single mouse (**d**) or tumor (**c, e-h**), and mean ± SD for each group is shown. (**b**) Repeated Measures ANOVA test, (**c-h**) Unpaired two-tailed Student's *t*-test; ns p>0.05, *p≤0.05, **p≤0.01, ***p≤0.001, ****p≤0.0001.

Subsequently, we analyzed the presence of CD3$^+$ T lymphocytes (CD45$^+$/CD11b$^-$/CD3$^+$ cells), CD4$^+$ T lymphocytes (CD3$^+$/CD4$^+$/CD8$^-$ cells), CD8$^+$ T lymphocytes (CD3$^+$/CD4$^-$/CD8$^+$ cells) and NK cells (CD11b$^+$/CD3$^-$/NK-1.1$^+$ cells) in IgG2b control and anti-TIGIT-treated tumors by FACS assays. We observed that the percentage of CD3$^+$ T cells significantly increased in anti-TIGIT-treated tumors compared to IgG2b control tumors (Figure 72e). While no changes in CD4$^+$ T lymphocytes were detected among the different treatment groups (Figure 72f), an increase of CD8$^+$

T lymphocytes was detected in anti-TIGIT-treated tumors (Figure 72g). In addition, no changes in the frequency of NK cells were observed upon anti-TIGIT treatment (Figure 72h).

Since this preliminary information seemed very interesting to us, we are currently analyzing more extensively the immune infiltrate and the IC expression profile upon anti-TIGIT treatment. As these results indicate that the reduction of tumor growth after anti-TIGIT treatment might be mediated by a high CTL and NK cell activity, we are currently studying if there is a reactivation of $CD8^+$ T lymphocytes and NK cells, through the loss of the expression of some IC receptors such as PD-1, TIM-3, LAG-3, and TIGIT, as well as a high expression of IFN-γ and GzmB, upon anti-TIGIT treatment. In addition, we are evaluating the impact of inhibiting the TIGIT pathway to reactivate CTL and NK activity in *in vitro* assays. Given that Treg cells facilitate tumor progression by interfering with the cytotoxic activity of T and NK cells (von Boehmer and Daniel, 2013), we are also evaluating whether the presence of this population is reduced in anti-TIGIT-treated tumors, that could explain the reactivation of T and NK-cell cytotoxic activities. Finally, we will evaluate whether the reactivation of $CD8^+$ and NK-cell activity might be associated with a reduced immunosuppressive cell recruitment in anti-TIGIT-treated mesenchymal tumors. To sum up, mesenchymal tumors exhibit a good response to anti-TIGIT therapy, in accordance to the increased expression of its ligand CD155 in mesenchymal-like cancer cells. However, further experiments will be necessary to evaluate the specific role of T and NK cells in mediating this response.

Summary Chapter 5: ICB therapies should be selected depending on the cancer-cell features

All the results presented in Chapter 5 demonstrate that mouse WD-SCCs, comprised by epithelial $EpCAM^+$ cancer cells, respond to anti-PD-L1 therapy, which is dependent on reactivated cytotoxic $CD8^+$ T cells and the reduction of immunosuppressive cell recruitment (M2-like macrophages and M-MDSCs). In addition, tumors showing moderate differentiation features (MD/PD-SCCs) could have an initial good response to anti-PD-L1 therapy due to a reactivation of $CD8^+$ T lymphocytes toward $EpCAM^{high}$ cancer cells and less infiltration of immunosuppressive M2-like macrophages. However, the enrichment of hybrid and mesenchymal-like $EpCAM^-$ cancer cells and the subsequent increased recruitment of immunosuppressive M-MDSCs at intermediate stages of progression makes it necessary to search for alternative therapies to combat them. In this sense, mouse PD/S-SCCs comprised by mesenchymal-like $EpCAM^-$ cancer cells were refractory to anti-PD-L1 therapy, but exhibit a good response to anti-TIGIT therapy in accordance to the increased expression of its ligand CD155 in mesenchymal-like $EpCAM^-$ cancer cells.

CHAPTER 6. ASSESSING THE BENEFITS OF TARGETING THE IMMUNOSUPPRESSIVE TUMOR MICROENVIRONMENT TO BLOCK CANCER-CELL PLASTICITY AND TO ENHANCE ANTI-TUMOR RESPONSES

The importance of the TME in dynamically regulating cancer progression and influencing therapeutic outcome is widely appreciated, and multiple therapies directed to various components of the TME have been developed in recent years (Bejarano et al., 2021). In this regard, due to the adverse side effects observed after the blockade of CTLA-4, PD-1 and combined therapies with different IC inhibitors in different tumor types (Dougan et al., 2021; Pauken et al., 2019), we hypothesized that an alternative strategy could be to target the immunosuppressive TME, which contributes to maintain the exhausted state of CTLs and NK cells, even after ICB therapy. Our studies indicated that, similarly to that reported in mesenchymal mouse tumors, advanced patient SCCs (G3 and G4 grade) showed an increased recruitment of immunosuppressive M2-like macrophages and Treg cells, concomitantly with an increased proportion of hybrid E-cadherin^{+}/Vimentin^{+} and mesenchymal E-cadherin^{-}/Vimentin^{+} cancer cells. However, it remained to be determined how the presence of these immunosuppressive immune cells may impair the function of CTLs and NK cells or promote the progression toward the mesenchymal phenotype. Since this plastic behavior occurs both in T-cell deficient mice and under the pressure of a full immune system in immunocompetent syngeneic mice (Figure 13), these data denote that T cells (Treg and CD4^{+} cells) may not be key drivers to promote this plastic behavior during SCC progression. Thus, we proposed to inhibit the recruitment of MDSCs and macrophages to target the immunosuppressive TME.

6.1- Depletion of MDSCs attenuates the growth of mixed mouse SCCs and reduces the infiltration of M2-like macrophages

MDSCs are a heterogenous population of immature myeloid cells than can promote tumor growth by suppressing T- and NK-cell activity (Law et al., 2020). In fact, several studies in melanoma, breast cancer, and rhabdomyosarcoma have revealed a correlation between MDSC abundance and resistance against ICB therapies, and ultimately resulting in poor patient outcomes (Diaz-Montero et al., 2009; Highfill et al., 2014; Meyer et al., 2014; Tarhini et al., 2014; Weber et al., 2016). To study the role of MDSCs promoting cancer-cell plasticity, mice bearing mixed SCCs (enriched in plastic cancer cells) were treated with IgG2b isotype control or anti-Gr1 antibodies the day before the engraftment of epithelial EpCAM^{+} cancer cells, and then 3 times per week during 41 days (18 doses) (Figure 73a). Our strategy was to deplete circulating and tumor-infiltrating MDSCs using an anti-Gr1 antibody, which is a rat IgG2b that induces cell death through complement-mediated membrane-complex attack (Boivin et al., 2020; Füst et al., 1980). Specifically, this antibody recognizes the differentiation antigens Ly6C, which is expressed in M-MDSCs, macrophages and

DC precursors, and Ly6G, which is expressed in PMN-MDSCs, neutrophils, monocytes and granulocytes (Youn et al., 2008). We observed that anti-Gr1 treatment significantly reduced mixed tumor growth as compared to IgG2b control tumors at the end of the treatment (day 41, Figure 73b), which was associated with a significant decrease in the weight of anti-Gr1-treated tumors (Figure 73c). However, no changes in spleen and liver weights were detected between both treatment groups (Figures 73d and 73e). We then quantified the percentage of necrotic areas relative to total tumor area from both treatment groups (Figures 73f and 73g; in collaboration with Adrià Archilla, PhD student). No significant differences in the percentage of necrotic areas were observed between IgG2b control and anti-Gr1-treated tumors (Figures 73f and 73g). These results demonstrate that anti-Gr1 treatment decreases mixed tumor growth at the end of the treatment, but this reduction may not be associated with a reduced cancer-cell viability in anti-Gr1-treated tumors. In accordance, no significant changes were detected in the total frequency of cancer cells ($GFP^+/CD45^-$ cells), fibroblasts ($GFP^-/CD45^-$ cells) and $CD45^+$ leukocytes between IgG2b control and anti-Gr1-treated tumors (Figures 74a to 74c).

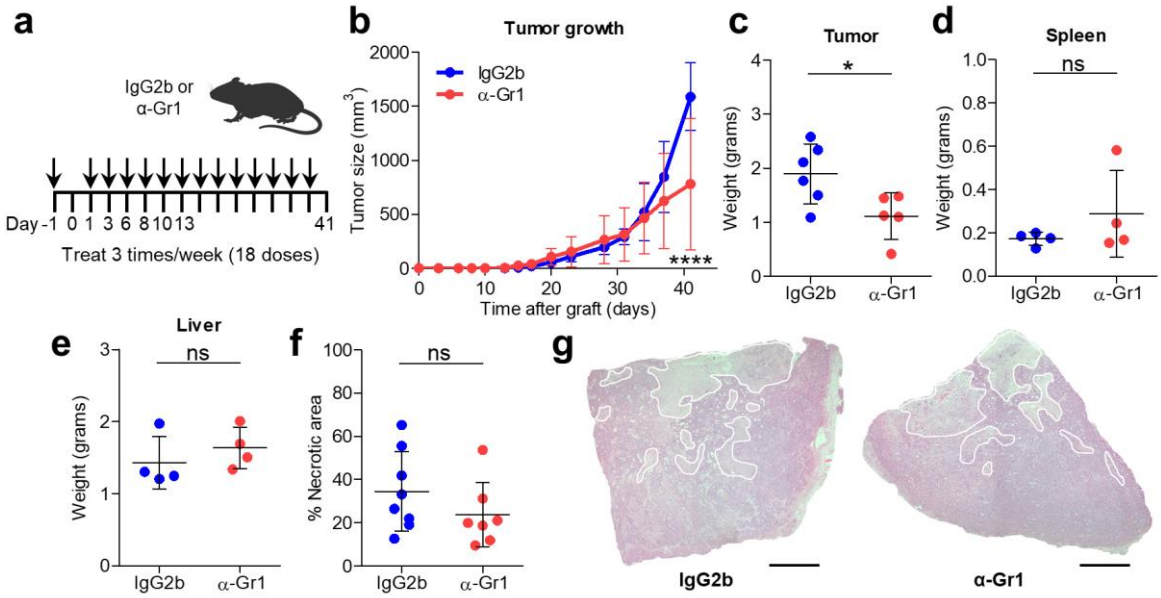

Figure 73. Anti-Gr1 treatment attenuates the growth of mixed SCCs. a. Experimental scheme for the treatment of mixed tumors, growing in immunocompetent syngeneic mice, with mouse IgG2b isotype control or anti-Gr1 antibodies. All treatments started on day -1, and then mice were administered intraperitoneally 3 days per week with 200 µg/dose until experimental endpoint (18 doses). **b.** Growth kinetics of IgG2b control and anti-Gr1-treated tumors (n=8). Weight of (**c**) tumor, (**d**) spleen and (**e**) liver in the indicated groups. **f.** Percentage of necrotic areas relative to total tumor area in the indicated groups (n=8). **g**. Representative hematoxylin/eosin (H/E) section of a mixed tumor treated with IgG2b control or anti-Gr1 antibodies, where necrotic areas are marked with white lines. Scale bar: 100 µm. Each symbol represents a single mouse (**d**, **e**) or tumor (**c, f**), and mean ± SD for each group is shown. (**b**) Repeated Measures ANOVA test, (**c**-**f**) unpaired two-tailed Student's *t*-test; ns $p>0.05$, *$p\leq0.05$, ****$p\leq0.0001$.

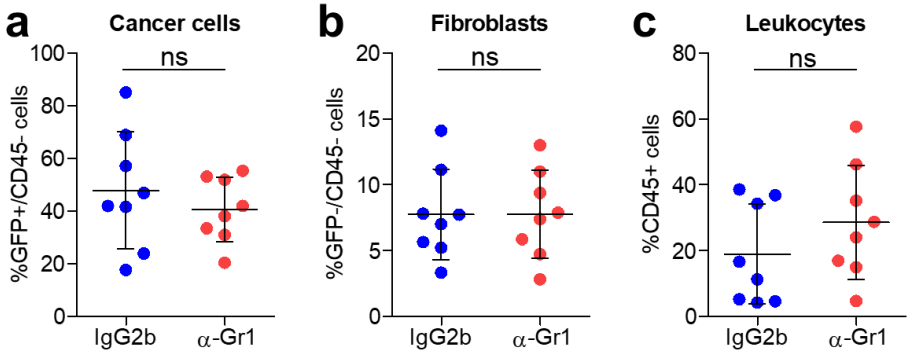

Figure 74. Tumor cell components do not change in mixed SCCs after anti-Gr1 treatment. Percentage of (**a**) cancer cells ($GFP^+/CD45^-$ cells), (**b**) fibroblasts ($GFP^-/CD45^-$ cells), and (**c**) leukocytes ($CD45^+$ cells) in IgG2b control and anti-Gr1-treated tumors (n=8), as determined by flow cytometry. Each symbol represents a single tumor and mean ± SD for each group is shown. (**a-c**) Unpaired two-tailed Student's *t*-test; ns p>0.05.

To evaluate the specificity of antibody-mediated MDSC depletion in response to the treatment, we compared the frequency of myeloid cells (MDSCs and macrophages) and DCs infiltrating IgG2b control and anti-Gr1 treated tumors (Figures 75a to 75i).

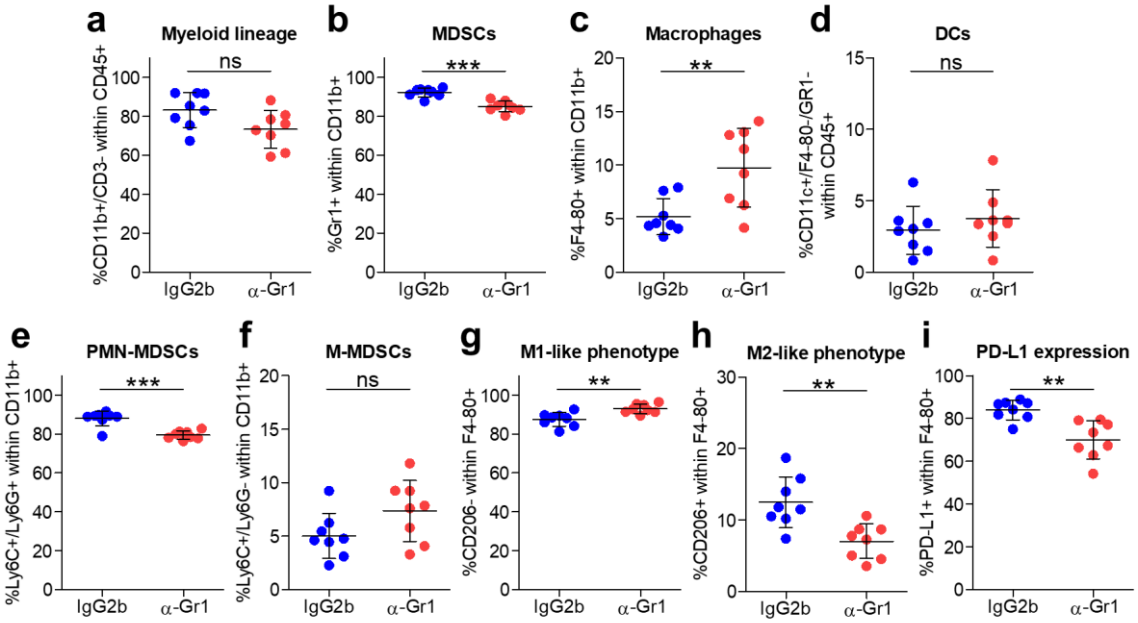

Figure 75. Anti-Gr1 treatment leads to a partial depletion of PMN-MDSCs and a decreased infiltration of M2-like macrophages. Percentage of (**a**) myeloid cells ($CD45^+/CD11b^+/CD3^-$ cells), (**b**) MDSCs ($CD11b^+/Gr1^+$ cells), (**c**) macrophages ($CD11b^+/F4\text{-}80^+/Gr1^-$ cells), (**d**) DCs ($CD45^+/CD11c^+/F4\text{-}80^-/Gr1^-$ cells), (**e**) PMN-MDSCs ($CD11b^+/Ly6C^+/Ly6G^+$ cells), (**f**) M-MDSCs ($CD11b^+/Ly6C^+/Ly6G^-$ cells), (**g**) M1-like macrophages ($CD11b^+/F4\text{-}80^+/Gr1^-/CD206^-$ cells), (**h**) M2-like macrophages ($CD11b^+/F4\text{-}80^+/Gr1^-/CD206^+$ cells), and (**i**) PD-$L1^+$ cells within $F4/80^+$ macrophages in IgG2b control and anti-Gr1-treated tumors (n=8), as determined by flow cytometry. Each symbol represents a single tumor and mean ± SD for each group is shown. (**a-i**) Unpaired two-tailed Student's *t*-test; ns p>0.05, **p≤0.01, ***p≤0.001.

FACS analysis showed no significant differences in the total frequency of myeloid cells ($CD45^+/CD11b^+/CD3^-$ cells) after anti-Gr1 treatment (Figure 75a). However, we observed a partial depletion of MDSCs ($CD11b^+/Gr1^+$ cells, Figure 75b) and a higher percentage of macrophages ($CD11b^+/F4\text{-}80^+/Gr1^-$ cells, Figure 75c) within the myeloid compartment in anti-Gr1-treated tumors as compared to IgG2b control tumors. No significant differences in the percentage of DCs ($CD45^+/CD11c^+/F4\text{-}80^-/Gr1^-$ cells) were detected after anti-Gr1 treatment (Figure 75d). Interestingly, whereas no changes in M-MDSCs ($CD11b^+/Ly6C^+/Ly6G^-$ cells) were detected (Figure 75f), a reduction of PMN-MDSCs ($CD11b^+/Ly6C^+/Ly6G^+$ cells) was observed in anti-Gr1-treated tumors (Figure 75e). These results indicate that anti-Gr1 treatment could mainly induce a depletion of PMN-MDSCs in mixed SCCs. Given that immunosuppressive MDSCs can influence the polarization of macrophages toward an M2-like phenotype (Law et al., 2020), we then analyzed the presence of M1- and M2-like macrophages by FACS analysis. Interestingly, anti-Gr1-treated tumors presented a higher infiltration of M1-like macrophages ($CD11b^+/F4\text{-}80^+/Gr1^-/CD206^-$ cells) and a lower percentage of M2-like macrophages ($CD11b^+/F4\text{-}80^+/Gr1^-/CD206^+$ cells) than IgG2b control tumors (Figures 75g and 75h), suggesting that anti-Gr1 treatment might favor the polarity of macrophages toward a pro-inflammatory M1-like phenotype. In addition, this change in the polarization phenotype of tumor-infiltrating macrophages was also corroborated by a reduced frequency of $PD\text{-}L1^+$ macrophages in anti-Gr1-treated tumors (Figure 75i).

To further characterize the alterations in tumor-infiltrating immune cells after anti-Gr1 treatment, we performed immunofluorescence and immunohistochemistry assays with anti-Gr1 (PMN-MDSCs and M-MDSCs), anti-CD68 (M1-like and M2-like macrophages) and anti-CD163 (M2-like macrophages) antibodies in IgG2b control and anti-Gr1-treated tumors (Figures 76a, 76d and 76g). In accordance with FACS results (Figure 75b), we observed a significant decrease of $Gr1^+$ cells per tumor area after anti-Gr1 treatment (Figures 76a and 76b). Interestingly, along with this decrease, we noticed that the majority of $Gr1^+$ MDSCs were located in the stromal area of anti-Gr1-treated tumors, so there could be an enhanced depletion and exclusion of $Gr1^+$ MDSCs from the tumor core (Figure 76c). In addition, we observed a significant increase in the frequency of $CD68^+$ macrophages (Figures 76d and 76e) and a mild decrease in the frequency of $CD163^+$ M2-like macrophages (Figures 76g and 76h) per tumor area after anti-Gr1 treatment, although these immune populations did not change their location after the treatment (Figures 76f and 76i). These results suggest that the increase of $CD68^+$ macrophages in anti-Gr1-treated tumors may be due to an enrichment of anti-tumorigenic M1-like macrophages, already indicated by FACS data (Figure 75g). Altogether, these results indicate that the partial depletion of PMN-MDSCs leads to a TME characterized by a high infiltration of anti-tumorigenic M1-like macrophages and less infiltration of immunosuppressive M2-like macrophages. This situation might generate a less immunosuppressive tumor microenvironment that could positively influence the immunotherapy response of mixed SCCs.

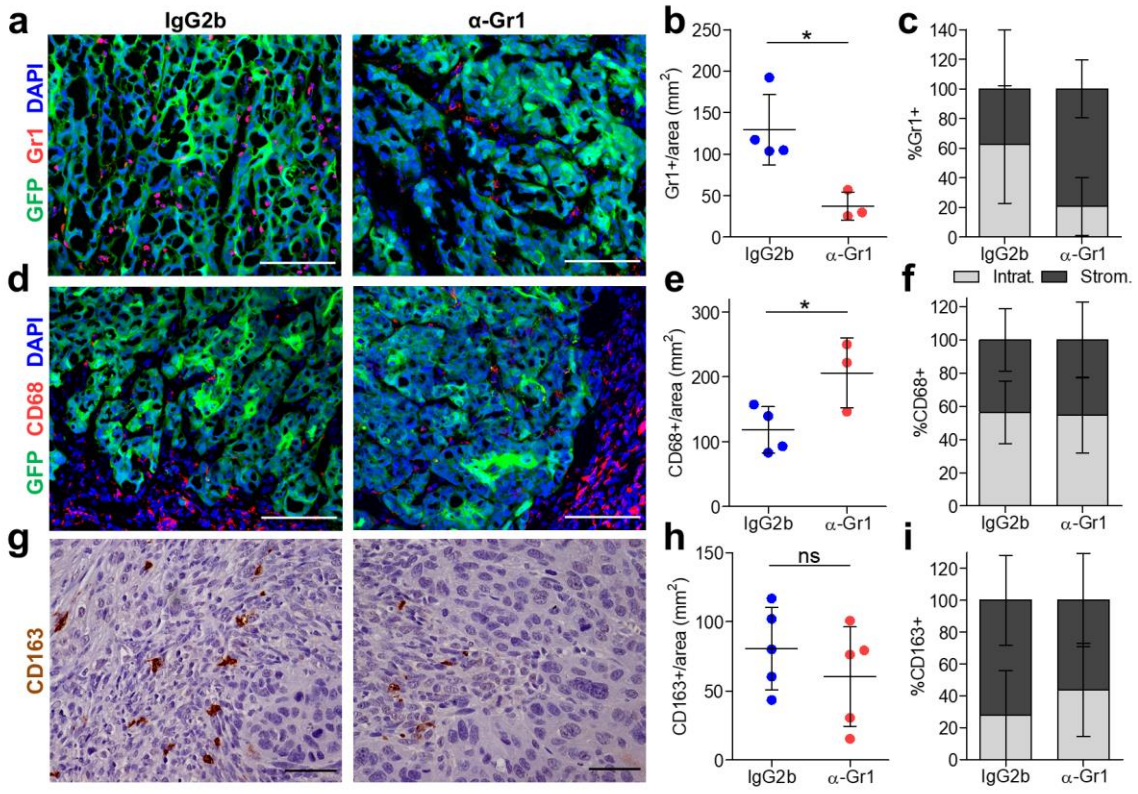

Figure 76. Anti-Gr1 treatment leads to a reduction of tumor-infiltrating Gr1$^+$ MDSCs and an increased frequency of tumor-infiltrating CD68$^+$ macrophages. (**a**, **d**) Representative immunofluorescence images of GFP$^+$ cancer cells, (**a**) Gr1$^+$ or (**d**) CD68$^+$ immune cells and DAPI labelled cell nuclei in IgG2b control and anti-Gr1-treated tumors. Scale bar: 100 µm. **g.** Representative immunohistochemistry images of CD163$^+$ cells in IgG2b control and anti-Gr1-treated tumors. Scale bar: 100 µm. Quantification of (**b**) Gr1$^+$, (**e**) CD68$^+$, and (**h**) CD163$^+$ cells per tumor area (mm^2) in IgG2b control and anti-Gr1-treated tumors (n≥3). At least 8 fields of different regions were quantified in each tumor. Each symbol represents a single tumor and mean ± SD for each group is shown. Percentage (mean ± SD) of intratumoral or stromal (**c**) Gr1$^+$, (**f**) CD68$^+$, and (**i**) CD163$^+$ cells in the indicated tumors. (**b, e, h**) Unpaired two-tailed Student's *t*-test; ns p>0.05, *p≤0.05.

6.2- Depletion of MDSCs blocks cancer-cell progression toward the mesenchymal state and enhances anti-tumor CTL responses

Subsequently, we evaluated whether PMN-MDSC depletion blocked the acquisition of cancer-cell plasticity and the progression toward the mesenchymal phenotype, as well as enhanced the anti-tumor immune responses of CTLs and NK cells.

To address the first objective, we quantified the percentage of epithelial EpCAM$^+$ and mesenchymal-like EpCAM$^-$ cancer cells at the end of the treatments by FACS analysis. We observed an increase in the percentage of epithelial EpCAM$^+$ cancer cells (Figure 77a) and a decrease in the frequency of mesenchymal-like EpCAM$^-$ cancer cells in anti-Gr1-treated tumors as compared to IgG2b control tumors (Figure 77b).

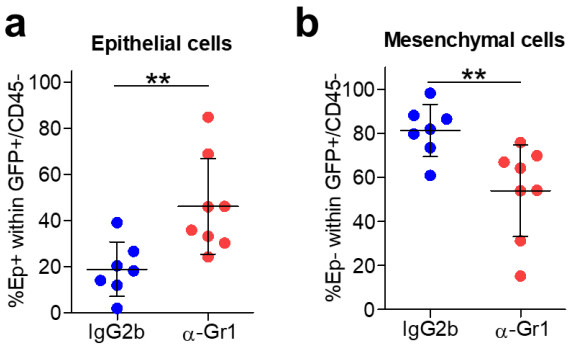

Figure 77. Partial depletion of PMN-MDSCs blocks cancer-cell progression toward the mesenchymal state. Percentage of (**a**) epithelial ($GFP^+/CD45^-/EpCAM^+$ cancer cells), and (**b**) mesenchymal ($GFP^+/CD45^-/EpCAM^-$ cancer cells) cancer cells in IgG2b control and anti-Gr1-treated tumors (n=8), as determined by flow cytometry. Each symbol represents a single tumor and mean ± SD for each group is shown. (**a-b**) Unpaired two-tailed Student's *t*-test; **p≤0.01.

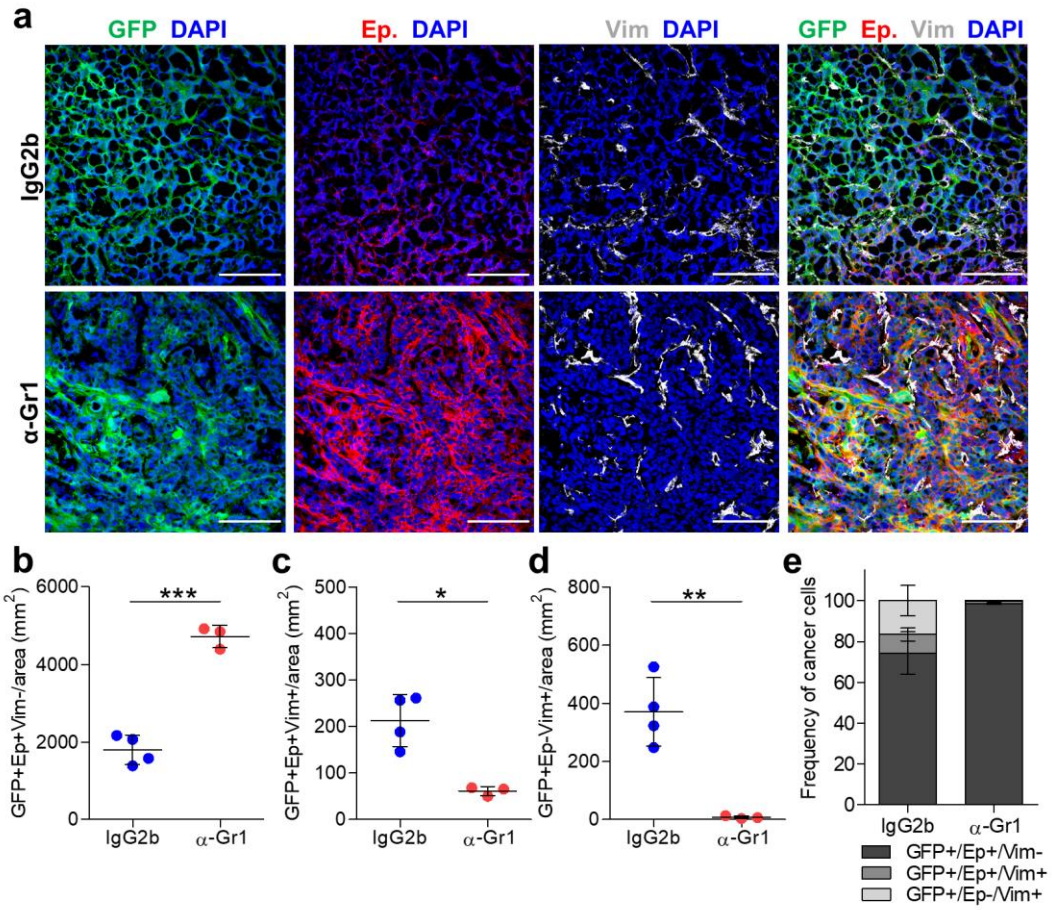

Figure 78. Partial depletion of PMN-MDSCs blocks the generation of hybrid $EpCAM^+/Vimentin^+$ and mesenchymal-like $EpCAM^-/Vimentin^+$ cancer cells. a. Representative immunofluorescence images of GFP^+, $EpCAM^+$, $Vimentin^+$ cancer cells and DAPI labelled cell nuclei in IgG2b control and anti-Gr1-treated tumors. Scale bar: 100 µm. Quantification of (**b**) epithelial $GFP^+/EpCAM^+/Vimentin^-$, (**c**) hybrid $GFP^+/EpCAM^+/Vimentin^+$, and (**d**) mesenchymal $GFP^+/EpCAM^-/Vimentin^+$ cancer cells per tumor area (mm^2) in IgG2b control (n=4) and anti-Gr1-treated (n=3) tumors. At least 9 fields of different regions were

quantified in each tumor. Each symbol represents a single tumor and mean ± SD for each group is shown. **e**. Percentage (mean ± SD) of $GFP^+/EpCAM^+/Vimentin^-$, $GFP^+/EpCAM^+/Vimentin^+$, and $GFP^+/EpCAM^-/Vimentin^+$ cancer cells relative to total cancer cells in the indicated tumors. (**b-d**) Unpaired two-tailed Student's *t*-test; *p≤0.05, **p≤0.01, ***p≤0.001.

Given that to evaluate the acquisition of cancer-cell plasticity we only monitored the loss of the epithelial marker EpCAM in FACS analysis (Figure 77b), we completed these studies by immunofluorescence assays, which allowed us to characterize cancer cells and their hybrid/plastic state by the expression of an epithelial (EpCAM) and a mesenchymal (Vimentin) marker (Figure 78a). We observed that the frequency of epithelial $GFP^+/EpCAM^+/Vimentin^-$ cancer cells per tumor area was significantly increased in anti-Gr1-treated tumors compared to IgG2b control tumors (Figures 78a, 78b and 78e), indicating that anti-Gr1-treated tumors had a more epithelial degree of differentiation. In line with this observation, we noticed that the frequency of hybrid $GFP^+/EpCAM^+/Vimentin^+$ and mesenchymal $GFP^+/EpCAM^-/Vimentin^+$ cancer cells per tumor area decreased after anti-Gr1 treatment (Figures 78a, 78c to 78e). With all these data, we hypothesized different scenarios. The first scenario would be that the depletion of PMN-MDSCs could block cancer-cell progression toward the mesenchymal state. Therefore, this suggest that cytokines and growth factors derived from PMN-MDSCs may promote cancer-cell plasticity, the acquisition of mesenchymal traits and SCC progression. The second scenario would be that the reduction of the mesenchymal component after anti-Gr1 treatment could be consequence of an increase of NK cells (Figure 79d), which could eliminate more efficiently hybrid and mesenchymal cancer cells.

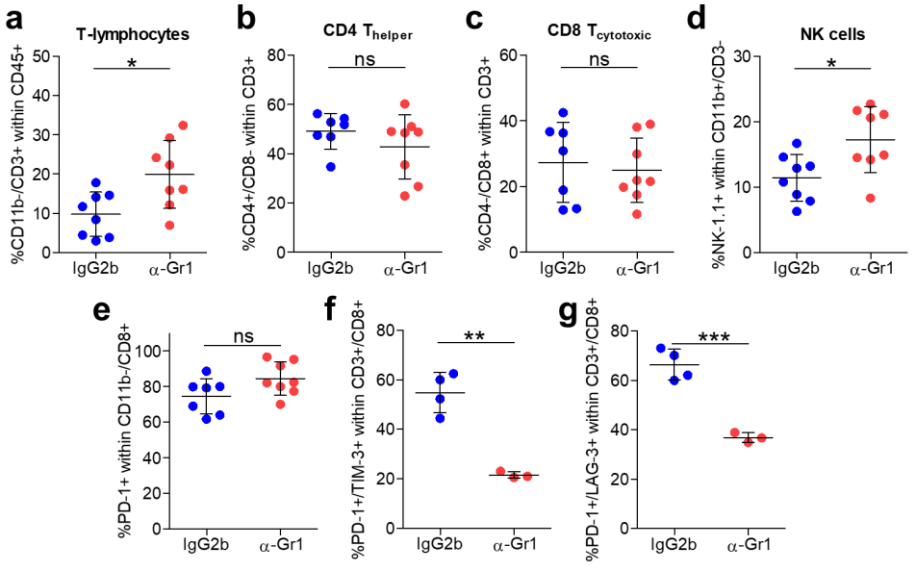

Figure 79. Partial depletion of PMN-MDSCs leads to a higher infiltration of T lymphocytes and NK cells, and a reactivation of CTLs. Percentage of (**a**) $CD3^+$ T lymphocytes ($CD45^+/CD11b^-/CD3^+$ cells), (**b**) $CD4^+$ T lymphocytes ($CD3^+/CD4^+/CD8^-$ cells), (**c**) $CD8^+$ T lymphocytes ($CD3^+/CD4^-/CD8^+$ cells), and (**d**) NK cells ($CD11b^+/CD3^-/NK\text{-}1.1^+$ cells) in IgG2b control and anti-Gr1-treated tumors (n=8), as determined by flow cytometry. Percentage of (**e**) $PD\text{-}1^+$, (**f**) $PD\text{-}1^+/TIM\text{-}3^+$, and (**g**) $PD\text{-}1^+/LAG\text{-}3^+$ cells within $CD3^+/CD8^+$

T lymphocyte population in the indicated groups (n≥3). Each symbol represents a single tumor and mean ± SD for each group is shown. (**a-g**) Unpaired two-tailed Student's *t*-test; ns p>0.05, *p≤0.05, **p≤0.01, ***p≤0.001.

To address whether anti-Gr1 treatment enhanced the anti-tumor responses of CTLs and NK cells, we analyzed the presence of $CD3^+$ T lymphocytes ($CD45^+/CD11b^-/CD3^+$ cells), $CD4^+$ T lymphocytes ($CD3^+/CD4^+/CD8^-$ cells), $CD8^+$ T lymphocytes ($CD3^+/CD4^-/CD8^+$ cells) and NK cells ($CD11b^+/CD3^-/NK\text{-}1.1^+$ cells) in IgG2b control and anti-Gr1-treated tumors by FACS assays. We observed that the percentage of $CD3^+$ T cells increased in anti-Gr1-treated tumors compared to IgG2b control tumors (Figure 79a), even though no changes were detected within $CD4^+$ and $CD8^+$ populations (Figures 79b and 79c). These results suggest that the depletion of PMN-MDSCs could favor a high frequency of $CD3^+$ T lymphocytes in anti-Gr1-treated tumors, indeed promoting the killing of cancer cells. Interestingly, a significant increase of NK cells was observed in anti-Gr1-treated tumors (Figure 79d), which could favor the elimination of those cells that do not express MHC-I. These results could be along the line that NK cells may be attacking hybrid and mesenchymal-like $EpCAM^-$ cancer cells and this could be another reason why we observed a reduction in their frequency after anti-Gr1 treatment (Figures 78c and 78d). In addition, we investigated the activation status of CTLs to evaluate whether there was a boost of anti-tumor responses after anti-Gr1 treatment. We observed that the percentage of $PD\text{-}1^+$ cells within $CD11b^-/CD8^+$ T lymphocyte population did not change in anti-Gr1-treated tumors compared to IgG2b control tumors (Figure 79e). In addition, the percentage of $PD\text{-}1^+/TIM\text{-}3^+$ and $PD\text{-}1^+/LAG\text{-}3^+$ T cells decreased after anti-Gr1 treatment (Figures 79f and 79g). This data indicates that $CD8^+$ T cells found in anti-Gr1-treated tumors could be less exhausted and mediate a pro-inflammatory immune response. Taken together, these results indicate that anti-Gr1 therapy induces an increase in T lymphocyte and NK cell frequency and might reactivate $CD8^+$ T cell activity. Given that the increase in NK cells could be key to the elimination of hybrid and mesenchymal cancer cells, we plan to evaluate in future experiments the activation status of this population, as well as the effect of combinatory therapies with IC antibodies to further prevent $CD8^+$ and NK cell exhaustion and to elicit a potent anti-tumor immunity.

Finally, we performed immunohistochemistry assays of CD8 (T cytotoxic lymphocytes) and FoxP3 (Treg cells) markers in IgG2b control and anti-Gr1-treated tumors (Figures 80a and 80d). In these assays, no changes were detected in the frequency of $CD8^+$ cells (Figures 80a and 80b) and immunosuppressive $FoxP3^+$ Treg cells per tumor area after anti-Gr1 treatment (Figures 80d and 80e). In addition, these immune populations did not change their spatial location after anti-Gr1 treatment (Figures 80c and 80f). These results indicate that the depletion of PMN-MDSCs does not lead to a reduction of Treg cells. Although it remains to be evaluated whether its immunosuppressive activity decreases after anti-Gr1 treatment.

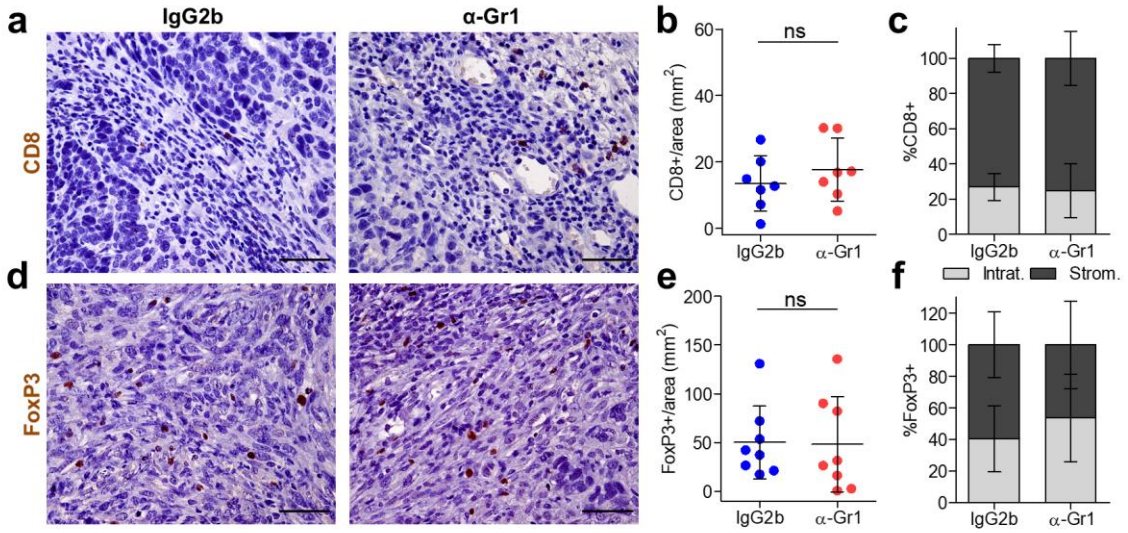

Figure 80. Anti-Gr1 treatment does not alter the tumor-infiltration of CD8$^+$ T lymphocytes and FoxP3$^+$ Treg cells. Representative immunohistochemistry images of (**a**) CD8$^+$ and (**d**) FoxP3$^+$ cells in IgG2b control and anti-Gr1-treated tumors. Scale bar: 100 µm. Quantification of (**b**) CD8$^+$ and (**e**) FoxP3$^+$ cells per tumor area (mm^2) in IgG2b control and anti-Gr1-treated tumors (n≥7). At least 10 fields of different regions were quantified in each tumor. Each symbol represents a single tumor and mean ± SD for each group is shown. Percentage (mean ± SD) of intratumoral or stromal (**c**) CD8$^+$ and (**f**) FoxP3$^+$ cells in the indicated tumors. (**b, e**) Unpaired two-tailed Student's *t*-test; ns p>0.05.

6.3- Anti-CSF1R treatment does not attenuate the growth of mixed SCCs, but decreases the frequency of M2-like macrophages and M-MDSCs

Several approaches have been used to ablate TAMs or inhibit their tumor-promoting functions in mouse models of cancer (Bejarano et al., 2021; Ruffell et al., 2012). One strategy is the CSF-1R inhibition, which is a tyrosine kinase receptor that when bound with its ligand CSF-1 promotes the differentiation and expansion of myeloid cells into MDSCs and TAMs in addition to promoting their migration to tumors (Holmgaard et al., 2016). Before starting the *in vivo* inhibition treatment, we evaluated the competence of MDSCs and TAMs for signaling via the CSF-1/CSF1R pathway. To address this, we isolated M1-like macrophages (F4-80$^+$/Gr1$^-$/CD206$^-$ cells), M2-like macrophages (F4-80$^+$/Gr1$^-$/CD206$^+$ cells), PMN-MDSCs (CD11b$^+$/Ly6C$^+$/Ly6G$^+$ cells) and M-MDSCs (CD11b$^+$/Ly6C$^+$/Ly6G$^-$ cells) from epithelial, mixed and mesenchymal SCCs by FACS sorting. *Csf1R* gene expression was similarly high in macrophages isolated from epithelial, mixed and mesenchymal tumors, and its expression did not vary according to their M1- or M2-like polarization phenotype (Figure 81a). In addition, M-MDSCs isolated from epithelial, mixed and mesenchymal tumors had a higher expression of *Csf1R* than PMN-MDSCs isolated from all SCC stages (Figure 81b). These results indicate that CSF1R inhibition may affect mainly M1-like and M2-like macrophages, and M-MDSCs.

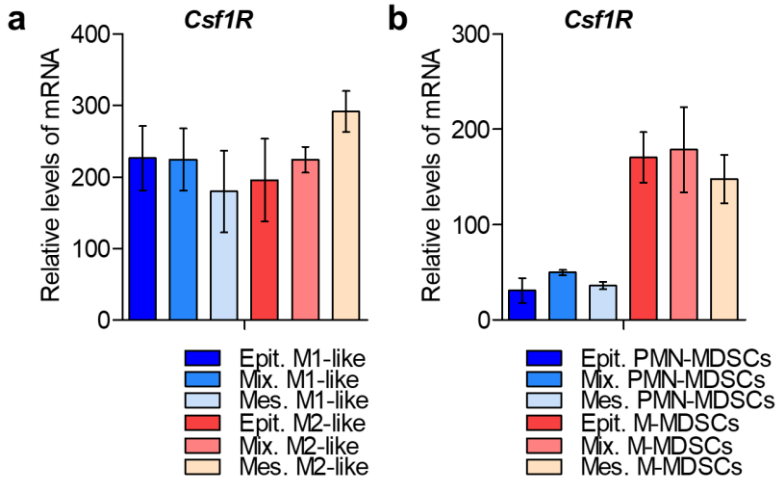

Figure 81. Csf1R expression in macrophages and MDSCs isolated from epithelial, mixed and mesenchymal SCCs. Gene expression levels of *Csf1R* (mean RNA levels relative to *Gapdh* mRNA ± SD) in (**a**) M1-like macrophages (F4-80$^+$/Gr1$^-$/CD206$^-$ cells) and M2-like macrophages (F4-80$^+$/Gr1$^-$/CD206$^+$ cells), or in (**b**) PMN-MDSCs (CD11b$^+$/Ly6C$^+$/Ly6G$^+$ cells) and M-MDSCs (CD11b$^+$/Ly6C$^+$/Ly6G$^-$ cells) isolated from epithelial, mixed and mesenchymal SCCs (n=3) by FACS-sorting, as quantified by qRT-PCR.

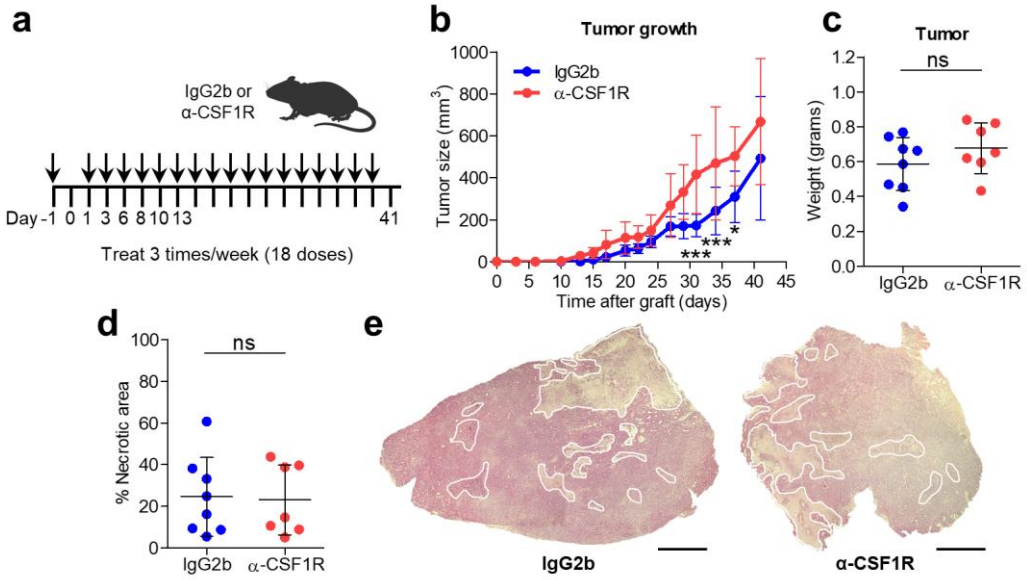

Figure 82. Anti-CSF1R treatment does not attenuate the growth of mixed SCCs. a. Experimental scheme for the treatment of mixed tumors, growing in immunocompetent syngeneic mice, with mouse IgG2b isotype control or anti-CSF1R antibodies. All treatments started on day -1, and then mice were administered intraperitoneally 3 days per week with 250 µg/dose (CSF1R) or 200 µg/dose (IgG2b) until experimental endpoint (18 doses). **b.** Growth kinetics of IgG2b control and anti-CSF1R-treated tumors (n=8). **c.** Weight of tumor in the indicated groups. **d.** Percentage of necrotic areas relative to total tumor area in the indicated groups (n=7). **e**. Representative hematoxylin/eosin (H/E) section of a mixed tumor treated with IgG2b control or anti-CSF1R antibodies, where necrotic areas are marked with white lines. Scale bar: 100 µm. Each symbol represents a single tumor and mean ± SD for each group is shown. (**b**) Repeated Measures ANOVA test, (**c**, **d**) unpaired two-tailed Student's *t*-test; ns $p>0.05$, *$p\leq0.05$, ***$p\leq0.001$.

To study the impact of preventing macrophage and M-MDSC recruitment in the acquisition of cancer-cell plasticity, mice bearing mixed SCCs were treated the day before the engraftment of epithelial EpCAM$^+$ cancer cells, and then three times per week during 41 days (18 doses) with IgG2b isotype control or anti-CSF1R antibodies (Figure 82a). Our analysis did not show any significant differences in mixed tumor growth at the end of the treatment (day 41, Figure 82b), which correlated with no changes in tumor weight (Figure 82c). Furthermore, the percentage of necrotic areas relative to total tumor area was similar in IgG2b and anti-CSF1R-treated tumors (Figures 82d and 82e; in collaboration with Adrià Archilla, PhD student), indicating that anti-CSF1R treatment did not affect the viability of mixed SCC cancer cells. These results were supported by the fact that no changes were detected in the total frequency of cancer cells (GFP$^+$/CD45$^-$ cells), fibroblasts (GFP$^-$/CD45$^-$ cells) and CD45$^+$ leukocytes between IgG2b control and anti-CSF1R-treated tumors (Figures 83a to 83c).

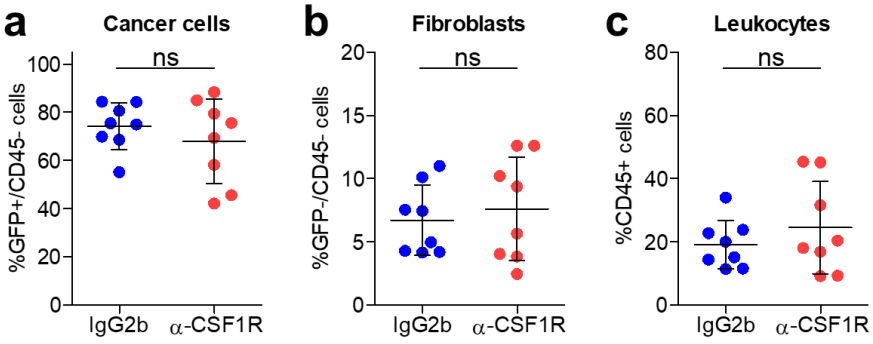

Figure 83. Tumor cell components do not change in mixed SCCs after anti-CSF1R treatment. Percentage of (**a**) cancer cells (GFP$^+$/CD45$^-$ cells), (**b**) fibroblasts (GFP$^-$/CD45$^-$ cells), and (**c**) leukocytes (CD45$^+$ cells) in IgG2b control and anti-CSF1R-treated tumors (n=8), as determined by flow cytometry. Each symbol represents a single tumor and mean ± SD for each group is shown. (**a-c**) Unpaired two-tailed Student's *t*-test; ns p>0.05.

Next, to evaluate the efficacy of the treatment, we studied whether there were changes within the different myeloid cell populations. FACS analysis showed no significant changes in the total frequency of myeloid cells (CD45$^+$/CD11b$^+$/CD3$^-$ cells) after anti-CSF1R treatment (Figure 84a). However, we observed a lower recruitment of macrophages (CD11b$^+$/F4-80$^+$/Gr1$^-$ cells, Figure 84b) and no changes in the percentage of MDSCs (CD11b$^+$/Gr1$^+$ cells, Figure 84c) after anti-CSF1R treatment. Furthermore, anti-CSF1R-treated tumors presented a higher infiltration of M1-like macrophages (CD11b$^+$/F4-80$^+$/Gr1$^-$/CD206$^-$ cells) and a lower percentage of M2-like macrophages (CD11b$^+$/F4-80$^+$/Gr1$^-$/CD206$^+$ cells) than IgG2b control tumors (Figures 84d and 84e), suggesting that anti-CSF1R treatment might block the recruitment of M2-like macrophages to the tumor core. This change in the polarization phenotype of macrophages was also corroborated by the reduced frequency of PD-L1$^+$ macrophages observed in anti-CSF1R-treated tumors (Figure 84f). In addition, whereas no changes in PMN-MDSCs (CD11b$^+$/Ly6C$^+$/Ly6G$^+$ cells) were detected, a reduction of

M-MDSCs ($CD11b^+/Ly6C^+/Ly6G^-$ cells) was observed in anti-CSF1R-treated tumors as compared to IgG2b control tumors (Figures 84g and 84h). Taken together, these results indicate that anti-CSF1R treatment mostly affected the recruitment of M2-like macrophages and M-MDSCs to the tumor core of mixed SCCs.

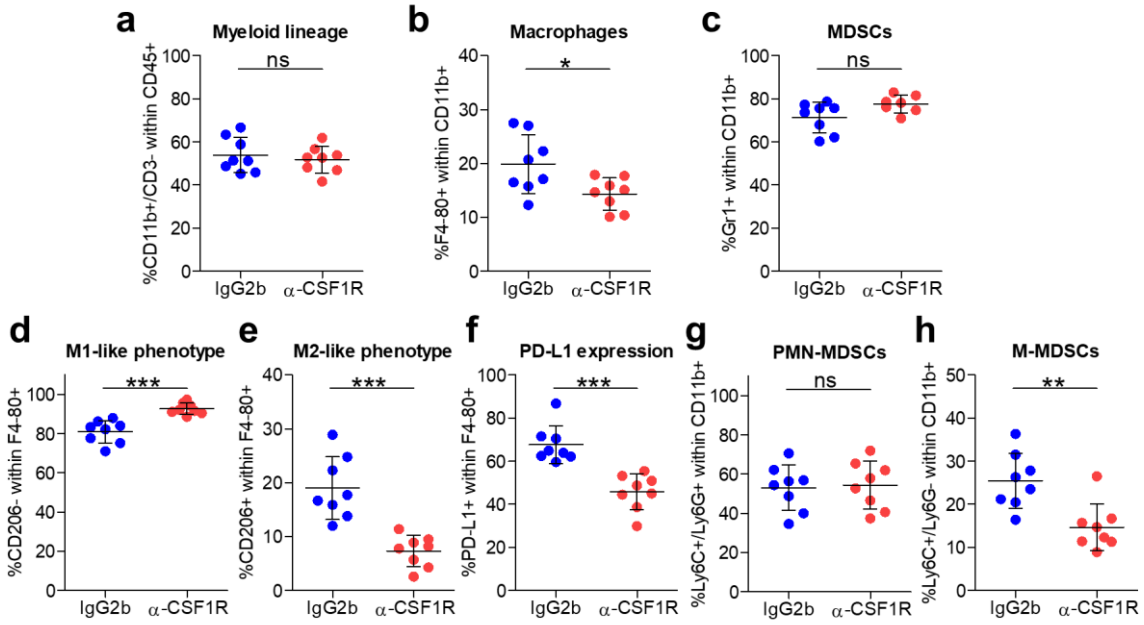

Figure 84. Anti-CSF1R treatment decreased the frequency of tumor-infiltrating M2-like macrophages and M-MDSCs. Percentage of (**a**) myeloid cells ($CD45^+/CD11b^+/CD3^-$ cells), (**b**) macrophages ($CD11b^+/F4\text{-}80^+/Gr1^-$ cells), (**c**) MDSCs ($CD11b^+/Gr1^+$ cells), (**d**) M1-like macrophages ($CD11b^+/F4\text{-}80^+/Gr1^-/CD206^-$ cells), (**e**) M2-like macrophages ($CD11b^+/F4\text{-}80^+/Gr1^-/CD206^+$ cells), (**f**) PD-$L1^+$ cells within $F4/80^+$ macrophages, (**g**) PMN-MDSCs ($CD11b^+/Ly6C^+/Ly6G^+$ cells) and (**h**) M-MDSCs ($CD11b^+/Ly6C^+/Ly6G^-$ cells) in IgG2b control and anti-CSF1R-treated tumors (n=8), as determined by flow cytometry. Each symbol represents a single tumor and mean ± SD for each group is shown. (**a-h**) Unpaired two-tailed Student's *t*-test; ns $p>0.05$, *$p\leq0.05$, **$p\leq0.01$, ***$p\leq0.001$.

To corroborate these observations, we performed immunofluorescence and immunohistochemistry assays with anti-CD68 (M1-like and M2-like macrophages), anti-CD163 (M2-like macrophages), and anti-Gr1 (PMN-MDSCs and M-MDSCs) antibodies in IgG2b control and anti-CSF1R-treated tumors (Figures 85a, 85d and 85g). In accordance with FACS results (Figure 84b), we observed a decrease of $CD68^+$ macrophages per tumor area in anti-CSF1R-treated tumors as compared to IgG2b control tumors (Figures 85a and 85b). In addition, we observed a decrease of $CD163^+$ M2-like macrophages (Figures 85d and 85e) and no changes of $Gr1^+$ MDSCs (Figures 85g and 85h) per tumor area in anti-CSF1R-treated tumors, and these immune populations did not change their tumor location after the treatment (Figures 85c, 85f and 85i). These results suggest that the decrease of $CD68^+$ macrophages in anti-CSF1R-treated tumors may be mainly due to a diminished pro-tumorigenic M2-like macrophage population, as already indicated by FACS data (Figure 84e).

Altogether, these results indicate that anti-CSF1R treatment leads to a TME characterized by a high infiltration of anti-tumorigenic M1-like macrophages and less infiltration of M2-like macrophages and M-MDSCs. This situation might generate a less immunosuppressive TME that could positively influence the immunotherapy response of mixed SCCs.

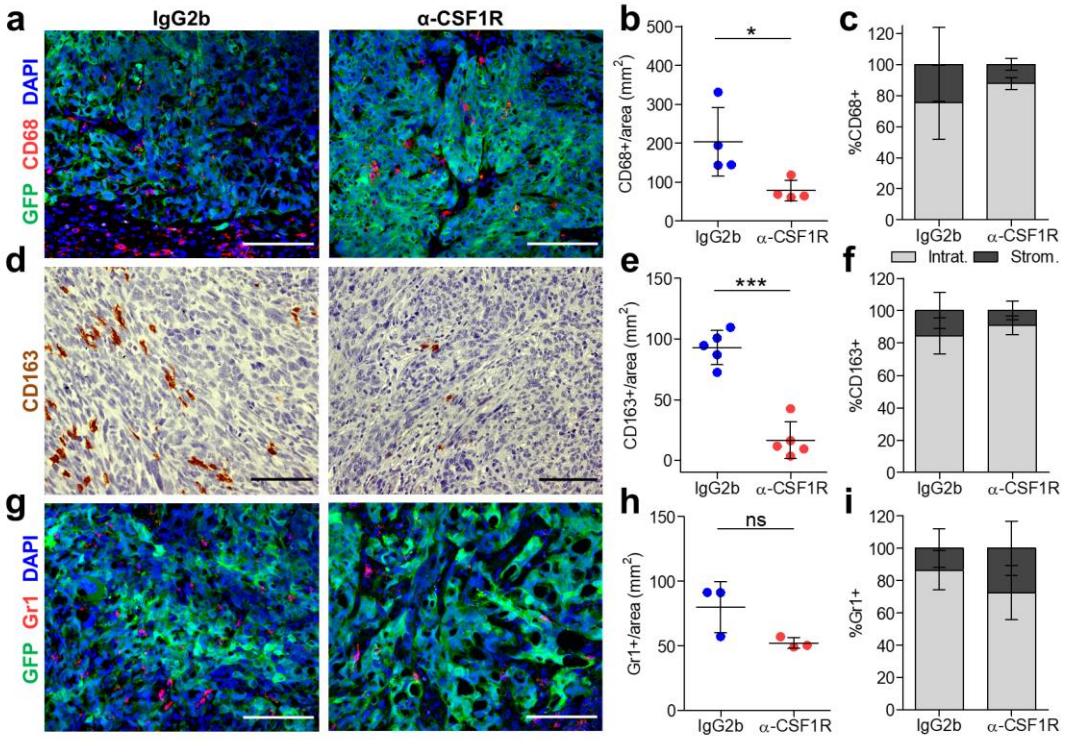

Figure 85. Anti-CSF1R treatment reduces the infiltration of CD68$^+$ macrophages and CD163$^+$ M2-like macrophages in mixed SCCs. (**a**, **g**) Representative immunofluorescence images of GFP$^+$ cancer cells, (**a**) CD68$^+$ or (**g**) Gr1$^+$ cells and DAPI labelled cell nuclei in IgG2b control and anti-CSF1R-treated tumors. Scale bar: 100 µm. **d.** Representative immunohistochemistry images of CD163$^+$ cells in IgG2b control and anti-CSF1R-treated tumors. Scale bar: 100 µm. Quantification of (**b**) CD68$^+$, (**e**) CD163$^+$, and (**h**) Gr1$^+$ cells per tumor area (mm^2) in IgG2b control and anti-CSF1R-treated tumors (n≥3). At least 10 fields of different regions were quantified in each tumor. Each symbol represents a single tumor and mean ± SD for each group is shown. Percentage (mean ± SD) of intratumoral or stromal (**c**) CD68$^+$, (**f**) CD163$^+$, and (**i**) Gr1$^+$ cells in the indicated tumors. (**b, e, h**) Unpaired two-tailed Student's *t*-test; ns p>0.05, *p≤0.05, ***p≤0.001.

6.4- Anti-CSF1R treatment does not block cancer-cell progression toward the mesenchymal state and does not enhance anti-tumor CTL responses

Subsequently, we wanted to evaluate the impact of the recruitment inhibition of M2-like macrophages and M-MDSCs on the acquisition of cancer-cell plasticity and the progression toward the mesenchymal phenotype, as well as on the anti-tumor responses of CTLs. To address the first objective, we quantified the percentage of epithelial EpCAM$^+$ and mesenchymal-like EpCAM$^-$ cancer cells at the end of the treatments by FACS analysis. No differences in the frequency of these cancer-cell populations were detected after anti-CSF1R treatment (Figures 86a and 86b).

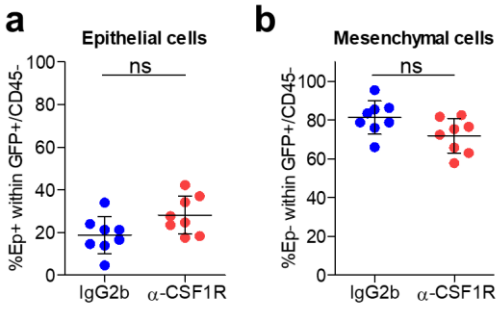

Figure 86. Anti-CSF1R treatment does not block cancer-cell progression toward the mesenchymal state. Percentage of (**a**) epithelial ($GFP^+/CD45^-/EpCAM^+$ cancer cells) and (**b**) mesenchymal ($GFP^+/CD45^-/EpCAM^-$ cancer cells) cancer cells in IgG2b control and anti-CSF1R-treated tumors (n=8), as determined by flow cytometry. Each symbol represents a single tumor and mean ± SD for each group is shown. (**a-b**) Unpaired two-tailed Student's *t*-test; ns p>0.05.

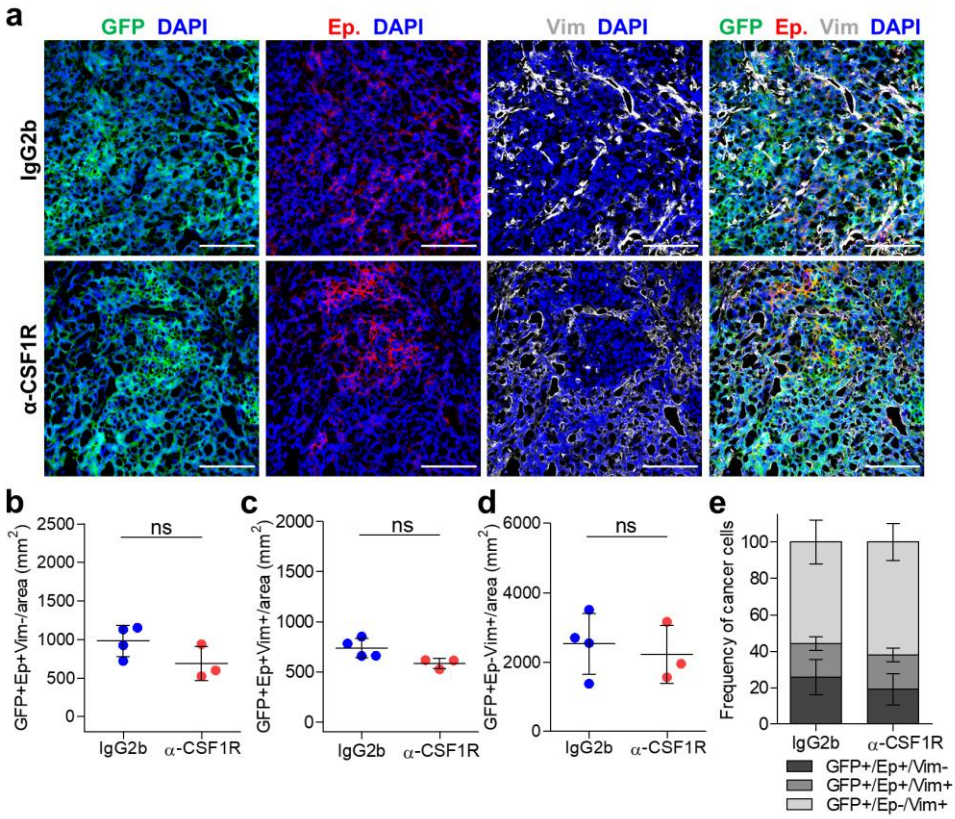

Figure 87. Anti-CSF1R treatment does not block cancer-cell progression toward the mesenchymal state. **a**. Representative immunofluorescence images of GFP^+, $EpCAM^+$, $Vimentin^+$ cancer cells and DAPI labelled cell nuclei in IgG2b control and anti-CSF1R-treated tumors. Scale bar: 100 µm. Quantification of (**b**) epithelial $GFP^+/EpCAM^+/Vimentin^-$, (**c**) hybrid $GFP^+/EpCAM^+/Vimentin^+$, and (**d**) mesenchymal $GFP^+/EpCAM^-/Vimentin^+$ cancer cells per tumor area (mm^2) in IgG2b control (n=4) and anti-CSF1R-treated (n=3) tumors. At least 10 fields of different regions were quantified in each tumor. Each symbol represents a single tumor and mean ± SD for each group is shown. **e**. Percentage (mean ± SD) of $GFP^+/EpCAM^+/Vimentin^-$, $GFP^+/EpCAM^+/Vimentin^+$, and $GFP^+/EpCAM^-/Vimentin^+$ cancer cells relative to total cancer cells in the indicated tumors. (**b-d**) Unpaired two-tailed Student's *t*-test; ns p>0.05.

Given that only the loss of the epithelial marker EpCAM was assessed to evaluate the acquisition of cancer-cell plasticity, we then completed these studies by immunofluorescence assays (Figure 87a). To do that, we determined the presence of epithelial GFP$^+$/EpCAM$^+$/Vimentin$^-$, hybrid GFP$^+$/EpCAM$^+$/Vimentin$^+$ and mesenchymal GFP$^+$/EpCAM$^-$/Vimentin$^+$ cancer cells in IgG2b control and anti-CSF1R-treated tumors (Figures 87a to 87e). We observed that the frequency of epithelial GFP$^+$/EpCAM$^+$/Vimentin$^-$ cancer cells, hybrid GFP$^+$/EpCAM$^+$/Vimentin$^+$ cancer cells, and mesenchymal GFP$^+$/EpCAM$^-$/Vimentin$^+$ cancer cells per tumor area did not change in anti-CSF1R-treated tumors compared to IgG2b control tumors (Figures 87a to 87e). Taken together, these results indicate that the depletion of M2-like macrophages and M-MDSCs does not block cancer-cell progression toward the mesenchymal state. Therefore, this suggests that cytokines and growth factors derived from these immune populations may not directly promote cancer-cell plasticity, the acquisition of mesenchymal traits and SCC progression.

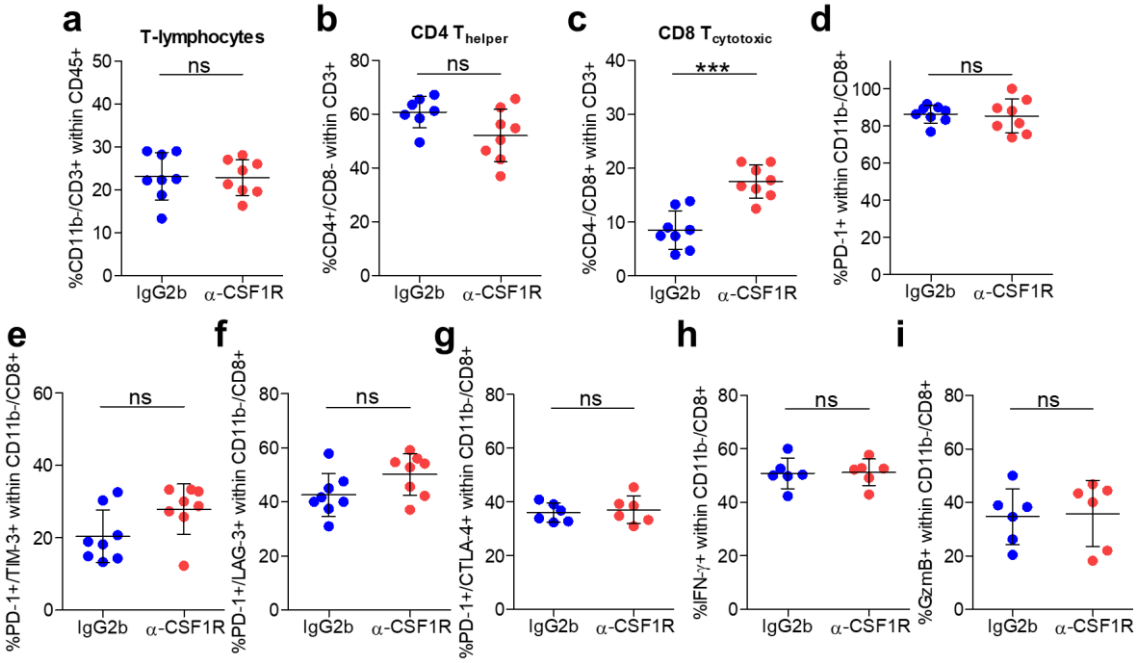

Figure 88. Anti-CSF1R treatment leads to a higher infiltration of CD8$^+$ T lymphocytes, but without changing their exhausted status. Percentage of (**a**) CD3$^+$ T lymphocytes (CD45$^+$/CD11b$^-$/CD3$^+$ cells), (**b**) CD4$^+$ T lymphocytes (CD3$^+$/CD4$^+$/CD8$^-$ cells), and (**c**) CD8$^+$ T lymphocytes (CD3$^+$/CD4$^-$/CD8$^+$ cells) in IgG2b control and anti-CSF1R-treated tumors (n=8), as determined by flow cytometry. Percentage of (**d**) PD-1$^+$, (**e**) PD-1$^+$/TIM-3$^+$, (**f**) PD-1$^+$/LAG-3$^+$, (**g**) PD-1$^+$/CTLA-4$^+$, (**h**) IFN-γ$^+$ and (**i**) GzmB$^+$ cells within CD11b$^-$/CD8$^+$ T lymphocyte population in the indicated groups (n≥6). Each symbol represents a single tumor and mean ± SD for each group is shown. (**a-i**) Unpaired two-tailed Student's *t*-test; ns p>0.05, ***p≤0.001.

To address whether anti-CSF1R treatment enhanced the anti-tumor responses of CTLs, we analyzed the presence of CD3$^+$ T lymphocytes (CD45$^+$/CD11b$^-$/CD3$^+$ cells), CD4$^+$ T lymphocytes (CD3$^+$/CD4$^+$/CD8$^-$ cells), and CD8$^+$ T lymphocytes (CD3$^+$/CD4$^-$/CD8$^+$ cells) in IgG2b control and anti-CSF1R-treated tumors by FACS assays. We observed no changes in the total frequency of

tumor-infiltrating CD3$^+$ T lymphocytes after anti-CSF1R treatment (Figure 88a). However, among the lymphoid cell populations, we observed no changes in CD4$^+$ T lymphocytes and a higher frequency of CD8$^+$ T lymphocytes after anti-CSF1R treatment (Figures 88b and 88c). In addition, we investigated the activation status of CTLs to evaluate whether there was a boost of anti-tumor responses after anti-CSF1R treatment. To this end, we evaluated by flow cytometry assays the expression of the IC inhibitory receptors PD-1, TIM-3, LAG-3, and CTLA-4, as well as IFN-γ and GzmB, within T lymphocytes. We observed that the percentage of PD-1$^+$ cells within CD11b$^-$/CD8$^+$ T lymphocytes did not change in anti-CSF1R-treated mixed tumors compared to IgG2b control tumors (Figure 88d). In addition, the percentage of PD-1$^+$/TIM-3$^+$, PD-1$^+$/LAG-3$^+$, PD-1$^+$/CTLA-4$^+$, IFN-γ$^+$ and Gzmb$^+$ T cells did not change in anti-CSF1R-treated tumors as compared to their respective IgG2b control tumors (Figures 88e and 88i). This data indicates that anti-CSF1R treatment does not change the exhausted status of CD8$^+$ T cells in mixed SCCs. In addition, we will evaluate in future experiments whether there could be a reactivation of NK cells after anti-CSF1R treatment.

Finally, we performed immunohistochemistry assays of CD8 (T cytotoxic lymphocytes) and FoxP3 (Treg cells) markers in IgG2b control and anti-CSF1R-treated tumors (Figures 89a and 89d). In these assays, an increase in the frequency of CD8$^+$ cells per tumor area was detected (Figures 89a and 89b), and no changes in the frequency of immunosuppressive FoxP3$^+$ Treg cells per tumor area were observed after anti-CSF1R treatment (Figures 89d and 89e). In addition, these immune populations did not change their spatial location after anti-CSF1R treatment (Figures 89c and 89f). These results indicate that anti-CSF1R treatment does not lead to a reduction of immunosuppressive Treg cells.

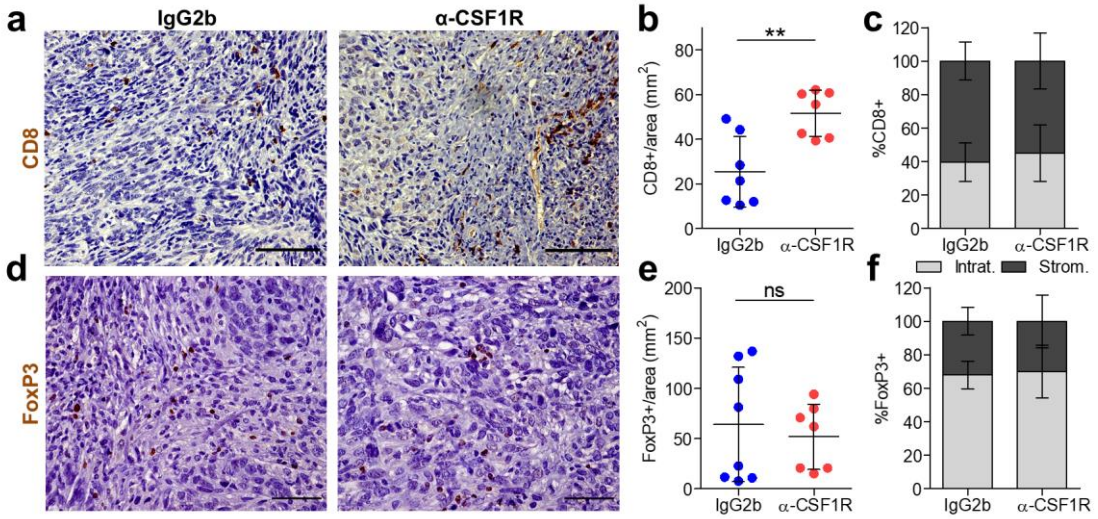

Figure 89. Anti-CSF1R treatment increases the frequency of CD8$^+$ T lymphocytes and does not change the frequency of FoxP3$^+$ Treg cells infiltrating mixed SCCs. Representative immunohistochemistry images of (**a**) CD8$^+$ and (**d**) FoxP3$^+$ immune cells in IgG2b control and anti-CSF1R-treated tumors. Scale bar: 100

μm. Quantification of (**b**) $CD8^+$ and (**e**) $FoxP3^+$ cells per tumor area (mm^2) in IgG2b control and anti-CSF1R-treated tumors ($n \geq 7$). At least 14 fields of different regions were quantified in each tumor. Each symbol represents a single tumor and mean ± SD for each group is shown. Percentage (mean ± SD) of intratumoral or stromal (**c**) $CD8^+$ and (**f**) $FoxP3^+$ cells in the indicated tumors. (**b, e**) Unpaired two-tailed Student's *t*-test; ns $p>0.05$, $^{**}p \leq 0.01$.

Summary Chapter 6: Targeting MDSCs and macrophages reduces the immunosuppressive tumor microenvironment and could boost anti-tumor immune responses

In Chapter 6, we demonstrate that anti-Gr1 treatment induces a partial depletion of PMN-MDSCs and a decreased infiltration of M2-like macrophages into the tumor core. At the same time, a reduction of hybrid and mesenchymal cancer cells is observed after anti-Gr1 treatment, suggesting that PMN-MDSCs could promote, together with other mechanisms, the acquisition of plasticity and the progression toward a mesenchymal state. Other possible scenario to explain the reduction of the mesenchymal component after anti-Gr1 treatment could be that this event is induced by an increase of tumor-infiltrating NK cells, which could more efficiently eliminate hybrid and mesenchymal cancer cells, although these experiments remain to be performed. In addition, as MDSCs are one of the immunosuppressive immune cells that abrogate T-cell activity, targeting this population led to a reactivation of CTL activity in mixed SCCs. On the other hand, anti-CSF1R treatment does not reduced mixed tumor growth, although it leads to a reduction of M2-like macrophages and M-MDSCs, which could favor the generation of a less immunosuppressive TME. The depletion of M2-like macrophages and M-MDSCs leads to an increased infiltration of $CD8^+$ T cells, although these cells did not change their activation status after the treatment, and does not block cancer-cell progression toward the mesenchymal state.

DISCUSSION

Despite most cases of skin SCCs are early detected and successfully eliminated by surgical excision, a considerable percentage of patients suffer recurrences, which frequently present an aggressive growth and enhanced metastasis prone. No prognostic markers are currently available to predict clinical outcomes, and advanced and metastatic SCCs, until recently, were commonly treated with radiotherapy and/or chemotherapy with poor clinical benefits (Franco et al., 2013b). In addition, it has been suggested that cSCCs could effectively respond to immunotherapy, as the disease risk is strongly associated with immunosuppression (Chalmers et al., 2017; Pickering et al., 2014) and cSCCs contain a high TMB that might lead to an increased neoantigen expression (Le et al., 2017; McGranahan et al., 2016; Rizvi et al., 2015). In this sense, two immunotherapies based on the PD-1 inhibition (cemiplimab and pembrolizumab) were approved by the FDA for the treatment of advanced or metastatic SCCs (Grob et al., 2020; Migden et al., 2018). Despite some patients present good responses, around 50% of patients do not respond (primary resistance) or develop resistance to therapy after an initial response (acquired resistance), which emphasizes the need for a better characterization of the TME (Keenan et al., 2019). It was proposed to combine different IC inhibitors to increase the response to these therapies. However, treated patients frequently suffer from immune-related adverse events (irAEs) given the physiological role of ICs regulating effector immunity (Pauken et al., 2019) and combined therapies further increase the irAEs (Dougan et al., 2021). Therefore, it is important to identify the mechanisms that promote tumor growth, metastasis development and therapy resistance, in order to design more efficient targeted therapies to increase the cSCC patient outcome without increasing irAEs. Following this line, we decided to identify the impact of cancer-cell plasticity, understood as the intratumoral heterogeneity observed within cSCCs, on the composition of the TME and on the response to immunotherapy, as limited information is available about these aspects in mouse and patient skin SCCs.

Cancer-cell features change during mouse and patient SCC progression

Previous studies from our laboratory demonstrated that during the progression from WD-SCCs that exhibit epithelial differentiation traits to mesenchymal-like PD/S-SCCs through the generation of intermediate states (MD/PD-SCCs), the CSC population was expanded and the EMT program was strongly induced, in accordance with the aggressive growth and the enhanced metastasis associated with advanced tumors (Lapouge et al., 2012; Silva-Diz et al., 2016). In fact, in our SCC mouse model, the progressive induction of the EMT program was also associated with the acquisition of cancer-cell plasticity, as previously described in other studies (Jolly et al., 2016; Pastushenko et al., 2018; Shibue and Weinberg, 2017). During this Thesis, we have demonstrated that at intermediate stages of SCC progression, epithelial $EpCAM^{+}$ cancer cells are a heterogeneous population that show different degrees of plasticity, which was evaluated by their capacity to switch toward the mesenchymal-like phenotype under *in vitro* and *in vivo* conditions. We detected the presence of two epithelial-like cancer cells in MD/PD-SCCs ($EpCAM^{high}$ and $EpCAM^{low}$ cancer cells), which present

a higher plasticity than full epithelial cancer cells from WD-SCCs. Surprisingly, whereas EpCAM^{high} cancer cells presented a moderate ability to generate mesenchymal-like EpCAM^{-} cancer cells and slightly induced the expression of mesenchymal genes, EpCAM^{low} cancer cells present a hybrid epithelial-mesenchymal phenotype and an enhanced capability to switch toward mesenchymal-like EpCAM^{-} cancer cells. By qRT-PCR assays, we have identified that this hybrid epithelial-mesenchymal SCC state is characterized by the expression of epithelial differentiation markers (*E-cadherin, EpCAM* and *K14*, among others) together with newly acquired mesenchymal ones (*Vimentin, Snail, Twist, Zeb1* and *Zeb2*). In addition, using co-immunofluorescence assays with an epithelial (EpCAM for mouse and E-cadherin for patient samples) and a mesenchymal (Vimentin) marker, we demonstrated that hybrid EpCAM^{+}/Vimentin^{+} or E-cadherin^{+}/Vimentin^{+} cancer cells can be frequently detected in mouse and patient cSCCs, and specifically increase in MD/PD-SCCs at intermediate stages of SCC progression. In this sense, Pastushenko et al. have revealed that multiple epithelial-mesenchymal cancer cell populations are identified in skin SCCs and mammary primary tumors based on the expression of K14 and Vimentin (Pastushenko et al., 2018), among other markers such as CD51, CD61 and CD106. In this study, they also demonstrated that cancer cells with a hybrid phenotype had a greater plasticity to generate mesenchymal cancer-cell phenotypes, were more efficient in reaching the circulation, colonizing and forming lung metastases (Pastushenko et al., 2018). In this sense, one of the most relevant aspects of our studies is that the presence of plastic/hybrid epithelial cancer cells, which are not histopathological detected by hematoxylin/eosin (H/E) assays by a pathologist, may be a risk factor of SCC progression and a key parameter in deciding which therapeutic strategy should be followed. In addition, these hybrid characteristics might provide cancer cells with an increased adaptability to respond to a variety of external cues and physiological stresses (Chaffer et al., 2016). These hybrid epithelial-mesenchymal cancer cells have been identified in other cancer types such as breast (Yu et al., 2013), ovarian (Strauss et al., 2009), HNSCC (Puram et al., 2017), pancreatic and prostate cancers (Rhim et al., 2012; Ruscetti et al., 2015), and its presence has been correlated with poor patient survival and resistance to chemotherapy and immunotherapies (Dongre and Weinberg, 2019; Grosse-Wilde et al., 2015; Smith and Bhowmick, 2016; Yamashita et al., 2018).

Given the clinical relevance of hybrid cancer cells, it was an unmet need to find new markers that more specifically identify cancer cell populations at different stages of SCC progression. In addition, it was necessary to unravel how cancer cells respond differently to external stimuli from the TME and vice versa, how changes in the cancer-cell features may impact on the TME and therefore, on therapy response. The first hypothesis was that this switch through the epithelial, hybrid and mesenchymal states may be produced through genetic and/or epigenetic changes in specific genes that control the EMT program and stemness in response to stromal factors during SCC progression. The second hypothesis was that this switch may be mediated by the crosstalk between tumor-

infiltrating immune cells and cancer cells, highlighting the need to study the impact of cancer-cell features on the recruitment of different immune populations and how this recruitment favors SCC progression and metastasis development.

Although the first hypothesis has not been extensively addressed in this Thesis, together with other members of the laboratory, we are currently evaluating the role of different signaling pathways identified from transcriptional and phosphoproteomic assays in the acquisition of cancer-cell plasticity by epithelial cancer cells. In this sense, we identified an induction of IGF-1R phosphorylation, among other kinases, in epithelial $EpCAM^+$ plastic cancer cells, which indicates that IGF-1R signaling pathway might be involved in the plasticity acquisition. This signaling pathway plays a key role in various aspects of cancer biology as transformation, cell growth and therapy resistance (Zha and Lackner, 2010), and IGF-1R activation is commonly upregulated in numerous tumor types. In fact, IGF-1R signaling is strongly associated with EMT program in hepatocellular and breast cancers (Rigiracciolo et al., 2020; Zhao et al., 2017). Despite different inhibitors of IGF-1R signaling have been developed, they showed a limited response in several clinical trials (Bruchim et al., 2014; Ekyalongo and Yee, 2017). Since IGF-1R inhibitors have not given very good clinical results, the studies of another member of the laboratory are currently addressed toward evaluating the role of IGF-1R signaling in the progression of epithelial SCC cells toward the mesenchymal state and their impact on the generation of immunosuppressive environments and in the response to ICB therapies. In this line, a recent study has demonstrated that the reduction of circulating insulin-like growth factor 1 (IGF-1) and a downregulation of IGF-1R signaling in cancer cells sensitize tumors to PD-1 blockade in preclinical models of NSCLC (Ajona et al., 2020). In addition, high levels of IGF-1 or high IGF-1R expression is associated with resistance to anti-PD-1/PD-L1 therapy (Ajona et al., 2020). We believe that it should be interesting to analyze whether hybrid/plastic cancer cells, characterized by the dual expression of epithelial and mesenchymal markers, also induces the expression of IGF-1R in primary cSCCs, among other markers, and if the presence of this population correlates with disease recurrence and poor prognosis or even with response to ICB therapy. Indeed, these studies are currently ongoing in our laboratory. Taken together, our studies suggest that targeting EMT and blocking the switch from epithelial to mesenchymal SCC states holds promise for overcoming resistance.

Our second hypothesis was that the changes in the cancer-cell features in cSCCs might impact the recruitment of different immune populations to favor SCC progression and metastasis development. The first evidence was that, by transcriptional assays, we observed that epithelial $EpCAM^+$ plastic cancer cells induce the expression of CXCL1, CXCL2, CXCL5, which may stimulate the recruitment of PMN-MDSCs (Gabrilovich et al., 2012; Kumar et al., 2016; Ostrand-Rosenberg, 2010). In contrast, the expression of CCL2, CCL5, Cyr61 and also of CCL7, CSF1 and GM-CSF was strongly induced in mesenchymal-like $EpCAM^-$ cancer cells, which may be associated with the

recruitment and polarization of M2-like macrophages and M-MDSCs, respectively, as previously reported in other tumor types (Fan et al., 2014). In addition, the comparison of the gene expression profile of tumor-infiltrating $CD45^+$ leukocytes isolated from WD-SCCs and MD/PD-SCCs showed significant changes in the TME signature during SCC progression. These preliminary results led to the development of the main objectives of this Thesis, which are focused on understanding how the presence and the functional state of different immune cell populations within the TME affect the development and progression of cSCCs, and how cancer cells are able to evade immune recognition and resist to some therapeutic strategies.

Immune landscape changes during mouse and patient SCC progression, concomitantly with the acquisition of cancer-cell plasticity and mesenchymal-like cell traits

The first interesting observation was that tumor-infiltrating $CD45^+$ leukocytes dramatically diminished during SCC progression, and that this reduction was not dependent of the expression of the E6/E7 viral oncoproteins on cancer cells (associated with our mouse model of SCC progression). We firstly identified that these changes could be originated by the different percentage of necrotic areas relative to total tumor area between epithelial, mixed and mesenchymal SCCs, as $CD45^+$ leukocytes were more recruited to these areas. Given the phagocytic activity of macrophages and neutrophils, it was expected to find them in the necrotic areas of the less aggressive epithelial and mixed SCCs, accomplishing their ongoing cleanup task by engulfing unwanted particles and dead cells (Brandau et al., 2013; Gabrilovich et al., 2012). These changes could also be mediated by the induction of a stronger pro-inflammatory response in epithelial and mixed tumors as compared to mesenchymal tumors. In our SCC model, we detected that these processes could be mediated by the expression of several pro-inflammatory cytokines such as IL-23A, TNF-α, IL-12b, IL18 and IL-1β by M1-like macrophages or IFN-γ, TNF-α and IL-2 by CTLs, which are well-defined cytokines that stimulate a proper pro-inflammatory immune response (DeNardo and Ruffell, 2019; Romagnani, 1997; Voskoboinik et al., 2015). Notably, it has been described that the immune infiltration density correlates with the expression of chemokines and other pro-inflammatory and pro-angiogenic molecules by cancer cells, suggesting that cancer cells attract and regulate the stromal cells that comprise their TME to support tumor growth, invasion and progression, and contribute directly to the spatial organization of cancer cell subpopulations (Lorenzo-Sanz and Muñoz, 2019; Pastushenko et al., 2018).

Our studies indicated that the immune landscape changes accordingly with the features of mouse and patient SCC cells, which was in line with several studies that have demonstrated that cancer-cell plasticity enhances the recruitment of immunosuppressive cells and reduces the response to ICB therapies (Binnewies et al., 2018; Kudo-Saito et al., 2009). Specifically, lung, breast and melanoma carcinomas whose cancer cells have predominantly mesenchymal features tend to be associated with

increased vascularity and immunosuppressive immune infiltrates, which leads to an impair cytotoxic function of CTLs and NK cells (Chockley and Keshamouni, 2016; Lou et al., 2016; Murciano-Goroff et al., 2020; Sharma et al., 2017; Thommen et al., 2015). In addition, tumors that are enriched for the EMT program, focal adhesion, ECM remodeling, angiogenesis, inflammation and hypoxia genes are also associated with the infiltration of immunosuppressive cells (Tamborero et al., 2018). This, in turn, may enable cancer cells to evade immune attack, rendering them resistant to the effect of IC blockade (Terry et al., 2017).

Surprisingly, we observed that the frequency of $CD8^+$ CTLs and NK cells in mouse SCCs and $CD8^+$ CTLs in patients SCCs was induced during SCC progression. These results were contradictory with the high cancer-cell viability and the aggressive growth of advanced mouse and patient SCCs. However, our results indicate that mesenchymal cancer cells could evade immunosurveillance through several common mechanisms in both mice and patient skin SCCs: (i) the action of infiltrating immunosuppressive cells such as M2-like macrophages, MDSCs and Treg cells; (ii) the activation of IC pathways that suppress cytotoxic immune responses, which involves the upregulation of IC receptors by CTLs and NK cells or the release of soluble factor or IC ligands by cancer cells, M2-like macrophages and DCs; or (iii) the downregulation of MHC molecules, thus becoming invisible to the recognition of T cells. Therefore, our results indicate that during mouse and patient skin SCC progression a switch from an anti-tumoral and pro-inflammatory to a pro-tumoral and immunosuppressive state is induced, which might favor the aggressive growth associated to advanced SCCs. These findings are in agreement with other studies that propose that TME can change in response to immune and cancer cell-derived signals to favor tumor growth and immune evasion, and negatively influence immunotherapy response (Quail and Joyce, 2013).

In this sense, our studies indicate that, during the dynamic process of SCC progression, the frequency of some immunosuppressive and pro-tumoral immune cells (M-MDSCs, Treg cells, $CD4^+$ Th2 cells, M2-like macrophages, and exhausted CTLs and NK cells) increased in the tumor core of mesenchymal SCCs, whereas immune cells associated with anti-tumoral activities such as M1-like macrophages, $CD4^+$ Th1 cells, active CTLs and NK cells, and neutrophils (TANs) were more abundant in epithelial SCCs. Indeed, these immunosuppressive cells could be involved in the acquisition or maintenance of the hybrid and mesenchymal state, but also in promoting the acquisition of the EMT program during SCC progression. The importance of our studies lies in the fact that our SCC model is able to progress from epithelial to mesenchymal stages, which allow us to identify dynamic changes in the composition of the TME as a consequence of the characteristics of the cancer cells within the tumor. This makes our studies stand out, as other works have focused solely on whether tumors formed from epithelial and mesenchymal cancer cell lines were differentially susceptible to immune attack. In this sense, Dongre et al. showed that epithelial or $Snail^{low}$ breast tumors contain active cytotoxic $CD8^+$ T cells, antitumoral M1-like macrophages, and

were sensitive to anti-CTLA-4 therapy. In contrast, mesenchymal or Snail^{high} breast tumors expressed low levels of MHC-I, contained Treg cells, M2-like macrophages, exhausted CD8$^+$ T cells, and were resistance to anti-CTLA-4 therapy (Dongre et al., 2017). The same authors have recently demonstrated that the abrogation of the mesenchymal cell-derived factors CD73, CSF1, or SPP1 prevents the generation of an immunosuppressive TME, specifically by decreasing the presence of M2-like macrophages and mobilizing functionally active T cells and DCs into the tumor core (Dongre et al., 2020). This situation sensitizes refractory mesenchymal tumors partially to anti-CTLA-4 therapy (Dongre et al., 2020). Likewise, melanomas that are resistant to anti-PD-1 treatment display a transcriptional signature reminiscent of EMT-related processes, including the downregulation of E-cadherin and the concomitant upregulation of factors involved in ECM remodeling, angiogenesis, and immunosuppression (Hugo et al., 2016). These observations suggest that the mesenchymal and the immunosuppressive phenotype might be associated with innate anti-PD-1 resistance. Recently, Cerezo-Wallis et al. have demonstrated that the cancer-cell secreted-growth factor midkine (MDK) rewires the molecular profile of melanoma cells to promote an immunosuppressive state. In the absence of MDK, this immunosuppressive state shifts to a pro-inflammatory IFN response, characterized by the presence of M1-like macrophages and cytotoxic CD8$^+$ T cells (Cerezo-Wallis et al., 2020). Finally, an increased T-cell exhaustion and Treg cell accumulation have been observed in mammary, pulmonary and pancreatic carcinomas (Bartoschek et al., 2018). Taken together, we hypothesized that factors derived from hybrid/plastic and mesenchymal SCC cells could drive the recruitment, differentiation and polarity of several immune populations such as macrophages, MDSCs and Treg cells, which in turn could promote the plasticity and progression of epithelial cancer cells to a mesenchymal state by a complex cytokine-mediated cross-talk. For that reason, other lines of research in the laboratory are currently focused on identifying cancer cell-derived cytokines involved in the recruitment of immunosuppressive cells by transcriptional and proteomic assays in order to increase the response to ICB therapy. Some cytokines that have been identified in our laboratory and in other studies associated with the mesenchymal SCC phenotype are Ccl2, Ccl7, Cxcl12, Csf1, Ccl11, Cxcl9, Cxcl10, IL6, Vegfc, Fgf1, Fgf2, Hgf, Angpt1, Thbs4 (Bernat-Peguera et al., 2019, 2021; Pastushenko et al., 2018), which will be evaluated if they are related to the recruitment of immunosuppressive cells in our mesenchymal-like SCC mouse models.

As it was not only important to assess the frequency of these immune populations within the tumors, but also their immunosuppressive and pro-tumoral activities, we characterized these populations by flow cytometry, qRT-PCR and immunohistochemistry assays. We observed that macrophages from WD-SCCs express MHC-II, which is required for the presentation of tumor-specific antigens, express some pro-inflammatory cytokines (*Il23a*, *Tnf-α*, *Il12b*, *Il18*, *Il1β*) and the Th1 cell-attracting chemokines *Cxcl9* and *Cxcl10*, which drive the polarization and recruitment of CD4$^+$ Th1 cells

(Griffith et al., 2014), as compared to macrophages isolated from PD/S-SCCs. Interestingly, macrophages isolated from PD/S-SCCs upregulate the expression of *Ccl2*, which could be involved in the high recruitment of M2-like macrophages and M-MDSCs to the mesenchymal tumor core, as previously described (Murray and Wynn, 2011; Qian et al., 2011), upregulate the expression of *Ccl22*, which could be involved in the recruitment of $CD4^+$ Th2 and Treg cells through its binding to CCR3 and CCR4 receptors (Röhrle et al., 2020b), and also induce the expression of IL-6. It has been described that IL-6 secretion promotes tumor growth and immunosuppression in the TME of various cancer types (Chanmee et al., 2014), and fosters the recruitment of MDSCs (Marvel and Gabrilovich, 2015), stimulating their inhibitory activity toward cytotoxic T cells (Groth et al., 2019). In addition, TAM-derived IL-6 induces STAT3-mediated expression of SC-related genes in breast, liver and pancreatic cancer cells (Yang et al., 2013; Wan et al., 2014; Yin et al., 2017). In addition, macrophages and M-MDSCs from PD/S-SCCs showed a stronger immunosuppressive signature compared to those isolated from WD-SCCs, which was characterized by an increased expression of immunosuppressive cytokines such as TGF-β, IL-10, iNOS, ARG1, VEGFA, and IC ligands such as PD-L1, Galectin 9, CD80, CD86 and CD155. This immunosuppressive signature of macrophages and M-MDSCs in PD/S-SCCs could explain the inhibition of T and NK-cell cytotoxic functions in these tumors. In addition, the macrophages of PD/S-SCCs induce the expression of CD47 compared to epithelial and mixed tumors. CD47 activation in immune cells has been linked to tumor immune evasion, decreased antigen-presentation, and impaired effector functions of NK and T cells (Veillette and Chen, 2018). Furthermore, CD47 also serves as an anti-phagocytic signal for macrophages upon binding to SIRPα (van den Berg and Valerius, 2019). These results indicate that a high activation of CD47 could be blocking macrophage-mediated phagocytosis and interfere the priming of CTLs against tumor antigens, as previously described (Liu et al., 2015; Veillette and Chen, 2018). Taken together, these results indicate that macrophages isolated from WD-SCCs have pro-inflammatory and tumoricidal functions, being classified as M1-like macrophages, whereas macrophages from PD/S-SCCs showed an immunosuppressive phenotype that could subvert anti-tumor immunity in mesenchymal tumors, and they were classed as M2-like macrophages.

In addition, our results indicate that MDSCs were the most frequent tumor-infiltrating myeloid cell, independently of the epithelial or mesenchymal features of the tumors. Given that MDSCs are a heterogeneous population of immature myeloid cells than can promote tumor growth by suppressing T- and NK-cell activity (Law et al., 2020), this was not consistent with the high presence of this population in epithelial and mixed SCCs. This data suggests that within the $Gr1^+$ MDSCs (PMN-MDSCs) detected in epithelial and mixed SCCs we might be considering tumor-associated neutrophils (TANs), which are phenotypically similar to PMN-MDSCs and their anti-tumoral or pro-tumoral activity is modulated by distinct TME signals (Brandau et al., 2013; Mantovani et al., 2011; Shaul and Fridlender, 2019). In this sense, we hypothesized that TANs in epithelial and mixed

tumors may have mostly anti-tumoral activity, as previously reported in colorectal cancer (Droeser et al., 2013; Sconocchia et al., 2011). Since the immunosuppressive activity of TANs could be in fact attributed to PMN-MDSCs (Brandau et al., 2013), we hypothesized that mesenchymal tumors might recruit mainly immunosuppressive PMN-MDSCs, which could interfere with the cytotoxic activity of T and NK cells, as well as play an essential role in tumor development and progression, as previously described (Condamine et al., 2015; Umansky et al., 2016). In contrast, epithelial tumors might recruit mostly anti-tumoral TANs. To corroborate whether these immune cells are either neutrophils or PMN-MDSCs, it has been widely established that we should evaluate their immunosuppressive ability to suppress other immune cells during SCC progression (Veglia et al., 2021). In this sense, we plan to evaluate in future experiments the expression level of some surface markers that have been reported between neutrophils and PMN-MDSCs, such as CD155, CD244 (Youn et al., 2012), and LOX-1 (Condamine et al., 2016), among others markers, as well as the *in vitro* capability of PMN-MDSCs and M-MDSCs isolated from epithelial, mixed and mesenchymal tumors to block the proliferation and activity of $CD8^+$ T and NK cells.

Given the increased frequency of $CD8^+$ CTLs in the blood and within the tumor core of mesenchymal SCCs, we hypothesized that the enrichment of cancer-effector T cells might occur in the lymph nodes and also within the tumor, as other studies have postulated (Joyce and Fearon, 2015) . Findings in preclinical models have suggested that the TME may be the major site of clonal expansion of T cells (Thompson et al., 2010) and that the $CD8^+$ T-cell replicative response within the tumor is orchestrated by the $CD103^+$ DCs, which can efficiently cross-present cancer-cell antigens (Broz et al., 2014). In line with these studies, we detected that tumor-infiltrating DCs increase during SCC progression. However, given the strong viability and aggressiveness of mesenchymal cancer cells, that prompted us to analyze whether T and NK cells were in an exhausted or inactive state. It has been recently described that the expression of the co-inhibitory receptor PD-1 is insufficient to define cell exhaustion, as it appears to coexist with a continuum of functional states, including states with at least some effector activity (Azizi et al., 2018; Li et al., 2019; Sade-Feldman et al., 2018). In addition, it has been reported that a high and sustained co-expression of IC inhibitory receptors is a hallmark of exhausted T and NK cells (Blackburn et al., 2009). These co-expression patterns are important, as the simultaneous blockade of multiple IC receptors results in a synergistic reversal of T and NK-cell exhaustion (Melero et al., 2015). We observed an increased expression of $PD\text{-}1^+/LAG\text{-}3^+$, $PD\text{-}1^+/TIM\text{-}3^+$ and $PD\text{-}1^+/TIGIT^+$ CTLs and NK cells in mouse mesenchymal SCCs, as well as a decreased expression of IFN-γ and GzmB, suggesting that they remained in an exhausted state. Interestingly, the expression of the activating receptor DNAM-1 was significantly induced in mesenchymal tumors. It has been described that the regulation of T and NK cells by DNAM-1 and TIGIT receptors is achieved by complex interactions that, depending on their binding affinity for the ligand CD155, will counteract or not their activation mediated through the

DNAM-1 receptor (Chauvin and Zarour, 2020; Sanchez-Correa et al., 2019). Studies on the affinity of these receptors for their ligands shows that TIGIT has a higher affinity than DNAM-1 for CD155 and competes for binding to CD155, which interrupts the activation mediated by DNAM-1 and delivers an inhibitory signal to T and NK cells (Stanietsky et al., 2009; Tahara-Hanaoka et al., 2004; Yu et al., 2009). These results suggest that, even with an increase of DNAM-1$^+$ T and NK cells in mesenchymal tumors, TIGIT recognition of the ligand CD155 could be stronger and might exert an inhibitory effect on T and NK cell-mediated cytotoxicity. Hence, we hypothesized that this axis represents a promising target for cancer immunotherapy, blocking TIGIT recognition of CD155 and activating the recognition of this ligand by DNAM-1 to potentiate T and NK cell-mediated cytotoxicity. To translate our results to cSCC and HNSCC patients, we are evaluating by immunohistochemistry and immunofluorescence assays the expression of PD-1 together with LAG-3, TIM-3, CTLA-4 and TIGIT in CD8$^+$ and NK cells to uncover which IC pathways may be being blocked in advanced and metastatic tumors. In addition, we are evaluating if the presence of dysfunctional/exhausted CTLs and NK cells, or if the exclusion of these cells from the tumor core, correlate with resistance or short-term response to ICB therapies. Altogether, our results strongly suggest that ICB therapies should be selected taking into account cancer-cell features.

In order to find the best combinatory therapies to target both the epithelial and mesenchymal component of SCCs, we are planning to compare the impact of the inhibition of different IC pathways to reactivate CTL and NK cell activity in *in vitro* assays. For this, we will test how the proliferation and activity of CD8$^+$ T and NK cells is modulated by the expression of alternative IC ligands. In addition, we plan to co-cultivate epithelial and mesenchymal cancer cells with *in vitro* activated CD8$^+$ T cells and NK cells, in order to compare the inhibitory effect of both cancer cell populations on the activity and cytotoxic cytokine release of CTLs and NK cells. As indicated by our previous results, we expect that mesenchymal-like EpCAM$^-$ cells more effectively block the proliferation and activity of these immune cells than epithelial-like cells. Then, we plan to add to the co-cultured medium, anti-PD-1, anti-CTLA-4, anti-TIGIT, anti-LAG-3, and anti-TIM-3 alone or in combination with other IC blocking antibodies, and identify the more effective treatments to bypass the dysfunction of these effector immune cells. Finally, after the results of our *in* vitro assays, we will select the combined treatments that most effectively reactivate effector cells in the presence of epithelial and mesenchymal cancer cells.

Furthermore, CD4$^+$ T lymphocytes isolated from mouse PD/S-SCCs showed a downregulation of some Th1 pro-inflammatory cytokines (*Il12b* and *Il2*), a slight induction of the expression of Th2 and Treg immunosuppressive cytokines such as *Il5*, *Il13*, *Gata3*, and *Tgf-β1*, as well as an upregulation of *Ccr3* compared to CD4$^+$ cells isolated from mouse WD-SCCs. The receptor CCR3 is important for the recruitment of Th2 cells and the amplification of polarized Th2 responses following the release of cytokines such as CCL17, CCL22, and CCL24 by M2-like macrophages

(Griffith et al., 2014). These results suggest that mesenchymal tumors exhibit a high infiltration of $CD4^+$ Th2 and Treg cells, which may secrete immunosuppressive cytokines to block T and NK-cell activity. Given that the frequency of $CD4^+$ T cells between epithelial and mesenchymal SCCs did not change, our results indicate that there was a change of cellular subtypes. While in epithelial tumors, most of $CD4^+$ T cells were Th1 cells and a very few Treg cells, in mesenchymal tumors there was an enrichment of Th2 cells and immunosuppressive Treg cells, probably related with the presence of hybrid and mesenchymal cancer cells.

IC profile changes during mouse and patient SCC progression

Another important result from this Thesis was that macrophages and DCs upregulate the expression of IC ligands such as PD-L1, MHC-II, Gal9, CD80/CD86, and CD155 during SCC progression, which might be also involved in the dysfunctional cytolytic activity of CTLs and NK cells when interacting with their co-inhibitory receptors in mesenchymal tumors (Kim et al., 2016). This has boosted interest in understanding how these coinhibitory receptors function in order to therapeutically block them, which includes ICB therapies (Sharma and Allison, 2015) and adoptive T-cell therapy (Lim and June, 2017; Rosenberg and Restifo, 2015).

In addition, one of the most promising results was that epithelial, mixed and mesenchymal SCCs have different immune evasion mechanisms to attenuate the effectiveness of T and NK cells. This is achieved by a change in the IC ligand expression during SCC progression, as well as corrupting antigen presentation to avoid T-cell recognition. Our results demonstrate that during the progression from the epithelial to the mesenchymal state, cancer cells loss progressively the expression of MHC-I, which might lead to an impaired T-cell recognition and activation. In addition, whereas PD-L1, MHC-II, Gal9, and CD86 are mostly expressed by epithelial cancer cells, mesenchymal cancer cells strongly downregulate their expression and upregulate a different repertoire of IC ligands. In particular, mesenchymal cancer cells significantly induce the expression of CD80 and CD155, ligands of CTLA-4 and TIGIT IC receptors, respectively. These results suggest that SCCs containing mostly epithelial differentiation features (WD-SCCs) might respond to ICB therapies based on monotherapy with anti-PD-1/PD-L1 antibodies, as well as in combination with anti-LAG-3, anti-TIM-3, or anti-CTLA-4. On the other hand, mixed and mesenchymal tumors (PD/S-SCCs) might be refractory to anti-PD-1/PD-L1 therapies, and the blockade of other IC receptors such as CTLA-4 and TIGIT should be tested to enhance anti-tumor responses. Our studies have revealed more extensive information of the role of other IC ligands in reducing the activity of CTLs and NK cells, as a lot of studies have only related that the EMT can induce the expression of PD-L1 by cancer cells (Chen et al., 2014; Dongre et al., 2017; Noman et al., 2017). Indeed, ZEB1-mediated EMT in NSCLC cells results in increased tumor PD-L1 expression, thus reducing the activity of tumor-infiltrating $CD8^+$ lymphocytes and increasing metastasis (Chen et al., 2014). However, it is possible

that mesenchymal cancer cells from different tumoral context acquire distinct evasion mechanism to elude the anti-tumor immune response, or even the differences between that observed in lung cancer cells and in our cSCC cells may be related with different levels of Zeb1 expression (ectopic overexpression of Zeb1 vs endogenous expression of EMT-TFs in our mouse cSCC mesenchymal cells).

With these results, we hypothesized that the major challenges should be to restore the expression of MHC-I molecules in mesenchymal cancer cells in order to be recognized by T cells, or testing the blockade of CTLA-4 and TIGIT receptors to diminish the inhibitory signals that the ligands CD80 and CD155 might cause on effector T and NK-cell functions. The loss of MHC-I expression and defects in the antigen-processing machinery have been observed in a large proportion of patients, such as in melanoma or lung cancers (Liu et al., 2019; Rosenthal et al., 2019). For instance, some defects imply the loss of function of B2M, which is required for MHC class I folding and transport to the cell surface, the dysregulation of the transporters that pump the antigenic fragments across the endoplasmic reticulum (TAP1, TAP2 and TAPBP), and the disruption of the IFN-γ-JAK-STAT signaling, which promotes MHC-I expression (Campo et al., 2014; Patel et al., 2017; Sade-Feldman et al., 2018). These alterations might impair T-cell recognition and activation, and comprise antitumor activity. Altogether, these results indicate that mesenchymal tumors could be refractory to ICB-based therapies. Furthermore, Verma and colleagues demonstrate that ICB treatment of $CD8^+$ T cells in the absence of antigen stimulation can induce, rather than alleviate, T-cell dysfunction (Verma et al., 2019). Therefore, enhancing MHC-I levels in mesenchymal cancer cells might be a promising strategy to improve ICB efficacy in SCC patients (Garrido et al., 2016). In addition, another strategy for the elimination of mesenchymal cancer cells could be through the boost of the cytotoxic functions of NK cells, since they are capable of recognizing cancer cells without prior antigen presentation by MHC molecules.

Interestingly, the induction of CD80 expression in cancer cells happens at intermediate stages of progression, concomitantly with the acquisition of cancer-cell plasticity, and mesenchymal-like $EpCAM^-$ cancer cells strongly induced the expression of this ligand. These results suggest that CD80 could impede the cytolytic activity of T and NK cells through its binding to CTLA-4 in mixed and mesenchymal tumors, protecting plastic/hybrid and mesenchymal cancer cells of the anti-tumor immune response. Other studies have revealed that cancer cells that actively respond to TGF-β are specifically equipped with surface CD80, endowing cancer cells with the power to not only orchestrate cytotoxic T-cell exhaustion but also fuel their own tumor growth (Miao et al., 2019). The importance of TGF-β in protecting cancer cells from anti-tumor immunity has also been reported for bladder and colon cancer, in this case with conventional PD-L1 immunotherapy (Ganesh and Massagué, 2018; Mariathasan et al., 2018; Tauriello et al., 2018). In addition, as the induction of CD80 could be associated with the acquisition of cancer-cell plasticity, we will evaluate

the *in vitro* and *in vivo* capability of $CD80^+$/$Vimentin^+$/$EpCAM^+$ cells to switch toward mesenchymal like phenotypes. It could be interesting also to evaluate the effect of anti-CTLA-4 treatment, the IC receptor of CD80, to release the blockade of T and NK cells in mesenchymal SCCs and to enhance antitumor immune responses. Finally, CD155 is induced specifically in mesenchymal cancer cells that have extensively induced the EMT program. This leads us to hypothesized that CD155 expression could be induced by microenvironment factors that promote EMT induction, although these experiments are still pending.

ICB therapies should be selected depending on the cancer-cell features

Given that we identified that cancer cell populations within SCCs might use different immune evasions mechanisms, we hypothesized that the resistance or short-term response of advanced SCC patients to ICB therapies could be consequence of cancer-cell plasticity. Moreover, not only the recruitment of immunosuppressive immune cells, but also the expression of a different repertoire of IC ligands in mesenchymal SCCs could activate immune evasion mechanisms different from those in epithelial and mixed SCCs. In order to test the relevance of the IC ligands expressed by cancer and immune cells in SCC immune evasion, we blocked different IC pathways to boost the anti-tumor immune response.

Our results demonstrate that mouse WD-SCCs, comprised by epithelial $EpCAM^+$ cancer cells that express high levels of PD-L1, respond to anti-PD-L1 therapy, which was translate to a reduced tumor growth and a lower cancer-cell viability. This boost of the anti-tumoral immune response was dependent on the reactivation of cytotoxic $CD8^+$ T cells (less expression of PD-1, TIM-3 and LAG-3 exhausted markers, and high expression of IFN-γ and GzmB after anti-PD-L1 treatment) toward the elimination of epithelial cancer cells and the reduction of immunosuppressive cell recruitment (M2-like macrophages and M-MDSCs). This change in the polarization phenotype of tumor-infiltrating macrophages toward the M1-like phenotype was also corroborated by the reduced frequency of $PD\text{-}L1^+$ cells within the macrophage population in anti-PD-L1-treated epithelial tumors, as previously identified (Cai et al., 2019). In addition, a significant increase of NK cells was observed in anti-PD-L1-treated epithelial tumors, which could mediate the elimination of those epithelial cancer cells with reduced expression of MHC-I. However, we are currently evaluating the activation state of NK cells, so these assays are deferred to future experiments. Interestingly, we observed that anti-PD-L1 therapy facilitate the entry of $CD8^+$ T lymphocytes, $CD68^+$ macrophages of the type M1, and $Gr1^+$ MDSCs, possibly of the neutrophil phenotype, toward the intratumoral areas and thus the direct contact with cancer cells. Probably, this increase of cytotoxic $CD8^+$ T cells and M1-like macrophages in the tumor core, whose main function is to eliminate cancer cells, was in line with the reduced cancer-cell viability and the decreased tumor growth of anti-PD-L1-treated tumors. In line with our results, other studies have demonstrated that PD-1 signaling blockade

decreases tumor growth and enhances T and NK antitumoral activity, and PD-1 blockade alongside other ICs has proven increased immune responses (Stecher et al., 2017).

In addition, tumors showing moderate differentiation features (MD/PD-SCCs) could have an initial good response to anti-PD-L1 therapy due to a reactivation of $CD8^+$ T lymphocytes toward $EpCAM^{high}$ cancer cells and less infiltration of immunosuppressive M2-like macrophages, which results in the reduction of the growth of mixed SCCs. However, this reduction of tumor growth was not associated with a low viability of anti-PD-L1-treated mixed tumors. In this sense, the observed enrichment of hybrid and mesenchymal-like $EpCAM^-$ cancer cells and the subsequent increased recruitment of immunosuppressive M-MDSCs at intermediate stages of progression suggest that the decrease in tumor growth of anti-PD-L1-treated tumors is due to the fact that these tumors are acquiring plasticity and have more mesenchymal components. This was confirmed by the fact that anti-PD-L1-treated mixed tumors follow a similar growth kinetics to those observed in the aggressive and mesenchymal SCCs. It is noteworthy that the enrichment of the mesenchymal-like $EpCAM^-$ cancer cell component of these tumors, could lead to a subsequent resistance or short-term response to this therapy, even with a very significant decrease in tumor growth after the treatment. These results also open the door to evaluate the action of other IC receptors in T cells, as well as the role of NK cells, to combat the hybrid and mesenchymal-like $EpCAM^-$ cancer cells.

Finally, mouse PD/S-SCCs comprised by mesenchymal-like $EpCAM^-$ cancer cells were refractory to anti-PD-L1 therapy, as $CD8^+$ T-cell activity was not completely recovered and a high percentage of exhausted T cells were still present upon anti-PD-L1 treatment. In addition, no changes in the immunosuppressive cell recruitment were detected in anti-PD-L1-treated mesenchymal SCCs. These results suggest that the PD-1/PD-L1 signaling is not primarily responsible for blocking the action of T lymphocytes and NK cells in mesenchymal SCCs. Interestingly, mesenchymal tumors exhibit a good response to anti-TIGIT therapy in accordance to the increased expression of its ligand CD155 in mesenchymal-like $EpCAM^-$ cancer cells, M2-like macrophages and DCs. As our preliminary results indicate that the reduction of tumor growth after anti-TIGIT treatment might be mediated by an enhanced CTL and NK cell activity, we are currently studying if there is a reactivation of $CD8^+$ T lymphocytes and NK cells, through the loss of the expression of some IC receptors such as PD-1, TIM-3, LAG-3, and TIGIT, as well as the expression of IFN-γ and GzmB, upon anti-TIGIT treatment. In addition, we will evaluate the impact of inhibiting the TIGIT pathway to reactivate CTL and NK cell activity in *in vitro* assays. Given that Treg cells facilitate tumor progression by interfering with the cytotoxic activity of T and NK cells (von Boehmer and Daniel, 2013), we are also evaluating whether the presence of this population is reduced in anti-TIGIT-treated tumors, that could explain a reactivation of T and NK-cell cytotoxic activities. Following this path, Zhang and colleagues demonstrated that the blockade of the IC receptor TIGIT prevents NK-cell exhaustion and elicits potent anti-tumor immunity in tumor-bearing mice and in patients

with colon cancer (Zhang et al., 2018). This and our work demonstrate that TIGIT constitutes a previously unappreciated immune checkpoint receptor in NK cells and that targeting TIGIT alone or in combination with other IC receptors is a promising anti-cancer therapeutic strategy for advanced mesenchymal SCC tumors, as they might kill cancer cells without previous antigen presentation. In this sense, there is currently much focus on synergistically combining cancer immunotherapies to modulate immune outcomes, combining different IC receptors, or in combination with chemotherapy, targeted therapies, radiotherapy, anti-angiogenic agents and partial surgical resections (Melero et al., 2015).

Altogether our results reveal the relevance of characterizing the cancer cell features before select the ICB therapy that better fits with a specific tumor. Furthermore, as tumors are not comprised by homogeneous cancer cell populations (in cSCC most of the analyzed tumors exhibited different percentage of hybrid/mesenchymal cancer cells), ICB based in a determined IC pathway could give an initial good response, which may be lost after short-time, probably due to the initial elimination of epithelial-like cancer cells, with the consequent enrichment of hybrid/mesenchymal cells between the survival cancer cell population. In this context, the response to this selected ICB therapy may dramatically change, due to the induction of alternative IC pathways and the recruitment of immunosuppressive cells. Therefore, we should consider tumor as a set of heterogeneous cancer cells that change dynamically, inducing concomitant changes in TME, which can deeply impact on ICB therapy response.

Targeting MDSCs and macrophages reduces the immunosuppressive tumor microenvironment and could boost the anti-tumor immune responses of SCCs

Finally, due to the adverse side effects observed after the blockade of CTLA-4, PD-1 and combined therapies with different IC inhibitors in different tumor types (Dougan et al., 2021; Pauken et al., 2019), we hypothesized that an alternative strategy for SCC treatment could be to target the immunosuppressive TME, which contributes to maintain the exhausted state of CTLs and NK cells, even after ICB therapy. Thus, we proposed to inhibit the recruitment of MDSCs and macrophages to target the immunosuppressive TME.

MDSCs are a heterogenous population of immature myeloid cells than can promote tumor growth by suppressing T- and NK-cell activity (Law et al., 2020). Our studies demonstrated that anti-Gr1 treatment induces a partial depletion of PMN-MDSCs. Given that immunosuppressive MDSCs can influence the polarization of macrophages toward an M2-like phenotype (Law et al., 2020), a decreased infiltration of M2-like macrophages was observed into the tumor core of anti-Gr1-treated mixed tumors. This change in the polarization phenotype of tumor-infiltrating macrophages was also corroborated by a reduced frequency of PD-L1^{+} macrophages in anti-Gr1-treated tumors. At the same time, an increase of epithelial cancer cells and a reduction of hybrid and mesenchymal

cancer cells was observed after anti-Gr1 treatment, suggesting that PMN-MDSCs could promote, together with other mechanisms, the acquisition of cancer-cell plasticity and the progression toward a mesenchymal state. Therefore, this suggest that cytokines and growth factors derived from PMN-MDSCs may promote cancer-cell plasticity, the acquisition of mesenchymal traits and SCC progression, which we are currently evaluating. Other possible scenario to explain the reduction of the mesenchymal component after anti-Gr1 treatment could be that this event is induced by an increase of tumor-infiltrating NK cells, which could more efficiently eliminate hybrid and mesenchymal cancer cells in the presence of a reduced immunosuppressive TME, although these experiments remain to be performed. In addition, as MDSCs are one of the immunosuppressive immune cells that abrogate T and NK cell activity, targeting this population might led to a reactivation of CTL and NK cell activity in mixed SCCs (Law et al., 2020).

On the other hand, anti-CSF1R treatment does not reduced mixed tumor growth, although it leads to a reduction of M2-like macrophages and M-MDSCs, which could favor the generation of a less immunosuppressive TME. The depletion of M2-like macrophages and M-MDSCs leads to an increased infiltration of $CD8^+$ T cells, although these cells did not change their activation status after the treatment, and does not block cancer-cell progression toward the mesenchymal state. These results suggest that anti-CSF1R therapy would be efficient to reduce the immunosuppressive component, but it would be necessary to combine it with IC inhibitors to stimulate the antitumor immune response of SCCs. In this sense, inhibiting CCR2 (Lesokhin et al., 2012), CSF1R (DeNardo et al., 2011; Strachan et al., 2013; Zhu et al., 2014) in preclinical models of melanoma, pancreatic, breast, and prostatic carcinoma increased intratumoral T cells and controlled tumor growth, especially when combined with anti-CTLA-4 or anti-PD-1/PD-L1. Although these studies did not determine whether the increases in T cells were a consequence of enhanced viability or replication, they emphasize again how elements of the TME regulate the accumulation of effector T cells. In accordance with our results, the inhibition of CSF1R in a preclinical model of glioblastoma or pancreatic ductal adenocarcinoma (PDAC) correlates also with the reprogramming of macrophages toward an M1-like phenotype that enhance antigen presentation (Pyonteck et al., 2013; Zhu et al., 2014). In the study with PDAC, they found that combining anti-CSF1R blockade with PD-1 and CTLA-4 antagonist potently elicited tumor regressions, even in larger established tumors (Zhu et al., 2014).

Taken together, our findings provide a rationale to reprogram immunosuppressive myeloid cell populations in the tumor microenvironment in order to empower the therapeutic effects of ICB therapeutic strategies.

CONCLUSIONS

Based on the results obtained in this Thesis, we conclude:

1. During mouse skin SCC progression, epithelial EpCAM^{high} cancer cells acquire plasticity and give rise to EpCAM^{low} cancer cells, which show a hybrid epithelial-mesenchymal phenotype and a higher ability to switch to mesenchymal-like EpCAM^{-} cancer cells.
2. The immune landscape switches from a pro-inflammatory to an immunosuppressive state during mouse and patient skin SCC progression, concomitantly with the acquisition of hybrid and mesenchymal-like features in cancer cells.
3. The immunosuppressive state is characterized by the high presence of M-MDSCs, M2-like macrophages, Treg cells, and exhausted CTLs and NK cells.
4. Epithelial, mixed and mesenchymal SCCs have evolved different mechanisms to attenuate the effectiveness of T and NK cells. During SCC progression, cancer cells loss the expression of MHC-I, which lead to an impaired T-cell recognition. In addition, whereas PD-L1, MHC-II, Galectin-9 and CD86 are mostly expressed by epithelial cancer cells, mesenchymal cancer cells upregulate the expression of a different repertoire of IC ligands, such as CD80 and CD155.
5. Mouse WD-SCCs, comprised by full epithelial cancer cells, respond to anti-PD-L1 therapy, which is dependent on reactivated cytotoxic CD8^{+} T cells and on the reduction of immunosuppressive cell recruitment (M2-like macrophages and M-MDSCs).
6. Mouse MD/PD-SCCs have an initial good response to anti-PD-L1 therapy due to a reactivation of CD8^{+} T lymphocytes toward EpCAM^{high} cells and to a less infiltration of immunosuppressive M2-like macrophages. However, the increased frequency of hybrid and mesenchymal-like EpCAM^{-} cancer cells and immunosuppressive M-MDSCs upon treatment makes it necessary to search for alternative or combined therapies to combat these immunosuppressive cells.
7. Mouse PD/S-SCCs comprised by mesenchymal-like EpCAM^{-} cancer cells are refractory to anti-PD-L1 therapy, but exhibit a good response to anti-TIGIT therapy, in accordance to the increased expression of its ligand CD155 in mesenchymal-like EpCAM^{-} cancer cells, M2-like macrophages and DCs.
8. A partial depletion of PMN-MDSCs after anti-Gr1 treatment blocks cancer-cell progression toward the mesenchymal state and reduces the infiltration of M2-like macrophages, which might contribute to enhance the anti-tumor response of CTLs and NK cells, leading to the attenuated mixed SCC growth observed upon treatment.
9. Anti-CSF1R treatment does not reduce mixed tumor growth, although it promotes a reduction of M1-like and M2-like macrophage, as well as M-MDSC populations, which could reduce the immunosuppressive TME.

BIBLIOGRAPHY

Aceto, N., Bardia, A., Miyamoto, D.T., Donaldson, M.C., Wittner, B.S., Spencer, J.A., Yu, M., Pely, A., Engstrom, A., Zhu, H., et al. (2014). Circulating Tumor Cell Clusters Are Oligoclonal Precursors of Breast Cancer Metastasis. Cell *158*, 1110–1122.

Acun, T., Oztas, E., Yagci, T., and Yakicier, M.C. (2011). SIP1 is downregulated in hepatocellular carcinoma by promoter hypermethylation. BMC Cancer *11*, 223.

Ahmadzadeh, M., Johnson, L.A., Heemskerk, B., Wunderlich, J.R., Dudley, M.E., White, D.E., and Rosenberg, S.A. (2009). Tumor antigen–specific CD8 T cells infiltrating the tumor express high levels of PD-1 and are functionally impaired. Blood *114*, 1537–1544.

Ahmed, S.R., Petersen, E., Patel, R., and Migden, M.R. (2019). Cemiplimab-rwlc as first and only treatment for advanced cutaneous squamous cell carcinoma. Expert Rev. Clin. Pharmacol. *12*, 947–951.

Aiello, N.M., Maddipati, R., Norgard, R.J., Balli, D., Li, J., Yuan, S., Yamazoe, T., Black, T., Sahmoud, A., Furth, E.E., et al. (2018). EMT Subtype Influences Epithelial Plasticity and Mode of Cell Migration. Dev. Cell *45*, 681-695.e4.

Ajona, D., Ortiz-Espinosa, S., Lozano, T., Exposito, F., Calvo, A., Valencia, K., Redrado, M., Remírez, A., Lecanda, F., Alignani, D., et al. (2020). Short-term starvation reduces IGF-1 levels to sensitize lung tumors to PD-1 immune checkpoint blockade. Nat. Cancer *1*, 75–85.

Alam, M., and Ratner, D. (2001). Cutaneous squamous-cell carcinoma. N. Engl. J. Med. *344*, 975–983.

Aldea, M., Andre, F., Marabelle, A., Dogan, S., Barlesi, F., and Soria, J.-C. (2021). Overcoming Resistance to Tumor-Targeted and Immune-Targeted Therapies. Cancer Discov. *11*, 874–899.

Almand, B., Clark, J.I., Nikitina, E., Beynen, J. van, English, N.R., Knight, S.C., Carbone, D.P., and Gabrilovich, D.I. (2001). Increased Production of Immature Myeloid Cells in Cancer Patients: A Mechanism of Immunosuppression in Cancer. J. Immunol. *166*, 678–689.

Anagnostou, V., Smith, K.N., Forde, P.M., Niknafs, N., Bhattacharya, R., White, J., Zhang, T., Adleff, V., Phallen, J., Wali, N., et al. (2017). Evolution of Neoantigen Landscape during Immune Checkpoint Blockade in Non–Small Cell Lung Cancer. Cancer Discov. *7*, 264–276.

Anderson, A.C. (2012). Tim-3, a negative regulator of anti-tumor immunity. Curr. Opin. Immunol. *24*, 213–216.

Anderson, A.C., Joller, N., and Kuchroo, V.K. (2016). Lag-3, Tim-3, and TIGIT: Co-inhibitory Receptors with Specialized Functions in Immune Regulation. Immunity *44*, 989–1004.

Appay, V., Douek, D.C., and Price, D.A. (2008). CD8 + T cell efficacy in vaccination and disease. Nat. Med. *14*, 623–628.

Aras, S., and Zaidi, M.R. (2017). TAMeless traitors: macrophages in cancer progression and metastasis. Br. J. Cancer *117*, 1583–1591.

Arase, H., Arase, N., and Saito, T. (1995). Fas-mediated cytotoxicity by freshly isolated natural killer cells. J. Exp. Med. *181*, 1235–1238.

Arbeit, J.M., Münger, K., Howley, P.M., and Hanahan, D. (1994). Progressive squamous epithelial neoplasia in K14-human papillomavirus type 16 transgenic mice. J. Virol. *68*, 4358–4368.

Armstrong, A.J., Marengo, M.S., Oltean, S., Kemeny, G., Bitting, R.L., Turnbull, J.D., Herold, C.I., Marcom, P.K., George, D.J., and Garcia-Blanco, M.A. (2011). Circulating Tumor Cells from Patients with Advanced Prostate and Breast Cancer Display Both Epithelial and Mesenchymal Markers. Mol. Cancer Res. *9*, 997–1007.

Arwert, E.N., Hoste, E., and Watt, F.M. (2012). Epithelial stem cells, wound healing and cancer. Nat. Rev. Cancer *12*, 170–180.

Ashford, B.G., Clark, J., Gupta, R., Iyer, N.G., Yu, B., and Ranson, M. (2017). Reviewing the genetic alterations in high-risk cutaneous squamous cell carcinoma: A search for prognostic markers and therapeutic targets. Head Neck *39*, 1462–1469.

Azizi, E., Carr, A.J., Plitas, G., Cornish, A.E., Konopacki, C., Prabhakaran, S., Nainys, J., Wu, K., Kiseliovas, V., Setty, M., et al. (2018). Single-Cell Map of Diverse Immune Phenotypes in the Breast Tumor Microenvironment. Cell *174*, 1293-1308.e36.

Baginska, J., Viry, E., Paggetti, J., Medves, S., Berchem, G., Moussay, E., and Janji, B. (2013). The Critical Role of the Tumor Microenvironment in Shaping Natural Killer Cell-Mediated Anti-Tumor Immunity. Front. Immunol. *4*.

Baixeras, E., Huard, B., Miossec, C., Jitsukawa, S., Martin, M., Hercend, T., Auffray, C., Triebel, F., and Piatier-Tonneau, D. (1992). Characterization of the lymphocyte activation gene 3-encoded protein. A new ligand for human leukocyte antigen class II antigens. J. Exp. Med. *176*, 327–337.

Bald, T., Krummel, M.F., Smyth, M.J., and Barry, K.C. (2020). The NK cell–cancer cycle: advances and new challenges in NK cell–based immunotherapies. Nat. Immunol. *21*, 835–847.

Barrow, A.D., Martin, C.J., and Colonna, M. (2019). The Natural Cytotoxicity Receptors in Health and Disease. Front. Immunol. *10*.

Bartoschek, M., Oskolkov, N., Bocci, M., Lövrot, J., Larsson, C., Sommarin, M., Madsen, C.D., Lindgren, D., Pekar, G., Karlsson, G., et al. (2018). Spatially and functionally distinct subclasses of breast cancer-associated fibroblasts revealed by single cell RNA sequencing. Nat. Commun. *9*, 5150.

Basu, R., Whitlock, B.M., Husson, J., Floc'h, A.L., Jin, W., Oyler-Yaniv, A., Dotiwala, F., Giannone, G., Hivroz, C., Biais, N., et al. (2016). Cytotoxic T Cells Use Mechanical Force to Potentiate Target Cell Killing. Cell *165*, 100–110.

Bates, G.J., Fox, S.B., Han, C., Leek, R.D., Garcia, J.F., Harris, A.L., and Banham, A.H. (2006). Quantification of Regulatory T Cells Enables the Identification of High-Risk Breast Cancer Patients and Those at Risk of Late Relapse. J. Clin. Oncol. *24*, 5373–5380.

Batlle, E., and Clevers, H. (2017). Cancer stem cells revisited. Nat. Med. *23*, 1124–1134.

Batlle, E., Sancho, E., Francí, C., Domínguez, D., Monfar, M., Baulida, J., and García de Herreros, A. (2000). The transcription factor Snail is a repressor of E-cadherin gene expression in epithelial tumour cells. Nat. Cell Biol. *2*, 84–89.

Baylin, S.B., and Jones, P.A. (2011). A decade of exploring the cancer epigenome — biological and translational implications. Nat. Rev. Cancer *11*, 726–734.

Beck, B., Lapouge, G., Rorive, S., Drogat, B., Desaedelaere, K., Delafaille, S., Dubois, C., Salmon, I., Willekens, K., Marine, J.-C., et al. (2015). Different Levels of Twist1 Regulate Skin Tumor Initiation, Stemness, and Progression. Cell Stem Cell *16*, 67–79.

Bedard, P.L., Hansen, A.R., Ratain, M.J., and Siu, L.L. (2013). Tumour heterogeneity in the clinic. Nature *501*, 355–364.

Beekhof, R., Alphen, C., Henneman, A.A., Knol, J.C., Pham, T.V., Rolfs, F., Labots, M., Henneberry, E., Le Large, T.Y., Haas, R.R., et al. (2019). INKA , an integrative data analysis pipeline for phosphoproteomic inference of active kinases. Mol. Syst. Biol. *15*.

Bejarano, L., Jordão, M.J.C., and Joyce, J.A. (2021). Therapeutic Targeting of the Tumor Microenvironment. Cancer Discov. *11*, 933–959.

Benci, J.L., Xu, B., Qiu, Y., Wu, T.J., Dada, H., Victor, C.T.-S., Cucolo, L., Lee, D.S.M., Pauken, K.E., Huang, A.C., et al. (2016). Tumor Interferon Signaling Regulates a Multigenic Resistance Program to Immune Checkpoint Blockade. Cell *167*, 1540-1554.e12.

van den Berg, T.K., and Valerius, T. (2019). Myeloid immune-checkpoint inhibition enters the clinical stage. Nat. Rev. Clin. Oncol. *16*, 275–276.

Bernat-Peguera, A., Simón-Extremera, P., da Silva-Diz, V., López de Munain, M., Díaz-Gil, L., Penin, R.M., González-Suárez, E., Pérez Sidelnikova, D., Bermejo, O., Viñals, J.M., et al. (2019). PDGFR-induced autocrine SDF-1 signaling in cancer cells promotes metastasis in advanced skin carcinoma. Oncogene *38*, 5021–5037.

Bernat-Peguera, A., Navarro-Ventura, J., Lorenzo-Sanz, L., Silva-Diz, V. da, Bosio, M., Palomero, L., Penin, R.M., Sidelnikova, D.P., Bermejo, J.O., Taberna, M., et al. (2021). FGFR Inhibition Overcomes Resistance to EGFR-targeted Therapy in Epithelial-like Cutaneous Carcinoma. Clin. Cancer Res. *27*, 1491–1504.

Bi, J., and Tian, Z. (2017). NK Cell Exhaustion. Front. Immunol. *8*.

Binnewies, M., Roberts, E.W., Kersten, K., Chan, V., Fearon, D.F., Merad, M., Coussens, L.M., Gabrilovich, D.I., Ostrand-Rosenberg, S., Hedrick, C.C., et al. (2018). Understanding the tumor immune microenvironment (TIME) for effective therapy. Nat. Med. *24*, 541–550.

Blackburn, S.D., Shin, H., Haining, W.N., Zou, T., Workman, C.J., Polley, A., Betts, M.R., Freeman, G.J., Vignali, D.A.A., and Wherry, E.J. (2009). Coregulation of CD8 + T cell exhaustion by multiple inhibitory receptors during chronic viral infection. Nat. Immunol. *10*, 29–37.

Blanpain, C., Lowry, W.E., Geoghegan, A., Polak, L., and Fuchs, E. (2004). Self-Renewal, Multipotency, and the Existence of Two Cell Populations within an Epithelial Stem Cell Niche. Cell *118*, 635–648.

Blum, J.S., Wearsch, P.A., and Cresswell, P. (2013). Pathways of Antigen Processing. Annu. Rev. Immunol. *31*, 443–473.

von Boehmer, H., and Daniel, C. (2013). Therapeutic opportunities for manipulating T(Reg) cells in autoimmunity and cancer. Nat. Rev. Drug Discov. *12*, 51–63.

Boivin, G., Faget, J., Ancey, P.-B., Gkasti, A., Mussard, J., Engblom, C., Pfirschke, C., Contat, C., Pascual, J., Vazquez, J., et al. (2020). Durable and controlled depletion of neutrophils in mice. Nat. Commun. *11*, 2762.

Bopp, T., Becker, C., Klein, M., Klein-Heßling, S., Palmetshofer, A., Serfling, E., Heib, V., Becker, M., Kubach, J., Schmitt, S., et al. (2007). Cyclic adenosine monophosphate is a key component of regulatory T cell–mediated suppression. J. Exp. Med. *204*, 1303–1310.

Borst, J., Ahrends, T., Bąbała, N., Melief, C.J.M., and Kastenmüller, W. (2018). CD4+ T cell help in cancer immunology and immunotherapy. Nat. Rev. Immunol. *18*, 635–647.

Bottino, C., Castriconi, R., Pende, D., Rivera, P., Nanni, M., Carnemolla, B., Cantoni, C., Grassi, J., Marcenaro, S., Reymond, N., et al. (2003). Identification of PVR (CD155) and Nectin-2 (CD112) as Cell Surface Ligands for the Human DNAM-1 (CD226) Activating Molecule. J. Exp. Med. *198*, 557–567.

Bottomley, M.J., Thomson, J., Harwood, C., and Leigh, I. (2019). The Role of the Immune System in Cutaneous Squamous Cell Carcinoma. Int. J. Mol. Sci. *20*.

Boumahdi, S., Driessens, G., Lapouge, G., Rorive, S., Nassar, D., Le Mercier, M., Delatte, B., Caauwe, A., Lenglez, S., Nkusi, E., et al. (2014). SOX2 controls tumour initiation and cancer stem-cell functions in squamous-cell carcinoma. Nature *511*, 246–250.

Brabletz, T. (2012). To differentiate or not — routes towards metastasis. Nat. Rev. Cancer *12*, 425–436.

Brandau, S., Dumitru, C.A., and Lang, S. (2013). Protumor and antitumor functions of neutrophil granulocytes. Semin. Immunopathol. *35*, 163–176.

Brantsch, K.D., Meisner, C., Schönfisch, B., Trilling, B., Wehner-Caroli, J., Röcken, M., and Breuninger, H. (2008). Analysis of risk factors determining prognosis of cutaneous squamous-cell carcinoma: a prospective study. Lancet Oncol. *9*, 713–720.

Brinkman, J.N., Hajder, E., van der Holt, B., Den Bakker, M.A., Hovius, S.E.R., and Mureau, M.A.M. (2015). The Effect of Differentiation Grade of Cutaneous Squamous Cell Carcinoma on Excision Margins, Local Recurrence, Metastasis, and Patient Survival: A Retrospective Follow-Up Study. Ann. Plast. Surg. *75*, 323–326.

van den Broek, T., Borghans, J.A.M., and van Wijk, F. (2018). The full spectrum of human naive T cells. Nat. Rev. Immunol. *18*, 363–373.

Bronte, V., Brandau, S., Chen, S.-H., Colombo, M.P., Frey, A.B., Greten, T.F., Mandruzzato, S., Murray, P.J., Ochoa, A., Ostrand-Rosenberg, S., et al. (2016). Recommendations for myeloid-derived suppressor cell nomenclature and characterization standards. Nat. Commun. *7*, 12150.

Broz, M.L., Binnewies, M., Boldajipour, B., Nelson, A.E., Pollack, J.L., Erle, D.J., Barczak, A., Rosenblum, M.D., Daud, A., Barber, D.L., et al. (2014). Dissecting the Tumor Myeloid Compartment Reveals Rare Activating Antigen-Presenting Cells Critical for T Cell Immunity. Cancer Cell *26*, 638–652.

Bruchim, I., Sarfstein, R., and Werner, H. (2014). The IGF Hormonal Network in Endometrial Cancer: Functions, Regulation, and Targeting Approaches. Front. Endocrinol. *5*.

Burk, U., Schubert, J., Wellner, U., Schmalhofer, O., Vincan, E., Spaderna, S., and Brabletz, T. (2008). A reciprocal repression between ZEB1 and members of the miR-200 family promotes EMT and invasion in cancer cells. EMBO Rep. *9*, 582–589.

Burova, E., Hermann, A., Dai, J., Ullman, E., Halasz, G., Potocky, T., Hong, S., Liu, M., Allbritton, O., Woodruff, A., et al. (2019). Preclinical Development of the Anti-LAG-3 Antibody REGN3767: Characterization and Activity in Combination with the Anti-PD-1 Antibody Cemiplimab in Human PD-1xLAG-3–Knockin Mice. Mol. Cancer Ther. *18*, 2051–2062.

Burton, K.A., Ashack, K.A., and Khachemoune, A. (2016). Cutaneous Squamous Cell Carcinoma: A Review of High-Risk and Metastatic Disease. Am. J. Clin. Dermatol. *17*, 491–508.

Cai, J., Qi, Q., Qian, X., Han, J., Zhu, X., Zhang, Q., and Xia, R. (2019). The role of PD-1/PD-L1 axis and macrophage in the progression and treatment of cancer. J. Cancer Res. Clin. Oncol. *145*, 1377–1385.

Camisaschi, C., Casati, C., Rini, F., Perego, M., Filippo, A.D., Triebel, F., Parmiani, G., Belli, F., Rivoltini, L., and Castelli, C. (2010). LAG-3 Expression Defines a Subset of CD4+CD25highFoxp3+ Regulatory T Cells That Are Expanded at Tumor Sites. J. Immunol. *184*, 6545–6551.

Campo, A.B. del, Kyte, J.A., Carretero, J., Zinchencko, S., Méndez, R., González-Aseguinolaza, G., Ruiz-Cabello, F., Aamdal, S., Gaudernack, G., Garrido, F., et al. (2014). Immune escape of cancer cells with beta2-microglobulin loss over the course of metastatic melanoma. Int. J. Cancer *134*, 102–113.

Cano, A., Pérez-Moreno, M.A., Rodrigo, I., Locascio, A., Blanco, M.J., del Barrio, M.G., Portillo, F., and Nieto, M.A. (2000). The transcription factor Snail controls epithelial–mesenchymal transitions by repressing E-cadherin expression. Nat. Cell Biol. *2*, 76–83.

Cañueto, J., Cardeñoso, E., García, J.L., Santos-Briz, Á., Castellanos-Martín, A., Fernández-López, E., Gómez, A.B., Pérez-Losada, J., and Román-Curto, C. (2017). Epidermal growth factor receptor expression is associated with poor outcome in cutaneous squamous cell carcinoma. Br. J. Dermatol. *176*, 1279–1287.

Cao, X., Cai, S.F., Fehniger, T.A., Song, J., Collins, L.I., Piwnica-Worms, D.R., and Ley, T.J. (2007). Granzyme B and Perforin Are Important for Regulatory T Cell-Mediated Suppression of Tumor Clearance. Immunity *27*, 635–646.

Cassetta, L., and Pollard, J.W. (2018). Targeting macrophages: therapeutic approaches in cancer. Nat. Rev. Drug Discov. *17*, 887–904.

Celià-Terrassa, T., Meca-Cortés, Ó., Mateo, F., Paz, A.M. de, Rubio, N., Arnal-Estapé, A., Ell, B.J., Bermudo, R., Díaz, A., Guerra-Rebollo, M., et al. (2012). Epithelial-mesenchymal transition can suppress major attributes of human epithelial tumor-initiating cells. J. Clin. Invest. *122*, 1849–1868.

Cerezo-Wallis, D., Contreras-Alcalde, M., Troulé, K., Catena, X., Mucientes, C., Calvo, T.G., Cañón, E., Tejedo, C., Pennacchi, P.C., Hogan, S., et al. (2020). Midkine rewires the melanoma microenvironment toward a tolerogenic and immune-resistant state. Nat. Med. *26*, 1865–1877.

Chaffer, C.L., San Juan, B.P., Lim, E., and Weinberg, R.A. (2016). EMT, cell plasticity and metastasis. Cancer Metastasis Rev. *35*, 645–654.

Chalmers, Z.R., Connelly, C.F., Fabrizio, D., Gay, L., Ali, S.M., Ennis, R., Schrock, A., Campbell, B., Shlien, A., Chmielecki, J., et al. (2017). Analysis of 100,000 human cancer genomes reveals the landscape of tumor mutational burden. Genome Med. *9*, 34.

Chan, C.J., Martinet, L., Gilfillan, S., Souza-Fonseca-Guimaraes, F., Chow, M.T., Town, L., Ritchie, D.S., Colonna, M., Andrews, D.M., and Smyth, M.J. (2014). The receptors CD96 and CD226 oppose each other in the regulation of natural killer cell functions. Nat. Immunol. *15*, 431–438.

Chang, Z.L., Lorenzini, M.H., Chen, X., Tran, U., Bangayan, N.J., and Chen, Y.Y. (2018). Rewiring T-cell responses to soluble factors with chimeric antigen receptors. Nat. Chem. Biol. *14*, 317–324.

Chanmee, T., Ontong, P., Konno, K., and Itano, N. (2014). Tumor-associated macrophages as major players in the tumor microenvironment. Cancers *6*, 1670–1690.

Chauvin, J.-M., and Zarour, H.M. (2020). TIGIT in cancer immunotherapy. J. Immunother. Cancer *8*, e000957.

Chen, L., and Flies, D.B. (2013). Molecular mechanisms of T cell co-stimulation and co-inhibition. Nat. Rev. Immunol. *13*, 227–242.

Chen, J., Li, Y., Yu, T.-S., McKay, R.M., Burns, D.K., Kernie, S.G., and Parada, L.F. (2012). A restricted cell population propagates glioblastoma growth after chemotherapy. Nature *488*, 522–526.

Chen, L., Gibbons, D.L., Goswami, S., Cortez, M.A., Ahn, Y.-H., Byers, L.A., Zhang, X., Yi, X., Dwyer, D., Lin, W., et al. (2014). Metastasis is regulated via microRNA-200/ZEB1 axis control of tumour cell PD-L1 expression and intratumoral immunosuppression. Nat. Commun. *5*, 5241.

Chen, X.-H., Liu, Z.-C., Zhang, G., Wei, W., Wang, X.-X., Wang, H., Ke, H.-P., Zhang, F., Wang, H.-S., Cai, S.-H., et al. (2015). TGF-β and EGF induced HLA-I downregulation is associated with epithelial-mesenchymal transition (EMT) through upregulation of snail in prostate cancer cells. Mol. Immunol. *65*, 34–42.

Cheng, P., Eksioglu, E.A., Chen, X., Kandell, W., Le Trinh, T., Cen, L., Qi, J., Sallman, D.A., Zhang, Y., Tu, N., et al. (2019). S100A9-induced overexpression of PD-1/PD-L1 contributes to ineffective hematopoiesis in myelodysplastic syndromes. Leukemia *33*, 2034–2046.

Chiba, S., Baghdadi, M., Akiba, H., Yoshiyama, H., Kinoshita, I., Dosaka-Akita, H., Fujioka, Y., Ohba, Y., Gorman, J.V., Colgan, J.D., et al. (2012). Tumor-infiltrating DCs suppress nucleic acid–mediated innate immune responses through interactions between the receptor TIM-3 and the alarmin HMGB1. Nat. Immunol. *13*, 832–842.

Chiossone, L., Dumas, P.-Y., Vienne, M., and Vivier, E. (2018). Natural killer cells and other innate lymphoid cells in cancer. Nat. Rev. Immunol. *18*, 671–688.

Chmielewski, M., Kopecky, C., Hombach, A.A., and Abken, H. (2011). IL-12 Release by Engineered T Cells Expressing Chimeric Antigen Receptors Can Effectively Muster an Antigen-Independent Macrophage Response on Tumor Cells That Have Shut Down Tumor Antigen Expression. Cancer Res. *71*, 5697–5706.

Chockley, P.J., and Keshamouni, V.G. (2016). Immunological Consequences of Epithelial–Mesenchymal Transition in Tumor Progression. J. Immunol. *197*, 691–698.

Clevers, H. (2011). The cancer stem cell: premises, promises and challenges. Nat. Med. *17*, 313–319.

Comijn, J., Berx, G., Vermassen, P., Verschueren, K., Grunsven, L. van, Bruyneel, E., Mareel, M., Huylebroeck, D., and Roy, F. van (2001). The Two-Handed E Box Binding Zinc Finger Protein SIP1 Downregulates E-Cadherin and Induces Invasion. Mol. Cell *7*, 1267–1278.

Condamine, T., Ramachandran, I., Youn, J.-I., and Gabrilovich, D.I. (2015). Regulation of Tumor Metastasis by Myeloid-Derived Suppressor Cells. Annu. Rev. Med. *66*, 97–110.

Condamine, T., Dominguez, G.A., Youn, J.-I., Kossenkov, A.V., Mony, S., Alicea-Torres, K., Tcyganov, E., Hashimoto, A., Nefedova, Y., Lin, C., et al. (2016). Lectin-type oxidized LDL receptor-1 distinguishes population of human polymorphonuclear myeloid-derived suppressor cells in cancer patients. Sci. Immunol. *1*, aaf8943–aaf8943.

Coniglio, S.J., Eugenin, E., Dobrenis, K., Stanley, E.R., West, B.L., Symons, M.H., and Segall, J.E. (2012). Microglial Stimulation of Glioblastoma Invasion Involves Epidermal Growth Factor

Receptor (EGFR) and Colony Stimulating Factor 1 Receptor (CSF-1R) Signaling. Mol. Med. *18*, 519–527.

Coussens, L.M., Hanahan, D., and Arbeit, J.M. (1996). Genetic predisposition and parameters of malignant progression in K14-HPV16 transgenic mice. Am. J. Pathol. *149*, 1899–1917.

Coussens, L.M., Zitvogel, L., and Palucka, A.K. (2013). Neutralizing Tumor-Promoting Chronic Inflammation: A Magic Bullet? Science *339*, 286–291.

Craene, B.D., and Berx, G. (2013). Regulatory networks defining EMT during cancer initiation and progression. Nat. Rev. Cancer *13*, 97–110.

Cranmer, L.D., Engelhardt, C., and Morgan, S.S. (2010). Treatment of Unresectable and Metastatic Cutaneous Squamous Cell Carcinoma. The Oncologist *15*, 1320–1328.

Cui, T.X., Kryczek, I., Zhao, L., Zhao, E., Kuick, R., Roh, M.H., Vatan, L., Szeliga, W., Mao, Y., Thomas, D.G., et al. (2013). Myeloid-Derived Suppressor Cells Enhance Stemness of Cancer Cells by Inducing MicroRNA101 and Suppressing the Corepressor CtBP2. Immunity *39*, 611–621.

Curran, M.A., Montalvo, W., Yagita, H., and Allison, J.P. (2010). PD-1 and CTLA-4 combination blockade expands infiltrating T cells and reduces regulatory T and myeloid cells within B16 melanoma tumors. Proc. Natl. Acad. Sci. *107*, 4275–4280.

Dagogo-Jack, I., and Shaw, A.T. (2018). Tumour heterogeneity and resistance to cancer therapies. Nat. Rev. Clin. Oncol. *15*, 81–94.

Darnell, J.E., Kerr, I.M., and Stark, G.R. (1994). Jak-STAT pathways and transcriptional activation in response to IFNs and other extracellular signaling proteins. Science *264*, 1415–1421.

Davis, M.M., Boniface, J.J., Reich, Z., Lyons, D., Hampl, J., Arden, B., and Chien, Y. (1998). LIGAND RECOGNITION BY αβ T CELL RECEPTORS. Annu. Rev. Immunol. *16*, 523–544.

Deaglio, S., Dwyer, K.M., Gao, W., Friedman, D., Usheva, A., Erat, A., Chen, J.-F., Enjyoji, K., Linden, J., Oukka, M., et al. (2007). Adenosine generation catalyzed by CD39 and CD73 expressed on regulatory T cells mediates immune suppression. J. Exp. Med. *204*, 1257–1265.

DeNardo, D.G., and Coussens, L.M. (2007). Inflammation and breast cancer. Balancing immune response: crosstalk between adaptive and innate immune cells during breast cancer progression. Breast Cancer Res. *9*, 212.

DeNardo, D.G., and Ruffell, B. (2019). Macrophages as regulators of tumour immunity and immunotherapy. Nat. Rev. Immunol. *19*, 369–382.

DeNardo, D.G., Barreto, J.B., Andreu, P., Vasquez, L., Tawfik, D., Kolhatkar, N., and Coussens, L.M. (2009). CD4+ T Cells Regulate Pulmonary Metastasis of Mammary Carcinomas by Enhancing Protumor Properties of Macrophages. Cancer Cell *16*, 91–102.

DeNardo, D.G., Brennan, D.J., Rexhepaj, E., Ruffell, B., Shiao, S.L., Madden, S.F., Gallagher, W.M., Wadhwani, N., Keil, S.D., Junaid, S.A., et al. (2011). Leukocyte Complexity Predicts Breast Cancer Survival and Functionally Regulates Response to Chemotherapy. Cancer Discov. *1*, 54–67.

Diaz-Montero, C.M., Salem, M.L., Nishimura, M.I., Garrett-Mayer, E., Cole, D.J., and Montero, A.J. (2009). Increased circulating myeloid-derived suppressor cells correlate with clinical cancer stage, metastatic tumor burden, and doxorubicin–cyclophosphamide chemotherapy. Cancer Immunol. Immunother. *58*, 49–59.

Didona, D., Paolino, G., Bottoni, U., and Cantisani, C. (2018). Non Melanoma Skin Cancer Pathogenesis Overview. Biomedicines *6*.

Dongre, A., and Weinberg, R.A. (2019). New insights into the mechanisms of epithelial–mesenchymal transition and implications for cancer. Nat. Rev. Mol. Cell Biol. *20*, 69–84.

Dongre, A., Rashidian, M., Reinhardt, F., Bagnato, A., Keckesova, Z., Ploegh, H.L., and Weinberg, R.A. (2017). Epithelial-to-Mesenchymal Transition Contributes to Immunosuppression in Breast Carcinomas. Cancer Res. *77*, 3982–3989.

Dongre, A., Rashidian, M., Eaton, E.N., Reinhardt, F., Thiru, P., Zagorulya, M., Nepal, S., Banaz, T., Martner, A., Spranger, S., et al. (2020). Direct and Indirect Regulators of Epithelial-Mesenchymal Transition (EMT)-mediated Immunosuppression in Breast Carcinomas. Cancer Discov.

Dotto, G.P., and Rustgi, A.K. (2016). Squamous Cell Cancers: A Unified Perspective on Biology and Genetics. Cancer Cell *29*, 622–637.

Dougan, M., Luoma, A.M., Dougan, S.K., and Wucherpfennig, K.W. (2021). Understanding and treating the inflammatory adverse events of cancer immunotherapy. Cell *184*, 1575–1588.

Drijvers, J.M., Sharpe, A.H., and Haigis, M.C. (2020). The effects of age and systemic metabolism on anti-tumor T cell responses. ELife *9*, e62420.

Droeser, R.A., Hirt, C., Eppenberger-Castori, S., Zlobec, I., Viehl, C.T., Frey, D.M., Nebiker, C.A., Rosso, R., Zuber, M., Amicarella, F., et al. (2013). High Myeloperoxidase Positive Cell Infiltration in Colorectal Cancer Is an Independent Favorable Prognostic Factor. PLOS ONE *8*, e64814.

Duan, Z., and Luo, Y. (2021). Targeting macrophages in cancer immunotherapy. Signal Transduct. Target. Ther. *6*, 1–21.

Dubina, M., and Goldenberg, G. (2009). Viral-Associated Nonmelanoma Skin Cancers: A Review. Am. J. Dermatopathol. *31*, 561–573.

Eisenhauer, E.A., Therasse, P., Bogaerts, J., Schwartz, L.H., Sargent, D., Ford, R., Dancey, J., Arbuck, S., Gwyther, S., Mooney, M., et al. (2009). New response evaluation criteria in solid tumours: Revised RECIST guideline (version 1.1). Eur. J. Cancer *45*, 228–247.

Ekyalongo, R.C., and Yee, D. (2017). Revisiting the IGF-1R as a breast cancer target. Npj Precis. Oncol. *1*, 1–7.

Fan, Q.-M., Jing, Y.-Y., Yu, G.-F., Kou, X.-R., Ye, F., Gao, L., Li, R., Zhao, Q.-D., Yang, Y., Lu, Z.-H., et al. (2014). Tumor-associated macrophages promote cancer stem cell-like properties via transforming growth factor-beta1-induced epithelial–mesenchymal transition in hepatocellular carcinoma. Cancer Lett. *352*, 160–168.

Festenstein, H., and Garrido, F. (1986). Tumour immunology: MHC antigens and malignancy. Nature *322*, 502–503.

Fife, B.T., and Bluestone, J.A. (2008). Control of peripheral T-cell tolerance and autoimmunity via the CTLA-4 and PD-1 pathways. Immunol. Rev. *224*, 166–182.

Francisco, L.M., Salinas, V.H., Brown, K.E., Vanguri, V.K., Freeman, G.J., Kuchroo, V.K., and Sharpe, A.H. (2009). PD-L1 regulates the development, maintenance, and function of induced regulatory T cells. J. Exp. Med. *206*, 3015–3029.

Franco, R., Nicoletti, G., Lombardi, A., Domenico, M.D., Botti, G., Marino, F.Z., and Caraglia, M. (2013a). Current treatment of cutaneous squamous cancer and molecular strategies for its sensitization to new target-based drugs. Expert Opin. Biol. Ther. *13*, 51–66.

Franco, R., Nicoletti, G., Lombardi, A., Domenico, M.D., Botti, G., Marino, F.Z., and Caraglia, M. (2013b). Current treatment of cutaneous squamous cancer and molecular strategies for its sensitization to new target-based drugs. Expert Opin. Biol. Ther. *13*, 51–66.

Freeman, G.J., Long, A.J., Iwai, Y., Bourque, K., Chernova, T., Nishimura, H., Fitz, L.J., Malenkovich, N., Okazaki, T., Byrne, M.C., et al. (2000). Engagement of the Pd-1 Immunoinhibitory Receptor by a Novel B7 Family Member Leads to Negative Regulation of Lymphocyte Activation. J. Exp. Med. *192*, 1027–1034.

Fridman, W.H., Zitvogel, L., Sautès–Fridman, C., and Kroemer, G. (2017). The immune contexture in cancer prognosis and treatment. Nat. Rev. Clin. Oncol. *14*, 717–734.

Fruci, D., Benevolo, M., Cifaldi, L., Lorenzi, S., Monaco, E.L., Tremante, E., and Giacomini, P. (2012). Major Histocompatibility Complex Class I and Tumour Immuno-Evasion: How to Fool T Cells and Natural Killer Cells at One Time. Curr. Oncol. *19*, 39–41.

Fu, J., Xu, D., Liu, Z., Shi, M., Zhao, P., Fu, B., Zhang, Z., Yang, H., Zhang, H., Zhou, C., et al. (2007). Increased Regulatory T Cells Correlate With CD8 T-Cell Impairment and Poor Survival in Hepatocellular Carcinoma Patients. Gastroenterology *132*, 2328–2339.

Fu, Q., Fu, T.-M., Cruz, A.C., Sengupta, P., Thomas, S.K., Wang, S., Siegel, R.M., Wu, H., and Chou, J.J. (2016). Structural Basis and Functional Role of Intramembrane Trimerization of the Fas/CD95 Death Receptor. Mol. Cell *61*, 602–613.

Fukagawa, A., Ishii, H., Miyazawa, K., and Saitoh, M. (2015). δEF1 associates with DNMT1 and maintains DNA methylation of the E-cadherin promoter in breast cancer cells. Cancer Med. *4*, 125–135.

Füst, G., Medgyesi, G.A., Bazin, H., and Gergely, J. (1980). Differences in the ability of rat IgG subclasses to consume complement in homologous and heterologous serum. Immunol. Lett. *1*, 249–253.

Gabrilovich, D.I., and Nagaraj, S. (2009). Myeloid-derived suppressor cells as regulators of the immune system. Nat. Rev. Immunol. *9*, 162–174.

Gabrilovich, D.I., Ostrand-Rosenberg, S., and Bronte, V. (2012). Coordinated regulation of myeloid cells by tumours. Nat. Rev. Immunol. *12*, 253–268.

Galván, J.A., Helbling, M., Koelzer, V.H., Tschan, M.P., Berger, M.D., Hädrich, M., Schnüriger, B., Karamitopoulou, E., Dawson, H., Inderbitzin, D., et al. (2014). TWIST1 and TWIST2 promoter methylation and protein expression in tumor stroma influence the epithelial-mesenchymal transition-like tumor budding phenotype in colorectal cancer. Oncotarget *6*, 874–885.

Ganesh, K., and Massagué, J. (2018). TGF-β Inhibition and Immunotherapy: Checkmate. Immunity *48*, 626–628.

Gao, J., Shi, L.Z., Zhao, H., Chen, J., Xiong, L., He, Q., Chen, T., Roszik, J., Bernatchez, C., Woodman, S.E., et al. (2016). Loss of IFN-γ Pathway Genes in Tumor Cells as a Mechanism of Resistance to Anti-CTLA-4 Therapy. Cell *167*, 397-404.e9.

Garrido, F., Aptsiauri, N., Doorduijn, E.M., Garcia Lora, A.M., and van Hall, T. (2016). The urgent need to recover MHC class I in cancers for effective immunotherapy. Curr. Opin. Immunol. *39*, 44–51.

Gasteiger, G., and Rudensky, A.Y. (2014). Interactions between innate and adaptive lymphocytes. Nat. Rev. Immunol. *14*, 631–639.

Gasteiger, G., Hemmers, S., Firth, M.A., Le Floc'h, A., Huse, M., Sun, J.C., and Rudensky, A.Y. (2013). IL-2–dependent tuning of NK cell sensitivity for target cells is controlled by regulatory T cells. J. Exp. Med. *210*, 1167–1178.

Gautron, A.-S., Dominguez-Villar, M., Marcken, M. de, and Hafler, D.A. (2014). Enhanced suppressor function of TIM-3+FoxP3+ regulatory T cells. Eur. J. Immunol. *44*, 2703–2711.

Gettinger, S., Choi, J., Hastings, K., Truini, A., Datar, I., Sowell, R., Wurtz, A., Dong, W., Cai, G., Melnick, M.A., et al. (2017). Impaired HLA Class I Antigen Processing and Presentation as a Mechanism of Acquired Resistance to Immune Checkpoint Inhibitors in Lung Cancer. Cancer Discov. *7*, 1420–1435.

Ghittoni, R., Accardi, R., Hasan, U., Gheit, T., Sylla, B., and Tommasino, M. (2010). The biological properties of E6 and E7 oncoproteins from human papillomaviruses. Virus Genes *40*, 1–13.

Gocheva, V., Wang, H.-W., Gadea, B.B., Shree, T., Hunter, K.E., Garfall, A.L., Berman, T., and Joyce, J.A. (2010). IL-4 induces cathepsin protease activity in tumor-associated macrophages to promote cancer growth and invasion. Genes Dev. *24*, 241–255.

Gold, K.A., Kies, M.S., William, W.N., Johnson, F.M., Lee, J.J., and Glisson, B.S. (2018). Erlotinib in the treatment of recurrent or metastatic cutaneous squamous cell carcinoma: A single-arm phase 2 clinical trial. Cancer *124*, 2169–2173.

Gonzalez-Roca, E., Garcia-Albéniz, X., Rodriguez-Mulero, S., Gomis, R.R., Kornacker, K., and Auer, H. (2010). Accurate Expression Profiling of Very Small Cell Populations. PLOS ONE *5*, e14418.

Gordon, S.R., Maute, R.L., Dulken, B.W., Hutter, G., George, B.M., McCracken, M.N., Gupta, R., Tsai, J.M., Sinha, R., Corey, D., et al. (2017). PD-1 expression by tumour-associated macrophages inhibits phagocytosis and tumour immunity. Nature *545*, 495–499.

Gordy, C., and He, Y.-W. (2012). Endocytosis by target cells: an essential means for perforin- and granzyme-mediated killing. Cell. Mol. Immunol. *9*, 5–6.

Goswami, S., Sahai, E., Wyckoff, J.B., Cammer, M., Cox, D., Pixley, F.J., Stanley, E.R., Segall, J.E., and Condeelis, J.S. (2005). Macrophages Promote the Invasion of Breast Carcinoma Cells via a Colony-Stimulating Factor-1/Epidermal Growth Factor Paracrine Loop. Cancer Res. *65*, 5278–5283.

Granot, Z., Henke, E., Comen, E.A., King, T.A., Norton, L., and Benezra, R. (2011). Tumor Entrained Neutrophils Inhibit Seeding in the Premetastatic Lung. Cancer Cell *20*, 300–314.

Griffith, J.W., Sokol, C.L., and Luster, A.D. (2014). Chemokines and chemokine receptors: positioning cells for host defense and immunity. Annu. Rev. Immunol. *32*, 659–702.

Grob, J.-J., Gonzalez, R., Basset-Seguin, N., Vornicova, O., Schachter, J., Joshi, A., Meyer, N., Grange, F., Piulats, J.M., Bauman, J.R., et al. (2020). Pembrolizumab Monotherapy for Recurrent or Metastatic Cutaneous Squamous Cell Carcinoma: A Single-Arm Phase II Trial (KEYNOTE-629). J. Clin. Oncol.

Grosse-Wilde, A., d'Hérouël, A.F., McIntosh, E., Ertaylan, G., Skupin, A., Kuestner, R.E., Sol, A. del, Walters, K.-A., and Huang, S. (2015). Stemness of the hybrid Epithelial/Mesenchymal State in Breast Cancer and Its Association with Poor Survival. PLOS ONE *10*, e0126522.

Groth, C., Hu, X., Weber, R., Fleming, V., Altevogt, P., Utikal, J., and Umansky, V. (2019). Immunosuppression mediated by myeloid-derived suppressor cells (MDSCs) during tumour progression. Br. J. Cancer *120*, 16–25.

Gubin, M.M., Zhang, X., Schuster, H., Caron, E., Ward, J.P., Noguchi, T., Ivanova, Y., Hundal, J., Arthur, C.D., Krebber, W.-J., et al. (2014). Checkpoint blockade cancer immunotherapy targets tumour-specific mutant antigens. Nature *515*, 577–581.

Gunasinghe, N.P.A.D., Wells, A., Thompson, E.W., and Hugo, H.J. (2012). Mesenchymal–epithelial transition (MET) as a mechanism for metastatic colonisation in breast cancer. Cancer Metastasis Rev. *31*, 469–478.

Gupta, P.B., Chaffer, C.L., and Weinberg, R.A. (2009). Cancer stem cells: mirage or reality? Nat. Med. *15*, 1010–1012.

Gupta, P.B., Fillmore, C.M., Jiang, G., Shapira, S.D., Tao, K., Kuperwasser, C., and Lander, E.S. (2011). Stochastic State Transitions Give Rise to Phenotypic Equilibrium in Populations of Cancer Cells. Cell *146*, 633–644.

Guthrie, T.H., Porubsky, E.S., Luxenberg, M.N., Shah, K.J., Wurtz, K.L., and Watson, P.R. (1990). Cisplatin-based chemotherapy in advanced basal and squamous cell carcinomas of the skin: results in 28 patients including 13 patients receiving multimodality therapy. J. Clin. Oncol. *8*, 342–346.

Hanahan, D., and Weinberg, R.A. (2011). Hallmarks of Cancer: The Next Generation. Cell *144*, 646–674.

Harwood, C.A., Surentheran, T., McGregor, J.M., Spink, P.J., Leigh, I.M., Breuer, J., and Proby, C.M. (2000). Human papillomavirus infection and non-melanoma skin cancer in immunosuppressed and immunocompetent individuals. J. Med. Virol. *61*, 289–297.

He, X., and Xu, C. (2020). Immune checkpoint signaling and cancer immunotherapy. Cell Res. *30*, 660–669.

Highfill, S.L., Cui, Y., Giles, A.J., Smith, J.P., Zhang, H., Morse, E., Kaplan, R.N., and Mackall, C.L. (2014). Disruption of CXCR2-Mediated MDSC Tumor Trafficking Enhances Anti-PD1 Efficacy. Sci. Transl. Med. *6*, 237ra67-237ra67.

Hiraoka, N., Onozato, K., Kosuge, T., and Hirohashi, S. (2006). Prevalence of FOXP3+ Regulatory T Cells Increases During the Progression of Pancreatic Ductal Adenocarcinoma and Its Premalignant Lesions. Clin. Cancer Res. *12*, 5423–5434.

Holmgaard, R.B., Zamarin, D., Lesokhin, A., Merghoub, T., and Wolchok, J.D. (2016). Targeting myeloid-derived suppressor cells with colony stimulating factor-1 receptor blockade can reverse immune resistance to immunotherapy in indoleamine 2,3-dioxygenase-expressing tumors. EBioMedicine *6*, 50–58.

Hong, M., Clubb, J.D., and Chen, Y.Y. (2020). Engineering CAR-T Cells for Next-Generation Cancer Therapy. Cancer Cell *38*, 473–488.

Huang, C.-T., Workman, C.J., Flies, D., Pan, X., Marson, A.L., Zhou, G., Hipkiss, E.L., Ravi, S., Kowalski, J., Levitsky, H.I., et al. (2004). Role of LAG-3 in Regulatory T Cells. Immunity *21*, 503–513.

Huang, R.-Y., Eppolito, C., Lele, S., Shrikant, P., Matsuzaki, J., and Odunsi, K. (2015a). LAG3 and PD1 co-inhibitory molecules collaborate to limit CD8 + T cell signaling and dampen antitumor immunity in a murine ovarian cancer model. Oncotarget *6*, 27359–27377.

Huang, Y.-H., Zhu, C., Kondo, Y., Anderson, A.C., Gandhi, A., Russell, A., Dougan, S.K., Petersen, B.-S., Melum, E., Pertel, T., et al. (2015b). CEACAM1 regulates TIM-3-mediated tolerance and exhaustion. Nature *517*, 386–390.

Hugo, W., Zaretsky, J.M., Sun, L., Song, C., Moreno, B.H., Hu-Lieskovan, S., Berent-Maoz, B., Pang, J., Chmielowski, B., Cherry, G., et al. (2016). Genomic and Transcriptomic Features of Response to Anti-PD-1 Therapy in Metastatic Melanoma. Cell *165*, 35–44.

Hung, A.L., Maxwell, R., Theodros, D., Belcaid, Z., Mathios, D., Luksik, A.S., Kim, E., Wu, A., Xia, Y., Garzon-Muvdi, T., et al. (2018). TIGIT and PD-1 dual checkpoint blockade enhances antitumor immunity and survival in GBM. OncoImmunology *7*, e1466769.

Hwang, W.-L., Jiang, J.-K., Yang, S.-H., Huang, T.-S., Lan, H.-Y., Teng, H.-W., Yang, C.-Y., Tsai, Y.-P., Lin, C.-H., Wang, H.-W., et al. (2014). MicroRNA-146a directs the symmetric division of Snail-dominant colorectal cancer stem cells. Nat. Cell Biol. *16*, 268–280.

Iams, W.T., and Lovly, C.M. (2015). Molecular Pathways: Clinical Applications and Future Direction of Insulin-like Growth Factor-1 Receptor Pathway Blockade. Clin. Cancer Res. *21*, 4270–4277.

Ikeda, H., Old, L.J., and Schreiber, R.D. (2002). The roles of IFNγ in protection against tumor development and cancer immunoediting. Cytokine Growth Factor Rev. *13*, 95–109.

Ishida, Y., Agata, Y., Shibahara, K., and Honjo, T. (1992a). Induced expression of PD-1, a novel member of the immunoglobulin gene superfamily, upon programmed cell death. EMBO J. *11*, 3887–3895.

Ishida, Y., Agata, Y., Shibahara, K., and Honjo, T. (1992b). Induced expression of PD-1, a novel member of the immunoglobulin gene superfamily, upon programmed cell death. EMBO J. *11*, 3887–3895.

Ishikawa, H., Ma, Z., and Barber, G.N. (2009). STING regulates intracellular DNA-mediated, type I interferon-dependent innate immunity. Nature *461*, 788–792.

Jackson, H.J., Rafiq, S., and Brentjens, R.J. (2016). Driving CAR T-cells forward. Nat. Rev. Clin. Oncol. *13*, 370–383.

Jenkins, R.W., Barbie, D.A., and Flaherty, K.T. (2018). Mechanisms of resistance to immune checkpoint inhibitors. Br. J. Cancer *118*, 9–16.

Ji, A.L., Rubin, A.J., Thrane, K., Jiang, S., Reynolds, D.L., Meyers, R.M., Guo, M.G., George, B.M., Mollbrink, A., Bergenstråhle, J., et al. (2020). Multimodal Analysis of Composition and Spatial Architecture in Human Squamous Cell Carcinoma. Cell *182*, 497-514.e22.

Joffroy, C.M., Buck, M.B., Stope, M.B., Popp, S.L., Pfizenmaier, K., and Knabbe, C. (2010). Antiestrogens Induce Transforming Growth Factor β–Mediated Immunosuppression in Breast Cancer. Cancer Res. *70*, 1314–1322.

Johnston, R.J., Comps-Agrar, L., Hackney, J., Yu, X., Huseni, M., Yang, Y., Park, S., Javinal, V., Chiu, H., Irving, B., et al. (2014). The Immunoreceptor TIGIT Regulates Antitumor and Antiviral CD8+ T Cell Effector Function. Cancer Cell *26*, 923–937.

Jolly, M.K., Tripathi, S.C., Jia, D., Mooney, S.M., Celiktas, M., Hanash, S.M., Mani, S.A., Pienta, K.J., Ben-Jacob, E., and Levine, H. (2016). Stability of the hybrid epithelial/mesenchymal phenotype. Oncotarget *7*, 27067–27084.

Joyce, J.A., and Fearon, D.T. (2015). T cell exclusion, immune privilege, and the tumor microenvironment. Science *348*, 74–80.

Junttila, M.R., and de Sauvage, F.J. (2013). Influence of tumour micro-environment heterogeneity on therapeutic response. Nature *501*, 346–354.

Kadakia, S., Ducic, Y., Marra, D., Chan, D., Saman, M., Sawhney, R., and Mourad, M. (2016). Cutaneous squamous cell carcinoma of the scalp in the immunocompromised patient: review of 53 cases. Oral Maxillofac. Surg. *20*, 171–175.

Kalbasi, A., and Ribas, A. (2020). Tumour-intrinsic resistance to immune checkpoint blockade. Nat. Rev. Immunol. *20*, 25–39.

Kaplan, D.H., Shankaran, V., Dighe, A.S., Stockert, E., Aguet, M., Old, L.J., and Schreiber, R.D. (1998). Demonstration of an interferon γ-dependent tumor surveillance system in immunocompetent mice. Proc. Natl. Acad. Sci. *95*, 7556–7561.

Kauvar, A.N., Arpey, C., Hruza, G., Olbricht, S., and Bennett, R. (2015). Consensus for Nonmelanoma Skin Cancer Treatment, Part II: Squamous Cell Carcinoma, Including a Cost Analysis of Treatment Methods. Dermatol. Surg. *41*, 1214–1240.

Kayagaki, N., Yamaguchi, N., Nakayama, M., Takeda, K., Akiba, H., Tsutsui, H., Okamura, H., Nakanishi, K., Okumura, K., and Yagita, H. (1999). Expression and Function of TNF-Related Apoptosis-Inducing Ligand on Murine Activated NK Cells. J. Immunol. *163*, 1906–1913.

Ke, X.-S., Qu, Y., Cheng, Y., Li, W.-C., Rotter, V., Øyan, A.M., and Kalland, K.-H. (2010). Global profiling of histone and DNA methylation reveals epigenetic-based regulation of gene expression during epithelial to mesenchymal transition in prostate cells. BMC Genomics *11*, 669.

Keenan, T.E., Burke, K.P., and Van Allen, E.M. (2019). Genomic correlates of response to immune checkpoint blockade. Nat. Med. *25*, 389–402.

Khan, M., Arooj, S., and Wang, H. (2020). NK Cell-Based Immune Checkpoint Inhibition. Front. Immunol. *11*.

Kim, E.S., Kim, J.E., Patel, M.A., Mangraviti, A., Ruzevick, J., and Lim, M. (2016). Immune Checkpoint Modulators: An Emerging Antiglioma Armamentarium. J. Immunol. Res. *2016*.

Kobayashi, N., Hiraoka, N., Yamagami, W., Ojima, H., Kanai, Y., Kosuge, T., Nakajima, A., and Hirohashi, S. (2007). FOXP3+ Regulatory T Cells Affect the Development and Progression of Hepatocarcinogenesis. Clin. Cancer Res. *13*, 902–911.

Kono, K., Kawaida, H., Takahashi, A., Sugai, H., Mimura, K., Miyagawa, N., Omata, H., and Fujii, H. (2006). CD4(+)CD25high regulatory T cells increase with tumor stage in patients with gastric and esophageal cancers. Cancer Immunol. Immunother. *55*, 1064–1071.

Kouo, T., Huang, L., Pucsek, A.B., Cao, M., Solt, S., Armstrong, T., and Jaffee, E. (2015). Galectin-3 Shapes Antitumor Immune Responses by Suppressing CD8+ T Cells via LAG-3 and Inhibiting Expansion of Plasmacytoid Dendritic Cells. Cancer Immunol. Res. *3*, 412–423.

Kudo-Saito, C., Shirako, H., Takeuchi, T., and Kawakami, Y. (2009). Cancer Metastasis Is Accelerated through Immunosuppression during Snail-Induced EMT of Cancer Cells. Cancer Cell *15*, 195–206.

Kumar, V., Patel, S., Tcyganov, E., and Gabrilovich, D.I. (2016). The Nature of Myeloid-Derived Suppressor Cells in the Tumor Microenvironment. Trends Immunol. *37*, 208–220.

Kwon, J., and Bakhoum, S.F. (2020). The Cytosolic DNA-Sensing cGAS–STING Pathway in Cancer. Cancer Discov. *10*, 26–39.

Labanieh, L., Majzner, R.G., and Mackall, C.L. (2018). Programming CAR-T cells to kill cancer. Nat. Biomed. Eng. *2*, 377–391.

Lambrechts, D., Wauters, E., Boeckx, B., Aibar, S., Nittner, D., Burton, O., Bassez, A., Decaluwé, H., Pircher, A., Eynde, K.V. den, et al. (2018). Phenotype molding of stromal cells in the lung tumor microenvironment. Nat. Med. *24*, 1277–1289.

Lamouille, S., Xu, J., and Derynck, R. (2014). Molecular mechanisms of epithelial–mesenchymal transition. Nat. Rev. Mol. Cell Biol. *15*, 178–196.

Landsberg, J., Kohlmeyer, J., Renn, M., Bald, T., Rogava, M., Cron, M., Fatho, M., Lennerz, V., Wölfel, T., Hölzel, M., et al. (2012). Melanomas resist T-cell therapy through inflammation-induced reversible dedifferentiation. Nature *490*, 412–416.

Lanitis, E., Coukos, G., and Irving, M. (2020). All systems go: converging synthetic biology and combinatorial treatment for CAR-T cell therapy. Curr. Opin. Biotechnol. *65*, 75–87.

Lapouge, G., Beck, B., Nassar, D., Dubois, C., Dekoninck, S., and Blanpain, C. (2012). Skin squamous cell carcinoma propagating cells increase with tumour progression and invasiveness. EMBO J. *31*, 4563–4575.

Larionova, I., Tuguzbaeva, G., Ponomaryova, A., Stakheyeva, M., Cherdyntseva, N., Pavlov, V., Choinzonov, E., and Kzhyshkowska, J. (2020). Tumor-Associated Macrophages in Human Breast, Colorectal, Lung, Ovarian and Prostate Cancers. Front. Oncol. *10*.

Latil, M., Nassar, D., Beck, B., Boumahdi, S., Wang, L., Brisebarre, A., Dubois, C., Nkusi, E., Lenglez, S., Checinska, A., et al. (2017). Cell-Type-Specific Chromatin States Differentially Prime Squamous Cell Carcinoma Tumor-Initiating Cells for Epithelial to Mesenchymal Transition. Cell Stem Cell *20*, 191-204.e5.

Lau, S.K., Chu, P.G., and Weiss, L.M. (2004). CD163: A Specific Marker of Macrophages in Paraffin-Embedded Tissue Samples. Am. J. Clin. Pathol. *122*, 794–801.

Law, A.M.K., Valdes-Mora, F., and Gallego-Ortega, D. (2020). Myeloid-Derived Suppressor Cells as a Therapeutic Target for Cancer. Cells *9*, 561.

Le, D.T., Durham, J.N., Smith, K.N., Wang, H., Bartlett, B.R., Aulakh, L.K., Lu, S., Kemberling, H., Wilt, C., Luber, B.S., et al. (2017). Mismatch repair deficiency predicts response of solid tumors to PD-1 blockade. Science *357*, 409–413.

Leach, D.R., Krummel, M.F., and Allison, J.P. (1996). Enhancement of Antitumor Immunity by CTLA-4 Blockade. Science *271*, 1734–1736.

Lee, J.H., Shklovskaya, E., Lim, S.Y., Carlino, M.S., Menzies, A.M., Stewart, A., Pedersen, B., Irvine, M., Alavi, S., Yang, J.Y.H., et al. (2020). Transcriptional downregulation of MHC class I and melanoma de- differentiation in resistance to PD-1 inhibition. Nat. Commun. *11*, 1897.

Leiter, U., Eigentler, T., and Garbe, C. (2014). Epidemiology of Skin Cancer. In Sunlight, Vitamin D and Skin Cancer, J. Reichrath, ed. (New York, NY: Springer), pp. 120–140.

Lesokhin, A.M., Hohl, T.M., Kitano, S., Cortez, C., Hirschhorn-Cymerman, D., Avogadri, F., Rizzuto, G.A., Lazarus, J.J., Pamer, E.G., Houghton, A.N., et al. (2012). Monocytic CCR2+ Myeloid-Derived Suppressor Cells Promote Immune Escape by Limiting Activated CD8 T-cell Infiltration into the Tumor Microenvironment. Cancer Res. *72*, 876–886.

Lewis, S.M., Williams, A., and Eisenbarth, S.C. (2019). Structure-function of the immune system in the spleen. Sci. Immunol. *4*.

Li, A., Omura, N., Hong, S.-M., Vincent, A., Walter, K., Griffith, M., Borges, M., and Goggins, M. (2010). Pancreatic Cancers Epigenetically Silence SIP1 and Hypomethylate and Overexpress miR-200a/200b in Association with Elevated Circulating miR-200a and miR-200b Levels. Cancer Res. *70*, 5226–5237.

Li, H., Leun, A.M. van der, Yofe, I., Lubling, Y., Gelbard-Solodkin, D., Akkooi, A.C.J. van, Braber, M. van den, Rozeman, E.A., Haanen, J.B.A.G., Blank, C.U., et al. (2019). Dysfunctional CD8 T Cells Form a Proliferative, Dynamically Regulated Compartment within Human Melanoma. Cell *176*, 775-789.e18.

Li, Z.-L., Ye, S.-B., OuYang, L.-Y., Zhang, H., Chen, Y.-S., He, J., Chen, Q.-Y., Qian, C.-N., Zhang, X.-S., Cui, J., et al. (2015). COX-2 promotes metastasis in nasopharyngeal carcinoma by mediating interactions between cancer cells and myeloid-derived suppressor cells. OncoImmunology *4*, e1044712.

Liang, B., Workman, C., Lee, J., Chew, C., Dale, B.M., Colonna, L., Flores, M., Li, N., Schweighoffer, E., Greenberg, S., et al. (2008). Regulatory T Cells Inhibit Dendritic Cells by Lymphocyte Activation Gene-3 Engagement of MHC Class II. J. Immunol. *180*, 5916–5926.

Lim, W.A., and June, C.H. (2017). The Principles of Engineering Immune Cells to Treat Cancer. Cell *168*, 724–740.

Lim, S.-O., Gu, J.-M., Kim, M.S., Kim, H.-S., Park, Y.N., Park, C.K., Cho, J.W., Park, Y.M., and Jung, G. (2008). Epigenetic Changes Induced by Reactive Oxygen Species in Hepatocellular Carcinoma: Methylation of the E-cadherin Promoter. Gastroenterology *135*, 2128-2140.e8.

Lin, E.Y., Nguyen, A.V., Russell, R.G., and Pollard, J.W. (2001). Colony-Stimulating Factor 1 Promotes Progression of Mammary Tumors to Malignancy. J. Exp. Med. *193*, 727–740.

Lin, E.Y., Li, J.-F., Gnatovskiy, L., Deng, Y., Zhu, L., Grzesik, D.A., Qian, H., Xue, X., and Pollard, J.W. (2006). Macrophages Regulate the Angiogenic Switch in a Mouse Model of Breast Cancer. Cancer Res. *66*, 11238–11246.

Linde, N., Lederle, W., Depner, S., Rooijen, N. van, Gutschalk, C.M., and Mueller, M.M. (2012). Vascular endothelial growth factor-induced skin carcinogenesis depends on recruitment and alternative activation of macrophages. J. Pathol. *227*, 17–28.

Liu, C.-Y., Xu, J.-Y., Shi, X.-Y., Huang, W., Ruan, T.-Y., Xie, P., and Ding, J.-L. (2013). M2-polarized tumor-associated macrophages promoted epithelial–mesenchymal transition in pancreatic cancer cells, partially through TLR4/IL-10 signaling pathway. Lab. Invest. *93*, 844–854.

Liu, D., Schilling, B., Liu, D., Sucker, A., Livingstone, E., Jerby-Arnon, L., Zimmer, L., Gutzmer, R., Satzger, I., Loquai, C., et al. (2019). Integrative molecular and clinical modeling of clinical outcomes to PD1 blockade in patients with metastatic melanoma. Nat. Med. *25*, 1916–1927.

Liu, X., Pu, Y., Cron, K., Deng, L., Kline, J., Frazier, W.A., Xu, H., Peng, H., Fu, Y.-X., and Xu, M.M. (2015). CD47 blockade triggers T cell–mediated destruction of immunogenic tumors. Nat. Med. *21*, 1209–1215.

Lomas, A., Leonardi-Bee, J., and Bath-Hextall, F. (2012). A systematic review of worldwide incidence of nonmelanoma skin cancer. Br. J. Dermatol. *166*, 1069–1080.

Long, E.O., Sik Kim, H., Liu, D., Peterson, M.E., and Rajagopalan, S. (2013). Controlling Natural Killer Cell Responses: Integration of Signals for Activation and Inhibition. Annu. Rev. Immunol. *31*, 227–258.

Lorenzo-Sanz, L., and Muñoz, P. (2019). Tumor-Infiltrating Immunosuppressive Cells in Cancer-Cell Plasticity, Tumor Progression and Therapy Response. Cancer Microenviron. *12*, 119–132.

Lou, Y., Diao, L., Cuentas, E.R.P., Denning, W.L., Chen, L., Fan, Y.H., Byers, L.A., Wang, J., Papadimitrakopoulou, V.A., Behrens, C., et al. (2016). Epithelial–Mesenchymal Transition Is Associated with a Distinct Tumor Microenvironment Including Elevation of Inflammatory Signals and Multiple Immune Checkpoints in Lung Adenocarcinoma. Clin. Cancer Res. *22*, 3630–3642.

Louis, C.U., Savoldo, B., Dotti, G., Pule, M., Yvon, E., Myers, G.D., Rossig, C., Russell, H.V., Diouf, O., Liu, E., et al. (2011). Antitumor activity and long-term fate of chimeric antigen receptor–positive T cells in patients with neuroblastoma. Blood *118*, 6050–6056.

Lu, H., Clauser, K.R., Tam, W.L., Fröse, J., Ye, X., Eaton, E.N., Reinhardt, F., Donnenberg, V.S., Bhargava, R., Carr, S.A., et al. (2014). A breast cancer stem cell niche supported by juxtacrine signalling from monocytes and macrophages. Nat. Cell Biol. *16*, 1105–1117.

Mackay, W.D. (1965). Role of Splenomegaly in Tumour-bearing Mice. Nature *205*, 918–919.

Madan, V., Lear, J.T., and Szeimies, R.-M. (2010). Non-melanoma skin cancer. The Lancet *375*, 673–685.

Maddipati, R., and Stanger, B.Z. (2015). Pancreatic Cancer Metastases Harbor Evidence of Polyclonality. Cancer Discov. *5*, 1086–1097.

Maimon, A., Levi-Yahid, V., Ben-Meir, K., Halpern, A., Talmi, Z., Priya, S., Mizraji, G., Mistriel-Zerbib, S., Berger, M., Baniyash, M., et al. (2021). Myeloid cell-derived PROS1 inhibits tumor metastasis by regulating inflammatory and immune responses via IL-10. J. Clin. Invest.

Malanchi, I., Peinado, H., Kassen, D., Hussenet, T., Metzger, D., Chambon, P., Huber, M., Hohl, D., Cano, A., Birchmeier, W., et al. (2008). Cutaneous cancer stem cell maintenance is dependent on β-catenin signalling. Nature *452*, 650–653.

Mani, S.A., Guo, W., Liao, M.-J., Eaton, E.N., Ayyanan, A., Zhou, A.Y., Brooks, M., Reinhard, F., Zhang, C.C., Shipitsin, M., et al. (2008). The Epithelial-Mesenchymal Transition Generates Cells with Properties of Stem Cells. Cell *133*, 704–715.

Mantovani, A. (2010). The growing diversity and spectrum of action of myeloid-derived suppressor cells. Eur. J. Immunol. *40*, 3317–3320.

Mantovani, A., Sozzani, S., Locati, M., Allavena, P., and Sica, A. (2002). Macrophage polarization: tumor-associated macrophages as a paradigm for polarized M2 mononuclear phagocytes. Trends Immunol. *23*, 549–555.

Mantovani, A., Cassatella, M.A., Costantini, C., and Jaillon, S. (2011). Neutrophils in the activation and regulation of innate and adaptive immunity. Nat. Rev. Immunol. *11*, 519–531.

Mantovani, A., Marchesi, F., Malesci, A., Laghi, L., and Allavena, P. (2017). Tumour-associated macrophages as treatment targets in oncology. Nat. Rev. Clin. Oncol. *14*, 399–416.

Mariathasan, S., Turley, S.J., Nickles, D., Castiglioni, A., Yuen, K., Wang, Y., Kadel Iii, E.E., Koeppen, H., Astarita, J.L., Cubas, R., et al. (2018). TGFβ attenuates tumour response to PD-L1 blockade by contributing to exclusion of T cells. Nature *554*, 544–548.

Marjanovic, N.D., Weinberg, R.A., and Chaffer, C.L. (2013). Cell Plasticity and Heterogeneity in Cancer. Clin. Chem. *59*, 168–179.

Martinet, L., Ferrari De Andrade, L., Guillerey, C., Lee, J.S., Liu, J., Souza-Fonseca-Guimaraes, F., Hutchinson, D.S., Kolesnik, T.B., Nicholson, S.E., Huntington, N.D., et al. (2015). DNAM-1 Expression Marks an Alternative Program of NK Cell Maturation. Cell Rep. *11*, 85–97.

Marvel, D., and Gabrilovich, D.I. (2015). Myeloid-derived suppressor cells in the tumor microenvironment: expect the unexpected. J. Clin. Invest. *125*, 3356–3364.

Massagué, J. (2008). TGFβ in Cancer. Cell *134*, 215–230.

Massagué, J., and Ganesh, K. (2021). Metastasis-Initiating Cells and Ecosystems. Cancer Discov. *11*, 971–994.

Maubec, E., Duvillard, P., Velasco, V., Crickx, B., and Avril, M.-F. (2005). Immunohistochemical Analysis of EGFR and HER-2 in Patients with Metastatic Squamous Cell Carcinoma of the Skin. Anticancer Res. *25*, 1205–1210.

Maubec, E., Petrow, P., Scheer-Senyarich, I., Duvillard, P., Lacroix, L., Gelly, J., Certain, A., Duval, X., Crickx, B., Buffard, V., et al. (2011). Phase II Study of Cetuximab As First-Line Single-Drug Therapy in Patients With Unresectable Squamous Cell Carcinoma of the Skin. J. Clin. Oncol. *29*, 3419–3426.

McGranahan, N., and Swanton, C. (2017). Clonal Heterogeneity and Tumor Evolution: Past, Present, and the Future. Cell *168*, 613–628.

McGranahan, N., Furness, A.J.S., Rosenthal, R., Ramskov, S., Lyngaa, R., Saini, S.K., Jamal-Hanjani, M., Wilson, G.A., Birkbak, N.J., Hiley, C.T., et al. (2016). Clonal neoantigens elicit T cell immunoreactivity and sensitivity to immune checkpoint blockade. Science *351*, 1463–1469.

Meacham, C.E., and Morrison, S.J. (2013). Tumour heterogeneity and cancer cell plasticity. Nature *501*, 328–337.

Melero, I., Berman, D.M., Aznar, M.A., Korman, A.J., Gracia, J.L.P., and Haanen, J. (2015). Evolving synergistic combinations of targeted immunotherapies to combat cancer. Nat. Rev. Cancer *15*, 457–472.

Messmer, M.N., Netherby, C.S., Banik, D., and Abrams, S.I. (2015). Tumor-induced myeloid dysfunction and its implications for cancer immunotherapy. Cancer Immunol. Immunother. *64*, 1–13.

Meyer, C., Cagnon, L., Costa-Nunes, C.M., Baumgaertner, P., Montandon, N., Leyvraz, L., Michielin, O., Romano, E., and Speiser, D.E. (2014). Frequencies of circulating MDSC correlate with clinical outcome of melanoma patients treated with ipilimumab. Cancer Immunol. Immunother. *63*, 247–257.

Miao, Y., Yang, H., Levorse, J., Yuan, S., Polak, L., Sribour, M., Singh, B., Rosenblum, M.D., and Fuchs, E. (2019). Adaptive Immune Resistance Emerges from Tumor-Initiating Stem Cells. Cell *177*, 1172-1186.e14.

Migden, M.R., Rischin, D., Schmults, C.D., Guminski, A., Hauschild, A., Lewis, K.D., Chung, C.H., Hernandez-Aya, L., Lim, A.M., Chang, A.L.S., et al. (2018). PD-1 Blockade with Cemiplimab in Advanced Cutaneous Squamous-Cell Carcinoma. N. Engl. J. Med. *379*, 341–351.

van der Mijn, J.C., Labots, M., Piersma, S.R., Pham, T.V., Knol, J.C., Broxterman, H.J., Verheul, H.M., and Jiménez, C.R. (2015). Evaluation of different phospho-tyrosine antibodies for label-free phosphoproteomics. J. Proteomics *127*, 259–263.

Moody, C.A., and Laimins, L.A. (2010). Human papillomavirus oncoproteins: pathways to transformation. Nat. Rev. Cancer *10*, 550–560.

Morel, A.-P., Lièvre, M., Thomas, C., Hinkal, G., Ansieau, S., and Puisieux, A. (2008). Generation of Breast Cancer Stem Cells through Epithelial-Mesenchymal Transition. PLOS ONE *3*, e2888.

Morel, K.L., Sheahan, A.V., Burkhart, D.L., Baca, S.C., Boufaied, N., Liu, Y., Qiu, X., Cañadas, I., Roehle, K., Heckler, M., et al. (2021). EZH2 inhibition activates a dsRNA–STING–interferon stress axis that potentiates response to PD-1 checkpoint blockade in prostate cancer. Nat. Cancer *2*, 444–456.

Moretta, A., Marcenaro, E., Parolini, S., Ferlazzo, G., and Moretta, L. (2008). NK cells at the interface between innate and adaptive immunity. Cell Death Differ. *15*, 226–233.

Morris, L.G.T., Kaufman, A.M., Gong, Y., Ramaswami, D., Walsh, L.A., Turcan, Ş., Eng, S., Kannan, K., Zou, Y., Peng, L., et al. (2013). Recurrent somatic mutation of FAT1 in multiple human cancers leads to aberrant Wnt activation. Nat. Genet. *45*, 253–261.

Mosser, D.M., and Edwards, J.P. (2008). Exploring the full spectrum of macrophage activation. Nat. Rev. Immunol. *8*, 958–969.

Muntasell, A., Ochoa, M.C., Cordeiro, L., Berraondo, P., López-Díaz de Cerio, A., Cabo, M., López-Botet, M., and Melero, I. (2017). Targeting NK-cell checkpoints for cancer immunotherapy. Curr. Opin. Immunol. *45*, 73–81.

Murciano-Goroff, Y.R., Warner, A.B., and Wolchok, J.D. (2020). The future of cancer immunotherapy: microenvironment-targeting combinations. Cell Res. *30*, 507–519.

Murray, P.J. (2017). Macrophage Polarization. Annu. Rev. Physiol. *79*, 541–566.

Murray, P.J., and Wynn, T.A. (2011). Protective and pathogenic functions of macrophage subsets. Nat. Rev. Immunol. *11*, 723–737.

Murray, P.J., Allen, J.E., Biswas, S.K., Fisher, E.A., Gilroy, D.W., Goerdt, S., Gordon, S., Hamilton, J.A., Ivashkiv, L.B., Lawrence, T., et al. (2014). Macrophage Activation and Polarization: Nomenclature and Experimental Guidelines. Immunity *41*, 14–20.

Nagarsheth, N., Wicha, M.S., and Zou, W. (2017). Chemokines in the cancer microenvironment and their relevance in cancer immunotherapy. Nat. Rev. Immunol. *17*, 559–572.

Narayanan, S., Ahl, P.J., Bijin, V.A., Kaliaperumal, N., Lim, S.G., Wang, C.-I., Fairhurst, A.-M., and Connolly, J.E. (2020). LAG3 is a Central Regulator of NK Cell Cytokine Production. BioRxiv 2020.01.31.928200.

Newick, K., Moon, E., and Albelda, S.M. (2016). Chimeric antigen receptor T-cell therapy for solid tumors. Mol. Ther. - Oncolytics *3*, 16006.

Nieto, M.A., Huang, R.Y.-J., Jackson, R.A., and Thiery, J.P. (2016). EMT: 2016. Cell *166*, 21–45.

Nikolich-Žugich, J., Slifka, M.K., and Messaoudi, I. (2004). The many important facets of T-cell repertoire diversity. Nat. Rev. Immunol. *4*, 123–132.

Nikolova, M., Lelievre, J.-D., Carriere, M., Bensussan, A., and Lévy, Y. (2009). Regulatory T cells differentially modulate the maturation and apoptosis of human CD8+ T-cell subsets. Blood *113*, 4556–4565.

Nishimura, H., Nose, M., Hiai, H., Minato, N., and Honjo, T. (1999). Development of Lupus-like Autoimmune Diseases by Disruption of the PD-1 Gene Encoding an ITIM Motif-Carrying Immunoreceptor. Immunity *11*, 141–151.

Noman, M.Z., Desantis, G., Janji, B., Hasmim, M., Karray, S., Dessen, P., Bronte, V., and Chouaib, S. (2014). PD-L1 is a novel direct target of HIF-1α, and its blockade under hypoxia enhanced MDSC-mediated T cell activation. J. Exp. Med. *211*, 781–790.

Noman, M.Z., Janji, B., Abdou, A., Hasmim, M., Terry, S., Tan, T.Z., Mami-Chouaib, F., Thiery, J.P., and Chouaib, S. (2017). The immune checkpoint ligand PD-L1 is upregulated in EMT-activated human breast cancer cells by a mechanism involving ZEB-1 and miR-200. OncoImmunology *6*, e1263412.

Nowell, P.C. (1976). The clonal evolution of tumor cell populations. Science *194*, 23–28.

Ocaña, O.H., Córcoles, R., Fabra, Á., Moreno-Bueno, G., Acloque, H., Vega, S., Barrallo-Gimeno, A., Cano, A., and Nieto, M.A. (2012). Metastatic Colonization Requires the Repression of the Epithelial-Mesenchymal Transition Inducer Prrx1. Cancer Cell *22*, 709–724.

Odorizzi, P.M., and Wherry, E.J. (2012). Inhibitory Receptors on Lymphocytes: Insights from Infections. J. Immunol. *188*, 2957–2965.

Oh, K., Lee, O.-Y., Shon, S.Y., Nam, O., Ryu, P.M., Seo, M.W., and Lee, D.-S. (2013). A mutual activation loop between breast cancer cells and myeloid-derived suppressor cells facilitates spontaneous metastasis through IL-6 trans-signaling in a murine model. Breast Cancer Res. *15*, R79.

Oh, S.A., Wu, D.-C., Cheung, J., Navarro, A., Xiong, H., Cubas, R., Totpal, K., Chiu, H., Wu, Y., Comps-Agrar, L., et al. (2020). PD-L1 expression by dendritic cells is a key regulator of T-cell immunity in cancer. Nat. Cancer *1*, 681–691.

Ostrand-Rosenberg, S. (2010). Myeloid-derived suppressor cells: more mechanisms for inhibiting antitumor immunity. Cancer Immunol. Immunother. *59*, 1593–1600.

Ouzounova, M., Lee, E., Piranlioglu, R., El Andaloussi, A., Kolhe, R., Demirci, M.F., Marasco, D., Asm, I., Chadli, A., Hassan, K.A., et al. (2017). Monocytic and granulocytic myeloid derived suppressor cells differentially regulate spatiotemporal tumour plasticity during metastatic cascade. Nat. Commun. *8*, 14979.

Pan, P.-Y., Ma, G., Weber, K.J., Ozao-Choy, J., Wang, G., Yin, B., Divino, C.M., and Chen, S.-H. (2010). Immune Stimulatory Receptor CD40 Is Required for T-Cell Suppression and T Regulatory Cell Activation Mediated by Myeloid-Derived Suppressor Cells in Cancer. Cancer Res. *70*, 99–108.

Panni, R.Z., Sanford, D.E., Belt, B.A., Mitchem, J.B., Worley, L.A., Goetz, B.D., Mukherjee, P., Wang-Gillam, A., Link, D.C., DeNardo, D.G., et al. (2014). Tumor-induced STAT3 activation in

monocytic myeloid-derived suppressor cells enhances stemness and mesenchymal properties in human pancreatic cancer. Cancer Immunol. Immunother. *63*, 513–528.

Pardoll, D.M. (2012). The blockade of immune checkpoints in cancer immunotherapy. Nat. Rev. Cancer *12*, 252–264.

Parham, P. (2005). MHC class I molecules and kirs in human history, health and survival. Nat. Rev. Immunol. *5*, 201–214.

Park, J.R., DiGiusto, D.L., Slovak, M., Wright, C., Naranjo, A., Wagner, J., Meechoovet, H.B., Bautista, C., Chang, W.-C., Ostberg, J.R., et al. (2007). Adoptive Transfer of Chimeric Antigen Receptor Re-directed Cytolytic T Lymphocyte Clones in Patients with Neuroblastoma. Mol. Ther. *15*, 825–833.

Park, S.-M., Gaur, A.B., Lengyel, E., and Peter, M.E. (2008). The miR-200 family determines the epithelial phenotype of cancer cells by targeting the E-cadherin repressors ZEB1 and ZEB2. Genes Dev. *22*, 894–907.

Parry, R.V., Chemnitz, J.M., Frauwirth, K.A., Lanfranco, A.R., Braunstein, I., Kobayashi, S.V., Linsley, P.S., Thompson, C.B., and Riley, J.L. (2005). CTLA-4 and PD-1 Receptors Inhibit T-Cell Activation by Distinct Mechanisms. Mol. Cell. Biol. *25*, 9543–9553.

Pastushenko, I., Brisebarre, A., Sifrim, A., Fioramonti, M., Revenco, T., Boumahdi, S., Van Keymeulen, A., Brown, D., Moers, V., Lemaire, S., et al. (2018). Identification of the tumour transition states occurring during EMT. Nature *556*, 463–468.

Pastushenko, I., Mauri, F., Song, Y., de Cock, F., Meeusen, B., Swedlund, B., Impens, F., Van Haver, D., Opitz, M., Thery, M., et al. (2021). Fat1 deletion promotes hybrid EMT state, tumour stemness and metastasis. Nature *589*, 448–455.

Patel, S.J., Sanjana, N.E., Kishton, R.J., Eidizadeh, A., Vodnala, S.K., Cam, M., Gartner, J.J., Jia, L., Steinberg, S.M., Yamamoto, T.N., et al. (2017). Identification of essential genes for cancer immunotherapy. Nature *548*, 537–542.

Pattabiraman, D.R., and Weinberg, R.A. (2014). Tackling the cancer stem cells — what challenges do they pose? Nat. Rev. Drug Discov. *13*, 497–512.

Pattabiraman, D.R., Bierie, B., Kober, K.I., Thiru, P., Krall, J.A., Zill, C., Reinhardt, F., Tam, W.L., and Weinberg, R.A. (2016). Activation of PKA leads to mesenchymal-to-epithelial transition and loss of tumor-initiating ability. Science *351*.

Pauken, K.E., Dougan, M., Rose, N.R., Lichtman, A.H., and Sharpe, A.H. (2019). Adverse Events Following Cancer Immunotherapy: Obstacles and Opportunities. Trends Immunol. *40*, 511–523.

Peggs, K.S., Quezada, S.A., Chambers, C.A., Korman, A.J., and Allison, J.P. (2009). Blockade of CTLA-4 on both effector and regulatory T cell compartments contributes to the antitumor activity of anti–CTLA-4 antibodies. J. Exp. Med. *206*, 1717–1725.

Peinado, H., Olmeda, D., and Cano, A. (2007). Snail, Zeb and bHLH factors in tumour progression: an alliance against the epithelial phenotype? Nat. Rev. Cancer *7*, 415–428.

Peng, D., Tanikawa, T., Li, W., Zhao, L., Vatan, L., Szeliga, W., Wan, S., Wei, S., Wang, Y., Liu, Y., et al. (2016). Myeloid-Derived Suppressor Cells Endow Stem-like Qualities to Breast Cancer Cells through IL6/STAT3 and NO/NOTCH Cross-talk Signaling. Cancer Res. *76*, 3156–3165.

Pesce, S., Greppi, M., Tabellini, G., Rampinelli, F., Parolini, S., Olive, D., Moretta, L., Moretta, A., and Marcenaro, E. (2017). Identification of a subset of human natural killer cells expressing high levels of programmed death 1: A phenotypic and functional characterization. J. Allergy Clin. Immunol. *139*, 335-346.e3.

Pickering, C.R., Zhou, J.H., Lee, J.J., Drummond, J.A., Peng, S.A., Saade, R.E., Tsai, K.Y., Curry, J.L., Tetzlaff, M.T., Lai, S.Y., et al. (2014). Mutational Landscape of Aggressive Cutaneous Squamous Cell Carcinoma. Clin. Cancer Res. *20*, 6582–6592.

Platanias, L.C. (2005). Mechanisms of type-I- and type-II-interferon-mediated signalling. Nat. Rev. Immunol. *5*, 375–386.

Polyak, K., and Weinberg, R.A. (2009). Transitions between epithelial and mesenchymal states: acquisition of malignant and stem cell traits. Nat. Rev. Cancer *9*, 265–273.

Psaila, B., and Lyden, D. (2009). The metastatic niche: adapting the foreign soil. Nat. Rev. Cancer *9*, 285–293.

Puisieux, A., Brabletz, T., and Caramel, J. (2014). Oncogenic roles of EMT-inducing transcription factors. Nat. Cell Biol. *16*, 488–494.

Puram, S.V., Tirosh, I., Parikh, A.S., Patel, A.P., Yizhak, K., Gillespie, S., Rodman, C., Luo, C.L., Mroz, E.A., Emerick, K.S., et al. (2017). Single-Cell Transcriptomic Analysis of Primary and Metastatic Tumor Ecosystems in Head and Neck Cancer. Cell *171*, 1611-1624.e24.

Pyonteck, S.M., Akkari, L., Schuhmacher, A.J., Bowman, R.L., Sevenich, L., Quail, D.F., Olson, O.C., Quick, M.L., Huse, J.T., Teijeiro, V., et al. (2013). CSF-1R inhibition alters macrophage polarization and blocks glioma progression. Nat. Med. *19*, 1264–1272.

Qi, X.-K., Han, H.-Q., Zhang, H.-J., Xu, M., Li, L., Chen, L., Xiang, T., Feng, Q.-S., Kang, T., Qian, C.-N., et al. (2018). OVOL2 links stemness and metastasis via fine-tuning epithelial-mesenchymal transition in nasopharyngeal carcinoma. Theranostics *8*, 2202–2216.

Qian, B., and Pollard, J.W. (2010). Macrophage Diversity Enhances Tumor Progression and Metastasis. Cell *141*, 39–51.

Qian, B., Deng, Y., Im, J.H., Muschel, R.J., Zou, Y., Li, J., Lang, R.A., and Pollard, J.W. (2009). A Distinct Macrophage Population Mediates Metastatic Breast Cancer Cell Extravasation, Establishment and Growth. PLOS ONE *4*, e6562.

Qian, B.-Z., Li, J., Zhang, H., Kitamura, T., Zhang, J., Campion, L.R., Kaiser, E.A., Snyder, L.A., and Pollard, J.W. (2011). CCL2 recruits inflammatory monocytes to facilitate breast-tumour metastasis. Nature *475*, 222–225.

Qin, S., Xu, L., Yi, M., Yu, S., Wu, K., and Luo, S. (2019). Novel immune checkpoint targets: moving beyond PD-1 and CTLA-4. Mol. Cancer *18*, 155.

Quail, D.F., and Joyce, J.A. (2013). Microenvironmental regulation of tumor progression and metastasis. Nat. Med. *19*, 1423–1437.

Rafiq, S., Hackett, C.S., and Brentjens, R.J. (2020). Engineering strategies to overcome the current roadblocks in CAR T cell therapy. Nat. Rev. Clin. Oncol. *17*, 147–167.

Ratushny, V., Gober, M.D., Hick, R., Ridky, T.W., and Seykora, J.T. (2012). From keratinocyte to cancer: the pathogenesis and modeling of cutaneous squamous cell carcinoma. J. Clin. Invest. *122*, 464–472.

Raulet, D.H., Vance, R.E., and McMahon, C.W. (2001). Regulation of the Natural Killer Cell Receptor Repertoire. Annu. Rev. Immunol. *19*, 291–330.

Read, S., Malmström, V., and Powrie, F. (2000). Cytotoxic T Lymphocyte–Associated Antigen 4 Plays an Essential Role in the Function of Cd25+Cd4+ Regulatory Cells That Control Intestinal Inflammation. J. Exp. Med. *192*, 295–302.

Restifo, N.P., Esquivel, F., Kawakami, Y., Yewdell, J.W., Mulé, J.J., Rosenberg, S.A., and Bennink, J.R. (1993). Identification of human cancers deficient in antigen processing. J. Exp. Med. *177*, 265–272.

Rhim, A.D., Mirek, E.T., Aiello, N.M., Maitra, A., Bailey, J.M., McAllister, F., Reichert, M., Beatty, G.L., Rustgi, A.K., Vonderheide, R.H., et al. (2012). EMT and Dissemination Precede Pancreatic Tumor Formation. Cell *148*, 349–361.

Rigiracciolo, D.C., Nohata, N., Lappano, R., Cirillo, F., Talia, M., Scordamaglia, D., Gutkind, J.S., and Maggiolini, M. (2020). IGF-1/IGF-1R/FAK/YAP Transduction Signaling Prompts Growth Effects in Triple-Negative Breast Cancer (TNBC) Cells. Cells *9*, 1010.

Rizvi, N.A., Hellmann, M.D., Snyder, A., Kvistborg, P., Makarov, V., Havel, J.J., Lee, W., Yuan, J., Wong, P., Ho, T.S., et al. (2015). Mutational landscape determines sensitivity to PD-1 blockade in non–small cell lung cancer. Science *348*, 124–128.

Röhrle, N., Knott, M.M.L., and Anz, D. (2020a). CCL22 Signaling in the Tumor Environment. In Tumor Microenvironment: The Role of Chemokines – Part A, A. Birbrair, ed. (Cham: Springer International Publishing), pp. 79–96.

Röhrle, N., Knott, M.M.L., and Anz, D. (2020b). CCL22 Signaling in the Tumor Environment. In Tumor Microenvironment: The Role of Chemokines – Part A, A. Birbrair, ed. (Cham: Springer International Publishing), pp. 79–96.

Romagnani, S. (1997). The Th1/Th2 paradigm. Immunol. Today *18*, 263–266.

Romano, M., Fanelli, G., Albany, C.J., Giganti, G., and Lombardi, G. (2019). Past, Present, and Future of Regulatory T Cell Therapy in Transplantation and Autoimmunity. Front. Immunol. *10*.

Rosenberg, S.A., and Restifo, N.P. (2015). Adoptive cell transfer as personalized immunotherapy for human cancer. Science *348*, 62–68.

Rosenthal, R., Cadieux, E.L., Salgado, R., Bakir, M.A., Moore, D.A., Hiley, C.T., Lund, T., Tanić, M., Reading, J.L., Joshi, K., et al. (2019). Neoantigen-directed immune escape in lung cancer evolution. Nature *567*, 479–485.

Ruffell, B., Affara, N.I., and Coussens, L.M. (2012). Differential macrophage programming in the tumor microenvironment. Trends Immunol. *33*, 119–126.

Ruscetti, M., Quach, B., Dadashian, E.L., Mulholland, D.J., and Wu, H. (2015). Tracking and Functional Characterization of Epithelial–Mesenchymal Transition and Mesenchymal Tumor Cells during Prostate Cancer Metastasis. Cancer Res. *75*, 2749–2759.

Sade-Feldman, M., Jiao, Y.J., Chen, J.H., Rooney, M.S., Barzily-Rokni, M., Eliane, J.-P., Bjorgaard, S.L., Hammond, M.R., Vitzthum, H., Blackmon, S.M., et al. (2017). Resistance to checkpoint blockade therapy through inactivation of antigen presentation. Nat. Commun. *8*, 1136.

Sade-Feldman, M., Yizhak, K., Bjorgaard, S.L., Ray, J.P., Boer, C.G. de, Jenkins, R.W., Lieb, D.J., Chen, J.H., Frederick, D.T., Barzily-Rokni, M., et al. (2018). Defining T Cell States Associated with Response to Checkpoint Immunotherapy in Melanoma. Cell *175*, 998-1013.e20.

Sadek, H., Azli, N., Wendling, J.L., Cvitkovic, E., Rahal, M., Mamelle, G., Guillaume, J.C., Armand, J.P., and Avril, M.F. (1990). Treatment of advanced squamous cell carcinoma of the skin with cisplatin, 5-fluorouracil, and bleomycin. Cancer *66*, 1692–1696.

Sainz, B., Carron, E., Vallespinós, M., and Machado, H.L. (2016). Cancer Stem Cells and Macrophages: Implications in Tumor Biology and Therapeutic Strategies. Mediators Inflamm.

Sakaguchi, S., Miyara, M., Costantino, C.M., and Hafler, D.A. (2010). FOXP3 + regulatory T cells in the human immune system. Nat. Rev. Immunol. *10*, 490–500.

Sakuishi, K., Apetoh, L., Sullivan, J.M., Blazar, B.R., Kuchroo, V.K., and Anderson, A.C. (2010). Targeting Tim-3 and PD-1 pathways to reverse T cell exhaustion and restore anti-tumor immunity. J. Exp. Med. *207*, 2187–2194.

Sanchez-Correa, B., Valhondo, I., Hassouneh, F., Lopez-Sejas, N., Pera, A., Bergua, J.M., Arcos, M.J., Bañas, H., Casas-Avilés, I., Durán, E., et al. (2019). DNAM-1 and the TIGIT/PVRIG/TACTILE Axis: Novel Immune Checkpoints for Natural Killer Cell-Based Cancer Immunotherapy. Cancers *11*, 877.

Sánchez-Danés, A., and Blanpain, C. (2018). Deciphering the cells of origin of squamous cell carcinomas. Nat. Rev. Cancer *18*, 549–561.

Santamaria, P.G., Moreno-Bueno, G., Portillo, F., and Cano, A. (2017). EMT: Present and future in clinical oncology. Mol. Oncol. *11*, 718–738.

Savagner, P., Yamada, K.M., and Thiery, J.P. (1997). The Zinc-Finger Protein Slug Causes Desmosome Dissociation, an Initial and Necessary Step for Growth Factor–induced Epithelial–Mesenchymal Transition. J. Cell Biol. *137*, 1403–1419.

Scheel, C., Eaton, E.N., Li, S.H.-J., Chaffer, C.L., Reinhardt, F., Kah, K.-J., Bell, G., Guo, W., Rubin, J., Richardson, A.L., et al. (2011). Paracrine and Autocrine Signals Induce and Maintain Mesenchymal and Stem Cell States in the Breast. Cell *145*, 926–940.

Schietinger, A., and Greenberg, P.D. (2014). Tolerance and exhaustion: defining mechanisms of T cell dysfunction. Trends Immunol. *35*, 51–60.

Schmidt, A., Oberle, N., and Krammer, P.H. (2012). Molecular Mechanisms of Treg-Mediated T Cell Suppression. Front. Immunol. *3*.

Schmidt, J.M., Panzilius, E., Bartsch, H.S., Irmler, M., Beckers, J., Kari, V., Linnemann, J.R., Dragoi, D., Hirschi, B., Kloos, U.J., et al. (2015). Stem-Cell-like Properties and Epithelial Plasticity Arise as Stable Traits after Transient Twist1 Activation. Cell Rep. *10*, 131–139.

Schneider, H., Downey, J., Smith, A., Zinselmeyer, B.H., Rush, C., Brewer, J.M., Wei, B., Hogg, N., Garside, P., and Rudd, C.E. (2006). Reversal of the TCR Stop Signal by CTLA-4. Science *313*, 1972–1975.

Schnell, A., Bod, L., Madi, A., and Kuchroo, V.K. (2020). The yin and yang of co-inhibitory receptors: toward anti-tumor immunity without autoimmunity. Cell Res. *30*, 285–299.

Schumacher, T.N., and Schreiber, R.D. (2015). Neoantigens in cancer immunotherapy. Science *348*, 69–74.

Schuster, I.S., Coudert, J.D., Andoniou, C.E., and Degli-Esposti, M.A. (2016). "Natural Regulators": NK Cells as Modulators of T Cell Immunity. Front. Immunol. *7*.

Sconocchia, G., Zlobec, I., Lugli, A., Calabrese, D., Iezzi, G., Karamitopoulou, E., Patsouris, E.S., Peros, G., Horcic, M., Tornillo, L., et al. (2011). Tumor infiltration by FcγRIII (CD16)+ myeloid cells is associated with improved survival in patients with colorectal carcinoma. Int. J. Cancer *128*, 2663–2672.

Seo, H., Kim, B.-S., Bae, E.-A., Min, B.S., Han, Y.D., Shin, S.J., and Kang, C.-Y. (2018). IL21 Therapy Combined with PD-1 and Tim-3 Blockade Provides Enhanced NK Cell Antitumor Activity against MHC Class I–Deficient Tumors. Cancer Immunol. Res. *6*, 685–695.

Sharma, P., and Allison, J.P. (2015). The future of immune checkpoint therapy. Science *348*, 56–61.

Sharma, P., Hu-Lieskovan, S., Wargo, J.A., and Ribas, A. (2017). Primary, Adaptive, and Acquired Resistance to Cancer Immunotherapy. Cell *168*, 707–723.

Shaul, M.E., and Fridlender, Z.G. (2019). Tumour-associated neutrophils in patients with cancer. Nat. Rev. Clin. Oncol. *16*, 601–620.

Shibue, T., and Weinberg, R.A. (2017). EMT, CSCs, and drug resistance: the mechanistic link and clinical implications. Nat. Rev. Clin. Oncol. *14*, 611–629.

Shin, D.M., Glisson, B.S., Khuri, F.R., Clifford, J.L., Clayman, G., Benner, S.E., Forastiere, A.A., Ginsberg, L., Liu, D., Lee, J.J., et al. (2016). Phase II and Biologic Study of Interferon Alfa, Retinoic Acid, and Cisplatin in Advanced Squamous Skin Cancer. J. Clin. Oncol.

Shin, D.S., Zaretsky, J.M., Escuin-Ordinas, H., Garcia-Diaz, A., Hu-Lieskovan, S., Kalbasi, A., Grasso, C.S., Hugo, W., Sandoval, S., Torrejon, D.Y., et al. (2017). Primary Resistance to PD-1 Blockade Mediated by JAK1/2 Mutations. Cancer Discov. *7*, 188–201.

Siegle, J.M., Basin, A., Sastre-Perona, A., Yonekubo, Y., Brown, J., Sennett, R., Rendl, M., Tsirigos, A., Carucci, J.A., and Schober, M. (2014). SOX2 is a cancer-specific regulator of tumour initiating potential in cutaneous squamous cell carcinoma. Nat. Commun. *5*, 4511.

Silva-Diz, V. da, Simón-Extremera, P., Bernat-Peguera, A., Sostoa, J. de, Urpí, M., Penín, R.M., Sidelnikova, D.P., Bermejo, O., Viñals, J.M., Rodolosse, A., et al. (2016). Cancer Stem-like Cells Act via Distinct Signaling Pathways in Promoting Late Stages of Malignant Progression. Cancer Res. *76*, 1245–1259.

da Silva-Diz, V., Simón-Extremera, P., Bernat-Peguera, A., de Sostoa, J., Urpí, M., Penín, R.M., Sidelnikova, D.P., Bermejo, O., Viñals, J.M., Rodolosse, A., et al. (2016). Cancer Stem-like Cells Act via Distinct Signaling Pathways in Promoting Late Stages of Malignant Progression. Cancer Res. *76*, 1245–1259.

da Silva-Diz, V., Lorenzo-Sanz, L., Bernat-Peguera, A., Lopez-Cerda, M., and Muñoz, P. (2018). Cancer cell plasticity: Impact on tumor progression and therapy response. Semin. Cancer Biol. *53*, 48–58.

Skoulidis, F., Goldberg, M.E., Greenawalt, D.M., Hellmann, M.D., Awad, M.M., Gainor, J.F., Schrock, A.B., Hartmaier, R.J., Trabucco, S.E., Gay, L., et al. (2018). STK11/LKB1 Mutations and PD-1 Inhibitor Resistance in KRAS-Mutant Lung Adenocarcinoma. Cancer Discov. *8*, 822–835.

Smith, B.N., and Bhowmick, N.A. (2016). Role of EMT in Metastasis and Therapy Resistance. J. Clin. Med. *5*, 17.

Smyth, M.J., Thia, K.Y.T., Cretney, E., Kelly, J.M., Snook, M.B., Forbes, C.A., and Scalzo, A.A. (1999). Perforin Is a Major Contributor to NK Cell Control of Tumor Metastasis. J. Immunol. *162*, 6658–6662.

Sojka, D.K., Huang, Y.-H., and Fowell, D.J. (2008). Mechanisms of regulatory T-cell suppression – a diverse arsenal for a moving target. Immunology *124*, 13–22.

Solito, S., Marigo, I., Pinton, L., Damuzzo, V., Mandruzzato, S., and Bronte, V. (2014). Myeloid-derived suppressor cell heterogeneity in human cancers. Ann. N. Y. Acad. Sci. *1319*, 47–65.

Spranger, S., and Gajewski, T.F. (2018). Impact of oncogenic pathways on evasion of antitumour immune responses. Nat. Rev. Cancer *18*, 139–147.

Spranger, S., Bao, R., and Gajewski, T.F. (2015). Melanoma-intrinsic β-catenin signalling prevents anti-tumour immunity. Nature *523*, 231–235.

Stanietsky, N., Simic, H., Arapovic, J., Toporik, A., Levy, O., Novik, A., Levine, Z., Beiman, M., Dassa, L., Achdout, H., et al. (2009). The interaction of TIGIT with PVR and PVRL2 inhibits human NK cell cytotoxicity. Proc. Natl. Acad. Sci. *106*, 17858–17863.

Stecher, C., Battin, C., Leitner, J., Zettl, M., Grabmeier-Pfistershammer, K., Höller, C., Zlabinger, G.J., and Steinberger, P. (2017). PD-1 Blockade Promotes Emerging Checkpoint Inhibitors in Enhancing T Cell Responses to Allogeneic Dendritic Cells. Front. Immunol. *8*.

Stiff, A., Trikha, P., Mundy-Bosse, B., McMichael, E., Mace, T.A., Benner, B., Kendra, K., Campbell, A., Gautam, S., Abood, D., et al. (2018). Nitric Oxide Production by Myeloid-Derived Suppressor Cells Plays a Role in Impairing Fc Receptor–Mediated Natural Killer Cell Function. Clin. Cancer Res. *24*, 1891–1904.

Strachan, D.C., Ruffell, B., Oei, Y., Bissell, M.J., Coussens, L.M., Pryer, N., and Daniel, D. (2013). CSF1R inhibition delays cervical and mammary tumor growth in murine models by attenuating the turnover of tumor-associated macrophages and enhancing infiltration by CD8+ T cells. OncoImmunology *2*, e26968.

Stratigos, A., Garbe, C., Lebbe, C., Malvehy, J., Marmol, V. del, Pehamberger, H., Peris, K., Becker, J.C., Zalaudek, I., Saiag, P., et al. (2015). Diagnosis and treatment of invasive squamous cell carcinoma of the skin: European consensus-based interdisciplinary guideline. Eur. J. Cancer *51*, 1989–2007.

Strauss, R., Sova, P., Liu, Y., Li, Z.Y., Tuve, S., Pritchard, D., Brinkkoetter, P., Möller, T., Wildner, O., Pesonen, S., et al. (2009). Epithelial Phenotype Confers Resistance of Ovarian Cancer Cells to Oncolytic Adenoviruses. Cancer Res. *69*, 5115–5125.

Su, S., Liu, Q., Chen, J., Chen, J., Chen, F., He, C., Huang, D., Wu, W., Lin, L., Huang, W., et al. (2014). A Positive Feedback Loop between Mesenchymal-like Cancer Cells and Macrophages Is Essential to Breast Cancer Metastasis. Cancer Cell *25*, 605–620.

Sucker, A., Zhao, F., Real, B., Heeke, C., Bielefeld, N., Maβen, S., Horn, S., Moll, I., Maltaner, R., Horn, P.A., et al. (2014). Genetic Evolution of T-cell Resistance in the Course of Melanoma Progression. Clin. Cancer Res. *20*, 6593–6604.

Sucker, A., Zhao, F., Pieper, N., Heeke, C., Maltaner, R., Stadtler, N., Real, B., Bielefeld, N., Howe, S., Weide, B., et al. (2017). Acquired IFNγ resistance impairs anti-tumor immunity and gives rise to T-cell-resistant melanoma lesions. Nat. Commun. *8*, 15440.

Tahara-Hanaoka, S., Shibuya, K., Onoda, Y., Zhang, H., Yamazaki, S., Miyamoto, A., Honda, S., Lanier, L.L., and Shibuya, A. (2004). Functional characterization of DNAM-1 (CD226) interaction with its ligands PVR (CD155) and nectin-2 (PRR-2/CD112). Int. Immunol. *16*, 533–538.

Tam, W.L., and Weinberg, R.A. (2013). The epigenetics of epithelial-mesenchymal plasticity in cancer. Nat. Med. *19*, 1438–1449.

Tamborero, D., Rubio-Perez, C., Muiños, F., Sabarinathan, R., Piulats, J.M., Muntasell, A., Dienstmann, R., Lopez-Bigas, N., and Gonzalez-Perez, A. (2018). A Pan-cancer Landscape of Interactions between Solid Tumors and Infiltrating Immune Cell Populations. Clin. Cancer Res. Off. J. Am. Assoc. Cancer Res. *24*, 3717–3728.

Tang, H., Qiao, J., and Fu, Y.-X. (2016). Immunotherapy and tumor microenvironment. Cancer Lett. *370*, 85–90.

Tang, T., Huang, X., Zhang, G., Hong, Z., Bai, X., and Liang, T. (2021). Advantages of targeting the tumor immune microenvironment over blocking immune checkpoint in cancer immunotherapy. Signal Transduct. Target. Ther. *6*, 1–13.

Tarhini, A.A., Edington, H., Butterfield, L.H., Lin, Y., Shuai, Y., Tawbi, H., Sander, C., Yin, Y., Holtzman, M., Johnson, J., et al. (2014). Immune Monitoring of the Circulation and the Tumor Microenvironment in Patients with Regionally Advanced Melanoma Receiving Neoadjuvant Ipilimumab. PLOS ONE *9*, e87705.

Tauriello, D.V.F., Palomo-Ponce, S., Stork, D., Berenguer-Llergo, A., Badia-Ramentol, J., Iglesias, M., Sevillano, M., Ibiza, S., Cañellas, A., Hernando-Momblona, X., et al. (2018). TGFβ drives immune evasion in genetically reconstituted colon cancer metastasis. Nature *554*, 538–543.

Terry, S., Savagner, P., Ortiz-Cuaran, S., Mahjoubi, L., Saintigny, P., Thiery, J.-P., and Chouaib, S. (2017). New insights into the role of EMT in tumor immune escape. Mol. Oncol. *11*, 824–846.

Thiery, J.P. (2002). Epithelial–mesenchymal transitions in tumour progression. Nat. Rev. Cancer *2*, 442–454.

Thiery, J.P., Acloque, H., Huang, R.Y.J., and Nieto, M.A. (2009). Epithelial-Mesenchymal Transitions in Development and Disease. Cell *139*, 871–890.

Thomas, D.A., and Massagué, J. (2005). TGF-β directly targets cytotoxic T cell functions during tumor evasion of immune surveillance. Cancer Cell *8*, 369–380.

Thommen, D.S., Schreiner, J., Müller, P., Herzig, P., Roller, A., Belousov, A., Umana, P., Pisa, P., Klein, C., Bacac, M., et al. (2015). Progression of Lung Cancer Is Associated with Increased Dysfunction of T Cells Defined by Coexpression of Multiple Inhibitory Receptors. Cancer Immunol. Res. *3*, 1344–1355.

Thompson, E.D., Enriquez, H.L., Fu, Y.-X., and Engelhard, V.H. (2010). Tumor masses support naive T cell infiltration, activation, and differentiation into effectors. J. Exp. Med. *207*, 1791–1804.

Tlsty, T.D., and Coussens, L.M. (2006). Tumor stroma and regulation of cancer development. Annu. Rev. Pathol. Mech. Dis. *1*, 119–150.

Tran, H.D., Luitel, K., Kim, M., Zhang, K., Longmore, G.D., and Tran, D.D. (2014). Transient SNAIL1 Expression Is Necessary for Metastatic Competence in Breast Cancer. Cancer Res. *74*, 6330–6340.

Trapani, J.A., and Smyth, M.J. (2002). Functional significance of the perforin/granzyme cell death pathway. Nat. Rev. Immunol. *2*, 735–747.

Trempus, C.S., Morris, R.J., Ehinger, M., Elmore, A., Bortner, C.D., Ito, M., Cotsarelis, G., Nijhof, J.G.W., Peckham, J., Flagler, N., et al. (2007). CD34 Expression by Hair Follicle Stem Cells Is Required for Skin Tumor Development in Mice. Cancer Res. *67*, 4173–4181.

Triebel, F., Jitsukawa, S., Baixeras, E., Roman-Roman, S., Genevee, C., Viegas-Pequignot, E., and Hercend, T. (1990). LAG-3, a novel lymphocyte activation gene closely related to CD4. J. Exp. Med. *171*, 1393–1405.

Tripathi, S.C., Peters, H.L., Taguchi, A., Katayama, H., Wang, H., Momin, A., Jolly, M.K., Celiktas, M., Rodriguez-Canales, J., Liu, H., et al. (2016). Immunoproteasome deficiency is a feature of non-small cell lung cancer with a mesenchymal phenotype and is associated with a poor outcome. Proc. Natl. Acad. Sci. *113*, E1555–E1564.

Tsai, J.H., Donaher, J.L., Murphy, D.A., Chau, S., and Yang, J. (2012). Spatiotemporal Regulation of Epithelial-Mesenchymal Transition Is Essential for Squamous Cell Carcinoma Metastasis. Cancer Cell *22*, 725–736.

Umansky, V., Blattner, C., Gebhardt, C., and Utikal, J. (2016). The Role of Myeloid-Derived Suppressor Cells (MDSC) in Cancer Progression. Vaccines *4*, 36.

Uzhachenko, R.V., and Shanker, A. (2019). CD8+ T Lymphocyte and NK Cell Network: Circuitry in the Cytotoxic Domain of Immunity. Front. Immunol. *10*.

Veglia, F., Sanseviero, E., and Gabrilovich, D.I. (2021). Myeloid-derived suppressor cells in the era of increasing myeloid cell diversity. Nat. Rev. Immunol. 1–14.

Veillette, A., and Chen, J. (2018). SIRPα–CD47 Immune Checkpoint Blockade in Anticancer Therapy. Trends Immunol. *39*, 173–184.

Verma, V., Shrimali, R.K., Ahmad, S., Dai, W., Wang, H., Lu, S., Nandre, R., Gaur, P., Lopez, J., Sade-Feldman, M., et al. (2019). PD-1 blockade in subprimed CD8 cells induces dysfunctional PD-1 + CD38 hi cells and anti-PD-1 resistance. Nat. Immunol. *20*, 1231–1243.

Viel, S., Marçais, A., Guimaraes, F.S.-F., Loftus, R., Rabilloud, J., Grau, M., Degouve, S., Djebali, S., Sanlaville, A., Charrier, E., et al. (2016). TGF-β inhibits the activation and functions of NK cells by repressing the mTOR pathway. Sci. Signal. *9*, ra19–ra19.

Vignali, D.A.A., Collison, L.W., and Workman, C.J. (2008). How regulatory T cells work. Nat. Rev. Immunol. *8*, 523–532.

Visvader, J.E. (2011). Cells of origin in cancer. Nature *469*, 314–322.

Vitale, I., Shema, E., Loi, S., and Galluzzi, L. (2021). Intratumoral heterogeneity in cancer progression and response to immunotherapy. Nat. Med. *27*, 212–224.

Vivier, E., Tomasello, E., Baratin, M., Walzer, T., and Ugolini, S. (2008). Functions of natural killer cells. Nat. Immunol. *9*, 503–510.

Vivier, E., Ugolini, S., Blaise, D., Chabannon, C., and Brossay, L. (2012). Targeting natural killer cells and natural killer T cells in cancer. Nat. Rev. Immunol. *12*, 239–252.

Vodnala, S.K., Eil, R., Kishton, R.J., Sukumar, M., Yamamoto, T.N., Ha, N.-H., Lee, P.-H., Shin, M., Patel, S.J., Yu, Z., et al. (2019). T cell stemness and dysfunction in tumors are triggered by a common mechanism. Science *363*.

Voskoboinik, I., Whisstock, J.C., and Trapani, J.A. (2015). Perforin and granzymes: function, dysfunction and human pathology. Nat. Rev. Immunol. *15*, 388–400.

Wajant, H., Pfizenmaier, K., and Scheurich, P. (2003). Tumor necrosis factor signaling. Cell Death Differ. *10*, 45–65.

Waldman, A.D., Fritz, J.M., and Lenardo, M.J. (2020). A guide to cancer immunotherapy: from T cell basic science to clinical practice. Nat. Rev. Immunol. *20*, 651–668.

Wan, S., Zhao, E., Kryczek, I., Vatan, L., Sadovskaya, A., Ludema, G., Simeone, D.M., Zou, W., and Welling, T.H. (2014). Tumor-Associated Macrophages Produce Interleukin 6 and Signal via STAT3 to Promote Expansion of Human Hepatocellular Carcinoma Stem Cells. Gastroenterology *147*, 1393–1404.

Wang, D., Yang, L., Yue, D., Cao, L., Li, L., Wang, D., Ping, Y., Shen, Z., Zheng, Y., Wang, L., et al. (2019a). Macrophage-derived CCL22 promotes an immunosuppressive tumor microenvironment via IL-8 in malignant pleural effusion. Cancer Lett. *452*, 244–253.

Wang, J., Sanmamed, M.F., Datar, I., Su, T.T., Ji, L., Sun, J., Chen, L., Chen, Y., Zhu, G., Yin, W., et al. (2019b). Fibrinogen-like Protein 1 Is a Major Immune Inhibitory Ligand of LAG-3. Cell *176*, 334-347.e12.

Wang, M., Zhao, J., Zhang, L., Wei, F., Lian, Y., Wu, Y., Gong, Z., Zhang, S., Zhou, J., Cao, K., et al. (2017). Role of tumor microenvironment in tumorigenesis. J. Cancer *8*, 761–773.

Wculek, S.K., Cueto, F.J., Mujal, A.M., Melero, I., Krummel, M.F., and Sancho, D. (2020). Dendritic cells in cancer immunology and immunotherapy. Nat. Rev. Immunol. *20*, 7–24.

Weber, J., Gibney, G., Kudchadkar, R., Yu, B., Cheng, P., Martinez, A.J., Kroeger, J., Richards, A., McCormick, L., Moberg, V., et al. (2016). Phase I/II Study of Metastatic Melanoma Patients Treated with Nivolumab Who Had Progressed after Ipilimumab. Cancer Immunol. Res. *4*, 345–353.

Wei, S.C., Duffy, C.R., and Allison, J.P. (2018). Fundamental Mechanisms of Immune Checkpoint Blockade Therapy. Cancer Discov. *8*, 1069–1086.

Wellner, U., Schubert, J., Burk, U.C., Schmalhofer, O., Zhu, F., Sonntag, A., Waldvogel, B., Vannier, C., Darling, D., Hausen, A. zur, et al. (2009). The EMT-activator ZEB1 promotes tumorigenicity by repressing stemness-inhibiting microRNAs. Nat. Cell Biol. *11*, 1487–1495.

Wessely, A., Steeb, T., Leiter, U., Garbe, C., Berking, C., and Heppt, M.V. (2020). Immune Checkpoint Blockade in Advanced Cutaneous Squamous Cell Carcinoma: What Do We Currently Know in 2020? Int. J. Mol. Sci. *21*, 9300.

Wherry, E.J. (2011). T cell exhaustion. Nat. Immunol. *12*, 492–499.

Wherry, E.J., and Kurachi, M. (2015). Molecular and cellular insights into T cell exhaustion. Nat. Rev. Immunol. *15*, 486–499.

Wierz, M., Pierson, S., Guyonnet, L., Viry, E., Lequeux, A., Oudin, A., Niclou, S.P., Ollert, M., Berchem, G., Janji, B., et al. (2018). Dual PD1/LAG3 immune checkpoint blockade limits tumor development in a murine model of chronic lymphocytic leukemia. Blood *131*, 1617–1621.

William, W.N., Feng, L., Ferrarotto, R., Ginsberg, L., Kies, M., Lippman, S., Glisson, B., and Kim, E.S. (2017). Gefitinib for patients with incurable cutaneous squamous cell carcinoma: A single-arm phase II clinical trial. J. Am. Acad. Dermatol. *77*, 1110-1113.e2.

Wing, K., Onishi, Y., Prieto-Martin, P., Yamaguchi, T., Miyara, M., Fehervari, Z., Nomura, T., and Sakaguchi, S. (2008). CTLA-4 Control over Foxp3+ Regulatory T Cell Function. Science *322*, 271–275.

Wollina, U., Hansel, G., Koch, A., and Köstler, E. (2005). Oral capecitabine plus subcutaneous interferon alpha in advanced squamous cell carcinoma of the skin. J. Cancer Res. Clin. Oncol. *131*, 300–304.

Xing, Y., and Hogquist, K.A. (2012). T-Cell Tolerance: Central and Peripheral. Cold Spring Harb. Perspect. Biol. *4*, a006957.

Xu, F., Liu, J., Liu, D., Liu, B., Wang, M., Hu, Z., Du, X., Tang, L., and He, F. (2014). LSECtin Expressed on Melanoma Cells Promotes Tumor Progression by Inhibiting Antitumor T-cell Responses. Cancer Res. *74*, 3418–3428.

Yamashita, N., Tokunaga, E., Iimori, M., Inoue, Y., Tanaka, K., Kitao, H., Saeki, H., Oki, E., and Maehara, Y. (2018). Epithelial Paradox: Clinical Significance of Coexpression of E-cadherin and Vimentin With Regard to Invasion and Metastasis of Breast Cancer. Clin. Breast Cancer *18*, e1003–e1009.

Yan, D., Wang, H.-W., Bowman, R.L., and Joyce, J.A. (2016). STAT3 and STAT6 Signaling Pathways Synergize to Promote Cathepsin Secretion from Macrophages via IRE1α Activation. Cell Rep. *16*, 2914–2927.

Yang, J., Mani, S.A., Donaher, J.L., Ramaswamy, S., Itzykson, R.A., Come, C., Savagner, P., Gitelman, I., Richardson, A., and Weinberg, R.A. (2004). Twist, a Master Regulator of Morphogenesis, Plays an Essential Role in Tumor Metastasis. Cell *117*, 927–939.

Yang, J., Liao, D., Chen, C., Liu, Y., Chuang, T.-H., Xiang, R., Markowitz, D., Reisfeld, R.A., and Luo, Y. (2013). Tumor-associated macrophages regulate murine breast cancer stem cells through a novel paracrine EGFR/Stat3/Sox-2 signaling pathway. Stem Cells Dayt. Ohio *31*, 248–258.

Yang, J., Antin, P., Berx, G., Blanpain, C., Brabletz, T., Bronner, M., Campbell, K., Cano, A., Casanova, J., Christofori, G., et al. (2020). Guidelines and definitions for research on epithelial–mesenchymal transition. Nat. Rev. Mol. Cell Biol. *21*, 341–352.

Yanofsky, V.R., Mercer, S.E., and Phelps, R.G. (2011). Histopathological variants of cutaneous squamous cell carcinoma: a review. J. Skin Cancer *2011*, 210813.

Ye, X., and Weinberg, R.A. (2015). Epithelial–Mesenchymal Plasticity: A Central Regulator of Cancer Progression. Trends Cell Biol. *25*, 675–686.

Yin, Y., Yao, S., Hu, Y., Feng, Y., Li, M., Bian, Z., Zhang, J., Qin, Y., Qi, X., Zhou, L., et al. (2017). The Immune-microenvironment Confers Chemoresistance of Colorectal Cancer through Macrophage-Derived IL6. Clin. Cancer Res. *23*, 7375–7387.

Youn, J.-I., Nagaraj, S., Collazo, M., and Gabrilovich, D.I. (2008). Subsets of Myeloid-Derived Suppressor Cells in Tumor Bearing Mice. J. Immunol. Baltim. Md 1950 *181*, 5791–5802.

Youn, J.-I., Collazo, M., Shalova, I.N., Biswas, S.K., and Gabrilovich, D.I. (2012). Characterization of the nature of granulocytic myeloid-derived suppressor cells in tumor-bearing mice. J. Leukoc. Biol. *91*, 167–181.

Yu, M., Bardia, A., Wittner, B.S., Stott, S.L., Smas, M.E., Ting, D.T., Isakoff, S.J., Ciciliano, J.C., Wells, M.N., Shah, A.M., et al. (2013). Circulating Breast Tumor Cells Exhibit Dynamic Changes in Epithelial and Mesenchymal Composition. Science *339*, 580–584.

Yu, X., Harden, K., Gonzalez, L.C., Francesco, M., Chiang, E., Irving, B., Tom, I., Ivelja, S., Refino, C.J., Clark, H., et al. (2009). The surface protein TIGIT suppresses T cell activation by promoting the generation of mature immunoregulatory dendritic cells. Nat. Immunol. *10*, 48–57.

Yuan, S., Norgard, R.J., and Stanger, B.Z. (2019). Cellular Plasticity in Cancer. Cancer Discov. *9*, 837–851.

Zaretsky, J.M., Garcia-Diaz, A., Shin, D.S., Escuin-Ordinas, H., Hugo, W., Hu-Lieskovan, S., Torrejon, D.Y., Abril-Rodriguez, G., Sandoval, S., Barthly, L., et al. (2016). Mutations Associated with Acquired Resistance to PD-1 Blockade in Melanoma. N. Engl. J. Med. *375*, 819–829.

Zha, J., and Lackner, M.R. (2010). Targeting the Insulin-like Growth Factor Receptor-1R Pathway for Cancer Therapy. Clin. Cancer Res. *16*, 2512–2517.

Zhang, N., and Bevan, M.J. (2011). CD8+ T Cells: Foot Soldiers of the Immune System. Immunity *35*, 161–168.

Zhang, P., Wei, Y., Wang, L., Debeb, B.G., Yuan, Y., Zhang, J., Yuan, J., Wang, M., Chen, D., Sun, Y., et al. (2014). ATM-mediated stabilization of ZEB1 promotes DNA damage response and radioresistance through CHK1. Nat. Cell Biol. *16*, 864–875.

Zhang, Q., Bi, J., Zheng, X., Chen, Y., Wang, H., Wu, W., Wang, Z., Wu, Q., Peng, H., Wei, H., et al. (2018). Blockade of the checkpoint receptor TIGIT prevents NK cell exhaustion and elicits potent anti-tumor immunity. Nat. Immunol. *19*, 723–732.

Zhang, Z.-N., Yi, N., Zhang, T.-W., Zhang, L.-L., Wu, X., Liu, M., Fu, Y.-J., He, S.-J., Jiang, Y.-J., Ding, H.-B., et al. (2017). Myeloid-Derived Suppressor Cells Associated With Disease Progression in Primary HIV Infection: PD-L1 Blockade Attenuates Inhibition. JAIDS J. Acquir. Immune Defic. Syndr. *76*, 200–208.

Zhao, L., and Cao, Y.J. (2019). Engineered T Cell Therapy for Cancer in the Clinic. Front. Immunol. *10*.

Zhao, C., Wang, Q., Wang, B., Sun, Q., He, Z., Hong, J., Kuehn, F., Liu, E., and Zhang, Z. (2017). IGF-1 induces the epithelial-mesenchymal transition via Stat5 in hepatocellular carcinoma. Oncotarget *8*, 111922–111930.

Zhao, J., Zhao, J., and Perlman, S. (2012). Differential Effects of IL-12 on Tregs and Non-Treg T Cells: Roles of IFN-γ, IL-2 and IL-2R. PLOS ONE *7*, e46241.

Zhao, Y., Yang, W., Huang, Y., Cui, R., Li, X., and Li, B. (2018). Evolving Roles for Targeting CTLA-4 in Cancer Immunotherapy. Cell. Physiol. Biochem. *47*, 721–734.

Zhu, C., Anderson, A.C., Schubart, A., Xiong, H., Imitola, J., Khoury, S.J., Zheng, X.X., Strom, T.B., and Kuchroo, V.K. (2005). The Tim-3 ligand galectin-9 negatively regulates T helper type 1 immunity. Nat. Immunol. *6*, 1245–1252.

Zhu, H., Gu, Y., Xue, Y., Yuan, M., Cao, X., and Liu, Q. (2017). CXCR2 + MDSCs promote breast cancer progression by inducing EMT and activated T cell exhaustion. Oncotarget *8*, 114554–114567.

Zhu, Y., Knolhoff, B.L., Meyer, M.A., Nywening, T.M., West, B.L., Luo, J., Wang-Gillam, A., Goedegebuure, S.P., Linehan, D.C., and DeNardo, D.G. (2014). CSF1/CSF1R Blockade Reprograms Tumor-Infiltrating Macrophages and Improves Response to T-cell Checkpoint Immunotherapy in Pancreatic Cancer Models. Cancer Res. *74*, 5057–5069.